Quasi-Static Hydraulic Control Systems and Energy Savings Potential Using Independent Metering Four-Valve Assembly Configuration

A Thesis
Presented to
The Academic Faculty

by

Amir Shenouda

In Partial Fulfillment
of the Requirements for the Degree
Doctor of Philosophy

Woodruff School of Mechanical Engineering
Georgia Institute of Technology
August 2006

Quasi-Static Hydraulic Control Systems and Energy Savings Potential Using Independent Metering Four-Valve Assembly Configuration

Approved by:

Wayne Book
School of Mechanical Engineering
Georgia Institute of Technology, Advisor

Nader Sadegh
School of Mechanical Engineering
Georgia Institute of Technology

Chris Paredis
School of Mechanical Engineering
Georgia Institute of Technology

Bonnie Heck
School of Electrical and Computer Engineering
Georgia Institute of Technology

Renato Monteiro
School of Industrial Systems Engineering
Georgia Institute of Technology

Roger Yang
HUSCO International

Date Approved: July 5, 2006

ACKNOWLEDGEMENTS

The author wishes to express sincere appreciation and thanks to Dr. Wayne Book, who thought about the idea of regenerative flow a long time ago, for his support and guidance throughout the process of obtaining a PhD, for giving me the opportunity to be part of his research group, and for the cooperative and supportive atmosphere that he creates in the group. The author also wishes to thank the other members of the committee for accepting to be part of this research experience.

Special thanks are due to Mr. Agustin Ramirez the Chairman and CEO of HUSCO International for sponsoring this research and facilitating the cooperation between Georgia Tech and HUSCO International. Thanks are also due to Mr. Dwight Stephenson the Vice President of Engineering at HUSCO International for his guidance, help, and support.

The help of the INCOVA engineering team at HUSCO International was invaluable to finishing this work. Special thanks are due to Keith Tabor for his help on the theoretical aspect of the project, preparing the author, and bringing him up to speed to start his research fast. Joe Pfaff, the manager of the Electronics Group at HUSCO International provided very valuable insight into the theoretical and experimental aspects of the project. His help with visualizing data has been indispensable. Joe and Keith also directed the author to the automatic transmission analogy. The experimental work would not have been possible without the help of Joe Pfaff, Dave Meliecke, Mike Fossell, and Andy Smjkle.

Appreciation and thanks are expressed for other member of the research group at Georgia Tech. Thanks are due to Patrick Opdenbosch for his help with the second order model of the poppet valves. Valuable discussions and encouragement from Matt Kontz, Ryan Krauss, and JD Huggins are deeply appreciated.

It is the continuous and unwavering support and love of family that makes going through the PhD process possible. Heartfelt thanks are due to my family.

SUMMARY

In this research, the four valve independent metering configuration is to be investigated. The Independent metering concept will be emphasized and compared to spool valve coupled metering conventional technologies. Research focuses on the energy savings potential of the four valve independent metering configuration in addition to improving performance.

The basic model of interest in this research is an actuator that is controlled by the four valve independent metering configuration to move beam like members of mobile hydraulic equipment such as tractor loader backhoes, excavators, and telehandlers.

Five distinct (or discrete) metering modes that exist in the literature are initially studied: Powered Extension, High Side Regeneration Extension, Low Side Regeneration Extension, Powered Retraction, and Low Side Regeneration Retraction. The energy saving potential of these modes is studied and comparisons between this system and a conventional spool valve controlled actuator are conducted.

The problem of switching between these five modes is treated as an optimal control problem of a switched dynamic system. Before solving the optimal control problem, a dynamic model for the system of interest is first derived. The model is experimentally validated.

General theory for the optimal control problem is derived and then applied to the hydraulic system of interest. The results are then interpreted and explained by looking into the force-speed capability of modes.

The effect of mode switching on system performance is studied as well. The basic mechanical system used for this analysis is a continuous rotating beam that undergoes structural vibrations due to mode switching in the driving hydraulic actuator. A fully coupled actuator-beam model is investigated. A non-dimensional analysis is pursued to generalize the study results. The optimal switching analysis and the vibrational study lead to the idea of Continuously Variable Modes (CVMs).

Instead of having five distinct modes that determines the flow path by opening two of the four valves in the assembly, three Continuously Variable Modes are presented as an alternative way of controlling the four-valve configuration. These three CVMs combine the distinct modes and use three of the four valves to provide the fluid flow path. The five distinct modes become a special case of these three CVMs. It is going to be shown that CVMs have more force-speed capabilities than the distinct modes and provide for better velocity and vibrational performance by virtue of always offering a continuous flow path. The theory behind CVMs is presented and experimental validation follows.

TABLE OF CONTENTS

LIST OF TABLES

LIST OF FIGURES

CHAPTER I

INTRODUCTION

1.1 General

Machines and robots can have movable members that can be operated by hydraulic actuators like a piston and cylinder arrangement that is controlled by a hydraulic valve. Hydraulic systems are used in many industrial applications because of their high power and force to weight ratio. Conventionally, in earth moving equipment for instance, the valve was located close to the operator cabin and the valves were operated manually to provide flow to the cylinders. However, the trend is to move away from the manual operation tradition and use electronics for control purposes. This makes the hydraulic plumbing much easier and provides the chance to implement modern control algorithms that are realized by an embedded microprocessor. Hydraulic system control is notorious for being difficult due to the many nonlinearities involved and the time varying characteristics that occur with temperature changes and wear, which makes microprocessor control capabilities even more valuable.

In existing electro-hydraulic systems, pressurized hydraulic fluid is supplied from a pump to the cylinder (actuator) and hydraulic fluid flows out of the actuator to a tank. The flow to the actuator and out of the actuator is controlled by a spool valve. The position of the spool controls the flow of the hydraulic fluid. A current is applied to an electro magnetic coil which moves an armature directly acting on the spool. Thus, the controller sends a certain current, which actuates the electro magnetic coil, moves the spool to a certain position proportional to the current applied to the coil, and controls the flow of hydraulic fluid to and from the actuator. Figure 1.1 shows a schematic of this system.

The construction of the four way spool valve is such that a given position of the spool determines the 'flow in' **and** the 'flow out' restriction sizes as shown in 1.2. Thus, metering-in and metering-out are coupled. A certain restriction size on the inlet corresponds to a

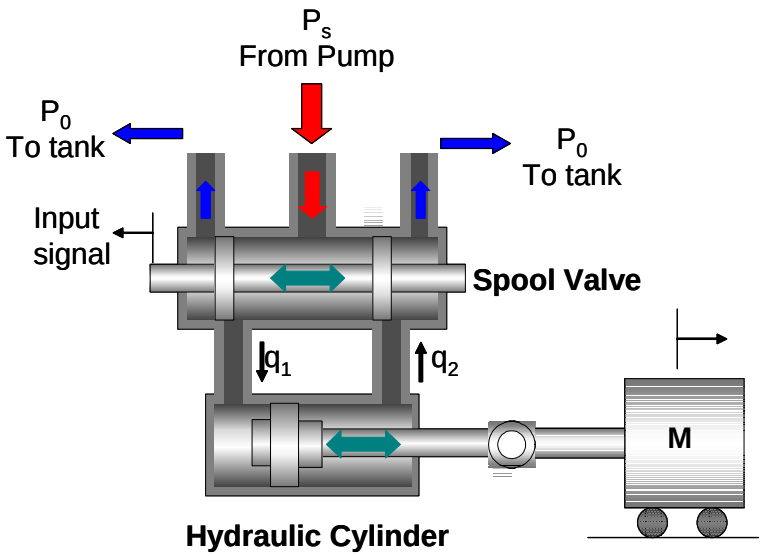

Figure 1.1: A Hydraulic Actuator Controlled by a Spool Valve

certain restriction size on the outlet. Therefore, we have one degree of freedom, and we can control either the speed of the actuator or the the pressure in just one chamber but not both. Thus, it can provide for good motion control but it cannot achieve energy saving potential at the same time [44]. In the case of an overrunning load, which happens when lowering a load with gravity assistance, for example, spool valves are designed such that the outlet restriction is used to control the flow so as to prevent the load from falling at uncontrollable speeds. However, in other operating conditions, such as lifting a load, this restriction is not needed yet it is inherent in the design of the spool valve. This causes energy loss that is unnecessary if the design would allow for separate meter-in and separate meter-out i.e. independent metering.

Moreover, conventional hydraulic systems that employ this kind of technology sense the pressure in the inlet chamber of the actuator alone, while being blind to the pressure in the other chamber. The control decisions are taken based on inlet chamber pressure alone. This technology is called Pressure Compensated Load Sense (PCLS). If changes happen in the other chamber, due to a force disturbance for instance, not in the chamber that is being sensed, the system will not react to these changes. In another instance, both chambers of

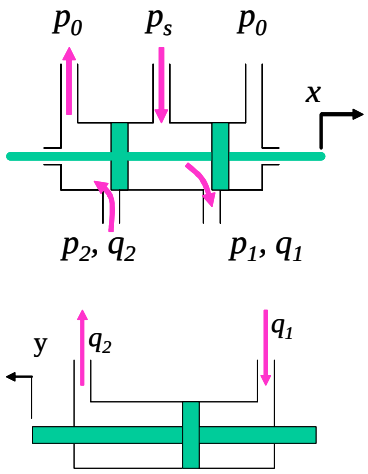

Figure 1.2: Coupled (dependent) Metering in a Spool Valve/Cylinder Assembly

the actuator can have a high trapped pressure with zero net force on the load. Thus it can be driven by minimum supply pressure and minimum flow from the pump, but since PCLS systems are blind to the pressure in the return chamber, it will drive the supply pressure high anyways, which means more energy consumption.

1.2 Literature Review

Proportional directional four-way control valves are the most frequently used valves in motion control in hydraulic applications [51]. Electronic control of hydraulic systems is becoming more and more common in industry [84]. The advent of electro-hydraulic valve technology and use of microprocessors have improved the performance of hydraulic systems significantly and promise a much needed energy savings. Advanced control algorithms were applied to spool valves with an electro-hydraulic pilot stage and an integral microcontroller added to each valve section [47]. A position measurement scheme can be added to determine the spool position with low hysteresis [48]. A typical four way directional proportional valve can meet high performance requirements of hydraulic systems as shown by Bu and Yao [14], but it just has one degree of freedom as explained above because of the dependence of metering in and metering out orifices openings on just one input, which is the position of the spool. Only one chamber's pressure can be controlled. Bu and Yao showed that this

one dimensional system is stable [14]. However, once the desired motion of the actuator is determined, the control input is uniquely determined. That means that it cannot provide precise motion control while controlling pressure in both actuator chambers. This further means that its potential for energy savings is low. Besides, different applications require different four way spool valve designs to accommodate the different needs of the various systems. The current trend in industry is to design a valve that can be adapted to the various systems in practice [26].

Most current systems use pressure compensators to keep a constant pressure margin across the spool valve inlet and thus achieve a linear relationship between the valve opening and flow [4]. As explained in the section above the traditional Pressure Compensated Load Sense (PCLS) systems are blind to the pressure in the return chamber and it will drive the supply pressure high even when not needed, which means more energy consumption. This can be a major source of inefficiency [54].

Independent metering promises to achieve higher system efficiency. Research has been done to achieve independent metering and thus to be able to have an extra control dimension. This has the potential of achieving precise motion control while controlling pressures in both actuator chambers for energy savings. The idea has been used in industry for several years. Aardema suggest using two conventional four way directional valves: one to control meter-in and the other to control meter-out [1]. But this is an expensive solution since it replaces one valve by two, and it does not achieve complete independence of meter-in and meter-out. Other more promising solutions replace the typical four way servo valve with four poppet type valves that can be controlled separately. Patents by Deere & Company [38], Caterpillar Inc [2], and Moog Inc [28] demonstrate the concept with minor variations. The "Smart Valve" [8] is another demonstration of the concept of a programmable valve that achieves independent metering control. The Electro Hydraulic Poppet Valve (EHPV) patented by HUSCO is also an example of this type of valve [97]. In EHPV valves, an electric current is used to actuate a solenoid armature that acts on a pilot poppet that controls the flow through a pilot passage in the main poppet. The main poppet moves and opens a passage for fluid that is proportional to the current supplied to the solenoid. In

other words, a certain current supplied to the solenoid of the valve translates into a certain valve opening or a valve flow coefficient K. This kind of valve can be adapted to the different hydraulic applications in the market with no hardware changes, which makes them "economically attractive" [34].

The independent metering concept replaces the four way spool valve with four valves in one package. Through software changes, this package can be adapted to several hydraulic system applications [9]. Four valves are needed to operate one cylinder. One valve connects one of the work ports of the cylinder to the supply line that contains pressurized oil. A second valve connects the other work port to the supply line. A third valve connects the first port to return line which leads to the tank. Finally a fourth valve is needed to connect the second port to the supply line. Using this four valve configuration, while only two valves will be active for a given condition, allows for independent metering and also allows for energy regeneration [38], which has the potential of reducing the requirement on the pump and thus achieve highly valuable energy saving. **Regeneration flow can be defined as pumping the fluid from one chamber to the other to achieve motion control of the load with using no or minimum flow from the pump**. This regeneration flow concept is almost impossible to achieve using a regular directional control valve [34]. Fig. 1.3 shows the transformation from spool valves to independent metering valve configuration. The spool valve can be represented by four restrictions that are not independent but mechanically coupled. The independent metering configuration breaks this mechanical linkage and uncouples the restrictions.

Liu and Yao investigated the use of a fifth valve to allow for cross port flow [44]. Their control scheme was composed of a task level controller and a valve level controller. The task level controller calculates the load that the cylinder has to move and determines which valves to be used i.e. what metering mode the valves should operate in. The valve level controller achieves pressure control and motion control of the hydraulic cylinder. It was proved that velocity control and energy efficiency can be achieved by pressure feedback [21]. Yao's work depends on online parameter estimation to achieve adaptive robust nonlinear control, and presented metering modes that will reduce the flow needed from the pump but

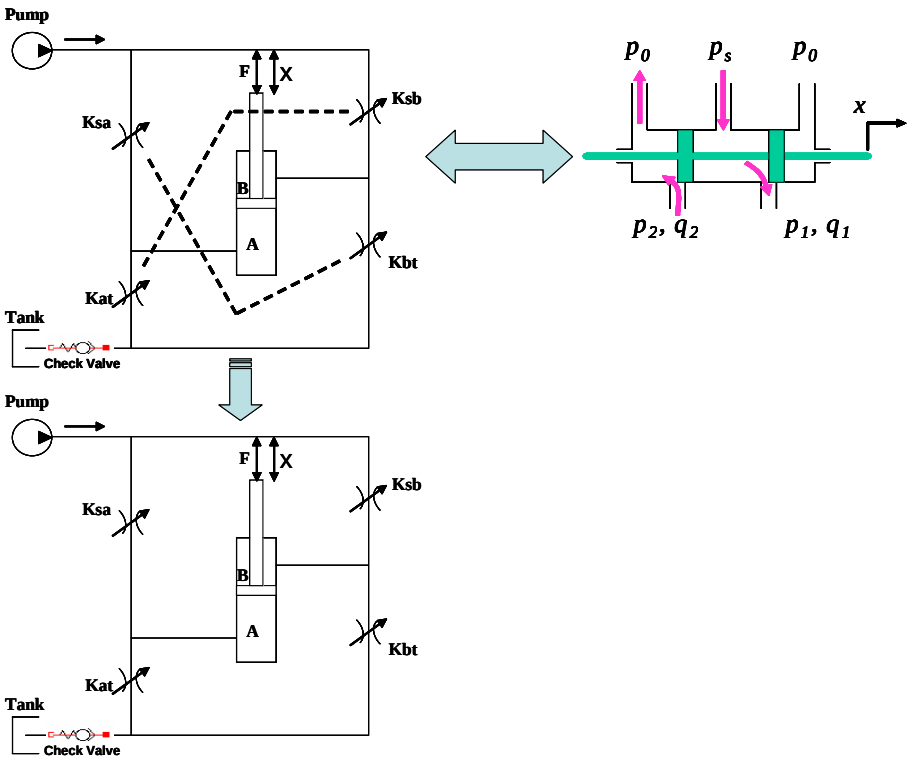

Figure 1.3: Evolution From Spool Valve To Independent Metering Valve Configuration

no optimization of the usage of these modes was used. His research used a robot arm setup that has three degrees of freedom and concentrated his work on boom motion control. The movements allowed for this setup were limited and slow (10°).

Ruth Book used a similar valve concept that she called the "Smart Valve" [9]. She attempted to apply advanced adaptive control algorithms to control a cylinder position. He used a five-valve configuration as well. The valves can be adapted to any other hydraulic systems through making software changes to the valves. She included anti-cavitation algorithms to control the pressure in the cylinder inlet chamber. Whenever cavitation occurred, the piston halted its movement until the void could be filled with oil. The idea was to draw oil from the retgturn port when the system senses an impending cavitation to fill the void in the inlet chamber. Due to the low flow capacity of the valves, the scheme was not successful all the times and cavitation occurred. She introduced the concept of "Inferred Flow Feedback" where the internal pressure measurements in the valves can be used to

calculate the flow through the valves. He was faced with hardware limitations and software / hardware compatibility issues and that prevented successful demonstration of his ideas.

Hydraulic systems are notorious for being hard to control due to the nonlinearities in the system, in addition to changes in fluid properties with temperature changes [23]. That is why researchers who worked on independent metering valves tried to apply adaptive control schemes to alleviate these problems inherent in hydraulic systems [68, 44, 9]. This technique involves continuous online plant identification and adapting the controller parameters accordingly. However, these nonlinear adaptive schemes require a lot of processing power that may not be practical for industrial application. Attempts at controlling cylinder movement under different load and velocity conditions used complex control algorithms that needed cylinder position and velocity feedback [25, 50]. **This is considered an impediment to industrial application due to the cost and complexity involved**. Simpler controllers are needed if this concept is going to be applied successfully in industry. For example, O'Hara was able to calculate a flow rate using an orifice equation [53], and a flow coefficient calibration equation with a 2% average error [58].

The ultimate goal of independent metering concepts is not only a more controllable system but a more energy efficient system as well. Because of fuel economy and the increasingly stringent environmental requirements, energy efficiency of hydraulic systems has been under research for a long time even before the concepts of programmable valves, independent metering, and regeneration flow appeared. Holzbock was interested in energy savings by combining conventional hydraulic systems with the versatility of microprocessors at times when microprocessors were starting to become feasible in industry [32]. The use of Adjustable-Frequency Drives to adapt a fixed displacement pump propeller speed to system requirements to save electrical energy was also studied [15]. Liang et al studied the effect of control valves on energy efficiency in a Loglift loader [40]. Current technology and future developments of load sense directional valves were studied in addition to analyzing the performance of mobile hydraulic valves and their power loss characteristics [5]. Different pump and valve control strategies have also been studied in the literature. Backe gave a general

description about the efficiency of these strategies [6], and Weber discussed pump control for performance and efficiency [88]. Using variable flow pumps with pressure control load sense systems proved to be better than fixed displacement pump systems, or variable flow pumps without pressure control load sense systems, or pressure control load sense systems without variable flow pump systems. However, even when using variable flow pumps with pressure control load sense systems, energy savings are still not high enough and hydraulic system utilization of energy is very poor [42]. Energy losses in hydraulic systems are due to several reasons including excess flow or pressure that is not needed, overrunning loads, and using a single pump to control multiple functions of a machine where it has to supply enough pressure to the function demanding highest pressure even if the other functions don't need such a high pressure. Research has been done on enhancing hydraulic system controls for more efficient usage of energy. Usage of multi-pump system, i.e. a pump for each function or joint, was investigated though without experimental verification [29]. Most of the research focused on how to minimize energy consumption by reducing the requirement to supply oil from the pump when it can be avoided.

Wieber used an optimal control mathematical description to analyze an electro-hydraulic servo system [89]. Optimal control strategy that can save energy in a hydraulic circuit was investigated by Punyapas and Book [69]. His circuit employed a conventional four way servo valve and a two way valve for regenerative flow to control a hydraulic cylinder. A very similar configuration was suggested again by Garnjost who also suggested other configurations that achieve regeneration flow for energy saving purposes [28]. Punyapas created a nonlinear model for the circuit and came up with an objective function that penalized steady state errors and energy consumption. He considered regenerative flow between the two cylinder chambers in his design to save energy. He argued that his solution of a bang-singular-bang input was a local minimum that is "very close" to the global minimum, and that it achieved a 30 % reduction in energy consumption.

Research also has been done on storing energy for later use. Excess flow in the system at high or low pressure can be stored in an accumulator, instead of dumping it in the tank. This excess energy can be used when needed instead of consuming pump energy. Liang

and Virvalo investigated a system with an accumulator and a balance cylinder to drive one of the joints of a mobile crane equipped with a hydraulic load sensing system [41]. They showed that during a period of operation involving overrunning load, instead of dissipating hydraulic energy as heat, it can be stored in an accumulator for later use. The excess flow in the system or the fluid stored directly in an accumulator or it can also be used to put energy back in the prime over. For example, the excess flow can be used to switch the driving pump into motoring mode and thus used to pump fluid at high pressure into the accumulator [70, 71]. Hybrid cars and trucks that used a hydraulic propulsion system in addition to its conventional diesel propulsion system has been under study due to the energy efficiency potential that can be achieved in this field. Similar research has been done on using accumulators in hybrid city buses [83, 19]. Wu et al, developed power management schemes of such a hybrid hydraulic power train to optimized the energy usage using dynamic programming [91]. In addition to hybrid cars, the benefit of potential energy storage was studied in metal forming machines [57].

Brief literature review of switched dynamic systems and coupled actuator-beam mechanical systems are presented in chapters 6 and 7 respectively.

1.3 Summary of Independent Metering Advantages

Independent metering promises to be more efficient. Independent metering valve configuration is a two degree of freedom system, which means that in addition to controlling speed of the actuator, pressure in one of chambers can be controlled as well. This can be used to achieve higher efficiency. As mentioned above, spool valve manufacturing is customized to the specific application. This customization means a high cost of manufacturing. Through software changes, the four-valve independent metering package can be adapted to several hydraulic system applications and that reduces the cost of manufacturing.

1.3.1 Distributed Valve Assembly Configuration

Independent metering using four valves is appealing and promises much more energy savings than the conventional spool valve technology.

In current practice, spool valves, a valve per cylinder, are stacked together and put

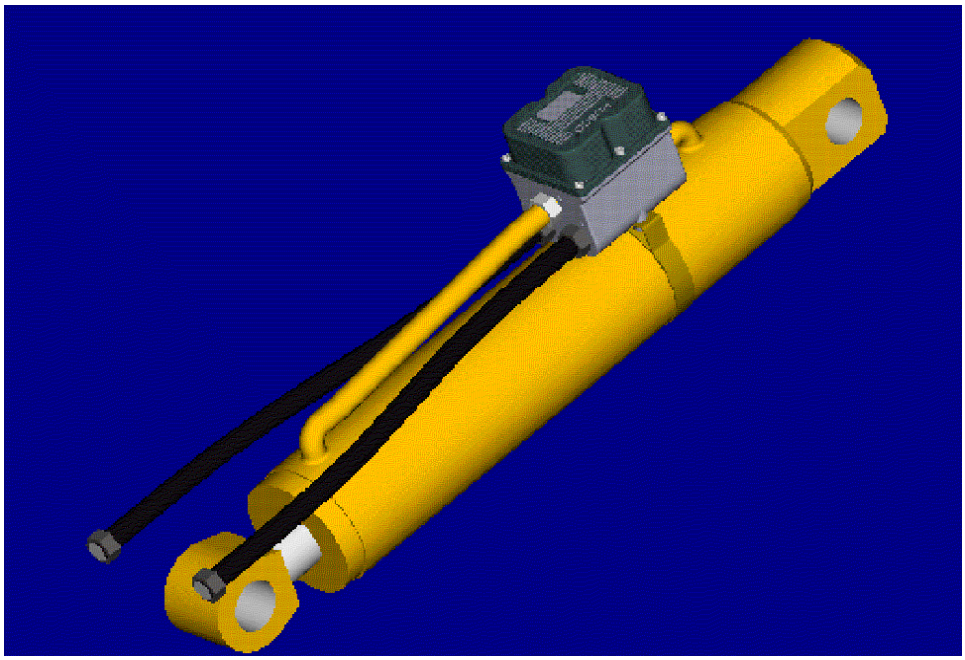

Figure 1.4: A four-valve assembly mounted directly on the cylinder it is controlling

under the operator cabin. Long pipes extend from that valve stack to the various cylinders. That constitutes major line losses as flow has to go all the way to the cylinder and back to through the valve to tank. It is obvious from the analysis above that regenerative flow uses minimum pump flow if any. Moreover, a four-valve assembly controlling one cylinder can be mounted directly on the cylinder it is controlling. This is shown in figure 1.4. Figure 1.5 shows the whole backhoe mechanism with the valve assemblies mounted directly on the cylinders. If any of these valve assemblies is operating in the regenerative modes, flow would be circulating within the assembly and does not have to go through long pipes and thus must save energy that would have been otherwise lost as hydraulic losses in the pipes.

1.3.2 Actuator Force Feedback System

As explained before, PCLS systems feedback only one chamber pressure and the pump is asked to add a margin to that pressure. The novel system being investigated in this research is essentially a force feedback system. Cylinder velocity, supply pressure, return pressure, and both chamber pressures are fed back to the controller and decisions are made based

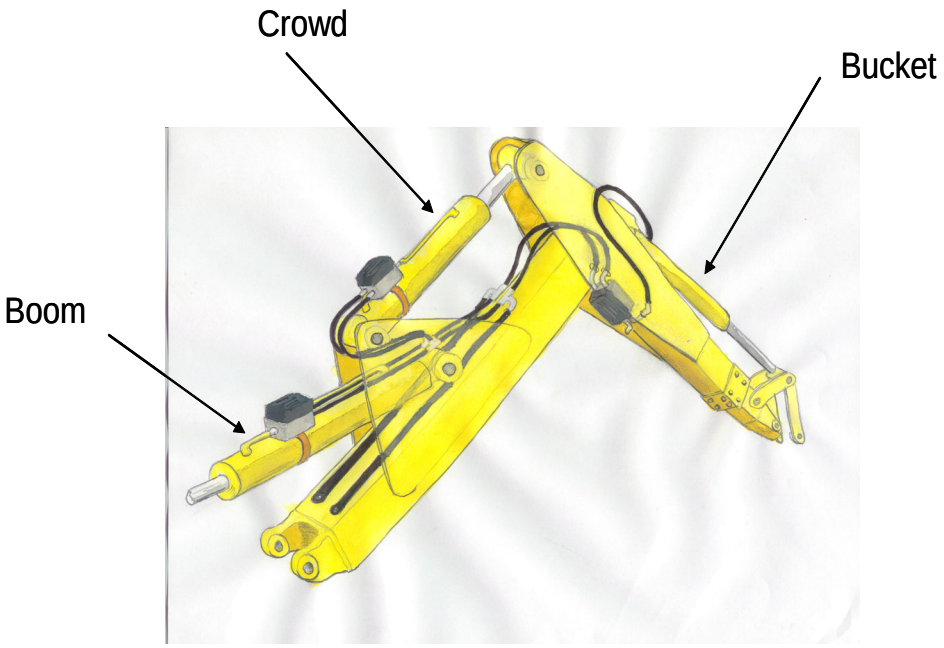

Figure 1.5: A backhoe mechanism showing the four-valve assembly mounted directly on the cylinders

upon all these inputs. If both chamber pressures are measured and the geometry of the cylinder is known, the force that the cylinder is subjected to is easily calculated, hence, it is called a force feedback system.

$$F_{hydraulic} = P_a A_a - P_b A_b \tag{1.1}$$

This force feedback characteristic makes the system capable of reacting faster and more accurately to disturbances and changes. The new control approach can be applied to spool valve controlled actuators. However, the full potential of the technology is achieved when using an independent metering valve configuration.

1.4 Goals of Present Research

The independent metering concept and microprocessor control have a huge potential of saving more energy than the concepts presented above because of the increased controllability of the system [35]. **This study is going to focus on use and control of a four-valve assembly for independent metering configuration and its potential of saving energy**.

Cavitation is a concern in hydraulic systems and studying anti-cavitation in this new system is one of the goals of this research.

This research aims at validating the hypothesis that this system is more energy efficient. The system under investigation is going to be compared to a conventional spool valve controlled PCLS system and the power savings is going to be quantified.

Some work has been done on a working metering mode selection controller but no optimization of mode selection was done. The metering modes that exist in the literature so far are discrete metering modes where two valves provide a flow path and switching to another mode involves closing a valve and opening another to provide for a different flow path. In this research, the optimal switching of these discrete metering modes is going to be studied. The problem is going to be investigated as a problem of optimal switching of a switched dynamics system. Switching from one mode to another changes the dynamics of the system. In addition to changes in system dynamics, the cost functional, which is energy consumption, also changes when mode switching occurs. Theoretical investigation of the general optimal control problem is first investigated and then the results are applied to the hydraulic system.

The short comings of these discrete modes are also explored in this research. For example, the effect of mode switching on vibrational behavior of a rotating beam actuated by a hydraulic cylinder controlled by the four-valve configuration is investigated. This configuration is encountered quite often in mobile hydraulic equipment. The basic mechanical system in this case is a continuous rotating beam that undergoes structural vibrations. The goal of this vibrational study is to investigate and quantify the effect of discrete mode switching on the beam vibration and coming up with a solution to the problem. This solution consists in the idea of continuously variable modes.

This research introduces, develops, and applys the concept of continuously variable modes that alleviate these short comings of discrete modes. The modeling of these modes is presented along with a technique for valve control. These modes can alleviate the vibration problem that occurs when switching between discrete modes. They also increase the force - speed capability of the system when compared to discrete modes. Experiments are done to

show that this idea of continuously variable modes achieve excellent velocity performance while saving energy.

Experiments in this research will be conducted on a full scale mobile hydraulic machines. This will help make the results directly related and applied to industrial application.

1.5 Summary of Chapters

The background for a four-valve independent metering configuration are presented in chapter 2. The five discrete modes are analyzed qualitatively and quantitatively. An overview of quasi-static modeling and control of four-valve independent metering configuration are also presented in this chapter. These results have been already developed in the literature and an overview of these results is given here for relevance to parts of the work done in this dissertation.

Since cavitation is a major concern in any hydraulic system, chapter 3 is focused on deriving the exact load that would cause cavitation to occur in an actuator controlled by the four-valve assembly. This is done for all five metering modes.

Independent metering promises intuitively to be more energy efficient than coupled metering. Chapter 4 validates this intuition mathematically. First it is shown that even if the independent metering four-valve assembly is used in a Pressure Compensated Load Sense (PCLS) type control strategy, power can be saved by virtue of having a two degrees of freedom system and being able to control the pressure in the return chamber in addition to the speed of the actuator. Then the power savings are quantified when using a actuator force feedback control method which takes full advantage of electronic control and independent metering configuration.

The complete mathematical model of a hydraulic cylinder controlled by a four-valve independent metering configuration is developed in chapter 5. First, the ***valve switching functions*** idea is introduced, which helps develop a unified mathematical representation for the dynamic model of the system despite having five different modes each with different dynamic characteristics. In order to develop the dynamic model of the whole system, a

simplified second order dynamic model of individual poppet valves is developed and experimentally validated first. Then the state space model of the system is presented. To experimentally validate the model, a telehandler machine is used to obtain experimental data to be compared with the model simulations. Since two of the telehandler functions, specifically its extender and boom functions, are used later in the research, both of these functions are simulated with the state space model and then the compared with experimental results.

Chapter 6 looks at mode switching. Specifically, it looks at the problem of switching between two modes as a problem of optimal switching of a switched dynamic system. This chapter develops the general theory for this problem first and then uses the dynamic model of chapter 5 to apply the theoretical results to the mode switching problem of the hydraulic system under investigation in this research. Not only the dynamics of the system changes upon mode switching, but the cost functional of the optimal control problem changes as well. The results of this chapter prove that mode switching bears resemblance to automotive automatic transmission gear shifting. This analogy leads to an idea for a real time algorithm for mode switching.

The effect of mode switching on vibrational behavior of a rotating beam actuated by a hydraulic cylinder controlled by the four-valve configuration is studied in chapter 7. This configuration is encountered quite often in mobile hydraulic equipment e.g. telehandlers, excavators and backhoes. The basic mechanical system in this case is a continuous rotating beam that undergoes structural vibrations due to mode switching in the driving hydraulic system. Since these beams are usually very rigid beams, only the rigid body mode and first vibration mode is looked at in this analysis. In order to make this analysis general to any beam, a non-dimensional analysis is pursued.

Chapter 8 introduces the concept of continuously variable modes. This chapter inspires their use and develops modeling equations for these modes. These modes promise to provide a smoother velocity performance and better energy efficiency when compared to using discrete modes and having to switch between them. These modes, however, are more involved from a controls point of view than the discrete modes. This chapter also develops

a valve control method for these continuously variable modes. It then proceeds to show that the force-speed capability of these new modes is better than the discrete modes and shows that a performance level can be achieved by these modes that cannot be obtained by the discrete modes. Also, it is shown in this chapter that the vibration problem of the previous chapter that results from discrete mode switching is assuaged when using these continuously variable modes.

In order to experimentally validate the concept of continuously variable modes, chapter 9 presents an experiment conducted on the crowd function of a mid size tractor loader backhoe. Four control techniques are tried. First technique involves using a conventional (or standard) mode that corresponds to using a spool valve with no regenerative modes possible. Then, two controllers allow for switching between regenerative modes and standard modes. Then, finally the continuously variable mode control is used. The crowd is given the same speed command in all four trials and the experiment conditions are the same. The experiment shows that that the continuously variable modes achieve superior velocity and energy consumption performance.

Finally, chapter 10 summarizes the research findings and draws conclusions. Some ideas for future research are also discussed.

CHAPTER II

BACKGROUND

2.1 General

As mentioned in the introduction, the hydraulic valve industry has seen the introduction of types of metering valves that can allow for independent metering. Four valves are needed to operate one cylinder. One valve connects one of the work ports of the cylinder to the supply line that contains pressurized oil. A second valve connects the other work port to the supply line. A third valve connects the first port to return line which leads to the tank. Finally a fourth valve is needed to connect the second port to the return line. Using this four valve configuration, while only two valves will be active for a given condition, allows for independent metering and also allows for energy regeneration, which has the potential for reducing the requirement on the pump and thus achieve highly valuable energy saving. Figure 2.1 is a schematic that shows the concept of using a four-valve configuration to achieve independent metering. This design provides for two degrees of freedom. This means more controllability of the machines can be achieved and thus more precise motion control. It also means that it is not necessary to design for a tight restriction on the return flow that is useful in overrunning load cases, but not needed otherwise. Depending on which pair of valves is selected to be opened, the cylinder can operate in different modes. Selection of the right mode can greatly reduce the energy required. **Keith Tabor and Joe Pfaff performed the mathematical analysis and valve control methods for this valve configuration and the discrete metering modes. This chapter gives an overview of these methods and results as a background because of its relevance to the rest of the dissertation**. The complete results and details are found in the references [78, 79, 66, 65, 80, 81].

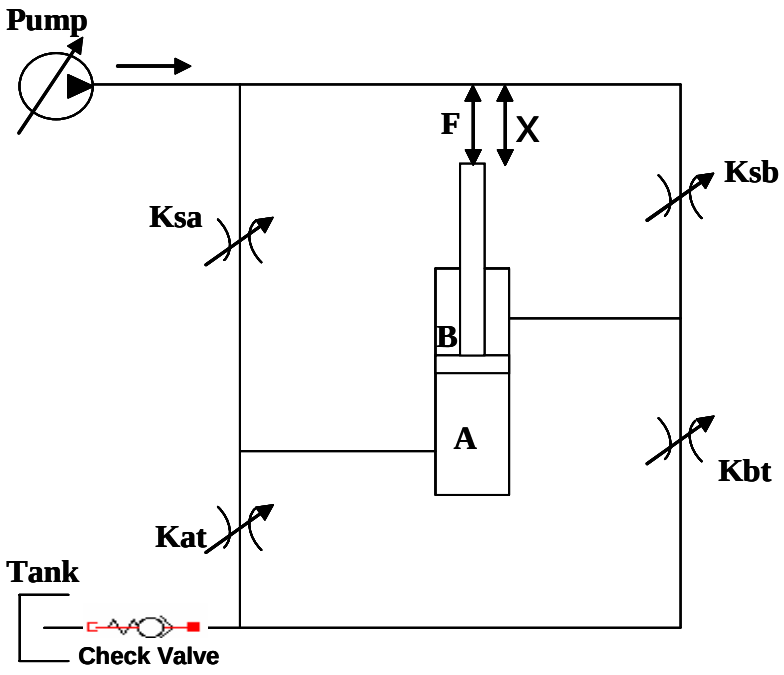

Figure 2.1: Four Valve Assembly to Achieve Independent Metering

2.2 Metering Modes

There are five metering modes that describe the operation of a hydraulic cylinder controlled by a four-valve assembly like the one shown in figure 2.1 [78]. A description of the operation of these modes is presented next.

2.2.1 Powered Extension Mode

The operation of this mode is not conceptually different from the operation of a cylinder controlled by a conventional proportional directional control valve. A schematic that describes this mode is shown in figure 2.2. Flow is supplied at high pressure from the pump through valve K_{sa} into head chamber A of the cylinder causing the piston to move (extend). This piston motion forces the flow out of rod chamber B through valve K_{bt} to the tank. The difference, however, is that in this four-valve configuration K_{sa} and K_{bt} can be controlled separately, while in a conventional proportional valve they cannot be controlled independently as explained in the introduction and thus flow to tank need not always be restricted.

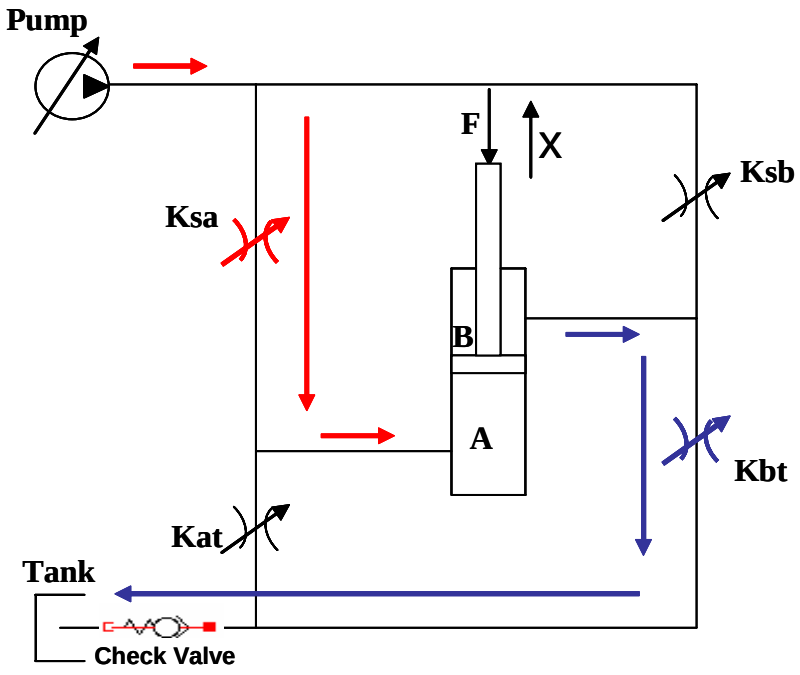

Figure 2.2: Powered Extension Mode

2.2.2 Powered Retraction Mode

Again, the operation of this mode is not conceptually different from the operation of a cylinder controlled by a conventional proportional directional control valve. A schematic that describes this mode is shown in figure 2.3 with arrows showing the essential directions of forces and velocities. Flow is supplied at high pressure from the pump through valve K_{sb} into rod chamber B of the cylinder causing the piston to move (retract). This piston motion forces the flow out of rod chamber A through valve K_{at} to the tank. Again, in this four-valve configuration K_{sb} and K_{at} can be controlled separately, while in a conventional proportional valve they cannot be controlled independently as explained in the introduction.

2.2.3 High Side Regeneration Extension Mode

This is one of the regenerative modes that can be achieved by the four-valve configuration and could not be achieved by a conventional proportional directional control valve. A schematic that describes this mode is shown in figure 2.4. Flow coming out of rod chamber

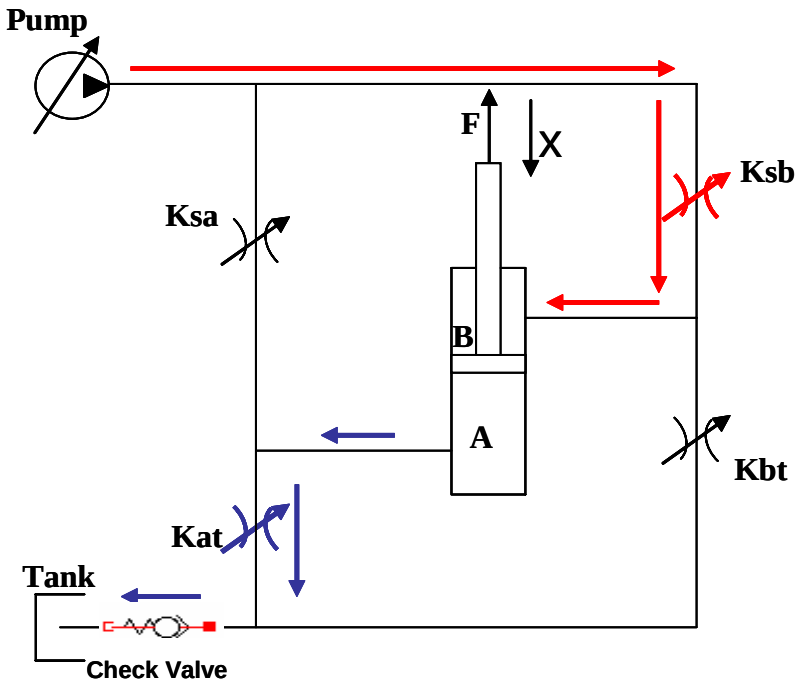

Figure 2.3: Powered Retraction Mode

B at high pressure does not go to tank through valve K_{bt}, but it circulates through valve K_{sb} and K_{sa} into head chamber A causing the piston to move (Extend). However, the flow coming out of chamber B is less than the flow needed in chamber A to achieve a certain speed because of the difference in areas ($A_a > A_b$). Flow out of either chamber is $Q = A \times \dot{x}$ and for a given velocity and with the difference in area ($Q_a > Q_b$). The remaining flow is supplied from the pump, but it is just enough to make up of the difference in flow while in powered extension mode all the flow is supplied from the pump. Thus, the high side regeneration extension mode has the potential to save energy. It is called high side because the flow goes through a path involving K_{sa} and K_{sb} that is on the pump side (high pressure side).

2.2.4 Low Side Regeneration Extension Mode

This is another one of the regenerative modes that can be achieved by the four-valve configuration and could not be achieved by a conventional proportional directional control valve. This mode is best suited for overrunning loads, which, for example, happens when lowering

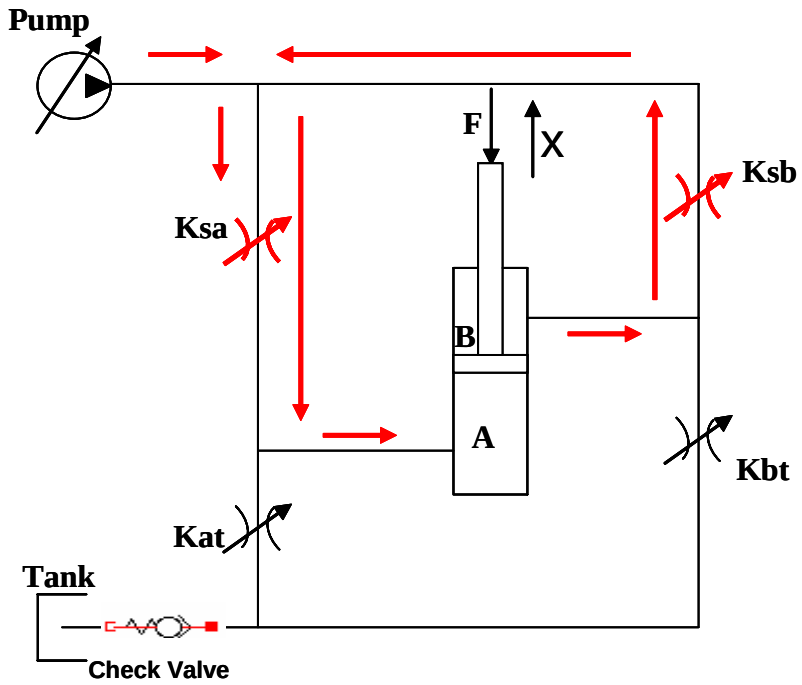

HSRE

Figure 2.4: High Side Regeneration Extension Mode

a load with gravity assistance. A schematic that describes this mode is shown in figure 2.5. Flow coming out of rod chamber B does not go to tank but it circulates through valve K_{bt} and K_{at} into head chamber A causing the piston to move (extend). However, the flow coming out of chamber B is less than the flow needed in chamber A to achieve a certain speed as explained above. The remaining flow can be supplied from the pump, but it is just enough to make up of the difference in flow and it is supplied at a low pressure. ***The remaining flow can also be supplied from the flow in the return line exhausted from other functions and will otherwise go to tank (cross-function regeneration)***. The check valve builds the pressure necessary for this operation. In conventional proportional directional control valves driven systems, the spools are designed such that the outlet restriction is used to control the flow so as to prevent the load from falling at uncontrollable speeds under gravity effects. However, in other operating conditions, such as lifting a load, this restriction is not needed yet it is inherent in the design of the spool valve. This causes energy loss that is unnecessary and this energy loss is avoided with this low side regeneration extension mode. Thus, the low side regeneration extension mode has

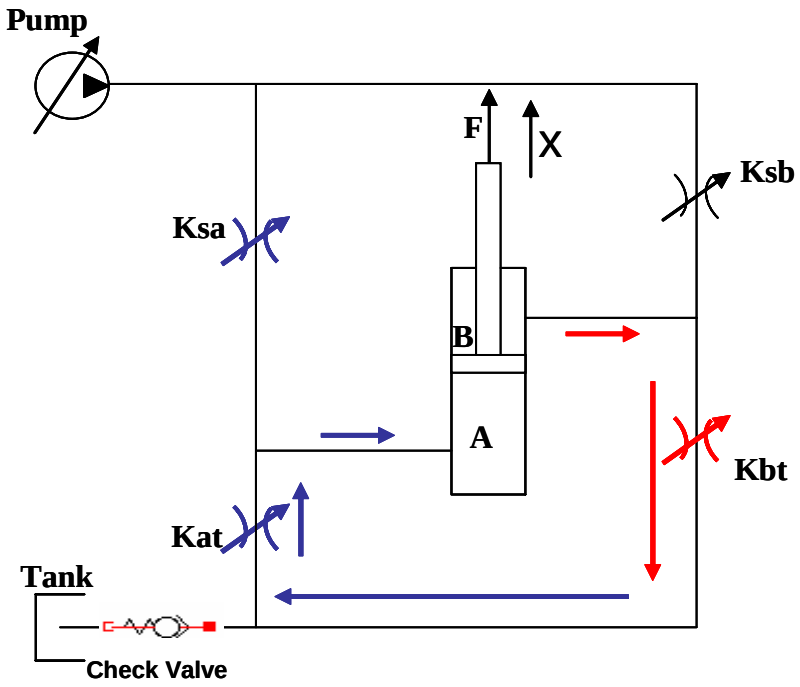

Figure 2.5: Low Side Regeneration Extension Mode

the potential to save energy. It is called low side because the flow goes through a path involving K_{bt} and K_{at} that is on the tank side (low pressure side).

2.2.5 Low Side Regeneration Retraction Mode

This is another one of the regenerative modes that can be achieved by the four-valve configuration and could not be achieved by a conventional proportional directional control valve. This mode is also best suited for overrunning loads, which, for example, happens when lowering a load with gravity assistance. A schematic that describes this mode is shown in figure 2.6. Flow coming out of head chamber A does not go to tank but it circulates through valve K_{at} and K_{bt} into rod chamber B causing the piston to move (retract). The flow coming out of chamber A is more than the flow needed in chamber B to achieve a certain speed as explained above. The extra flow goes to tank through the check valve. Thus, no pump flow is needed at all for this mode, which means a high potential for saving energy whenever this mode is used. It is called low side because the flow goes through a path involving K_{at} and K_{bt} that is on the tank side (low pressure side).

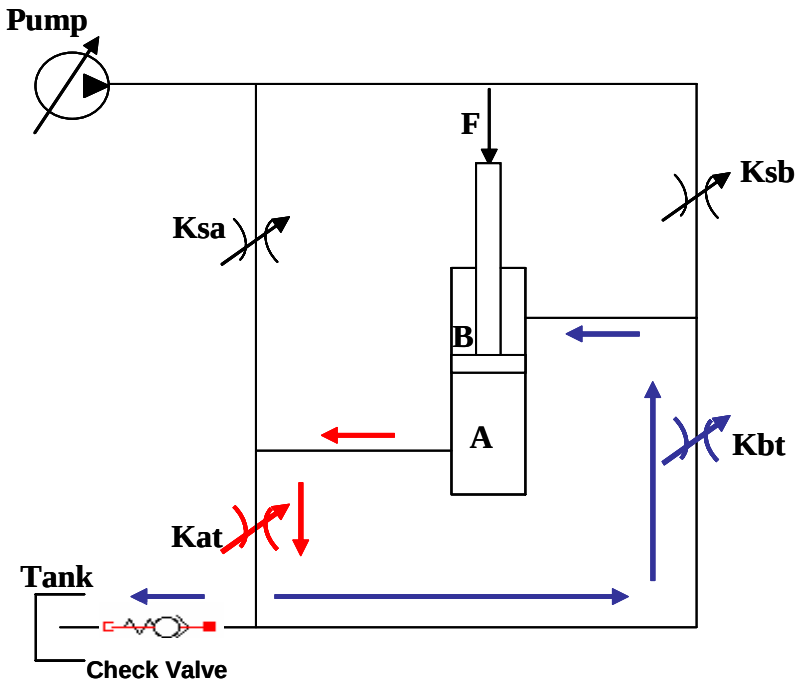

Figure 2.6: Low Side Regeneration Retraction Mode

2.3 Quasi-Static System Modeling

This section presents an overview of system modeling for the four-valve configuration. Note that from this point on, the parameters K_{sa}, K_{sb}, K_{at}, and K_{bt} will refer to the valves themselves or to the valve conductance coefficients.

2.3.1 Assumptions

In this modeling section and in the valve control section 2.4 a quasi-static system is assumed. That means that the plant dynamics are slowly changing and that the capacitances of the cylinder chambers and hydraulic lines are neglected.

2.3.2 Powered Extension Mode

Figure 2.7 shows a schematic of a system in Powered Extension Mode. Only the two active valves K_{sa} and K_{bt} are shown in this figure. This system is mathematically equivalent to a simplified system where you have an equivalent pressure source P_{eq} and an equivalent valve conductance K_{eq} as shown in the figure. This is proved next.

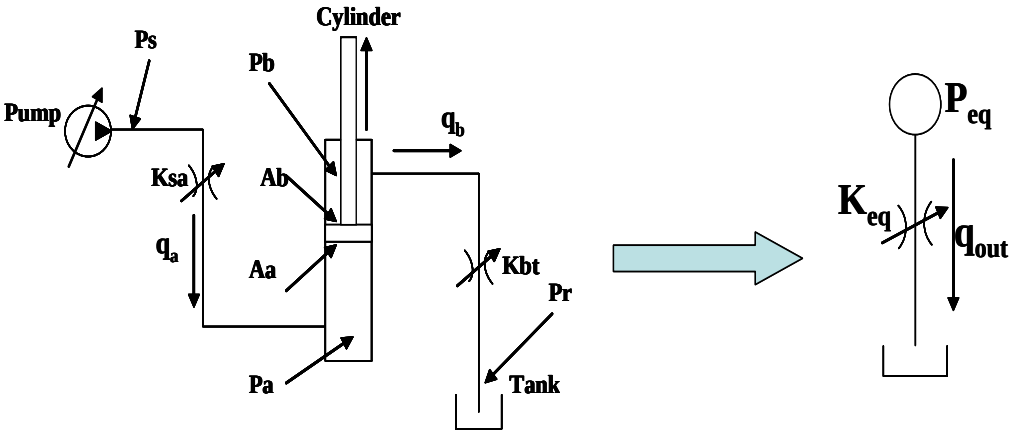

Figure 2.7: Powered Extension Mode-Mathematical Analysis & Equivalent System

The valve conductance coefficients K_{sa}, and K_{bt}, can be controlled separately by the controller and that is why this configuration provides for independent metering. Valves are represented as variable orifice restrictions [53]. Define:

$$\Delta P_1 \equiv P_s - P_a \tag{2.1}$$

$$\Delta P_2 \equiv P_b - P_r \tag{2.2}$$

Thus,

$$q_{in} = K_{sa}\sqrt{\Delta P_1} = K_{sa}\sqrt{P_s - P_a} = A_a\dot{x} \tag{2.3}$$

$$q_{out} = K_{bt}\sqrt{\Delta P_2} = K_{bt}\sqrt{P_b - P_r} = A_b\dot{x} \tag{2.4}$$

The following equation can be written:

$$P_sA_a - P_rA_b = \Delta P_1A_a + (P_aA_a - P_bA_b) + \Delta P_2A_b \tag{2.5}$$

Dividing through by A_b and calling the ratio $\frac{A_a}{A_b} = R$:

$$RP_s - P_r = R\Delta P_1 + (RP_a - P_b) + \Delta P_2 \tag{2.6}$$

$$(RP_s - P_r) + (-RP_a + P_b) = R\Delta P_1 + \Delta P_2 \tag{2.7}$$

From equations 2.3, 2.4, and 2.7 define:

$$P_{eq} = (RP_s - P_r) + (-RP_a + P_b) = R\frac{q_{in}^2}{K_{sa}^2} + \frac{q_{out}^2}{K_{bt}^2} \tag{2.8}$$

But from 2.3 and 2.4:

$$R = \frac{q_{in}}{q_{out}} \tag{2.9}$$

Thus, equation 2.8 can be written as:

$$P_{eq} = \frac{R^3 q_{out}^2}{K_{sa}^2} + \frac{q_{out}^2}{K_{bt}^2} = q_{out}^2 \left[\frac{R^3 K_{bt}^2 + K_{sa}^2}{K_{sa}^2 K_{bt}^2} \right] \tag{2.10}$$

$$\Rightarrow q_{out} = \frac{K_{sa} K_{bt}}{\sqrt{R^3 K_{bt}^2 + K_{sa}^2}} \sqrt{P_{eq}} = K_{eq} \sqrt{P_{eq}} \tag{2.11}$$

Where:

$$K_{eq} = \frac{K_{sa} K_{bt}}{\sqrt{R^3 K_{bt}^2 + K_{sa}^2}} \tag{2.12}$$

$$P_{eq} = (RP_s - P_r) + (-RP_a + P_b) \tag{2.13}$$

K_{eq} represents an equivalent conductance coefficient of the two valves opened in this mode, namely K_{sa} and K_{bt}. An infinite number of combinations of K_{sa} and K_{bt} can be used to achieve a certain K_{eq} which achieves a certain flow and thus a certain speed for the cylinder. In other words, the amount of flow through the valves and thus the speed of the cylinder depends upon how much we open both valves K_{sa} and K_{bt} given a specific load force, supply pressure, and return pressure. From equations 2.4 and 2.11 the following equation can be deduced [80, 81]:

$$K_{eq} = \frac{A_b \dot{x}}{\sqrt{P_{eq}}} = \frac{A_b \dot{x}}{\sqrt{(RP_s - P_r) + (-RP_a + P_b)}} \tag{2.14}$$

From equation 2.14 it is clear that if the velocity $\dot{x} = 0$ then $K_{eq} = 0$ implying that all valves are closed. The relationship between K_{eq} and both K_{sa} and K_{bt} will be discussed in section 2.4

2.3.3 Powered Retraction Mode

A similar analysis like the one done for the Powered Extension Mode can be done for the Powered Retraction Mode. To avoid repetition of a similar derivation, the results for K_{eq} and P_{eq} are directly given here:

$$K_{eq} = \frac{K_{sb} K_{at}}{\sqrt{K_{at}^2 + R^3 K_{sb}^2}} \tag{2.15}$$

$$P_{eq} = (P_s - RP_r) + (-P_b + RP_a) \tag{2.16}$$

Again, K_{eq} represents and equivalent conductance coefficient of the two valves open in this mode, namely K_{sb} and K_{at}. The following equation can be deduced:

$$K_{eq} = -\frac{A_b\dot{x}}{\sqrt{P_{eq}}} = -\frac{A_b\dot{x}}{\sqrt{(P_s - RP_r) + (-P_b + RP_a)}} \tag{2.17}$$

With $\dot{x} < 0$ since the cylinder is in retraction.

2.3.4 High Side Regeneration Extension Mode

Again, a similar analysis can lead to the following K_{eq} and P_{eq} equations for the High Side Regeneration Mode case

$$K_{eq} = \frac{K_{sa}K_{sb}}{\sqrt{R^3K_{sb}^2 + K_{sa}^2}} \tag{2.18}$$

$$P_{eq} = (R-1)P_s + (-RP_a + P_b) \tag{2.19}$$

K_{eq} represents an equivalent conductance coefficient of the two valves open in this mode, namely K_{sa} and K_{sb}. Also, this equation can be deduced:

$$K_{eq} = \frac{A_b\dot{x}}{\sqrt{P_{eq}}} = \frac{A_b\dot{x}}{\sqrt{(R-1)P_s + (-RP_a + P_b)}} \tag{2.20}$$

2.3.5 Low Side Regeneration Extension Mode

For this mode:

$$K_{eq} = \frac{K_{at}K_{bt}}{\sqrt{R^3K_{bt}^2 + K_{at}^2}} \tag{2.21}$$

$$P_{eq} = (R-1)P_r + (-RP_a + P_b) \tag{2.22}$$

K_{eq} represents and equivalent conductance coefficient of the two valves open in this mode, namely K_{at} and K_{bt}. The relationship between K_{eq} and the actuator speed $\dot{x}$ in this case is:

$$K_{eq} = \frac{A_b\dot{x}}{\sqrt{P_{eq}}} = \frac{A_b\dot{x}}{\sqrt{(R-1)P_r + (-RP_a + P_b)}} \tag{2.23}$$

2.3.6 Low Side Regeneration Retraction Mode

Finally for the fifth mode:

$$K_{eq} = \frac{K_{bt}K_{at}}{\sqrt{K_{at}^2 + R^3K_{bt}^2}} \tag{2.24}$$

$$P_{eq} = -(R-1)P_r + (-P_b + RP_a) \tag{2.25}$$

Again, K_{eq} represents and equivalent conductance coefficient of the two valves open in this mode, namely K_{at} and K_{bt}. K_{eq} is expressed in terms of $\dot{x}$ as follows:

$$K_{eq} = -\frac{A_b\dot{x}}{\sqrt{P_{eq}}} = \frac{A_b\dot{x}}{\sqrt{(-(R-1)P_r + (-P_b + RP_a)}} \tag{2.26}$$

With $\dot{x} < 0$ since the cylinder is in retraction.

2.4 Quasi-Static Valve Control

Valve control implies choosing individual valve openings that achieve a specific K_{eq} which translates into a specific actuator speed. Assuming that the commanded speed is $\dot{x}_{com}$, K_{eq} can be calculated for a given load and supply and return pressures according to the following formula:

$$K_{eq} = \frac{A_b\dot{x}_{com}}{\sqrt{P_{eq}}} \tag{2.27}$$

Although the expression for K_{eq} is slightly different for each mode depending upon which two valves are open for a given mode, a general expression for K_{eq} that is valid for all modes can be written as:

$$K_{eq} = \frac{K_a K_b}{\sqrt{K_a^2 + R^3 K_b^2}} \tag{2.28}$$

Where K_a can be either K_{sa} or K_{at}, which is either the valve that connects the *head* chamber to the supply line or the valve that connects the *head* chamber to the return line depending on the mode. K_b can be either K_{sb} or K_{bt}, which is either the valve that connects the *rod* chamber to the supply line or the valve that connects the *rod* chamber to the return line depending on the mode.

A $3D$ surface plot for K_{eq} versus variations in K_a and K_b obtained from equation 2.28 for a typical value of $R = \frac{A_a}{A_b} = 1.3405$ is shown in figure 2.8. Figure 2.9 shows the contour plot obtained from figure 2.8. It shows that an infinite number of combinations of K_a and K_b can be used to achieve a specific K_{eq}, which corresponds to a given cylinder speed. Each curve in figure 2.9 corresponds to a certain value of K_{eq}. This section is concerned with choosing the best individual valve openings out of the infinite possible combinations.

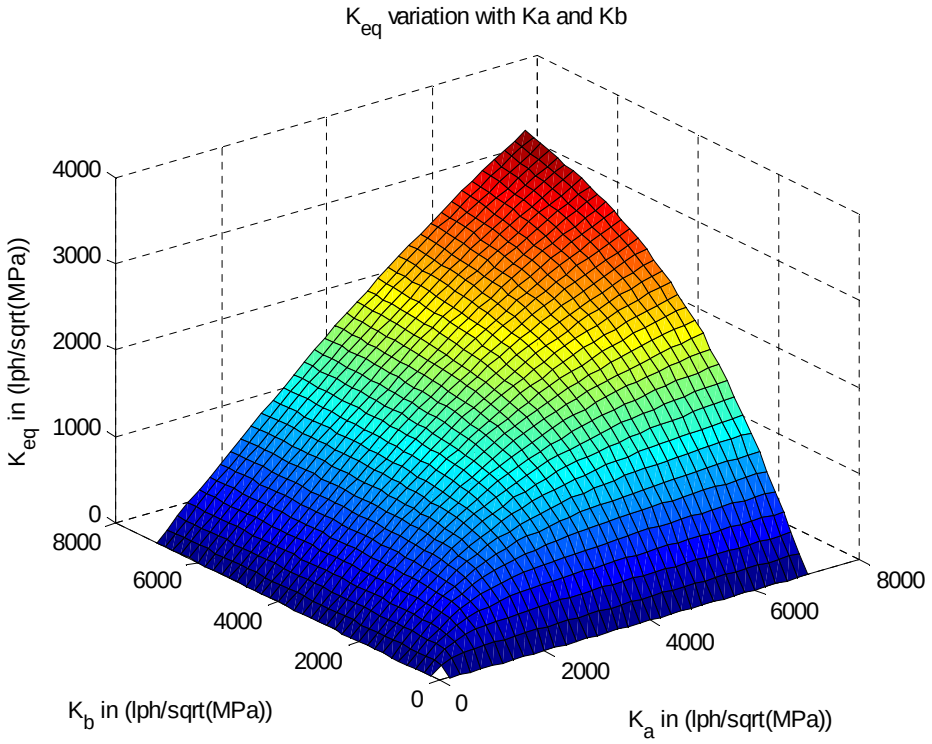

Figure 2.8: 3D surface showing variations of K_{eq} with K_a and K_b

2.4.1 Valve Sensitivity

A commanded current that is expected to achieve a certain valve opening, i.e. a certain Keq, may not result in the required opening at all operating pressures and temperatures. K_{eq} is proportional to velocity actuator velocity. Thus, it is imperative that for a certain K_{eq} represented by one the curves in figure 2.9, the controller should operate in the region of the curve that achieves the least sensitivity to valve inaccuracies. To measure the sensitivity of K_{eq} to errors in K_a and K_b, Tabor used the magnitude of the gradient of K_{eq} with respect to K_a and K_b [80, 81]:

$$|\nabla K_{eq}| = \sqrt{\frac{K_a^6 + R^6 K_b^6}{(K_a^2 + R^3 K_b^2)^3}} \tag{2.29}$$

Figure 2.10 shows a 3D surface of how the magnitude of the gradient of K_{eq} expressed in equation 2.29 varies with K_a and K_b. It can be observed from figure 2.29 that there is a valley in the surface where the gradient is minimized. This valley is clearer in figure 2.11,

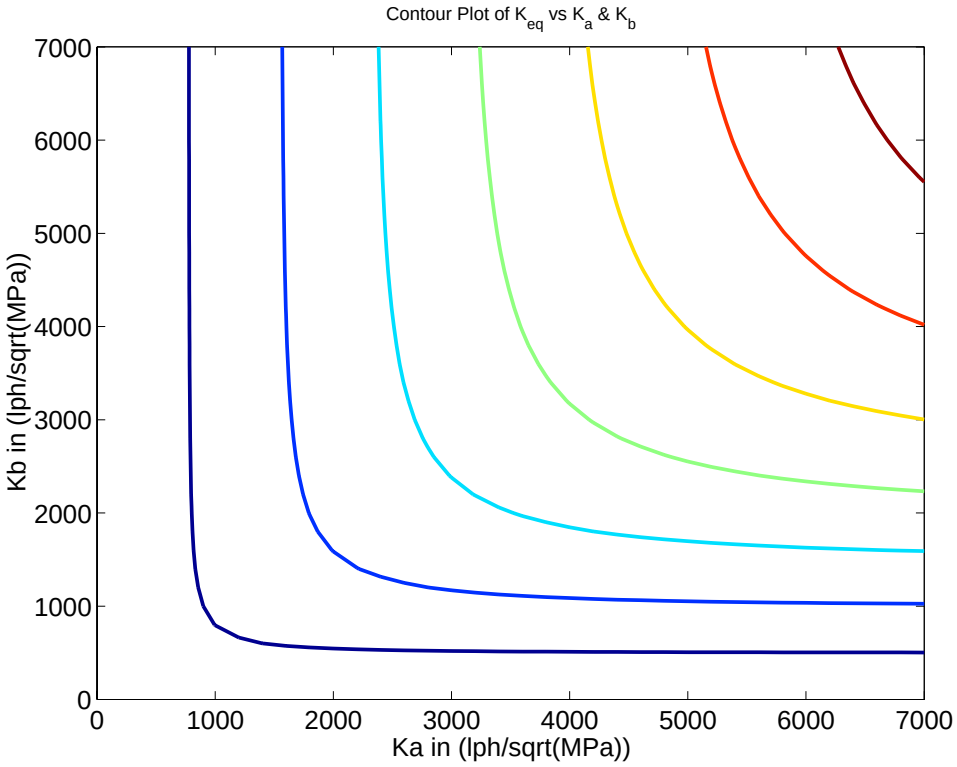

Figure 2.9: Contour Plot showing variations of K_{eq} with K_a and K_b

which shows the magnitude of the gradient of K_{eq} versus K_b for a given value of K_a. The bottom of the valley suggests a straight line relationship between K_a and K_b that minimizes the gradient [81]:

$$\mathbf{K_a} = \alpha_{\mathbf{opt}}\mathbf{K_b} \tag{2.30}$$

Where α_{opt} is found to be

$$\alpha_{\mathbf{opt}} = \mathbf{R^{3/4}} \tag{2.31}$$

Thus, the optimal combination for K_a and K_b that minimizes the valve sensitivity to errors lie along a line where $K_a = \alpha_{opt}K_b = R^{3/4}K_b$. Figure 2.12 show contour plot like figure 2.9 for $R = 1.5$ with the optimal line imposed on it.

It can be observed that the optimal line is along the maximum spacing regions between the K_{eq} curves, which is intuitively correct. In these maximum spacing regions, an error in K_a or K_b does not result in as a significant error in K_{eq} as much as it would in other regions. In conclusion, choosing the K_a, K_b combination that achieves a certain K_{eq} to lie on that

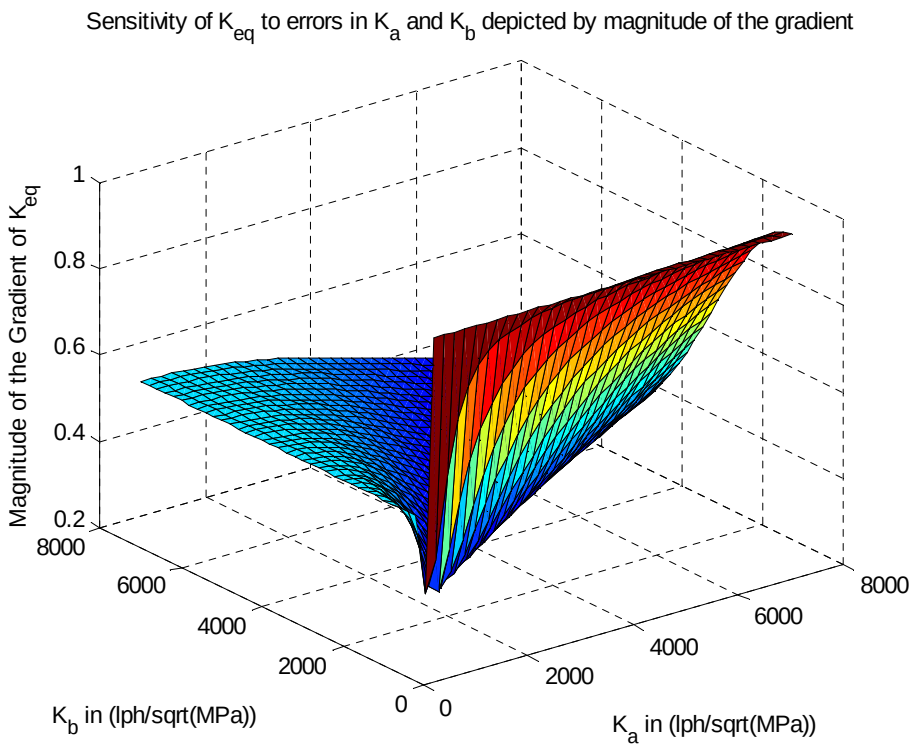

Figure 2.10: Sensitivity of K_{eq} to errors in K_a and K_b depicted by magnitude of the gradient

optimal line minimizes the sensitivity to valve errors and imperfections. However, there are other factors that have to be taken into consideration beside sensitivity, like maximum and minimum pressure limitations.

Note that from this point on in this document, this contour plot will be called ***valve control plot***. It will show K_{eq} curve(s) in addition to control and physical limitations as explained in the following sections.

2.4.2 Physical Valve Limitations

There is a limitation on how much the valve can be physically opened. Figure 2.13 shows how these physical design limitations are interpreted on the valve control plot. The figure shows an arbitrary K_{eq} curve and a vertical line representing the maximum inlet valve opening by the value Kin_{max} and a horizontal line representing the maximum outlet valve opening by the value $Kout_{max}$. These lines represent physical constraints on the valve control plot. The controller cannot choose inlet valve opening Kin to the right of Kin_{max}

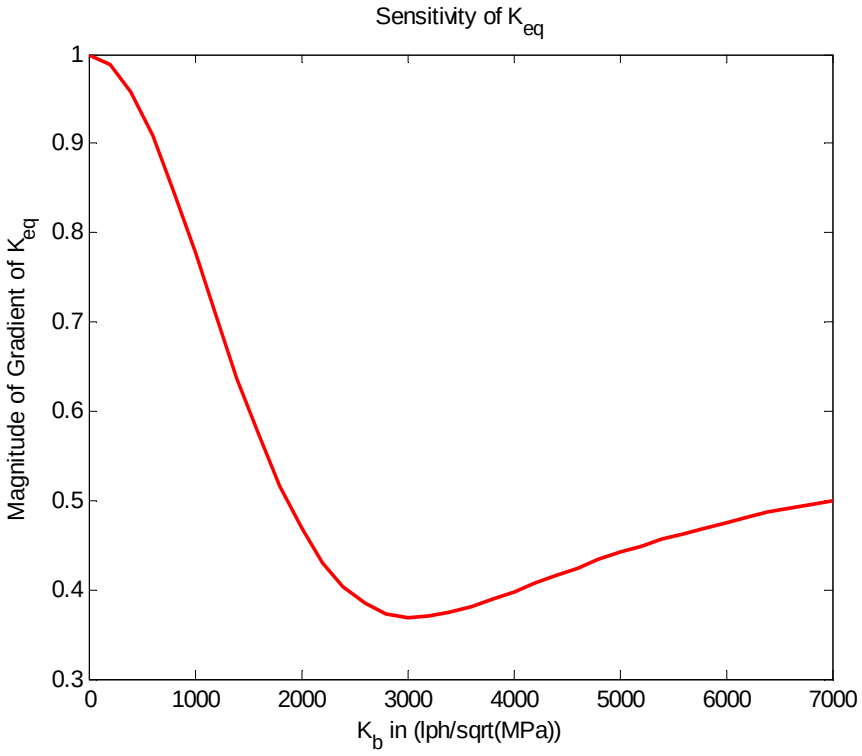

Figure 2.11: Magnitude of the gradient of K_{eq} versus K_b for a given K_a

or outlet valve opening $Kout$ above $Kout_{max}$. Note that Kin and $Kout$ were used here instead of K_a and K_b for generality. K_a can be Kin or $Kout$ depending on the metering mode and the same is true for K_b. Using Kin and $Kout$ makes this analysis more general.

2.4.3 Workport Pressure Control

Achieving required velocity with the least sensitivity to valve error is desirable. However, limitations on workport pressures are also very important. This four-valve independent metering system is a two degrees of freedom system as mentioned before, and the extra degree of freedom can be used to control pressure in one of the chambers. In many circumstances workport pressures should not decrease under a certain threshold pressure otherwise ***cavitation*** will occur. When the load the actuator is pushing (or pulling) causes one of the cylinder chambers to expand at a rate higher than the rate it is being filled with oil, cavitation occurs. When cavitation occurs, control algorithms do not apply anymore. In order to preserve controllability of the actuator, cavitation should be prevented. **A cavitation**

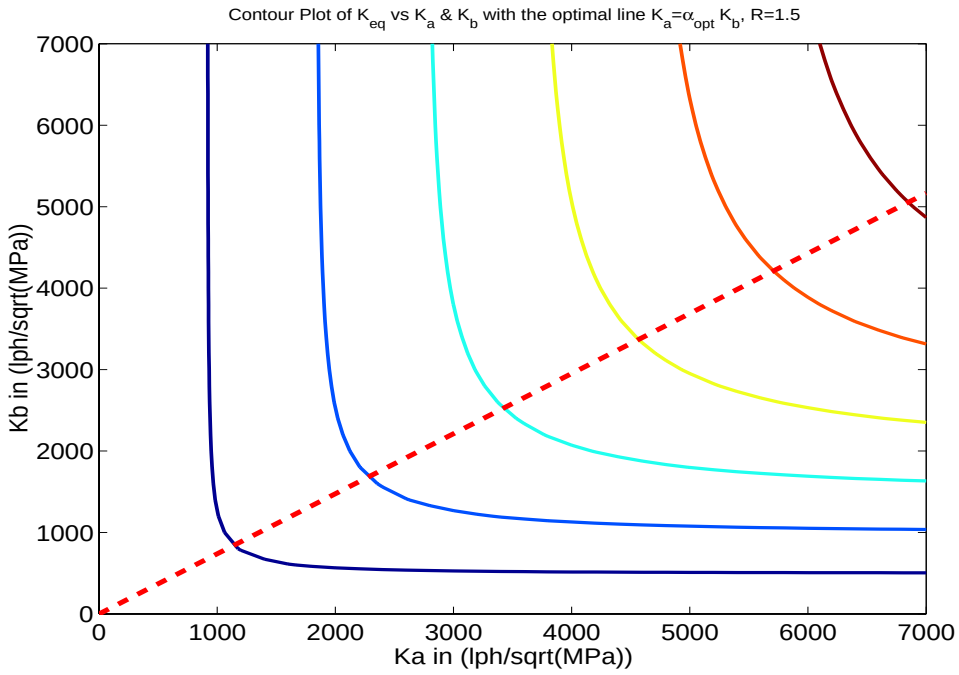

Figure 2.12: **Contour Plot of K_{eq} vs K_a and K_b with the optimal line $K_a = \alpha_{opt} K_b$, $R = 1.5$**

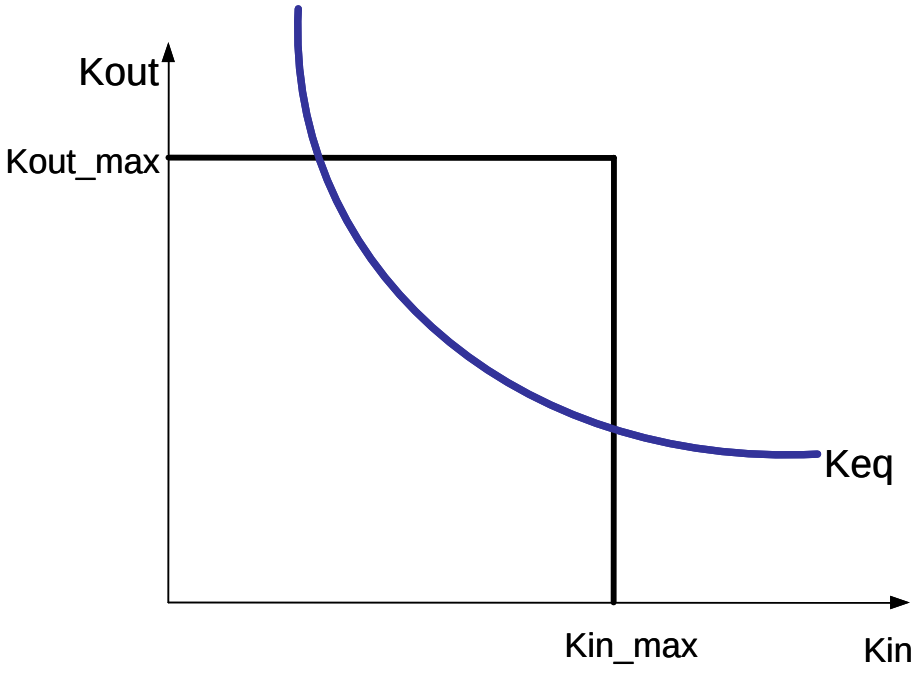

Figure 2.13: **Maximum and minimum valve openings as constraints on valve control plot**

prevention algorithm that determines the exact valve ratio that would cause cavitation for a given load is detailed in chapter 3.

On the other hand, workport pressures should not increase beyond a certain threshold due to design limitations of system piping and the different system components strength. If that pressure is exceeded damage of hydraulic circuitry can occur. Both of these limitations, i.e. minimum and maximum pressures, can be defined for head chamber or rod chamber or both. **In other circumstances, it may be desired to command the outlet pressure to be a particular pressure to save energy as will be explained in chapter 4**. A threshold pressure defined for head chamber will be called P_{tha}, and a threshold pressure defined for rod chamber will be called P_{thb}.

As in the case of physical valve limitations described in section 2.4.2, these threshold pressures can be represented by vertical and horizontal lines on the valve control plot. The general equations governing this relationship between threshold pressures and K_{in} or K_{out} are:

$$Kin_{th} = \frac{q_{in}}{\sqrt{\Delta P_{in}}} \tag{2.32}$$

$$Kout_{th} = \frac{q_{out}}{\sqrt{\Delta P_{out}}} \tag{2.33}$$

The specifics of these two equations differ according to the metering mode as will be detailed next.

2.4.3.1 Inlet Chamber Pressure Control

Equation 2.32 can be written for the different modes. In this section Powered Extension mode is going to be used as an illustrative example. More details can be found in reference [79]. For Powered Extension Mode:

$$Kin_{th} = Ksa_{th} = \frac{|\dot{x}|\, A_a}{\sqrt{P_s - P_{tha}}} \tag{2.34}$$

This threshold pressure can be a minimum inlet pressure and thus the inlet valve opening should be greater than Kin_{th} as shown in figure 2.14 in order to prevent cavitation. On the other hand, the threshold pressure can be a maximum inlet pressure that should not

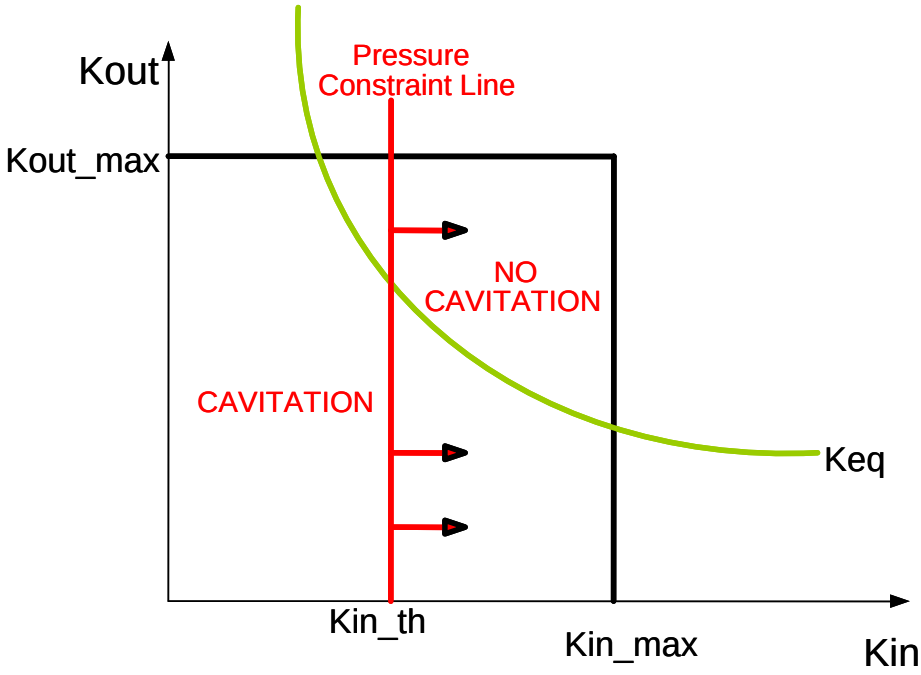

Figure 2.14: Minimum inlet valve opening representing a minimum pressure as a cavitation prevention constraint on valve control plot

be exceeded as a design limit and thus the inlet valve opening should be less than Kin_{th} as shown in figure 2.15. This can be understood by observing that as the inlet valve opening is increased then less pressure drop occurs across the valve and thus the inlet chamber pressure is higher. If the inlet valve opening is decreased then more pressure drop occurs across it and the inlet chamber pressure decreases.

2.4.3.2 Outlet Chamber Pressure Control

Again Powered Extension Mode is used as an illustrative example.

$$Kout_{th} = Kbt_{th} = \frac{|\dot{x}|\, A_b}{\sqrt{P_{thb} - P_r}} \tag{2.35}$$

Usually the outlet chamber is connected to tank directly or through check valve with a small cracking pressure. Thus, the minimum pressure in the outlet chamber is not very critical. Maximum pressure is more critical. The threshold pressure in this case is a maximum outlet pressure that should not be exceeded as a design limit and thus the outlet valve opening should be greater than $Kout_{th}$ as shown in figure 2.16. This can be understood by observing that as the outlet valve opening is increased then less pressure drop occurs across

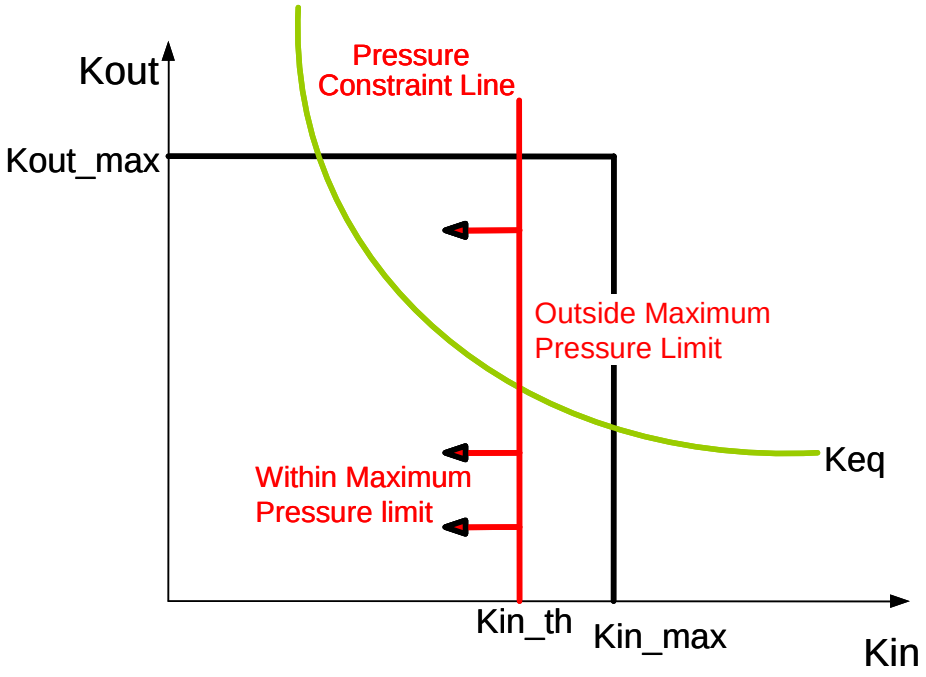

Figure 2.15: Maximum inlet valve opening representing a maximum pressure as a design limit constraint on valve control plot

the valve, i.e. the pressure in the outlet chamber does not build up very high above the return pressure.

2.4.4 Summary of Valve Control

A commanded current that is expected to achieve a particular valve opening, i.e. a certain Keq, may not result in the required opening at all operating pressures and temperatures. K_{eq} is proportional to actuator velocity. Thus, it is imperative that for a certain K_{eq} represented by one the curves in figure 2.9, the controller should operate in the region of the curve that achieves the least sensitivity to valve inaccuracies.

Furthermore, there are usually minimum pressure limitations on the actuator (cylinder) chambers to prevent cavitation, and a maximum pressure limitation that the system can handle before relief valves are opened to protect the system from high pressures. These pressure limitations appear as vertical and horizontal lines on the plot in figure 2.9 that limit the range of K_a and Kb that can be chosen. To ensure controllability, these limitations need to be taken into consideration when calculating individual valve openings [78, 79].

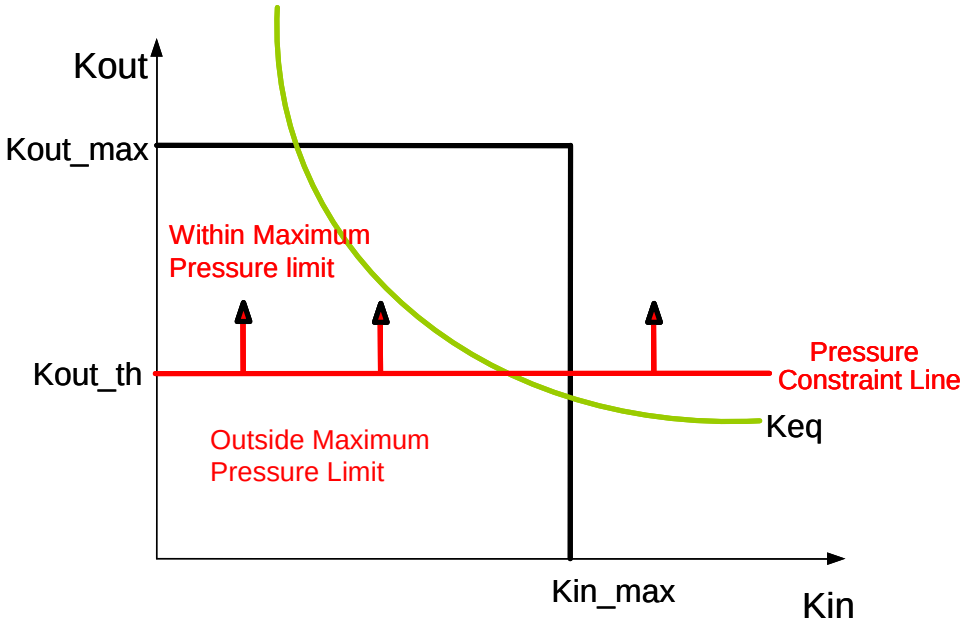

Figure 2.16: Maximum outlet valve opening representing a maximum pressure as a design limit constraint on valve control plot

With this valve control system it is possible to control the velocity of the hydraulic actuator while limiting pressure in both chambers. The final operating point on the valve control plot should take into consideration physical limitations of the valve, workport pressure limitations, achieving the commanded actuator speed, and valve sensitivity to errors. These considerations should be prioritized. For example, priority in operating the valves is given to physically possible valve openings, limiting the pressure in either chambers to prevent cavitation and to prevent pressure from increasing beyond a design limit, achieving the required speed of the actuator, and finally operating on the optimum line that achieves minimum sensitivity to valve errors [81].

2.5 Supply Pressure Set-Point

Based on the load that the actuator has to move and the speed required, a particular pump supply pressure is needed. This section presents equations for the supply pressure needed for the different modes, which is called the Supply Pressure Set Point, or the pressure that the pump needs to supply to move the load at the required speed.

2.5.1 Powered Extension Mode

Equation 2.14 can be easily manipulated to obtain and expression for P_s that the pump needs to supply for an actuator operating in Powered Extension mode [78, 80]

$$Ps_{set-point1} = \frac{\dot{x}^2 A_b^2}{RK_{eq}^2} + \frac{(RP_a - P_b)}{R} + \frac{P_r}{R} \tag{2.36}$$

EHPV valves need a minimum pressure ΔP_{min} across them for optimum performance. $Ps_{set-point}$ needs to supply this minimum pressure across the valves even if the velocity requirements do not demand such a $Ps_{set-point}$. Figure 2.17 shows a schematic to clarify this concept. Peq_{min} and $Ps_{set-point2}$ can be deduced from equation 2.13

$$Peq_{min} = (R+1)\Delta P_{min} \tag{2.37}$$

$$Ps_{set-point2} = \frac{Peq_{min}}{R} + \frac{(RP_a - P_b)}{R} + \frac{P_r}{R} \tag{2.38}$$

$$Ps_{set-point} = max(Ps_{set-point1}, Ps_{set-point2}) \tag{2.39}$$

Similar analysis can be done for the other five modes and the final results are presented next.

2.5.2 Powered Retraction Mode

$$Ps_{set-point1} = \frac{\dot{x}^2 A_b^2}{K_{eq}^2} - RP_a + P_b + RP_r \tag{2.40}$$

$$Ps_{set-point2} = Peq_{min} - RP_a + P_b + RP_r \tag{2.41}$$

2.5.3 High Side Regeneration Extension Mode

$$Ps_{set-point1} = \frac{\dot{x}^2 A_b^2}{(R-1)K_{eq}^2} + \frac{(RP_a - P_b)}{R-1} \tag{2.42}$$

$$Ps_{set-point2} = \frac{Peq_{min}}{R-1} + \frac{(RP_a - P_b)}{R-1} \tag{2.43}$$

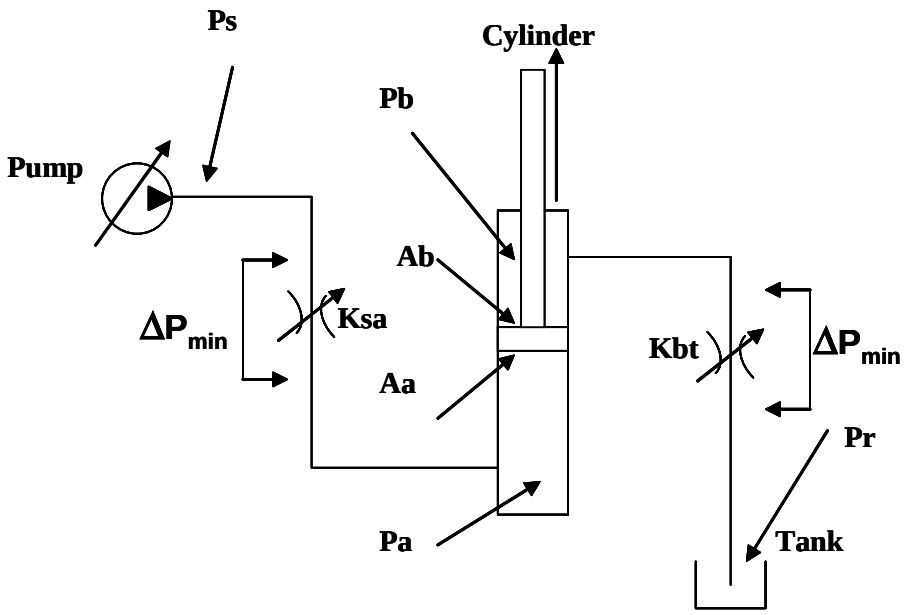

Figure 2.17: Peq_{min} **needed to maintain a** ΔP_{min} **across the valves in Powered Extension mode**

2.5.4 Low Side Regeneration Modes

For Low Side Regenerative modes, no supply pressure from the pump is needed but rather a minimum return pressure is needed to allow for flow recirculation. The minimum return set point pressure needed can be derived in the same way the supply pressure set point was derived

$$Pr_{set-point1} = \frac{\dot{x}^2 A_b^2}{(R-1)K_{eq}^2} + \frac{(RP_a - P_b)}{R-1} \tag{2.44}$$

$$Pr_{set-point2} = \frac{Peq_{min}}{R-1} + \frac{(RP_a - P_b)}{R-1} \tag{2.45}$$

$$Pr_{set-point} = max(Pr_{set-point1}, Pr_{set-point2}) \tag{2.46}$$

For low Side Regeneration Retraction mode return pressure P_r is set to the minimum value.

If the system has a multiple actuators, these calculations are done for the different actuators depending on the metering modes and the highest required $Ps_{set-point}$ amongst all actuators is determined and this becomes the System $Ps_{set-point}$ that the pump needs to supply.

CHAPTER III

ANTI CAVIATION ANALYSIS

3.1 Anti-cavitation Algorithm

As explained in chapter 2 in many circumstances workport pressures should not decrease under a certain threshold pressure or ***cavitation*** will occur. When the load the actuator is pushing (or pulling) causes one of the cylinder chambers to expand at a rate higher than the rate it is being filled with oil, a negative or zero pressure occurs in the inlet chamber. This causes cavitation. When cavitation occurs, control algorithms do not apply anymore. In order to preserve controllability of the actuator, cavitation should be prevented.

It has been explained in section 2.4.3 and in reference [81] how cavitation can be prevented. A threshold pressure, which the pressure in the inlet chamber should not decrease below it, is fixedly chosen and is translated into a vertical line on the valve control plot. This section approaches the problem differently and focuses on the critical load that would cause cavitation. The load that would cause cavitation could be calculated as a function of the valve openings ratio $\alpha = \frac{K_a}{K_b}$ depending on the metering mode.

$$F_{L,\,cav} = F(\alpha) \tag{3.1}$$

Thus, a particular load that can cause cavitation in specific conditions may not cause cavitation anymore if the valve ratio α is changed to a different value. This is the general idea of the suggested algorithm and next the mathematics will be detailed for the different metering modes.

3.2 Cavitation in Powered Extension Mode

Figure 3.1 shows a cylinder in Powered Extension mode subjected to an overrunning load. That is the cylinder is extending in the same direction the load is acting (a negative load case). This can happen for example when a load is moved vertically down by a cylinder

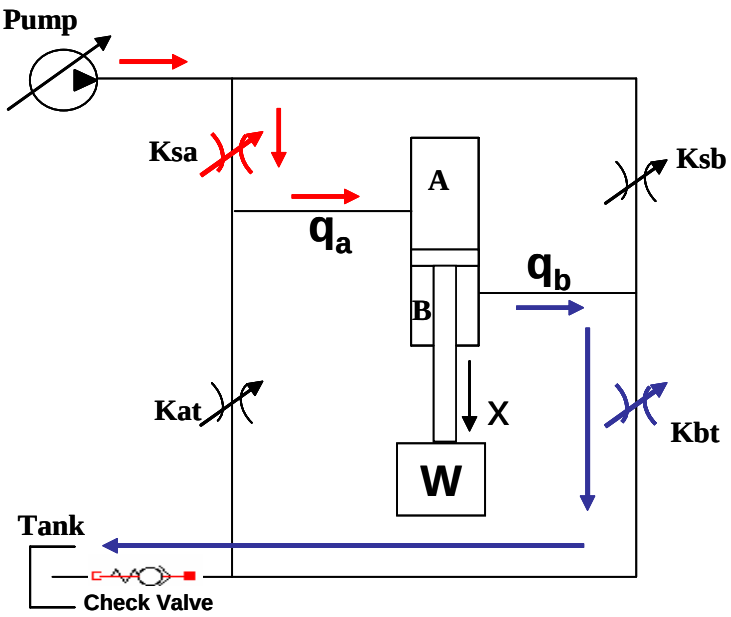

Figure 3.1: A cylinder in Powered Extension mode subjected to an overrunning load

while it is assisted by gravity. Hydraulic force can be expressed as:

$$F_{Hydraulic} = P_a A_a - P_b A_b = F_L - F_f \tag{3.2}$$

Where F_L is the load force and thus $F_L = W$. F_f is friction force in the cylinder. From equation 3.2, and noting that F_L is negative, pressure in chamber B can be written as

$$P_b = \frac{P_a A_a + F_L - F_f}{A_b} \tag{3.3}$$

Also:

$$q_a = A_a \dot{x} = K_{sa}\sqrt{\Delta P_1} = K_{sa}\sqrt{P_s - P_a} \tag{3.4}$$

$$q_b = A_b \dot{x} = K_{bt}\sqrt{\Delta P_2} = K_{bt}\sqrt{P_b - P_r} \tag{3.5}$$

Dividing equation 3.4 by 3.5 we obtain:

$$\frac{q_a}{q_b} = R = \alpha\sqrt{\frac{\Delta P_1}{\Delta P_2}} \tag{3.6}$$

Where $R = \frac{A_a}{A_b}$ and $\alpha = \frac{K_{sa}}{K_{bt}}$. Squaring equation 3.6 and rearranging we obtain

$$\Delta P_2 = \left(\frac{\alpha}{R}\right)^2 \Delta P_1 \tag{3.7}$$

$$\Rightarrow P_b - P_r = \left(\frac{\alpha}{R}\right)^2 (P_s - P_a) \tag{3.8}$$

$$\Rightarrow P_b = \left(\frac{\alpha}{R}\right)^2 (P_s - P_a) + P_r \tag{3.9}$$

Equating 3.9 and 3.3 we get:

$$\frac{P_a A_a + F_L - F_f}{A_b} = \left(\frac{\alpha}{R}\right)^2 (P_s - P_a) + P_r \tag{3.10}$$

Now solving for P_a

$$P_a A_a + F_L - F_f = P_r A_b + \left(\left(\frac{\alpha}{R}\right)^2 P_s - \left(\frac{\alpha}{R}\right)^2 P_a\right) A_b \tag{3.11}$$

$$\Rightarrow P_a \left[A_a + \left(\frac{\alpha}{R}\right)^2 A_b\right] = \left(\frac{\alpha}{R}\right)^2 A_b P_s - (F_L - F_f) + P_r A_b \tag{3.12}$$

$$P_a = \frac{(\frac{\alpha}{R})^2 A_b P_s - (F_L - F_f) + P_r A_b}{\left[A_a + (\frac{\alpha}{R})^2 A_b\right]} \tag{3.13}$$

Dividing numerator and denominator by A_b

$$\Rightarrow P_a = \frac{(\frac{\alpha}{R})^2 P_s - \frac{(F_L - F_f)}{A_b} + P_r}{\left[R + (\frac{\alpha}{R})^2\right]} \tag{3.14}$$

For cavitation to happen, P_a would have to be negative or zero. So, we put $P_a = 0$ in equation 3.14 and solve for F_L which is the load that would cause cavitation:

$$\left(\frac{\alpha}{R}\right)^2 A_b P_s + P_r A_b = \frac{F_L}{A_b} - \frac{F_f}{A_b} \tag{3.15}$$

$$\Rightarrow F_L = \left(\frac{\alpha}{R}\right)^2 A_b P_s + P_r A_b + F_f \tag{3.16}$$

For illustration, some numerical values are used from an actual tractor loader backhoe bucket cylinder can be used. If F_L, which would cause cavitation, is plotted as a function of α figure 3.2 is obtained with the following values used: $R = 1.6580$, $A_b = 4737\,mm^2$, $P_s = 20\,MPa$, $P_r = 0.7\,MPa$, and friction is neglected i.e. $F_f = 0$ or lumped in F_L. The dashed line on the plot is the line passing through $\alpha_{opt} = R^{3/4} = 1.4611$ and the corresponding Load is $F_L \approx 77kN$.

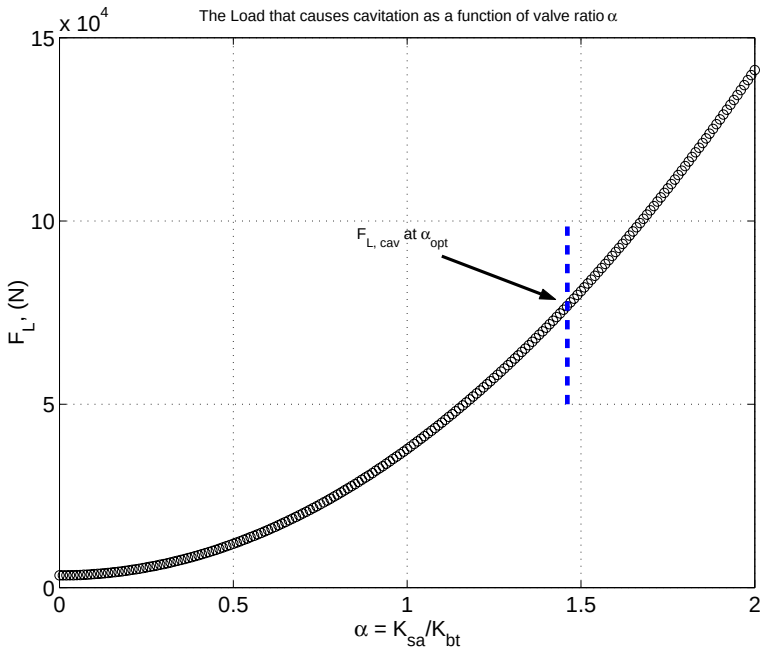

Figure 3.2: The Load F_L that causes cavitation as a function of valve ratio α for Powered Extension Mode

To explain how this can be used, it is observed that an electronic controller has access to the values of R, A_b, P_s, and P_r, while friction can be estimated as a function of pressures or it can be neglected. The hydraulic force in equation 3.2 can be calculated because the controller has access to work port pressures P_a and P_b, and thus F_L can be calculated. The valve openings ratio that would allow cavitation to happen at this load can be calculated by rearranging equation 3.16:

$$\alpha = R\sqrt{\frac{F_L - F_f - P_r A_b}{P_s A_b}} \tag{3.17}$$

Another α can be chosen by the controller to ***avoid cavitation***. By restricting the output valve K_{bt} and opening the input valve K_{sa}, higher loads are needed to cause cavitation as expected, but by virtue of this derivation the exact load that would cause cavitation can be calculated given the system parameters.

3.3 Cavitation in High Side Regeneration Extension Mode

Figure 3.3 shows a cylinder in High Side Regeneration Extension mode subjected to an overrunning load. Just as in the Powered Extension case, P_b can be expressed as:

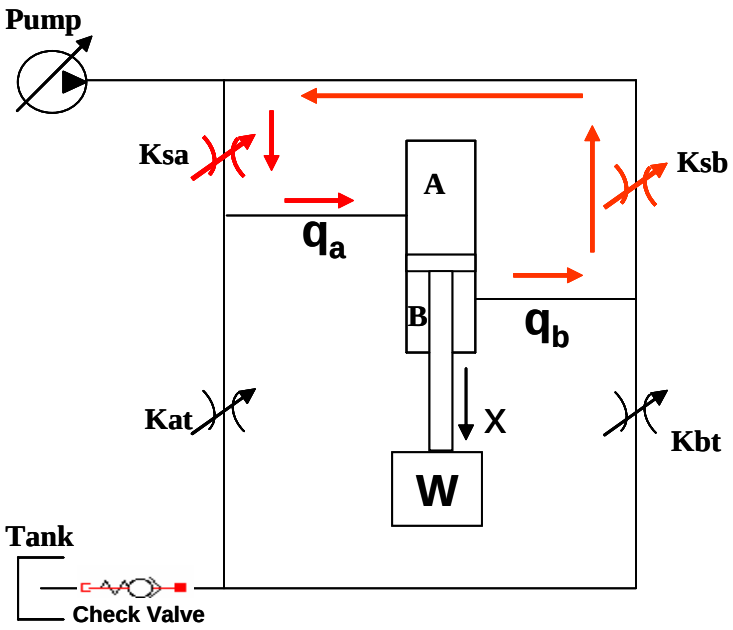

Figure 3.3: A cylinder in High Side Regeneration Extension mode subjected to an overrunning load

$$P_b = \frac{P_a A_a + F_L - F_f}{A_b} = RP_a + \frac{F_L - F_f}{A_b} \tag{3.18}$$

In this case, flow can be characterized with the following orifice equations:

$$q_a = A_a \dot{x} = K_{sa}\sqrt{\Delta P_1} = K_{sa}\sqrt{P_s - P_a} \tag{3.19}$$

$$q_b = A_b \dot{x} = K_{sb}\sqrt{\Delta P_2} = K_{bt}\sqrt{P_b - P_s} \tag{3.20}$$

Dividing equation 3.19 by 3.20 we obtain:

$$\frac{q_a}{q_b} = R = \alpha\sqrt{\frac{\Delta P_1}{\Delta P_2}} \tag{3.21}$$

Where $R = \frac{A_a}{A_b}$ and $\alpha = \frac{K_{sa}}{K_{sb}}$. Squaring equation 3.21 and rearranging we obtain

$$\Delta P_2 = \left(\frac{\alpha}{R}\right)^2 \Delta P_1 \tag{3.22}$$

$$\Rightarrow P_b = \left(\frac{\alpha}{R}\right)^2 (P_s - P_a) + P_s \tag{3.23}$$

Equating 3.23 and 3.18 we get:

$$RP_a + \frac{F_L - F_f}{A_b} = \left(\frac{\alpha}{R}\right)^2 (P_s - P_a) + P_s \tag{3.24}$$

Now we solve for P_a

$$P_a = \frac{[1 + (\frac{\alpha}{R})^2]P_s - \frac{F_L - F_f}{A_b}}{R + (\frac{\alpha}{R})^2} \tag{3.25}$$

For cavitation to happen, P_a would have to be negative or zero. So, we put $P_a = 0$ in equation 3.25 and solve for F_L which is the load that would cause cavitation:

$$\frac{F_L}{A_b} = [1 + (\frac{\alpha}{R})^2]P_s + \frac{F_f}{A_b} \tag{3.26}$$

$$\Rightarrow F_L = [1 + (\frac{\alpha}{R})^2]A_b P_s + F_f \tag{3.27}$$

Now, if F_L, which would cause cavitation, is plotted as a function of α we get figure 3.4 with the following values used: $R = 1.6580$, $A_b = 4737\,mm^2$, $P_s = 20\,MPa$, $P_r = 0.7\,MPa$, and friction is neglected i.e. $F_f = 0$ or lumped in F_L. Again, the dashed line on the plot is the line passing through α_{opt} and the corresponding Load is $F_L \approx 168kN$. It is noticed that a much higher load is needed to cause cavitation in High Side Regeneration Extension mode than Powered Extension Mode for a given ratio α.

3.4 Cavitation in Low Side Regeneration Extension Mode

Figure 3.5 shows a cylinder in Low Side Regeneration Extension mode subjected to an overrunning load. The anti-cavitation analysis for this mode uses just two valves K_{at} and K_{bt} and ignores the make up flow needed to compensate for piston area difference. This make up flow can theoretically be supplied at no pressure and consequently does not affect the cavitation pressure. Again, P_b can be expressed as:

$$P_b = RP_a + \frac{F_L - F_f}{A_b} \tag{3.28}$$

In this case, flow can be characterized with the following orifice equations:

$$q_a = A_a\dot{x} = K_{at}\sqrt{\Delta P_1} = K_{at}\sqrt{P_r - P_a} \tag{3.29}$$

$$q_b = A_b\dot{x} = K_{bt}\sqrt{\Delta P_2} = K_{bt}\sqrt{P_b - P_r} \tag{3.30}$$

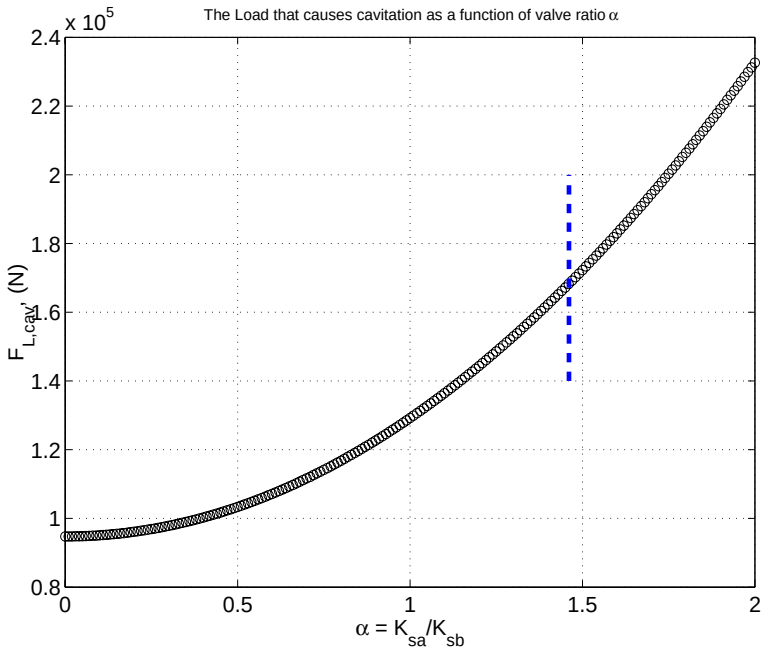

Figure 3.4: The Load F_L that causes cavitation as a function of valve ratio α for High Side Regeneration Extension Mode

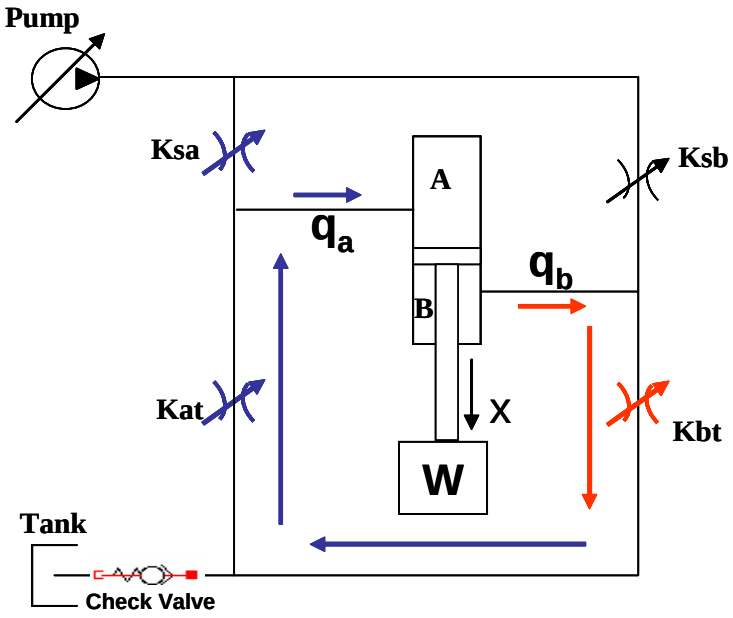

Figure 3.5: A cylinder in Low Side Regeneration Extension mode subjected to an overrunning load

Dividing equation 3.29 by 3.30 we obtain:

$$\frac{q_a}{q_b} = R = \alpha\sqrt{\frac{\Delta P_1}{\Delta P_2}} \tag{3.31}$$

Where $R = \frac{A_a}{A_b}$ and $\alpha = \frac{K_{at}}{K_{bt}}$. Squaring equation 3.21 and rearranging we obtain

$$\Delta P_2 = \left(\frac{\alpha}{R}\right)^2 \Delta P_1 \tag{3.32}$$

$$\Rightarrow P_b = \left(\frac{\alpha}{R}\right)^2 (P_r - P_a) + P_r \tag{3.33}$$

Equating 3.33 and 3.28 we get:

$$RP_a + \frac{F_L - F_f}{A_b} = \left(\frac{\alpha}{R}\right)^2 (P_r - P_a) + P_r \tag{3.34}$$

Now we solve for P_a

$$P_a = \frac{[1 + (\frac{\alpha}{R})^2]P_r - \frac{F_L - F_f}{A_b}}{R + (\frac{\alpha}{R})^2} \tag{3.35}$$

Again, for cavitation to happen, P_a would have to be negative or zero. So, we put $P_a = 0$ in equation 3.35 and solve for F_L which is the load that would cause cavitation:

$$\frac{F_L}{A_b} = [1 + (\frac{\alpha}{R})^2]P_r + \frac{F_f}{A_b} \tag{3.36}$$

$$\Rightarrow F_L = [1 + (\frac{\alpha}{R})^2]A_b P_r + F_f \tag{3.37}$$

Again, F_L, which would cause cavitation, is plotted as a function of α in figure 3.6 with the following values used: $R = 1.6580$, $A_b = 4737\,mm^2$, $P_r = 0.7\,MPa$, and friction is neglected i.e. $F_f = 0$ or lumped in F_L. Again, the dashed line on the plot is the line passing through α_{opt} and the corresponding Load is $F_L \approx 5900N$. It is observed that a much lower load can cause cavitation than in Powered Extension or in High Side Regeneration Extension modes for a given valve ratio α.

3.5 Cavitation in Powered Retraction Mode

Figure 3.7 shows a cylinder in Powered Retraction mode subjected to an overrunning load. From equation 3.2 P_a can be expressed as:

$$P_a = \frac{P_b}{R} + \frac{F_L - F_f}{A_a} \tag{3.38}$$

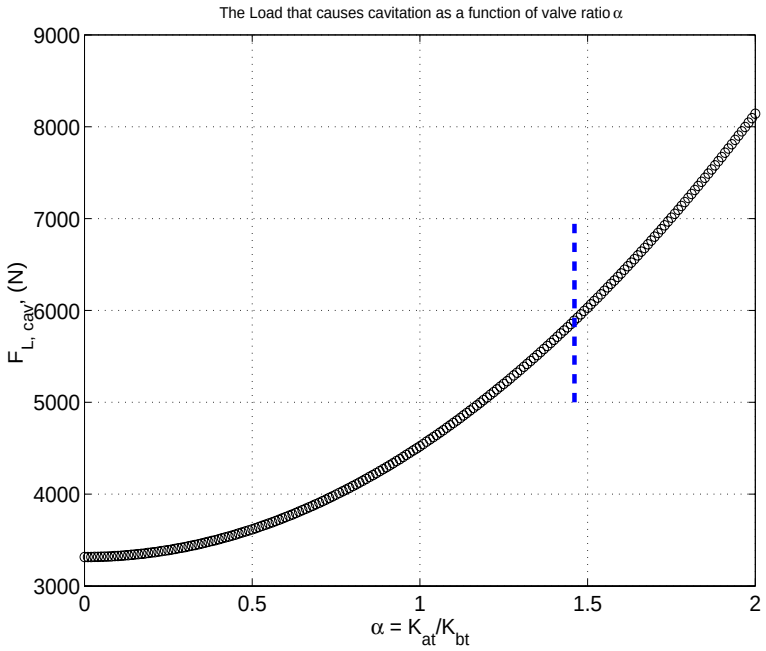

Figure 3.6: The Load F_L that causes cavitation as a function of valve ratio α for Low Side Regeneration Extension Mode

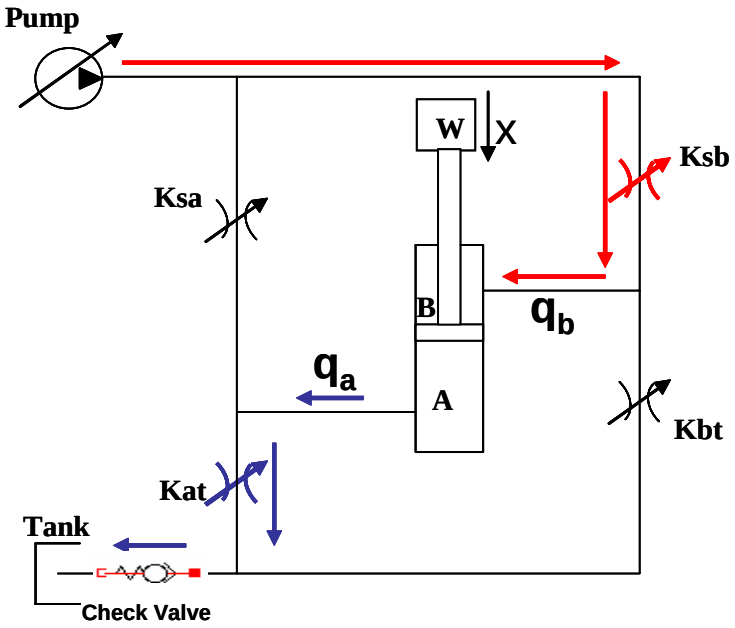

Figure 3.7: A cylinder in Powered Retraction mode subjected to an overrunning load

In this case, flow can be characterized with the following orifice equations:

$$q_a = A_a\dot{x} = K_{at}\sqrt{\Delta P_1} = K_{at}\sqrt{P_a - P_r} \tag{3.39}$$

$$q_b = A_b\dot{x} = K_{sb}\sqrt{\Delta P_2} = K_{sb}\sqrt{P_s - P_b} \tag{3.40}$$

Dividing equation 3.39 by 3.40 we obtain:

$$\frac{q_a}{q_b} = R = \alpha\sqrt{\frac{\Delta P_1}{\Delta P_2}} \tag{3.41}$$

Where $R = \frac{A_a}{A_b}$ and $\alpha = \frac{K_{at}}{K_{sb}}$. Squaring equation 3.41 and rearranging we obtain

$$\Delta P_1 = \left(\frac{R}{\alpha}\right)^2 \Delta P_2 \tag{3.42}$$

$$\Rightarrow P_a = \left(\frac{R}{\alpha}\right)^2 (P_s - P_b) + P_r \tag{3.43}$$

Equating 3.43 and 3.38 we get:

$$\frac{P_b}{R} + \frac{F_L - F_f}{A_a} = \left(\frac{R}{\alpha}\right)^2 (P_s - P_b) + P_r \tag{3.44}$$

Now we solve for P_b

$$P_b = \frac{(\frac{R}{\alpha})^2 P_s - \frac{F_L - F_f}{A_a} + P_r}{\frac{1}{R} + \frac{R}{\alpha}} \tag{3.45}$$

For cavitation to happen in Powered Retraction mode, P_b would have to be negative or zero. So, we put $P_b = 0$ in equation 3.45 and solve for F_L which is the load that would cause cavitation:

$$\frac{F_L}{A_a} = \frac{R}{\alpha})^2 P_s + P_r + \frac{F_f}{A_a} \tag{3.46}$$

$$\Rightarrow F_L = (\frac{\alpha}{R})^2 A_a P_s + A_a P_r + F_f \tag{3.47}$$

As in the previous three cases, the force F_L, which would cause cavitation, is plotted as a function of α in figure 3.8 with the following values used: $R = 1.6580$, $A_a = 7854\,mm^2$, $P_s = 20\,MPa$ $P_r = 0.7\,MPa$, and friction is neglected i.e. $F_f = 0$ or lumped in F_L. Again, the dashed line on the plot is the line passing through α_{opt} and the corresponding Load is $F_L \approx 210kN$. It can be noticed that a much larger load is necessary to cause cavitation than in the three extension modes for a given valve ratio α.

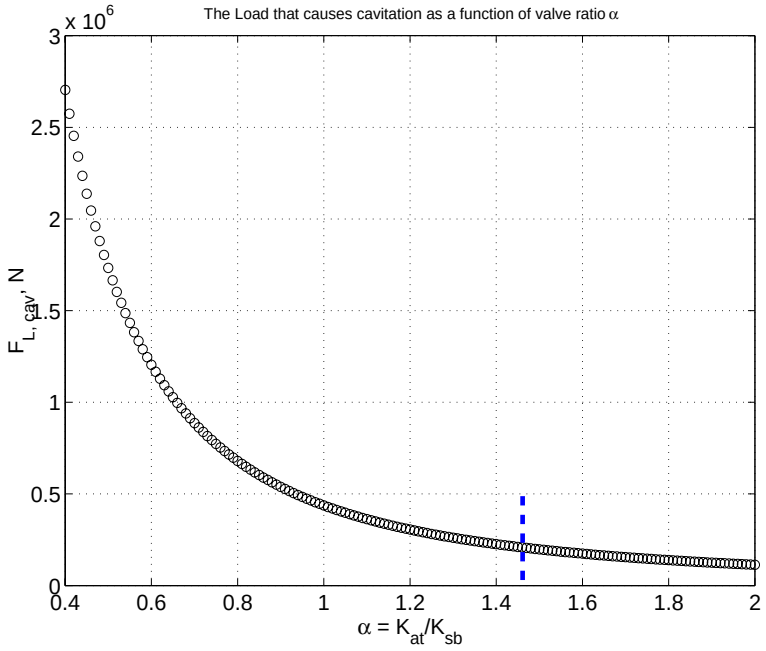

Figure 3.8: The Load F_L that causes cavitation as a function of valve ratio α for Powered Retraction Mode

3.6 Cavitation in Low Side Regeneration Retraction Mode

Figure 3.9 shows a cylinder in Low Side Regeneration Retraction mode subjected to an overrunning load.

In this case, flow can be characterized with the following orifice equations:

$$q_a = A_a\dot{x} = K_{at}\sqrt{\Delta P_1} = K_{at}\sqrt{P_a - P_r} \tag{3.48}$$

$$q_b = A_b\dot{x} = K_{bt}\sqrt{\Delta P_2} = K_{bt}\sqrt{P_r - P_b} \tag{3.49}$$

Dividing equation 3.48 by 3.49 we obtain:

$$\frac{q_a}{q_b} = R = \alpha\sqrt{\frac{\Delta P_1}{\Delta P_2}} \tag{3.50}$$

Where $R = \frac{A_a}{A_b}$ and $\alpha = \frac{K_{at}}{K_{bt}}$. Squaring equation 3.50 and rearranging we obtain

$$\Delta P_1 = \left(\frac{R}{\alpha}\right)^2 \Delta P_2 \tag{3.51}$$

$$\Rightarrow P_a = \left(\frac{R}{\alpha}\right)^2 (P_r - P_b) + P_r \tag{3.52}$$

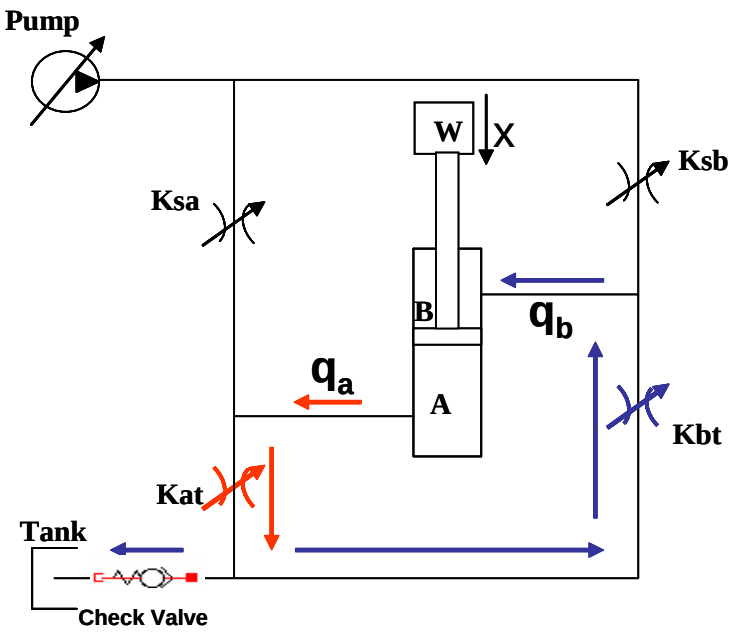

Figure 3.9: A cylinder in Low Side Regeneration Retraction mode subjected to an overrunning load

Equating 3.52 and 3.38 we get:

$$\frac{P_b}{R} + \frac{F_L - F_f}{A_a} = \left(\frac{R}{\alpha}\right)^2 (P_r - P_b) + P_r \tag{3.53}$$

Now solving for P_b

$$P_b = \frac{\left[1 + \left(\frac{R}{\alpha}\right)^2\right] P_r - \frac{F_L - F_f}{A_a} + P_r}{\frac{1}{R} + \left(\frac{R}{\alpha}\right)^2} \tag{3.54}$$

Like the previous modes we set $P_b = 0$ in equation 3.54 and solve for F_L which is the load that would cause cavitation:

$$\frac{F_L}{A_a} = [1 + (\frac{R}{\alpha})^2]P_r + \frac{F_f}{A_a} \tag{3.55}$$

$$\Rightarrow F_L = [1 + (\frac{\alpha}{R})^2]A_a P_r + F_f \tag{3.56}$$

Figure 3.10 shows the variation of $F_{L,cav}$ as a function of α with the same values used: $R = 1.6580$, $A_a = 7854\,mm^2$, $P_r = 0.7\,MPa$, and friction is neglected i.e. $F_f = 0$ or lumped in F_L. Again, the dashed line on the plot is the line passing through α_{opt} and the corresponding Load is $F_L \approx 12.5kN$. It is of course a much lower force than the force

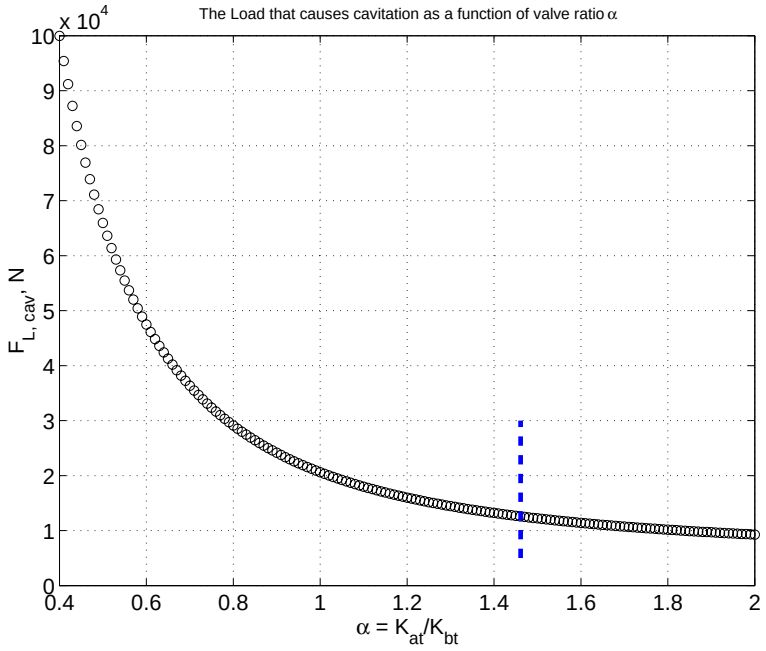

Figure 3.10: The Load F_L that causes cavitation as a function of valve ratio α for Low Side Regeneration Retraction Mode

needed in Powered Retraction but still if compared with Low side Regeneration Extension, it is larger.

3.7 Remarks

The analysis in this chapter shows that a much higher load is needed to cause cavitation in High Side Regeneration Extension Mode than Powered Extension Mode given the same system parameters. A lower load can cause cavitation in Low Side Regeneration Extension mode than in Powered Extension or in High Side Regeneration Extension modes given the same system parameters and thus cavitation is more likely to happen. For retraction modes, much larger load can cause cavitation than in the three extension modes given the same system parameters, which is expected given the difference in the piston area for retraction and extension cases.

It is insightful to look at how this analysis can be explained on the valve control plot. Considering the Powered Extension Mode and looking at the valve control plot, it is noticed that any valve ratio α appears as a straight line as shown in figure 3.11. Now, assuming that

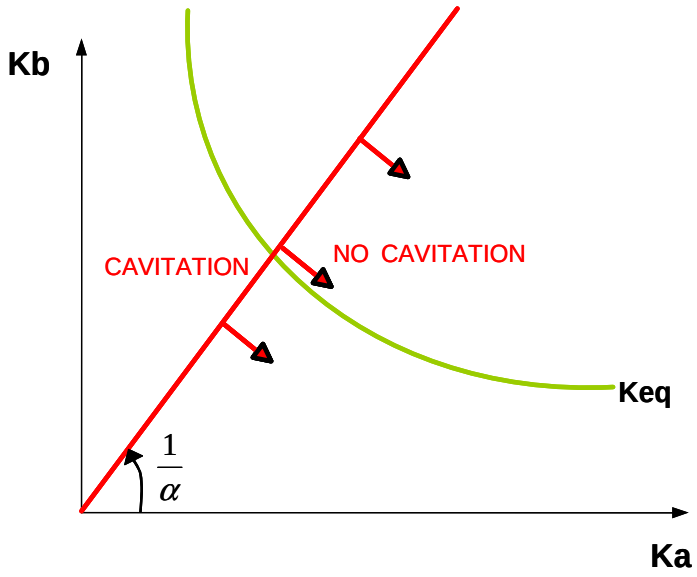

Figure 3.11: Valve openings ratio α can be interpreted as a line on the valve control plot

this is the critical ratio α_{crit} that would cause cavitation at the given load, the intersection of this line and the K_{eq} is an operating point that would achieve the required actuator speed but the actuator would be on the verge of cavitating. Any point below (or to the right of) that line means a higher α than the critical α_{cav} that would cause cavitation. By choosing a higher α, another line like the line shown in figure 3.11 can be drawn with a smaller slope. The intersection of this line with the K_{eq} alleviates cavitation and still achieves the commanded speed.

CHAPTER IV

POWER SAVINGS COMPARISON AND ANALYSIS

4.1 General

Chapter 2 presented the independent metering concept and showed qualitatively and instinctively that it promises energy savings when compared with the conventional spool valve based hydraulic systems. This chapter attempts a more rigorous analysis to mathematically validate the hypothesis that the independent metering system promises more energy savings.

First the analysis will be done assuming a typical conventional load sense pump system is used with the independent metering valve assembly explained in chapter 2. In this case only Powered Extension and Powered Retraction modes are going to be analyzed. Then the full potential of the system will be explored with all the five modes analyzed.

4.2 Using a Conventional Load Sensing Pump Control

PCLS (Pressure Compensated Load Sense) systems simply senses the pressure in the inlet chamber of the hydraulic cylinder and asks the pump to add a certain pressure margin P_m in order to maintain a fixed pressure drop across the valve and thus obtain a linear relationship between the spool position and the flow through the valve. Only Powered Extension and Powered Retraction modes are going to be analyzed in this section in order to compare the independent metering configuration with a spool valve controlled system that is capable of operating in Powered Extension-like and Powered Retraction-like modes only.

The following analysis assumes quasi-static or steady state behavior. All dynamic effects like compressibility of the oil, line capacitances and valve dynamics are ignored in this analysis. The power consumed in actuating the valves is assumed to be very small compared to the hydraulic power and thus ignored.

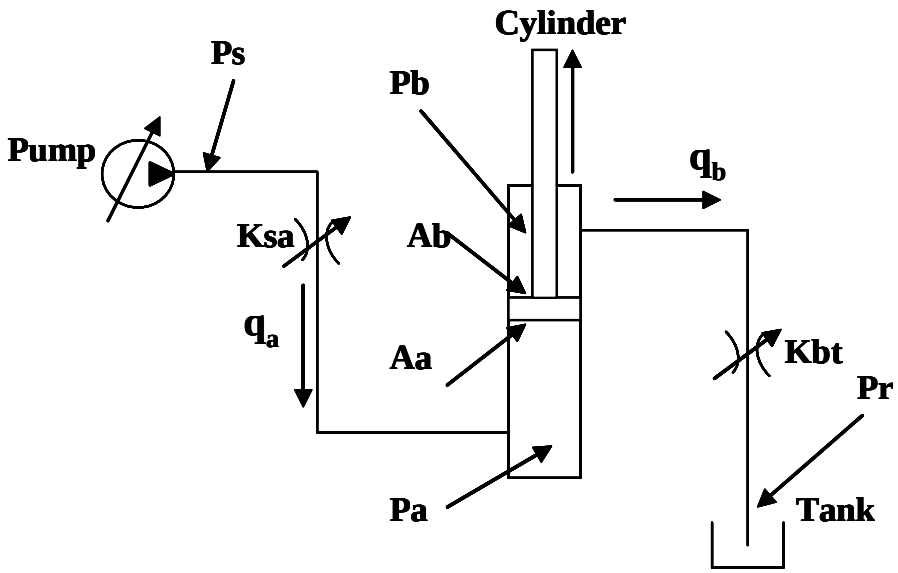

Figure 4.1: Powered Extension Mode

4.2.1 Powered Extension Mode

Figure 4.1 shows the Powered Extension Mode topology. Flow-in valve K_{sa} and valve K_{bt} can be characterized by the following equations:

$$q_a = K_{sa}\sqrt{\Delta P_1} = K_{sa}\sqrt{P_s - P_a} = A_a\dot{x} \tag{4.1}$$

$$q_b = K_{bt}\sqrt{\Delta P_2} = K_{bt}\sqrt{P_b - P_r} = A_b\dot{x} \tag{4.2}$$

Dividing equation 4.1 by 4.2 we obtain:

$$\frac{q_a}{q_b} = R = \alpha\sqrt{\frac{P_s - P_a}{P_b - P_r}} \tag{4.3}$$

Where $R = \frac{A_a}{A_b}$ and $\alpha = \frac{K_{sa}}{K_{bt}}$. Squaring equation 4.3 and rearranging we obtain

$$P_s - P_a = \left(\frac{R}{\alpha}\right)^2 (P_b - P_r) \tag{4.4}$$

$$P_s = P_a + \left(\frac{R}{\alpha}\right)^2 P_b - \left(\frac{R}{\alpha}\right)^2 P_r \tag{4.5}$$

But as shown before, the hydraulic force can be expressed as:

$$F_{Hyd} = P_a A_a - P_b A_b \tag{4.6}$$

$$\Rightarrow P_a = \frac{F_{Hyd}}{A_a} + \frac{P_b}{R} = P_s - \left(\frac{R}{\alpha}\right)^2 P_b + \left(\frac{R}{\alpha}\right)^2 P_r \tag{4.7}$$

$$\Rightarrow \left[\frac{1}{R} + \left(\frac{R}{\alpha}\right)^2\right] P_b = P_s - \frac{F_{Hyd}}{A_a} + \left(\frac{R}{\alpha}\right)^2 P_r \tag{4.8}$$

$$\Rightarrow P_b = \frac{R}{1 + (\frac{R^3}{\alpha^2})} P_s - \frac{1}{1 + (\frac{R^3}{\alpha^2})} \frac{F_{Hyd}}{A_b} + \frac{R^3}{\alpha^2 + R^3} P_r \tag{4.9}$$

Similarly:

$$\Rightarrow P_b = RP_a - \frac{F_{Hyd}}{A_b} = (\frac{\alpha}{R})^2 P_s - (\frac{\alpha}{R})^2 P_a + P_r \tag{4.10}$$

$$\Rightarrow \left[R + \left(\frac{\alpha}{R}\right)^2\right] P_a = (\frac{\alpha}{R})^2 P_s + \frac{F_{Hyd}}{A_b} + P_r \tag{4.11}$$

$$\Rightarrow P_a = \frac{1}{1 + (\frac{R^3}{\alpha^2})} P_s - \frac{R^2}{\alpha^2 + R^3} \frac{F_{Hyd}}{A_b} + \frac{R^2}{\alpha^2 + R^3} P_r \tag{4.12}$$

It is assumed that a Pressure Compensated Load Sense system (PCLS) is used to control this independent metering four-valve configuration. The cylinder is operating under a Powered Extension mode and thus head chamber (a) is the input chamber. So, the PCLS system senses the pressure in chamber a P_a and commands the pump to supply a certain pressure margin P_m above P_a:

$$P_s = P_a + P_m \tag{4.13}$$

From equation 4.12:

$$\Rightarrow P_s = \frac{1}{1 + (\frac{R^3}{\alpha^2})} P_s - \frac{R^2}{\alpha^2 + R^3} \frac{F_{Hyd}}{A_b} + \frac{R^2}{\alpha^2 + R^3} P_r + P_m \tag{4.14}$$

$$\Rightarrow P_s \left[\frac{R^3}{\alpha^2 + R^3}\right] = -\frac{R^2}{\alpha^2 + R^3} \frac{F_{Hyd}}{A_b} + \frac{R^2}{\alpha^2 + R^3} P_r + P_m \tag{4.15}$$

$$\Rightarrow P_s = \left[\frac{\alpha^2 + R^3}{R^3}\right] P_m - \frac{1}{R} \frac{F_{Hyd}}{A_b} + \frac{1}{R} P_r \tag{4.16}$$

But:

$$P_a = P_s - P_m \tag{4.17}$$

$$\Rightarrow P_a = \frac{\alpha^2}{R^3} P_m + \frac{1}{R} \frac{F_{Hyd}}{A_b} + \frac{1}{R} P_r \tag{4.18}$$

Also, from equation 4.4 P_b can be expressed as follows:

$$P_b = \left(\frac{\alpha}{R}\right)^2 (P_s - P_a) + P_r \tag{4.19}$$

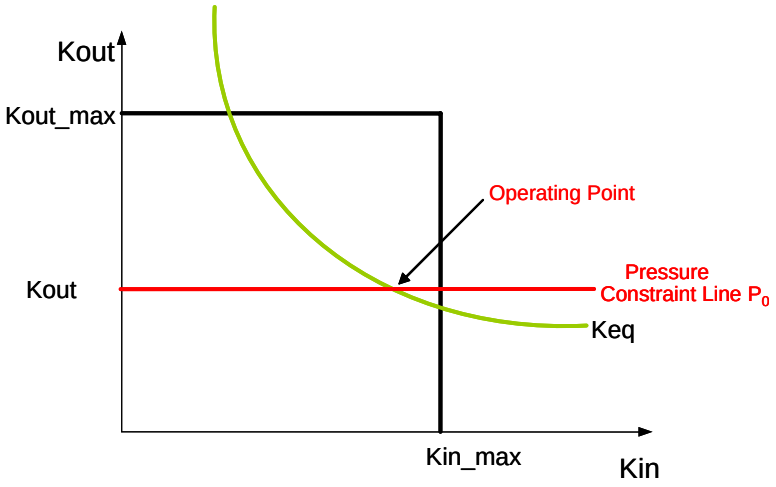

Figure 4.2: Back Pressure Regulation

4.2.1.1 Back Pressure Regulation for Powered Extension Case with PCLS Logic

The derivation in the previous section is the same for an independent metering configuration as for a conventional spool valve controlled system. However, as explained in chapter 2, by virtue of having a two degree of freedom control system, the pressure in the return chamber can be controlled in an independent metering configuration. In other words, the return chamber pressure P_b can be controlled to be a certain desired pressure P_0. A specific desired return chamber pressure P_0 appears as a horizontal line on the valve control plot that represents the outlet valve opening that would achieve that return pressure. If the operating point is selected as the intersection of that line with the K_{eq} line representing a particular required speed, then that return pressure would be achieved. This is shown in figure 4.2. Any point below that horizontal line translates to a pressure lower than P_0. Thus, the controller can command a specific return (back) pressure P_0, or:

$$P_b = P_0 \tag{4.20}$$

From equation 4.19 P_0 can be expressed as:

$$P_0 = \left(\frac{\alpha}{R}\right)^2 (P_s - P_a) + P_r \tag{4.21}$$

Equation for P_s can be rewritten as follows:

$$P_s = \left(\frac{\alpha^2}{R^3}\right) P_m + \frac{1}{R} P_r + \frac{1}{R} \frac{F_{Hyd}}{A_b} + P_m \tag{4.22}$$

$$\Rightarrow P_s = \frac{1}{R}\left(\frac{\alpha^2}{R^2}P_m + P_r\right) + \frac{1}{R}\frac{F_{Hyd}}{A_b} + P_m \tag{4.23}$$

$$\Rightarrow P_s = \frac{1}{R}P_0 + \frac{1}{R}\frac{F_{Hyd}}{A_b} + P_m \tag{4.24}$$

And from equation 4.24, P_a, which is the difference between P_s and P_m in this case, can be expressed as:

$$P_a = \frac{1}{R}P_0 + \frac{1}{R}\frac{F_{Hyd}}{A_b} \tag{4.25}$$

4.2.1.2 Difference in Pump Power Required for Powered Extension Case

To show that this new system can save more energy than a conventional system, an expression for pump required from the pump is written as:

$$Power = P_s \cdot Q_s \tag{4.26}$$

The pressure needed for a conventional spool valve controlled system is given in equation 4.16, while the pressure needed for the independent metering configuration is given in equation 4.24. The difference between the two equations is the pressure difference that is saved as a result of the control advantage of the latter system.

$$\Delta Power = \Delta P_s \cdot Q_s \tag{4.27}$$

$$\Delta P_s = \left[\left(\frac{\alpha^2 + R^3}{R^3}\right)P_m + \frac{1}{R}\frac{F_{Hyd}}{A_b} + \frac{1}{R}P_r\right] - \left[\frac{1}{R}P_0 + \frac{1}{R}\frac{F_{Hyd}}{A_b} + P_m\right] \tag{4.28}$$

$$\Rightarrow \Delta P_s = \left(\frac{\alpha^2}{R^3}\right)P_m + \frac{1}{R}(P_r - P_0) \tag{4.29}$$

Defining the supply pressure required by a spool valve conventional system as P_s, while the pressure required by an independent metering four-valve system as P'_s, the power savings can be expressed as:

$$\Delta Power = P_s Q_s - P'_s Q_s = \left[\left(\frac{\alpha^2}{R^3}\right)P_m + \frac{1}{R}(P_r - P_0)\right]Q_s \tag{4.30}$$

Assuming that the load and speed requirement on the actuator are the same, then the useful work is the same in both cases. Also, since the same pressure margin is maintained across the inlet valve in both cases, then the power loss across the inlet valve (throttling losses) are the same. However, since the independent metering system is a two degree of

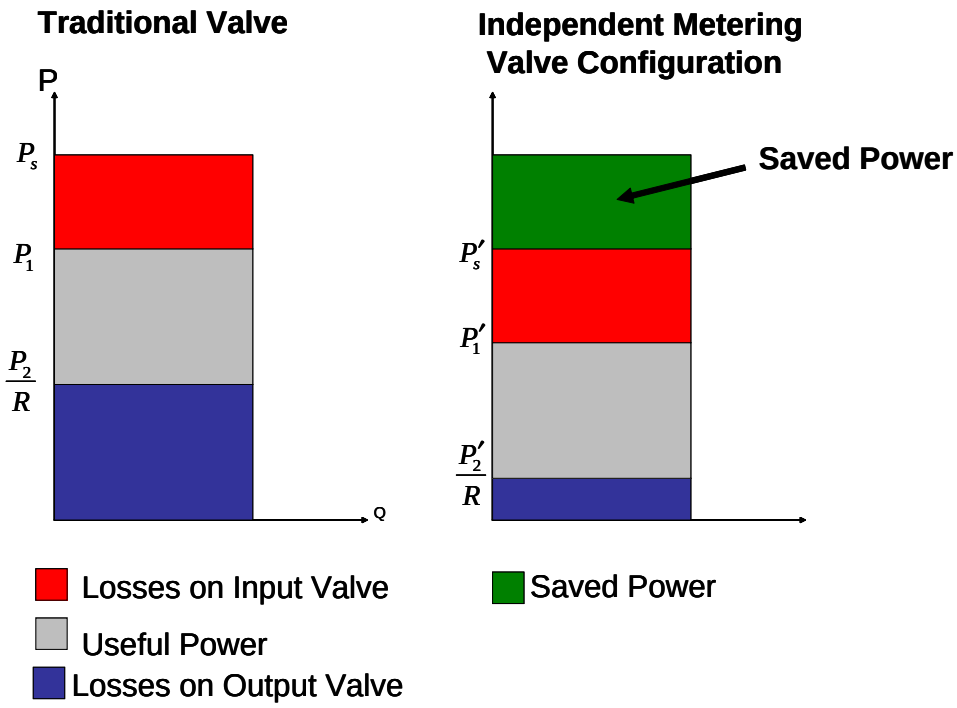

Figure 4.3: Power Savings when using an independent metering valve configuration versus using a traditional spool valve

freedom system and that the return chamber pressure can be controlled as explained earlier, the throttling losses across the outlet valve can be decreased. This is shown graphically in figure 4.3

As a numerical example, consider a case where return pressure $P_r = 0$, piston area ratio $R = 1.4$, valve openings ratio $\alpha = 1.3$, the pressure margin $P_m = 1.7\,MPa$, and the return pressure is controlled to be $P_0 = 0.7\,MPa$. For this case:

$$\Delta P_s \approx 0.55\,MPa \tag{4.31}$$

$$Power\ Ratio = \frac{P_s' Q_S}{P_s Q_S} \approx 37\% \tag{4.32}$$

Next the variation of the saved power area in figure 4.3 is studied as the parameters P_m, R, and P_0 are changed. Since the flow is assumed to be the same, changes in supply pressure difference is a representative of changes in saved power as shown by equations 4.27 and 4.30.

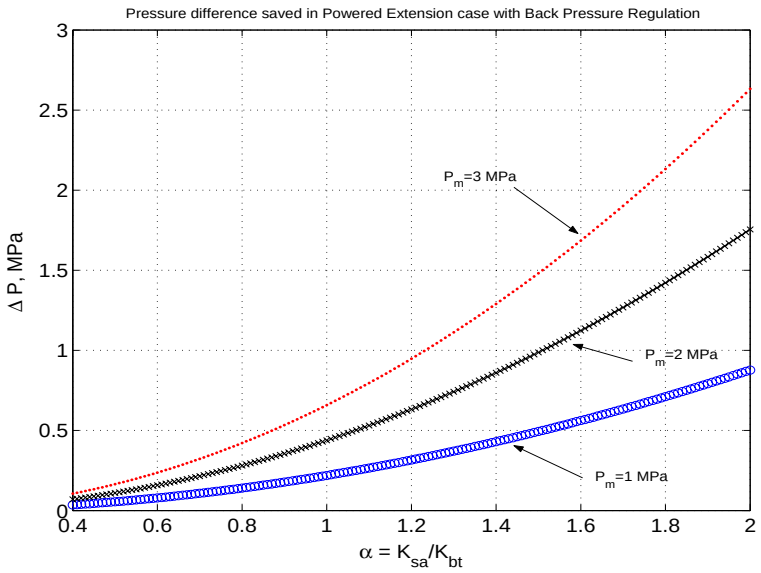

Figure 4.4: ΔP_s Saved in Powered Extension Case with Back Pressure Regulation with Variation in Pressure Margin P_m

4.2.1.3 Power Savings Variation

If P_0 is set equal to P_r, then ΔP_s depends on the valve coefficient ratio α and the pressure margin P_m. Figure 4.4 shows the variation in ΔP_s saved as a function of α for three values of P_m: $1\,MPa$, $2\,MPa$, and $3\,MPa$ for a value of $R = 1.658$. It is clear that more energy is saved for a given ratio α when the pressure margin is increased. One of the limitations on increasing the ratio is the desire to operate with limits on the maximum pressure that is allowed in the inlet chamber. Opening the inlet valve more and more increases the pressure in head chamber (a). The figure also shows that increasing the pressure margin has more potential for saving energy for a given valve ratio. Figure 4.5 shows the variation of ΔP_s saved as a function of α for three values of R: 1, 1.658, and 2 for a value of $P_m = 1\,MPa$. It shows that the potential for energy savings is higher for a smaller area ratio R. Figure 4.6 shows the variation of ΔP_s saved as a function of α for three values of P_0: Pr, $2Pr$, and $3Pr$ for a value of $P_m = 1\,MPa$ and $R = 1.658$. It shows that the potential for energy savings is higher for P_0 closer to P_r. The figure shows that in fact more energy would be needed (i.e. $\Delta P < 0$)for independent metering design case than conventional spool valve design case when $P_0 = 3P_r$ for almost all values of α, and for some values of α when $P_0 = 2P_r$.

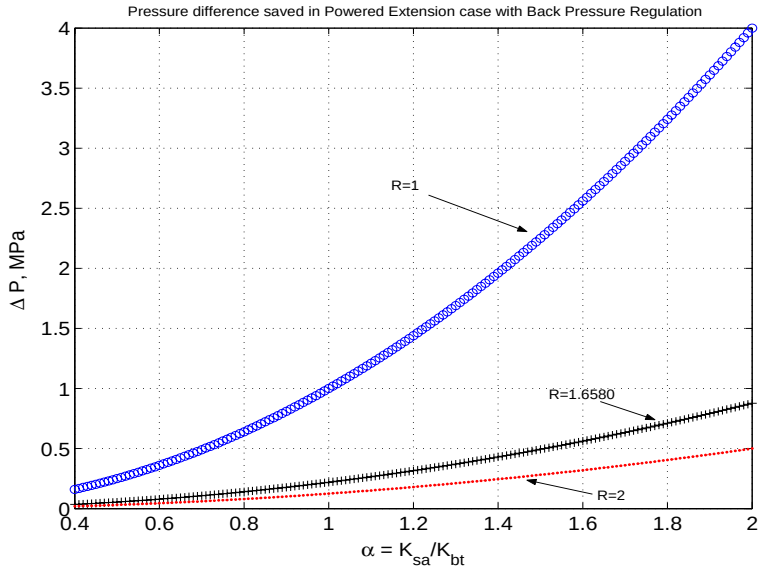

Figure 4.5: ΔP_s **Saved in Powered Extension Case with Back Pressure Regulation with Variation in Area Ratio** R

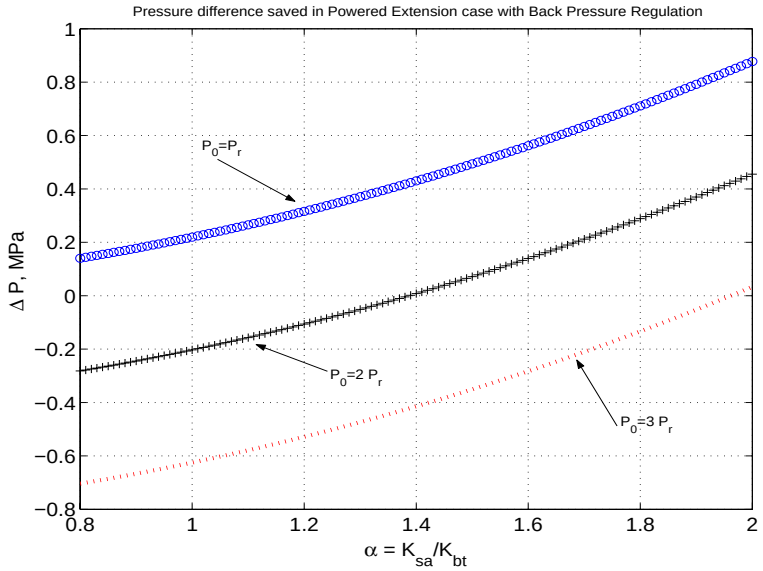

Figure 4.6: ΔP_s **Saved in Powered Extension Case with Back Pressure Regulation with Variation in Back Pressure** P_0

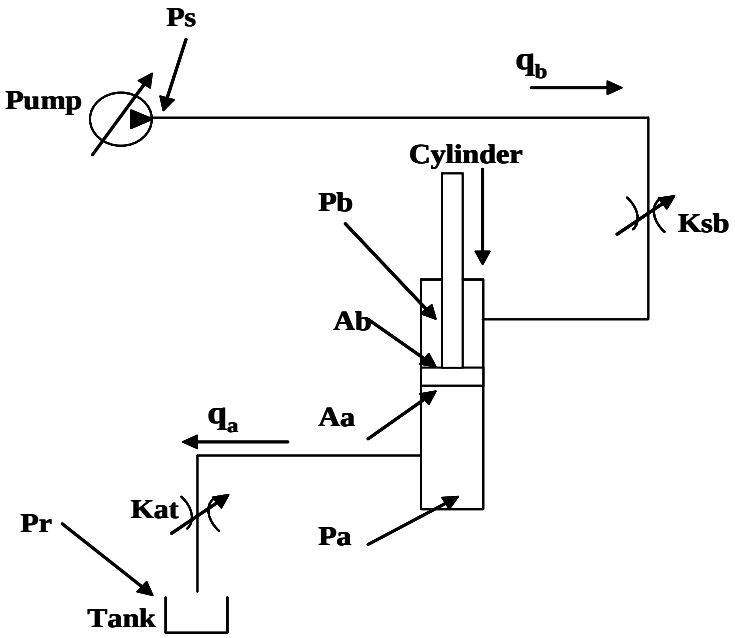

Figure 4.7: Powered Retraction Mode-Mathematical Analysis

4.2.2 Powered Retraction Mode

Similar analysis can be done for Powered Retraction Mode. Flow in valve K_{sa} and valve K_{bt} can be characterized by the following equations:

$$q_a = K_{at}\sqrt{\Delta P_1} = K_{at}\sqrt{P_a - P_r} = A_a\dot{x} \tag{4.33}$$

$$q_b = K_{sb}\sqrt{\Delta P_2} = K_{sb}\sqrt{P_s - P_b} = A_b\dot{x} \tag{4.34}$$

Dividing equation 4.33 by 4.34 we obtain:

$$\frac{q_a}{q_b} = R = \alpha\sqrt{\frac{P_a - P_r}{P_s - P_b}} \tag{4.35}$$

Where $R = \frac{A_a}{A_b}$ and $\alpha = \frac{K_{at}}{K_{sb}}$. Squaring equation 4.35 and rearranging we obtain

$$P_a - P_r = \left(\frac{R}{\alpha}\right)^2 (P_s + P_b) \tag{4.36}$$

$$P_s = P_b + \left(\frac{\alpha}{R}\right)^2 P_a - \left(\frac{\alpha}{R}\right)^2 P_r \tag{4.37}$$

In this case the hydraulic force can be expressed as follows:

$$F_{Hyd} = P_b A_b - P_a A_a \tag{4.38}$$

$$\Rightarrow P_b = \frac{F_{Hyd}}{A_b} + RP_a = P_s - \left(\frac{\alpha}{R}\right)^2 P_a + \left(\frac{\alpha}{R}\right)^2 P_r \tag{4.39}$$

$$\Rightarrow \left[\frac{\alpha^2 + R^3}{R^2}\right] P_a = P_s - \frac{F_{Hyd}}{A_b} + \left(\frac{\alpha}{R}\right)^2 P_r \tag{4.40}$$

$$\Rightarrow P_a = \frac{R^2}{\alpha^2 + R^3} P_s - \frac{R^2}{\alpha^2 + R^3} \frac{F_{Hyd}}{A_b} + \frac{\alpha^2}{\alpha^2 + R^3} P_r \tag{4.41}$$

Similarly:

$$P_a = \frac{P_b}{R} - \frac{F_{Hyd}}{A_a} = \left(\frac{R}{\alpha}\right)^2 P_s - \left(\frac{R}{\alpha}\right)^2 P_b + P_r \tag{4.42}$$

$$\Rightarrow \left[\frac{R^3 + \alpha^2}{R\alpha^2}\right] P_b = \left(\frac{R}{\alpha}\right)^2 P_s + \frac{F_{Hyd}}{A_a} + P_r \tag{4.43}$$

$$\Rightarrow P_b = \frac{R^3}{\alpha^2 + R^3} P_s + \frac{\alpha^2}{\alpha^2 + R^3} \frac{F_{Hyd}}{A_b} + \frac{R\alpha^2}{\alpha^2 + R^3} P_r \tag{4.44}$$

As in the previous section on Powered Extension case it is assumed that a Pressure Compensated Load Sense system (PCLS) is used to control this independent metering four-valve configuration. The cylinder is operating under a Powered Retraction mode and thus rod chamber (b) is the input chamber. So, the PCLS system sense the pressure in chamber a P_b and commands the pump to supply a certain pressure margin P_m above P_b:

$$P_s = P_b + P_m \tag{4.45}$$

From equation 4.44:

$$\Rightarrow P_s = \frac{R^3}{\alpha^2 + R^3} P_s + \frac{\alpha^2}{\alpha^2 + R^3} \frac{F_{Hyd}}{A_b} + \frac{R\alpha^2}{\alpha^2 + R^3} P_r + P_m \tag{4.46}$$

$$\Rightarrow P_s \left[\frac{\alpha^2}{\alpha^2 + R^3}\right] = \frac{\alpha^2}{\alpha^2 + R^3} \frac{F_{Hyd}}{A_b} + \frac{R\alpha^2}{\alpha^2 + R^3} P_r + P_m \tag{4.47}$$

$$\Rightarrow P_s = \left[\frac{R^3}{\alpha^2} + 1\right] P_m + \frac{F_{Hyd}}{A_b} + RP_r \tag{4.48}$$

But:

$$P_b = P_s - P_m \tag{4.49}$$

$$\Rightarrow P_b = \left(\frac{R^3}{\alpha^2}\right) P_m + \frac{F_{Hyd}}{A_b} + RP_r \tag{4.50}$$

Also, from equation 4.36 P_a can be expressed as follows:

$$P_a = \left(\frac{R}{\alpha}\right)^2 (P_s - P_b) + P_r = \left(\frac{R}{\alpha}\right)^2 P_m + P_r \tag{4.51}$$

4.2.2.1 Back Pressure Regulation for Powered Retraction Case with PCLS Logic

As explained in section 4.2.1.1, the controller can command a specific return pressure P_a in this case:

$$P_a = P_0 \tag{4.52}$$

From equation 4.19 P_0 can be expressed as:

$$P_0 = \left(\frac{R}{\alpha}\right)^2 P_m + P_r \tag{4.53}$$

Equation for P_s can be rewritten as follows:

$$P_s = \left(\frac{R^3}{\alpha^2}\right) P_m + RP_r + P_m + \frac{F_{Hyd}}{A_b} \tag{4.54}$$

$$\Rightarrow P_s = RP_0 + P_m + \frac{F_{Hyd}}{A_b} \tag{4.55}$$

And from equation 4.55, P_b, which is the difference between P_s and P_m in this case, can be expressed as:

$$P_a = RP_0 + \frac{F_{Hyd}}{A_b} \tag{4.56}$$

4.2.2.2 Difference in Pump Power Required for Powered Retraction Case

To show how much power can be saved in this case, the same procedures are followed as for Powered Extension case. The pressure needed for a conventional spool valve controlled system is given in equation 4.48, while the pressure needed for the independent metering configuration is given in equation 4.55. The difference between the two equations is the pressure difference that is saved as a result of the control advantage of the latter system.

$$\Delta Power = \Delta P_s \cdot Q_s \tag{4.57}$$

$$\Delta P_s = \left[\left(\frac{R^3}{\alpha^2} + 1\right) P_m + \frac{F_{Hyd}}{A_b} + RP_r\right] - \left[RP_0 + P_m + \frac{F_{Hyd}}{A_b}\right] \tag{4.58}$$

$$\Rightarrow \Delta P_s = \left(\frac{R^3}{\alpha^2}\right) P_m + R(P_r - P_0) \tag{4.59}$$

4.2.2.3 Power Savings Variation

If P_0 is set equal to P_r, then ΔP_s depends on the valve coefficients ratio α and the pressure margin P_m. Figure 4.8 shows the variation in ΔP_s saved as a function of α for three values

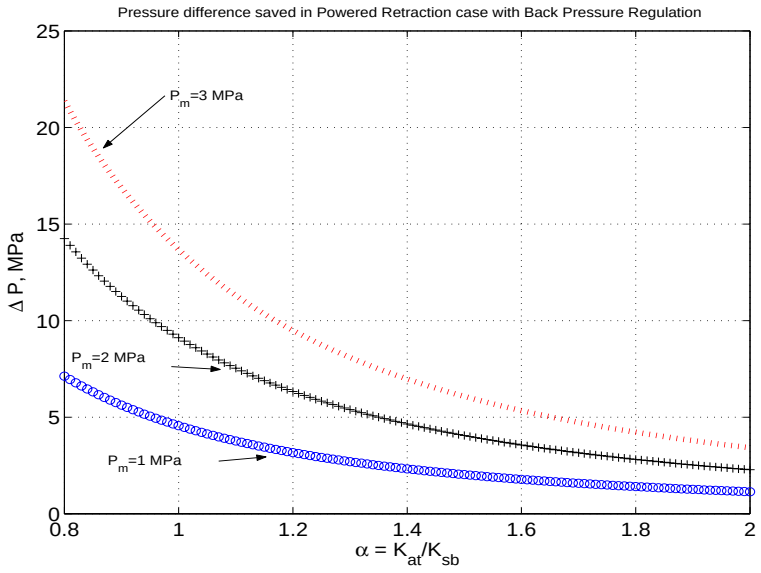

Figure 4.8: ΔP_s Saved in Powered Retraction Case with Back Pressure Regulation with Variation in Pressure Margin P_m

of P_m: $1\,MPa$, $2\,MPa$, and $3\,MPa$ for a value of $R = 1.658$. Operating at a low valve coefficient ratio α saves more pressure and thus power when compared to a conventional system in the retract case. The figure also shows that more energy is saved for a given ratio α when the pressure margin is increased.

Figure 4.9 shows the variation of ΔP_s saved as a function of α for three values of R: 1, 1.658, and 2 for a value of $P_m = 1\,MPa$. It shows that the potential for energy savings is higher for a larger area ratio R in this case as opposed to the Powered Extension case.

Figure 4.10 shows the variation of ΔP_s saved as a function of α for three values of P_0: P_r, $2P_r$, and $3P_r$ for a value of $P_m = 1\,MPa$ and $R = 1.658$. It shows that the potential for energy savings is higher for P_0 closer to P_r.

4.3 Using Powered Extension Supply Pressure Set Point Calculations

The previous section 4.1 compared the conventional system with a independent metering valve configurations that was assumed to be controlled by a PCLS-like control system. That means sensing the pressure in the inlet chamber and adding a certain pressure margin to it and commanding the pump to supply that pressure. This section explores the power savings

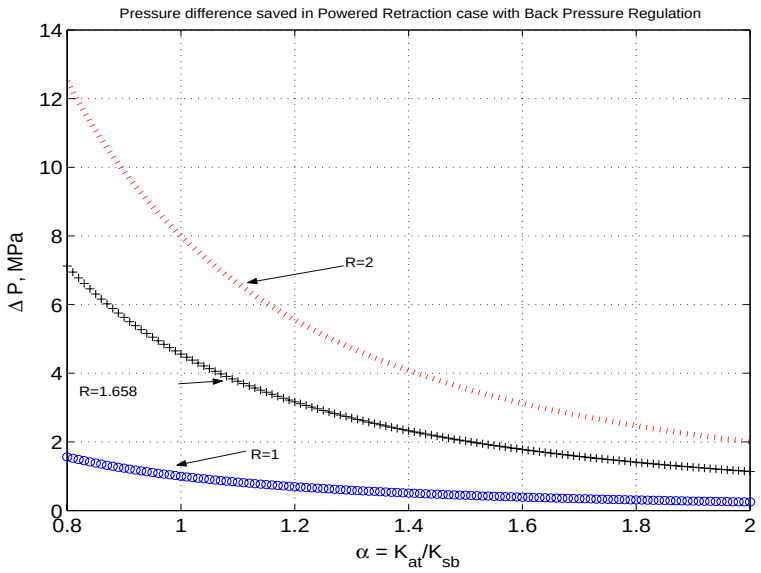

Figure 4.9: ΔP_s **Saved in Powered Retraction Case with Back Pressure Regulation with Variation in Area Ratio** R

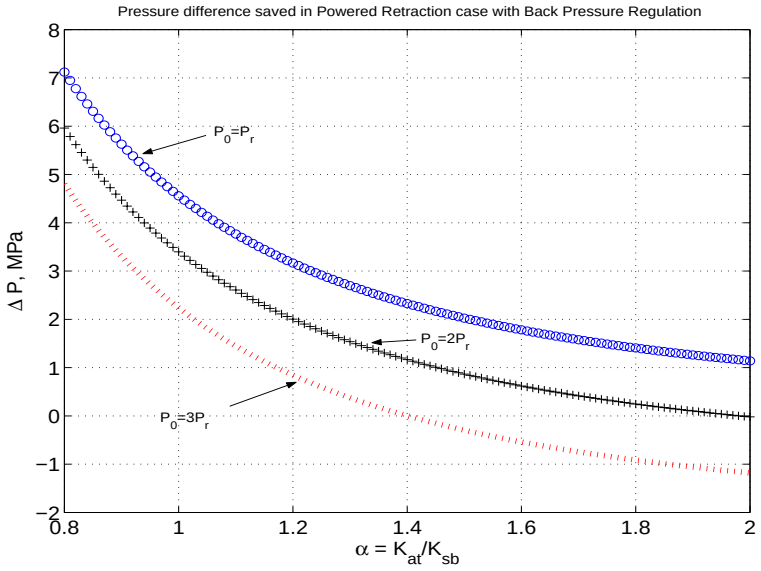

Figure 4.10: ΔP_s **Saved in Powered Retraction Case with Back Pressure Regulation with Variation in Back Pressure** P_0

potential of the independent metering four-valve configuration used with the control system outlined in chapter 2. In other words, instead of using a PCLS like algorithm, the $Ps_{setpoint}$ calculations explained in section 2.5 are used instead.

The conventional spool valve controlled system can perform Powered Extension-like and Powered Retraction-like modes, and calculation of required supply pressure has been presented in section 4.1. Section 2.5 has presented the calculations for pressure set point using the control system presented in chapter 2. Using this latter control system, extension of the cylinder can be done by Powered Extension, or High Side Regeneration Extension, or Low side Regeneration Extension modes. While cylinder retraction can be achieved by Powered Retraction or Low Side Regeneration Retraction. The pressures needed by this control system is to be compared to the conventional spool valve based PCLS hydraulic control systems to quantify how much pressure, and thus power, is saved when using the new control system.

Two equations were given in section 2.5 for $Ps_{set-point}$ for each mode and the maximum of the two is to be used. Practice showed that $Ps_{set-point2} > Ps_{set-point1}$ most of the time and therefore $Ps_{set-point2}$ is used in the following analysis.

$$\Delta Power = \Delta P_s \cdot Q_s \tag{4.60}$$

$$\Delta P_s = \left[\left(\frac{\alpha^2 + R^3}{R^3}\right)P_m + \frac{1}{R}\frac{F_{Hyd}}{A_b} + \frac{1}{R}P_r\right] - \left[\frac{Peq_{min}}{R} + \frac{(RP_a - P_b)}{R} + \frac{P_r}{R}\right] \tag{4.61}$$

$$Peq_{min} = (R+1)\Delta P_{min} \tag{4.62}$$

$$\Rightarrow \Delta P_s = \left(\frac{\alpha^2 + R^3}{R^3}\right)P_m - \frac{Peq_{min}}{R} \tag{4.63}$$

This can be represented as a power saving like that shown in figure 4.3 and again the variation of this power savings depends on several parameters in equation 4.63. This equation shows that the power saved depends on P_m, R, and ΔP_{min}, which is the minimum pressure that needs to be maintained across the poppet valves for proper functioning. Next, the effect of these parameters on the saved power is considered.

Figure 4.11 shows the variation of pressure saved, and power saved in turn, as the pressure margin across the inlet valve of a conventional spool valve controlled system is

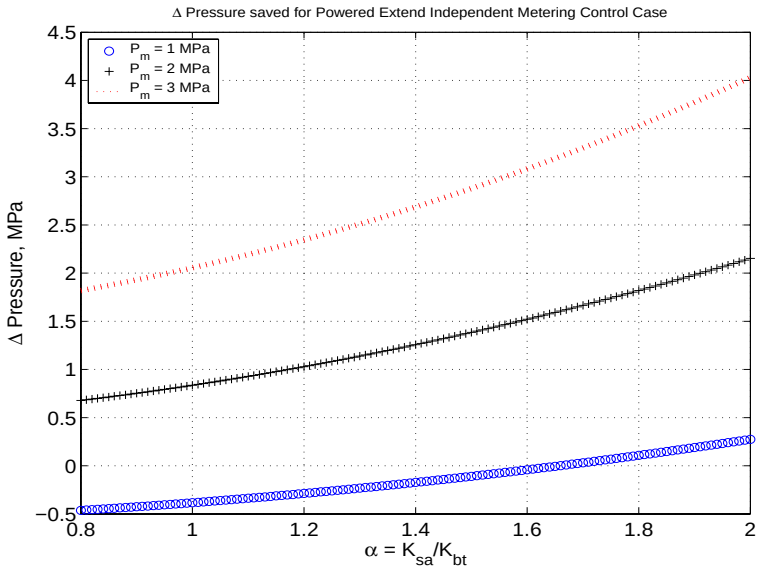

Figure 4.11: ΔP_s Saved in Powered Extension Case with independent metering control with Variation in Pressure Margin P_m

changed from $P_m = 1\,MPa$ to $P_m = 2\,MPa$ and finally to $P_m = 3\,MPa$ while $R = 1.658$ and $\Delta P_{min} = 1\,MPa$. This figure shows that for $P_m = 1\,MPa$ the pressure saved is negative for range of values of α and it means that the spool valve system is more efficient! However, for larger values of P_m power is saved when using the independent metering pressure set point control method.

Next the effect of piston area ratio R is shown. Three values of R are used: 1, 1.658, and 2 for a value of $P_m = 1\,MPa$ and $\Delta P_{min} = 1\,MPa$. The variation is shown in figure 4.12 which shows that as the value of R increases, no pressure is saved but on the contrary the pressure difference is negative and the spool valve PCLS control is more efficient. Finally the effect of ΔP_{min} is studied. Three values of ΔP_{min} are used: $0.5\,MPa$, $1\,MPa$, and $1.5\,MPa$ for a value of $P_m = 1\,MPa$ and $R = 1.658$. This is the pressure that has to be kept across the poppet valves for their proper functioning as aforementioned. Thus, this is a pressure that is totally lost as a throttling loss across the valve. Therefore, an increase in this pressure diminishes the power savings of the independent metering configuration which is confirmed by looking at equation 4.63 and by figure 4.13.

It is therefore concluded that a smaller piston area ratio R, a smaller ΔP_{min},

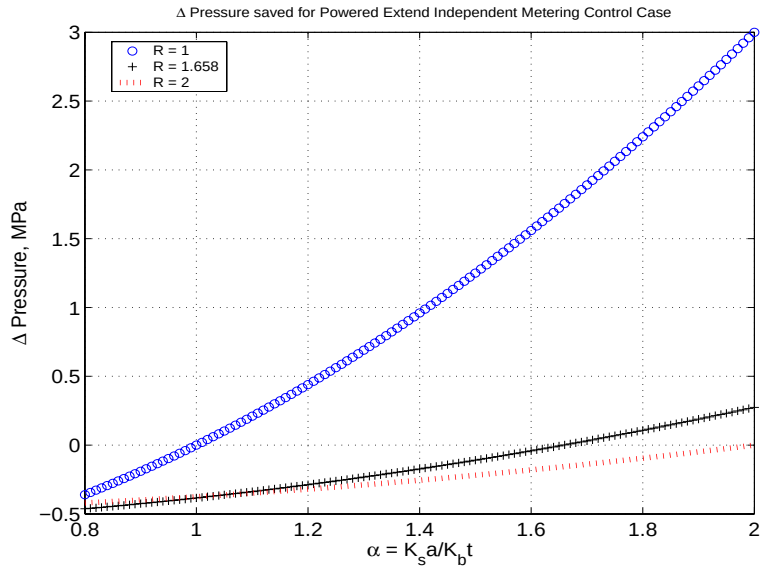

Figure 4.12: ΔP_s Saved in Powered Extension Case with independent metering control with Variation in R

and a larger pressure margin P_m are required to warrant independent metering control method explained in chapter 2 better than the conventional spool valve PCLS controlled systems in terms of power savings. A similar analysis can be done to compare Powered Retraction Mode with Pressure Set Point calculations to a spool valve PCLS controlled system and similar conclusions can be drawn.

Next we compare the regenerative modes with standard modes e.g. High Side Regenerative Mode and Powered Extension Mode

4.4 Regenerative Modes versus Standard Powered Modes

The High Side and Low Side Regeneration Extension modes are compared with Powered Extension Mode next.

4.4.1 Comparison Between High Side Regeneration Extension and Powered Extension Modes

Figure 4.14 shows a cylinder in two different modes: High Side Regeneration Extension (HSRE) mode and Powered Extension (PE) mode. Assuming the return pressure $P_r = 0$, the maximum force that can be achieved in both modes can be easily derived to be:

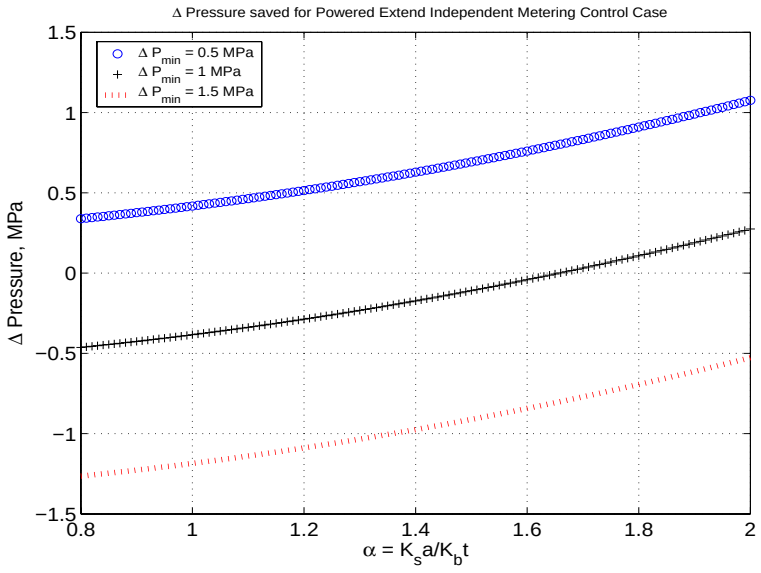

Figure 4.13: ΔP_s Saved in Powered Extension Case with independent metering control with Variation in R

$$Fmax_{PE} = P_s A_a \tag{4.64}$$

$$Fmax_{HSRE} = P_s(A_a - A_b) \tag{4.65}$$

Where P_s is the supply pressure. Similarly, the achievable speed can be derived in both modes to be:

$$\dot{x}_{PE} = \frac{Q_s}{A_a} \tag{4.66}$$

$$\dot{x}_{HSRE} = \frac{Q_s}{(A_a - A_b)} \tag{4.67}$$

Where Q_s is the supply flow

For the same Q_s and P_s it is clear from these equations that Powered Extension is capable of providing a larger maximum force than High Side Regeneration Extension, while High Side Regeneration Extension is capable of achieving higher maximum speeds than Powered Extension.

There are regions of performance overlap where both modes can drive a load at a desired speed with different supply pressure and flow. On the other hand, there are regions of performance where only one mode can achieve the desired performance and this mode has

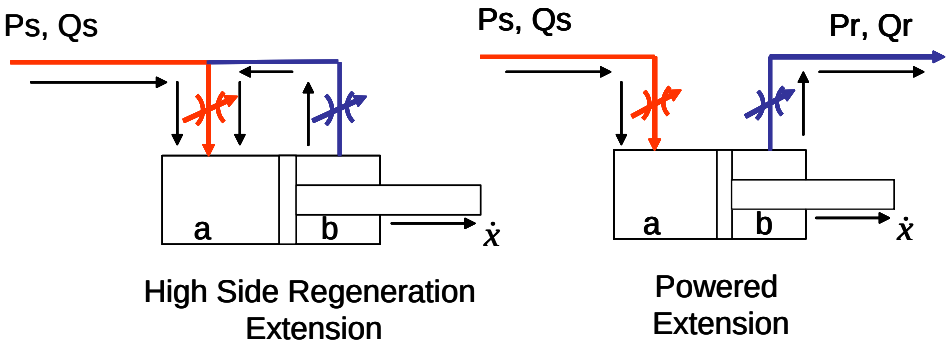

Figure 4.14: Comparison between characteristics of High Side Regeneration Extension and Powered Extension Modes

to be chosen. Similar comparison can be easily made between the different modes. **This comparison of mode capability is elaborated upon in chapter 6**.

If we compare the power requirements by both modes we get the following set of equations:

$$\Delta Power = P_{s,PE}Q_a - P_{s,HSRE}Q_r \quad (4.68)$$

$$Q_a = A_a\dot{x} \quad (4.69)$$

$$Q_r = (A_a - A_b)\dot{x} \quad (4.70)$$

$$\Delta Power = \left[\frac{Peq_{min}}{R} + \frac{(RP_a - P_b)}{R} + \frac{P_r}{R}\right]A_a\dot{x} - \left[\frac{Peq_{min}}{R-1} + \frac{(RP_a - P_b)}{R-1}\right]A_r\dot{x} \quad (4.71)$$

$$Peq_{min} = (R+1)\Delta P_{min} \quad (4.72)$$

$$\Rightarrow \Delta Power = \left[\left(\frac{Peq_{min}}{R} + \frac{(RP_a - P_b)}{R} + \frac{P_r}{R}\right)A_a - \left(\frac{Peq_{min}}{R-1} + \frac{(RP_a - P_b)}{R-1}\right)A_r\right]\dot{x} \quad (4.73)$$

$$\Delta Power = \Delta Force \cdot \dot{x} \quad (4.74)$$

Because the force and speed required from the actuator are the same in both cases, the $\Delta Force$ terms will be equal to zero. However, suppose in a multi-actuator system, which is very common in mobile hydraulics, that one actuator has to move a large load and thus demands a high pressure from the pump. Another actuator may be moving a smaller load but because the pump is already supplying a high pressure to the former actuator, it would save pump flow and thus pump power for the latter actuator to be operating in High Side Regeneration Mode (HSRE) than Powered Extension Mode (PE). This is explained

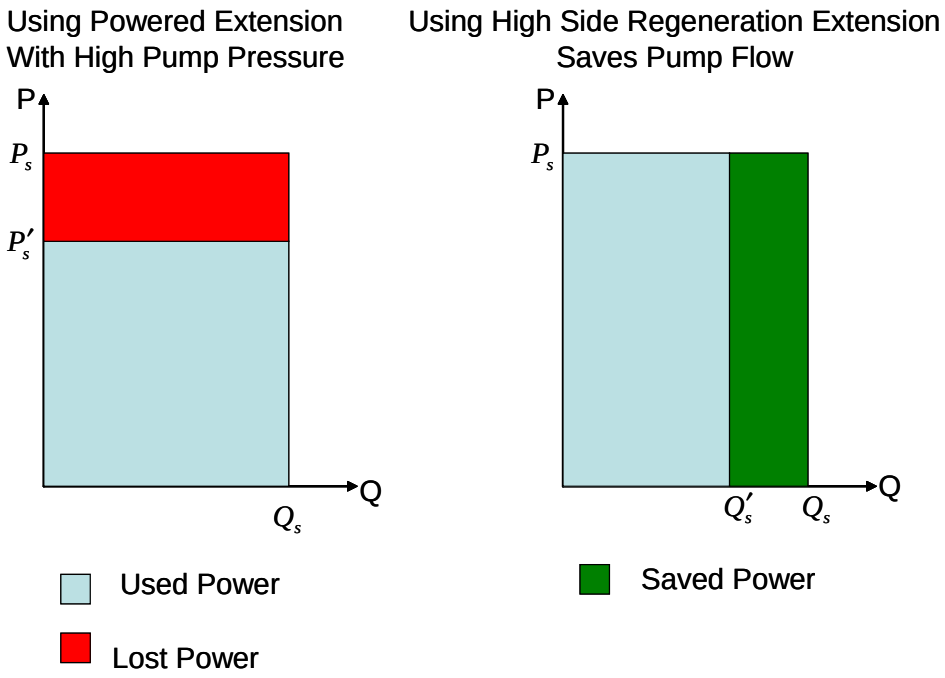

Figure 4.15: High Side Regeneration Extension Mode saves flow when compared with Powered Extension Mode provided the overall system pressure is high enough.

by figure 4.15. If the pump pressure P_s is higher than what PE mode needs P_s', the extra pressure $P_s - P_s'$, and therefore power, is lost. That is indicated by the red area. However, if HSRE is used, it makes full use of the already high pressure P_s but saves flow because of recirculation. This is indicated by the green area.

4.4.2 Low Side Regeneration Extension versus Powered Extension Modes

A similar comparison can be done between Low Side Regeneration Extension Mode (LSRE) and Powered Extension Mode (PE). The recirculation flow in LSRE case goes through the low pressure line as shown in chapter 2. LSRE not only saves pump flow but also saves pump pressure. LSRE needs a very small pump pressure to just supply a pump flow needed to supplement the recirculation flow $Q_a - Q_b$. Thus it saves power by saving pump flow and pump pressure as shown in figure 4.16.

A similar analysis can be done to compare Low Side Regeneration Retraction Mode (LSRR) and Powered Retraction Mode (PR). LSRR does not need pump pressure or flow because it completely depends on flow recirculation from head chamber to rod side chamber

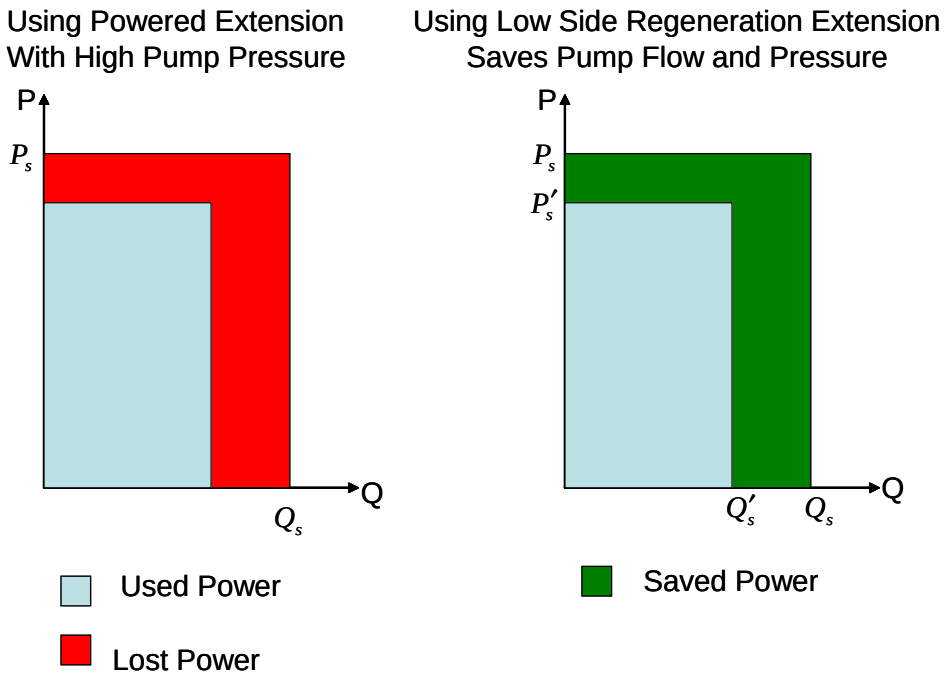

Figure 4.16: Low Side Regeneration Extension Mode saves flow and pressure when compared with Powered Extension Mode

and the extra flow goes to tank, while PR supplies pump pressure and flow in order to drive the actuator.

It should be emphasized however, that both Low Side Regeneration modes are only useful whenever there is gravity assistance i.e. the load is negative. The four-valve configuration allows for this kind of regenerative flow while a conventional spool valve does not and thus has to use pump flow and pressure which is a waste of energy.

4.5 Inlet / Outlet Valve Power Dissipation Comparison

In this section the throttling losses or the power dissipated across the inlet and outlet valves are compared. A Powered Extension Mode setup is used and then the result is generalized for the rest of the modes.

Considering figure 4.17, the following analysis can be conducted:

$$q_a = K_{sa}\sqrt{\Delta P_a} = A_a\dot{x} \tag{4.75}$$

$$q_b = K_{bt}\sqrt{\Delta P_b} = A_b\dot{x} \tag{4.76}$$

$$\Rightarrow q_a = Rq_b \tag{4.77}$$

$$\Rightarrow K_{sa}\sqrt{\Delta P_a} = RK_{bt}\sqrt{\Delta P_b} \tag{4.78}$$

Squaring:

$$\Rightarrow K_{sa}^2\Delta P_a = R^2K_{bt}^2\Delta P_b \tag{4.79}$$

$$\Rightarrow \Delta P_a = R^2\frac{K_{bt}^2}{K_{sa}^2}\Delta P_b \tag{4.80}$$

$$\Rightarrow \Delta P_a = \frac{R^2}{\alpha^2}\Delta P_b \tag{4.81}$$

The throttling power loss across the valve is equal to the pressure drop across the valve multiplied by the flow through the valve:

$$\mathbb{P}_a = q_a\Delta P_a \tag{4.82}$$

$$\mathbb{P}_b = q_b\Delta P_b \tag{4.83}$$

$$\Rightarrow \mathbb{P}_a = q_a\Delta P_b\frac{R^2}{\alpha^2} = \frac{R^3}{\alpha^2}\mathbb{P}_b \tag{4.84}$$

$$\Rightarrow \frac{\mathbb{P}_\mathbf{a}}{\mathbb{P}_\mathbf{b}} = \frac{\mathbf{R^3}}{\boldsymbol{\alpha^2}} \tag{4.85}$$

This result can be generalized by replacing K_{sa} by K_a ,which represents the valve connected to the head side of the actuator, and by replacing K_{bt} by K_b, which represents the valve connected to the rod side of the actuator, in the equations above.

In order for the throttling losses across both valves to be equal, then the following must be true:

$$\frac{R^3}{\alpha^2} = 1 \tag{4.86}$$

This means that the valve openings ratio corresponding to Equal Throttling Power Loss or α_{ETPL} is:

$$\alpha_{ETPL} = R^{\frac{3}{2}} \tag{4.87}$$

In chapter 2 it has been indicated that the valve openings ratio that minimizes sensitivities to errors is $\alpha_{opt} = R^{\frac{3}{4}}$. Therefore,

$$\alpha_{ETPL} = \alpha_{opt}^2 \tag{4.88}$$

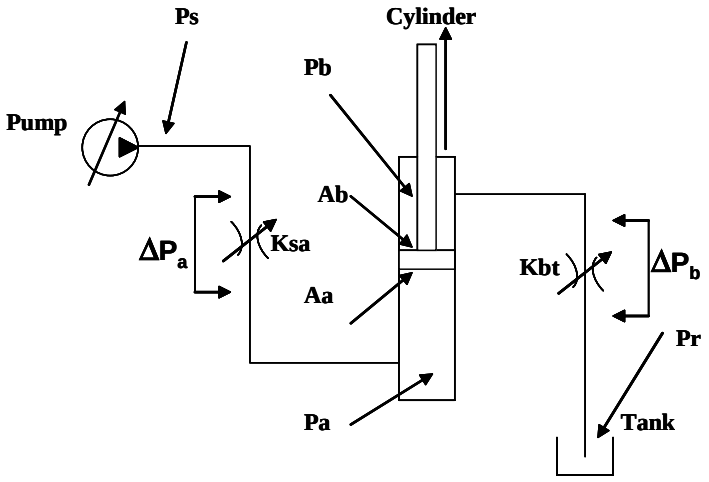

Figure 4.17: Inlet / Outlet valves throttling losses comparison

Figure 4.18 shows the variation of the ratio of throttling power loss of head side valve to that of rod side valve as a function of ratio α. Note that if the optimal ratio α_{opt} is used, the power loss ratio is ≈ 2.1 which means that the power loss across the head side valve is more than double the loss across the rod side valve.

The power loss across the outlet valve can be minimized by controlling the return pressure to decrease the pressure drop across the valve. Choosing a large α according to figure 4.18 can decrease the ratio of power loss between the two valves, and thus the power loss across the inlet valve is decreased as well. **It is therefore concluded that operating at α_{opt} is good for valve sensitivity but is not optimum for decreasing throttling losses**.

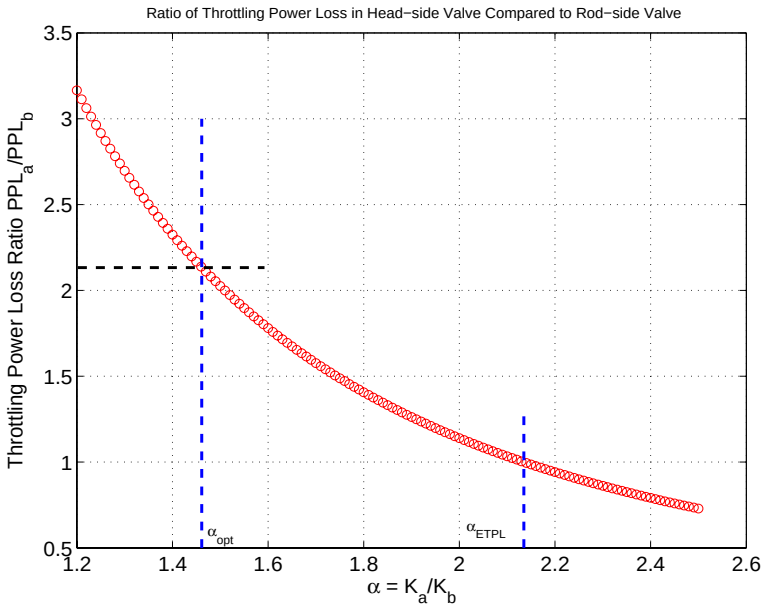

Figure 4.18: Throttling power loss ratio as a function of α

CHAPTER V

SYSTEM DYNAMIC MODEL AND EXPERIMENTAL VALIDATION

5.1 General

The complete mathematical model of a hydraulic cylinder controlled by a four-valve independent metering configuration is developed in this chapter. First, the ***valve switching functions*** idea is introduced, which helps develop a unified mathematical representation for the dynamic model of the system despite having five different modes each with different dynamic characteristics. In order to develop the dynamic model of the whole system, a simplified second order dynamic model of individual poppet valves is developed and experimentally validated. Then the state space model of the system is presented. To experimentally validate the model, a telehandler machine is used to obtain experimental data for matching with the model simulations. Since two of the telehandler functions, specifically its extender and boom functions, are used later in the research, both of these functions are simulated with the state space model and then compared with experimental results.

5.2 Valve Switching Functions

Each of the five metering modes presented earlier has its own set of equations for supply pressure set point, equivalent valve conductance, equivalent pressure and so on. This makes dynamic modeling and analysis difficult and cumbersome since they have to be repeated five times. This section presents an idea that unifies the mathematical representation of the five modes. The core idea is the *valve switching functions*.

Considering figure 5.1, it is noticed that the branch consisting of valves K_{sa} and K_{at} is called branch a since it includes the valves connected to head chamber a. Similarly, the branch consisting of valves K_{sb} and K_{bt} is called branch b since it includes the valves connected to rod chamber b. The following valve switching functions can be defined:

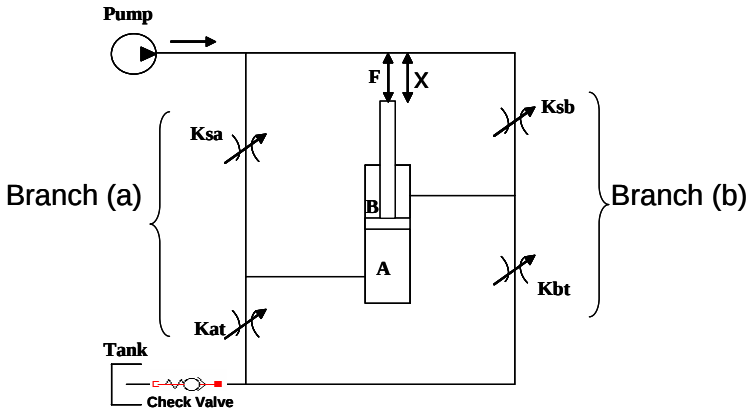

Figure 5.1: Valve Switching Functions

$$S_a = \begin{cases} 1 & \text{when } K_{sa} \text{ is open} \\ \\ -1 & \text{when } K_{at} \text{ is open} \end{cases}$$

Similarly,

$$S_b = \begin{cases} 1 & \text{when } K_{sb} \text{ is open} \\ \\ -1 & \text{when } K_{bt} \text{ is open} \end{cases}$$

If a parameter D is defined as the actuator direction of motion i.e. $D = 1$ if actuator is extending and $D = -1$ if the actuator is retracting, then all metering modes can be represented by the combination (S_a, S_b, D):

$$\begin{aligned} PoweredExtension(PE) = & \quad (1, -1, 1) \\ PoweredRetraction(PR) = & \quad (-1, 1, -1) \\ HighSideRegenerationExtension(HSRE) = & \quad (1, 1, 1) \\ LowSideRegenerationExtension(LSRE) = & \quad (-1, -1, 1) \\ LowSideRegenerationRetraction(LSRR) = & \quad (-1, -1, -1) \end{aligned}$$

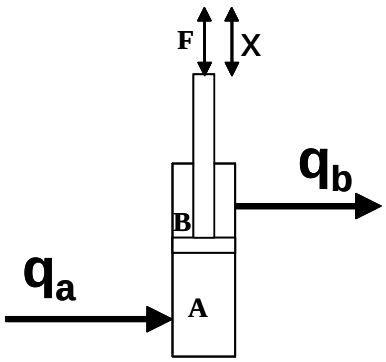

Figure 5.2: Positive flow direction

5.2.1 Flow Representation

Supply and return flows can be expressed using the valve switching functions. Referring to figure 5.2, supply flow can be expressed as:

$$Q_s = \frac{S_a + 1}{2} q_a - \frac{S_b + 1}{2} q_b \tag{5.1}$$

Notice that the flow directions in figure 5.2 are positive and flow in the opposite direction is negative. This is a general equation that represents the supply flow for all five modes. For example, if the actuator is operating in PE mode, $S_a = 1$ and $S_b = -1$, then $Q_s = q_a$. If the actuator is in HSRE mode, $S_a = 1$ and $S_b = 1$, then $Q_s = q_a - q_b$. If the actuator is in PR mode, then $S_a = -1$ and $S_b = 1$, then $Q_s = -q_b$ and so on. Similarly, the return flow can be expressed as:

$$Q_r = \frac{1 - S_b}{2} q_b - \frac{1 - S_a}{2} q_a \tag{5.2}$$

5.2.2 Equivalent Valve Conductance and Equivalent Pressure Representation

Next, valve switching functions are used to unify the representation of valve openings, pressure drop across valves, equivalent valve conductance, and equivalent pressure as well. A general valve opening on branch a can be defined as:

$$K_a = \frac{S_a + 1}{2} K_{sa} + \frac{1 - S_a}{2} K_{at} \tag{5.3}$$

Similarly, for branch b:

$$K_b = \frac{S_b + 1}{2} K_{sb} + \frac{1 - S_b}{2} K_{bt} \tag{5.4}$$

As a result of this representation that gives the correct valve openings based on S_a and S_b values, a general equivalent valve conductance Keq is:

$$K_{eq} = \frac{K_a\, K_b}{\sqrt{K_a^2 + R^3 K_b^2}} \tag{5.5}$$

Flow into head chamber (a) can be represented as $q_a = K_a\sqrt{\Delta P_1}$ where ΔP_1 depends on the mode the actuator is operating in according to the following:

$$\Delta P_1 = \begin{cases} P_s - P_a & \text{in PE mode} \\ P_a - P_r & \text{in PR mode} \\ P_s - P_a & \text{in HSRE mode} \\ P_r - P_a & \text{in LSRE mode} \\ P_a - P_r & \text{in LSRR mode} \end{cases}$$

Valve switching functions can be used to represent ΔP_1 by a single equation:

$$\Delta P_1 = D\left[\frac{S_a + 1}{2}(P_s - P_a) + \frac{1 - S_a}{2}(P_r - P_a)\right] \tag{5.6}$$

Similarly, for ΔP_2:

$$\Delta P_2 = \begin{cases} P_b - P_r & \text{in PE mode} \\ P_s - P_b & \text{in PR mode} \\ P_b - P_s & \text{in HSRE mode} \\ P_b - P_r & \text{in LSRE mode} \\ P_r - P_b & \text{in LSRR mode} \end{cases}$$

And the general representation using valve switching functions is:

$$\Delta P_2 = D\left[\frac{S_b + 1}{2}(P_b - P_s) + \frac{1 - S_b}{2}(P_b - P_r)\right] \tag{5.7}$$

Equivalent pressure P_{eq} has been shown in equations 2.8, 2.16, 2.19, 2.22, and 2.25. These five equations can be represented in a single expression using 5.6 and 5.7:

$$P_{eq} = R\Delta P_1 + \Delta P_2 \tag{5.8}$$

Finally, the different equations representing supply pressure set point for the different modes 2.38, 2.41, and 2.43 can be unified in one expression using valve switching functions

as follows:

$$Ps_{setpoint} = \frac{\Delta P_{min}}{\frac{S_a+1}{2}R - \frac{S_a+S_b}{2}} + \frac{\frac{S_a+1}{2}(RP_a - P_b) + \frac{S_a-1}{2}(RP_a - P_b)}{\frac{S_a+1}{2}R - \frac{S_a+S_b}{2} + \frac{1-S_a}{2}} + \frac{\frac{1-S_a}{2}R + \frac{1-S_b}{2}}{\frac{1-S_b}{2}R + \frac{1-S_a}{2} + \frac{S_a+S_b}{2}} P_r \tag{5.9}$$

The simplification enabled by these valve switching functions unifies the representation of the system and makes simulations and programming of these equations straightforward. They are used in the computer simulations in section 5.5.

5.3 Second Order Dynamic Model for Electro Hydraulic Poppet Valves (EHPV)

In order to simulate the dynamics of a hydraulic actuator controlled by a four-valve independent metering configuration, a dynamic model for the individual poppet valves is needed. Extensive work is being done to accurately model these valves and to perform online correction and estimation of the valve conductance coefficient value as a function of electric current input based on neural networks [59, 60]. However, For the purposes of modeling and simulating the dynamics of hydraulic actuator needed for this dissertation, a simplified second order model is developed and validated experimentally in this section. This model was developed and validated experimentally by Georgia Tech fellow researcher Patrick Opdenbosch. It is his conclusion that the second order model presented in this section matches the experimental results well.

5.3.1 EHPV Components and Operation

Figure 5.3 shows EHPV construction and components. Details of the working principles of EHPV can be found in references [97, 90, 95, 96]. A brief description of operation basics of EHPV are described next.

The EHPV consists of two stages: the first stage of the valve includes a main poppet, a pressure compensation mechanism consisting of a compensating piston, and a spring. The second stage houses the armature and the pilot pin. These two stages are separated by a pressure control chamber. In order to achieve flow through the valve, high pressure flow is delivered through a small passage in the main poppet to the control chamber. When

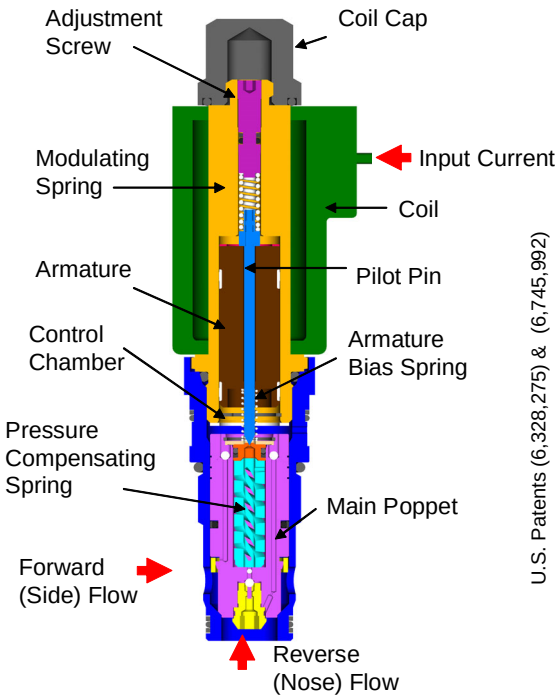

Figure 5.3: Flow directions

the solenoid is activated by an electric current, the pilot pin is pulled and fluid flows from the control pressure chamber through the piston and tubular spring to the low pressure side. This causes the pressure in the control chamber to decrease. The resulting pressure imbalance across the main poppet displaces the main poppet away from the valve seat creating a direct passage between the inlet and outlet connections of the valve. EHPV has bidirectional flow capability because the control can receive high-pressure flow from either port of the valve.

5.3.2 A Simplified Second Order Model

The approach taken here is modeling the valve as a linear second order parametric model with a nonlinear gain, where the nonlinear gain represents the steady state response of the valve. The nonlinear gain is a function of input solenoid current, pressure drop across the valve, and whether the valve is in forward or reverse flow $f(i_{sol}, \Delta P, \Phi)$. $\Phi = +1$ when the valve is in forward flow mode, and $\Phi = -1$ when the valve is in reverse flow mode. Refer to figure 5.3 for flow direction convention. The nonlinear gain is also a function of

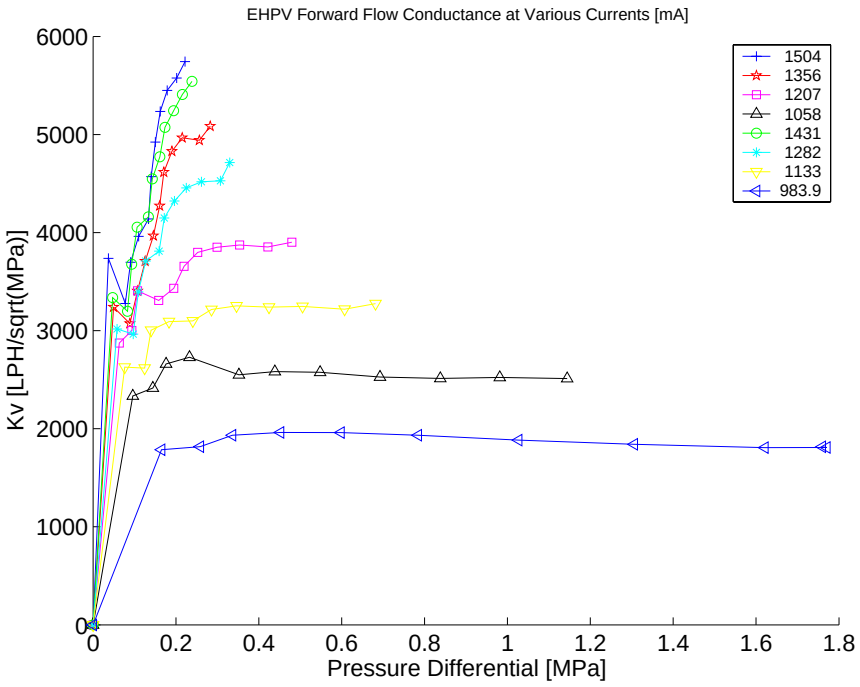

Figure 5.4: Valve conductance K_v for forward flow as a function of pressure drop and solenoid current

oil temperature. However, since temperature effects were insignificant, temperature was neglected in the nonlinear gain representing the steady state response.

The input to the model is the current sent to the solenoid i_{sol}, and the output of the model is the valve's flow conductance parameter K_v. The simplified mathematical model is accordingly:

$$\ddot{K}_v + 2\zeta\omega_n\dot{K}_v + \omega_n^2 K_v = \omega_n^2 f(i_{sol}, \Delta P, \Phi) \tag{5.10}$$

5.3.3 Experimental Validation of Second Order Model with Nonlinear Gain

Experimental dynamic data are needed to optimize the coefficients of the parametric linear model. Steady state data are required to generate the nonlinear gain. Data are collected from the EHPV at several input solenoid current values. The steady state values of valve conductance K_v as functions of pressure drop and input solenoid current in *milliamps* are shown in figure 5.4 and 5.5 for forward and reverse flow respectively. It can be noticed that from pressure drops greater than $0.4MPa$, K_v is merely a function of the input solenoid current.

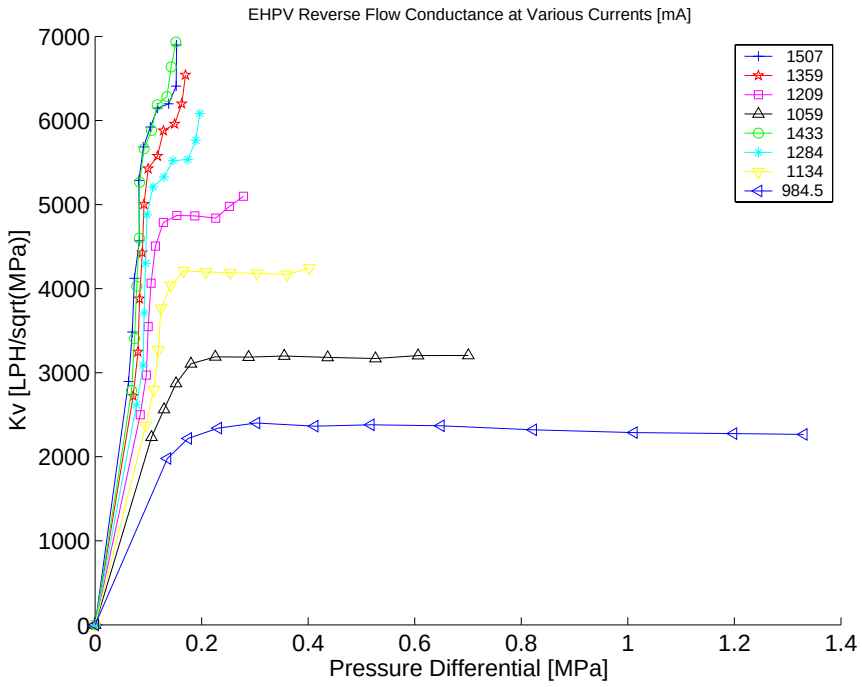

Figure 5.5: Valve conductance K_v for reverse flow as a function of pressure drop and solenoid current

If the pressure drop across EHPV is maintained above $\Delta P = 0.4\,MPa$ then valve conductance K_v is not a function of pressure drop as shown in both figures above. Consequently, the model can be further simplified to:

$$\ddot{K}_v + 2\zeta\omega_n\dot{K}_v + \omega_n^2 K_v = \omega_n^2 f(i_{sol}, \Phi) \tag{5.11}$$

The natural frequency of the valve is found to be $\omega_n = 72.05\,rad/sec$ and damping ratio is found to be $\zeta = 1.25$

It is worth noting that in figures 5.4, 5.5 when the current is higher than $1300\,mA$, and due to power limitation on the test bench, it is not clear that valve conductance ceases to be a function of ΔP. Hence, the nonlinear gain for this range of currents is furnished from manufacturer's (HUSCO International) data according to figure 5.6

To validate the mathematical model, the step response of the valve is obtained experimentally and compared to model prediction for various input currents. Forward flow comparison is shown in figure 5.7 and reverse flow comparison is shown in figure 5.8. The experimental data is passed through a filter with $25\,Hz$ cutoff frequency to attenuate the

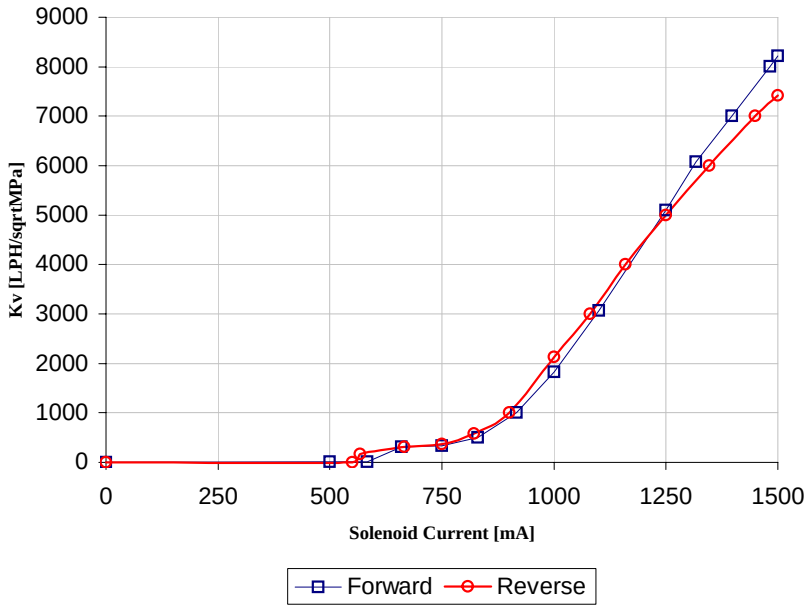

Figure 5.6: Valve conductance as a function of solenoid current (manufacturer's data)

noise effect.

5.4 Actuator Dynamic Model

5.4.1 General

In order to do analysis and draw sound conclusions on the dynamic behavior of a hydraulic actuator controlled by four-valve assembly, it is necessary to develop a dynamic model. This dynamic modeling process involves constructing a control volume around the system and applying fundamental laws such as conservation of momentum and mass to describe the system in the form of differential equations.

To depict this system as accurately as possible, the model has to take into consideration nonlinearities inherent in hydraulic systems as well as compressibility effects. Computer is then necessary to simulate the system. In order to validate the model, its prediction has to be compared to experimental results, which is done in section 5.5.

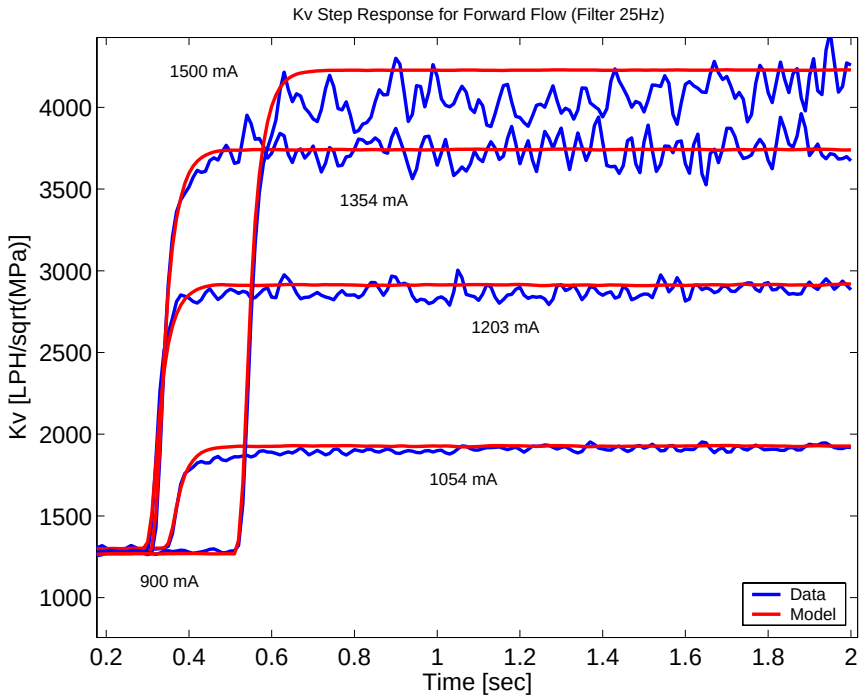

Figure 5.7: **Experimental results versus model for forward flow valve conductance** K_v

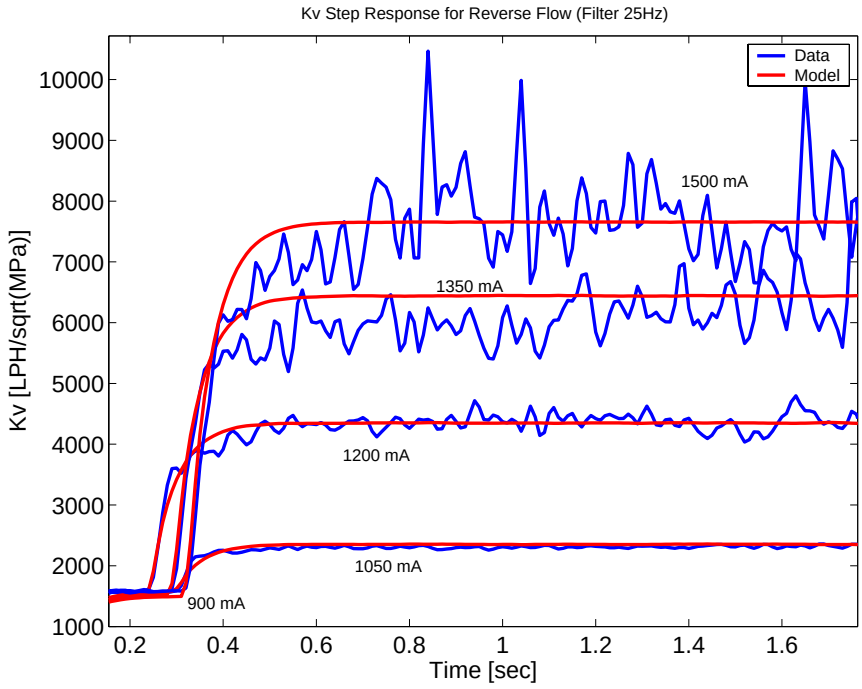

Figure 5.8: **Experimental results versus model for reverse flow valve conductance** K_v

5.4.1.1 Assumptions

In any modeling process, some assumptions have to be made to restrict the applicability of the model. The following major assumptions are made:

1. The orifice edges of the poppet valves are assumed to be sharp edges.
2. Flow through the poppet valve is assumed to be a simple orifice type inviscid flow and that the square root relationship between flow and pressure applied $Q = K\sqrt{\Delta P}$ [53].
3. There is not time delay between a change in pressure or orifice area and the corresponding change in flow.
4. Fluid inductance is ignored i.e. pipes are assumed to be short and wide.
5. Hydraulic oil Bulk Modulus is assumed to be constant across the operation range of pressure.
6. It is assumed that the temperature of the system remains constant, which is called isothermal condition. In this case the energy equation is not necessary since it does not add new information to the other equations.
7. Hydraulic line losses are neglected.

5.4.2 Dynamic Model Derivation

The dynamic model of the system shown in figure 5.9 is derived next. A general model is developed regardless of which mode the system is operating in. The dynamics of the system shown in figure 5.9 include the dynamics of the oil path from a pressure source (a variable displacement pump) through a poppet valve to a piston that has some differential pressure across it that depends on the load, and subsequent return of oil to a tank through another poppet valve. This path, consequently, contains oil lines, poppet control valves, and expanding and compressing chambers (volumes). Poppet valves have their own dynamics explained earlier in the chapter and will be included in the simulations. Valve openings are considered the input to the model developed here.

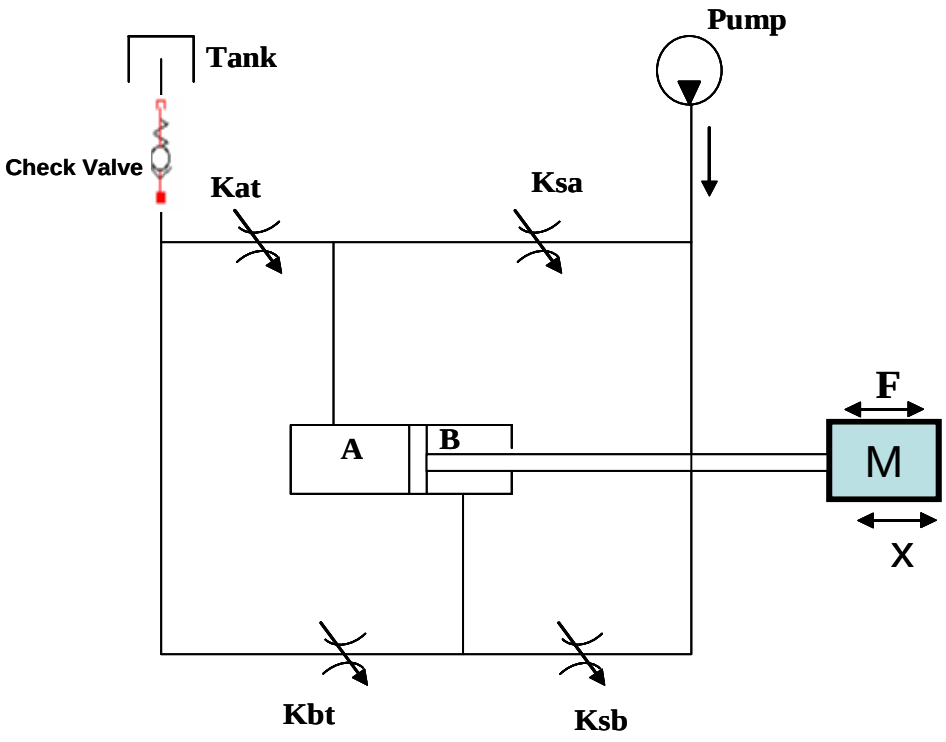

Figure 5.9: Independent metering four-valve configuration controlling a hydraulic cylinder

Orifice Flows: Assuming a turbulent flow, the following square root relationship between flow and pressure can be used [53]

$$\begin{aligned} Q_{sa} &= K_{sa}\sqrt{|P_s - P_a|}sgn(P_s - P_a) \\ Q_{sb} &= K_{sb}\sqrt{|P_s - P_b|}sgn(P_s - P_b) \\ Q_{at} &= K_{at}\sqrt{|P_a - P_r|}sgn(P_a - P_r) \\ Q_{bt} &= K_{bt}\sqrt{|P_b - P_r|}sgn(P_b - P_r) \end{aligned} \tag{5.12}$$

Compressibility:

$$\begin{aligned} Q_{ca} &= \frac{CV_a}{B_e}\dot{P}_a \\ Q_{cb} &= \frac{CV_b}{B_e}\dot{P}_b \end{aligned} \tag{5.13}$$

where,

$$\begin{aligned} CV_a &= V0_a + A_a x \\ CV_b &= V0_b - A_b x \end{aligned} \tag{5.14}$$

$V0_a$ is the initial volume of head chamber (a), and $V0_b$ is the initial volume of rod chamber (b)

Conservation of Mass:

$$Q_{sa} - Q_{at} - Q_L = Q_{ca} + A_a\dot{x}$$
$$Q_{sb} - Q_{bt} + Q_L = Q_{cb} - A_b\dot{x} \tag{5.15}$$

Where Q_L is the leakage flow from one chamber to the other around the piston, which is too small and it will be neglected.

The following equations result:

$$K_{sa}\sqrt{|P_s - P_a|}sgn(P_s - P_a) - K_{at}\sqrt{|P_a - P_r|}sgn(P_a - P_r) = \frac{CV_a}{B_e}\dot{P}_a + A_a\dot{x} \tag{5.16}$$
$$K_{sb}\sqrt{|P_s - P_b|}sgn(P_s - P_b) - K_{bt}\sqrt{|P_b - P_r|}sgn(P_b - P_r) = \frac{CV_b}{B_e}\dot{P}_b - A_b\dot{x} \tag{5.17}$$

Conservation of Momentum:

$$P_aA_a - P_bA_b = M\ddot{x} + F + F_f \tag{5.18}$$

Where F is the external force applied on the piston and can be dependent on position. F_f is the cylinder friction force.

5.4.2.1 Cylinder Friction

Cylinder friction estimation is a difficult issue that has gained research attention for a long time. As performance requirements increase and technology progresses, accurate estimation of friction in mechanical parts becomes more of an important issue. Adaptive controllers in high performance machines need to estimate friction in order to adapt to changes. Changing the metering mode of certain function changes the pressure in both chambers of the cylinder. Bonchis et al. argued that friction force depends heavily on chamber pressures [3]. It was shown that a model of the following format gives a very accurate estimation of friction in hydraulic cylinders:

$$F_f = a_1e^{a_2v} + a_3(P_a - P_b) + a_4P_b + a_5v \tag{5.19}$$

Where: F_f is friction force acting on the piston, $a_1 \dots a_5$ are coefficients to be determined, P_a and P_b are workport pressures in the two cylinder chambers, and v is piston

speed. Bonchis further proved that an accurate model can be obtained by ignoring the terms including the speed v. In this dissertation, just the first term is ignored and the the model used is accordingly reduced to:

$$F_f = a_1(P_a - P_b) + a_2 P_b + Cv \tag{5.20}$$

Where a_1, a_2, and C, which is viscous friction parameter, are all determined experimentally.

5.4.3 State Space Representation

This system can be considered as a multi-input system where the inputs are valve conductances: K_{sa}, K_{sb}, K_{at}, and K_{bt}. The equations above can be easily expressed in state space format of the form:

$$\dot{x} = f(x, u) \tag{5.21}$$

Consequently, the following set of first order differential equations can be written and will be used for simulation and analysis. The state variables are actuator position, actuator speed, and workport pressures.

$$\begin{aligned}
x_1 &= x \\
x_2 &= \dot{x} \\
x_3 &= P_a \\
x_4 &= P_b \\
\dot{x_1} &= x_2 \\
\dot{x_2} &= -F_{ext} - \frac{Cx_2}{M} + \frac{(A_a - a_1)}{M} x_3 + \frac{(a_1 - a_2 - A_b)}{M} x_4 \\
\dot{x_3} &= \frac{B_e}{CV_a}\left[K_{sa}\sqrt{P_s - x_3} - K_{at}\sqrt{x_3 - P_r} - A_a x_2\right] \\
\dot{x_4} &= \frac{B_e}{CV_b}\left[K_{sb}\sqrt{P_s - x_4} - K_{bt}\sqrt{x_4 - P_r} + A_b x_2\right]
\end{aligned} \tag{5.22}$$

Supply pressure P_s depends on the mode, but could be represented with a single equation using valve switching functions as shown in equation 5.9.

5.4.4 Model for a Two-Actuator System

In mobile hydraulic environments, systems usually have more than one actuator operating simultaneously. A two actuator system is shown in figure 5.10. An example would be the

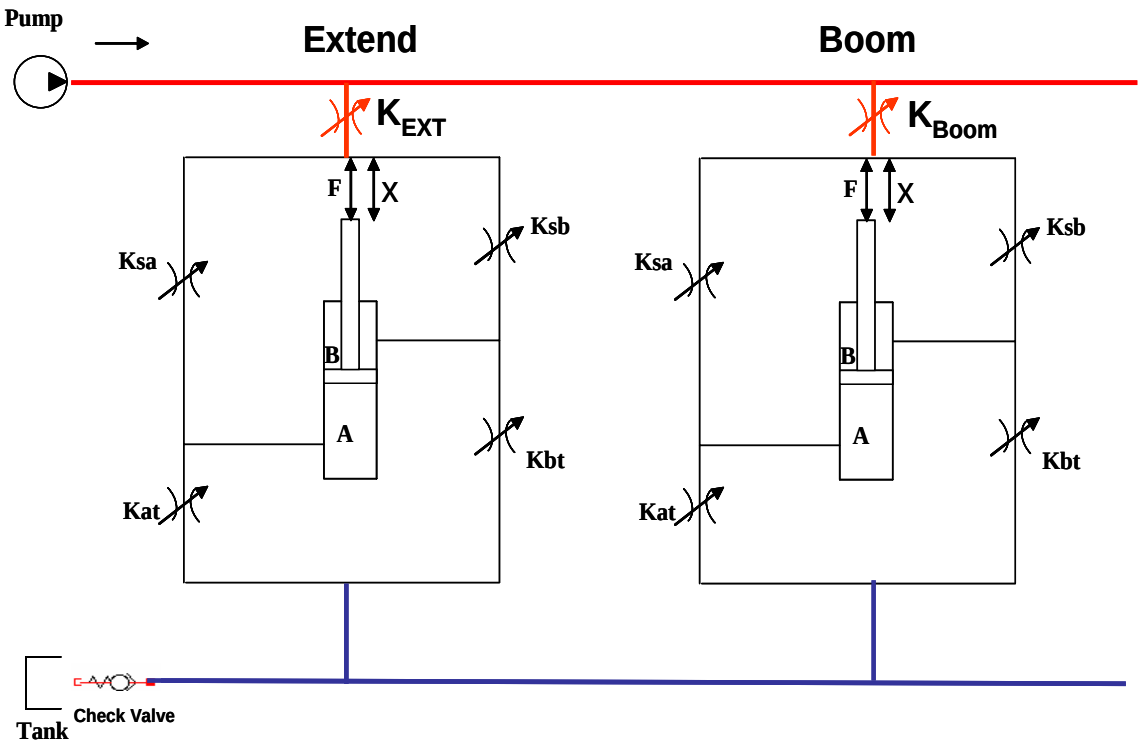

Figure 5.10: A two-actuator system

extender and boom functions of the telehandler operating at the same time.

Model derivation in this case is very similar to a one actuator model derivation. Instead of having four states, piston position, piston speed, and workport pressures for a single actuator, the model would have eight states the additional four being the same states for the other actuator.

The dilemma is in supply pressure set point calculations. For single actuator model, the supply pressure set point is calculated and then it is assumed that the pump would supply that pressure. For two actuators operating simultaneously, each one of them has its own requirement for supply pressure. One of them requires a higher pressure than the other depending on the load and speed required from it. The pump should supply that higher pressure. But the other actuator that requires the lower supply pressure cannot operate at the higher supply pressure since it would make velocity calculations and valve conductances erroneous.

In practice, the poppet valves are modulated and restricted in order to accommodate the higher pressure and achieve the same required speed. To accommodate this in modeling, the system is treated as if another valve exists in the flow path from the pump to the four-valve assembly and actuator. This other valve is assumed to drop the pressure to the required pressure set by the actuator. This valve is represented in figure 5.10 by K_{Ext} and K_{Boom}. With this assumption, both actuator operate independently and it is as if they are separate actuators modeled by the equations presented in section 5.4.2.

5.5 Experimental Validation

To validate the dynamic model derived in the previous section, the telehandler machine shown in figure 5.11 is used. A schematic of this machine is also shown in figure 5.12 pointing out the extender and boom cylinders of the machine. Both the extender and boom functions of this telehandler are used in the following chapters for experimental work. Therefore, the dynamic model is validated through experimental results from both of these functions to justify the use of the model when either functions is utilized. For example, the extend function is used in the optimal switching experiments in chapter 6, while the boom function is used for vibration analysis in chapter 7.

The experiments presented in this section were repeated several times to ensure repeatability. The results presented are representative samples of these experiments.

5.5.1 Parameter Estimation

The model parameters were estimated based on:

- Data given by manufacturers
- Experimental measurements
- Some parameters, like friction model variables a_1, a_2, and viscous friction parameter C in equation 5.20 cannot be measured directly. These were estimated and tuned by comparing model simulation results with experimental data and trying to minimize the discrepancy between them.

Figure 5.11: Telehandler Machine

System characteristics and model parameters are shown in table 5.1. The effective bulk modulus used is a value that leads to reliable results and takes into consideration that there is some trapped air in the fluid that decreases its bulk modulus [53].

5.5.1.1 Mass Estimation

To estimate the mass of the fork, which is important when simulating the extender cylinder, the boom cylinder is extended and the angle between the boom and a horizontal line is measured. Then while the boom is at that specific angle and the extender cylinder is extended slightly and both workport pressures are recorded. Given the cylinder geometries from the manufacturer's data and with simple calculation, the mass that the extender cylinder sees can be estimated from:

$$P_a A_a - P_b A_b = mg \sin\theta \tag{5.23}$$

This is shown in figure 5.13.

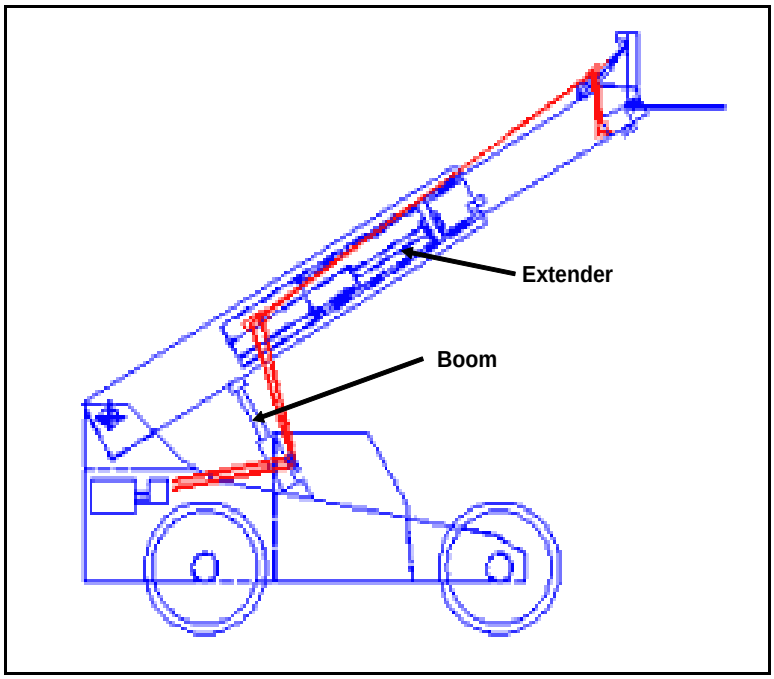

Figure 5.12: Schematic of the telehandler machine with extender and boom cylinders point out

5.5.2 Extender Cylinder Simulations

The boom of the machine is positioned horizontally so that the external load on the extender due to gravity is approximately zero. The joystick that controls the motion was moved to its extreme position, which translates into requiring highest speed possible by cylinder for this mode. The experimental results for the full stroke of the extender performed fully in Powered Extension mode along with the corresponding model predictions are shown in figures 5.14 and 5.15. The valve conductance coefficients K_{sa} and K_{bt} are compared in figure 5.14, while velocity and workport pressures are compared in figure 5.15. It is noticed that the load on the extender is increasing due to the increase in structural friction as the length of the extender increases and becomes more cantilevered. That is why the workport pressures of the experimental results increases as time passes and the cylinder is further extended.

The same motion was repeated in High Side Regeneration Extension mode and the results are shown in figures 5.16 and 5.17.

Table 5.1: System Characteristics and Model Parameters

Parameter	Value	Units
P_s Supply pressure	$2.9 - 25.6$	MPa
B_e Bulk Modulus	689.476	MPa
A_a Head area for Extender	3848	mm^2
A_b Rod area for Extender	9444	mm^2
Extender Cylinder Stroke	2350	mm
A_a Head area for Boom	12272	mm^2
A_b Rod area for Boom	$9444e$	mm^2
Extender Cylinder Stroke	845	mm
a_1 Friction Coefficient	$7.1400e - 06$	mm^2
a_2 Friction Coefficient	475.03	mm^2
C_Ext Viscous Friction Coefficient for Extender	10000	$N.s/m$
C_Boom Viscous Friction Coefficient for Boom	90000	$N.s/m$
M Mass (Pushed by Extender)	478.4	Kg

In both cases, in the dynamic model simulation the initial conditions for pressures are set to zero. However, in the real experiment the chamber pressures are whatever the trapped pressures are before the experiment started, hence the difference in pressures at the beginning of motion.

It remains to test the model validity when switching modes after motion commenced. In other words, the cylinder starts to operate in PE mode, for example, and then at some point in the stroke, mode is switched to HSRE to achieve higher speed. Again, an experiment is done on the extender where mode switching happens in mid-stroke. The valve conductance coefficients K_{sa} and K_{bt} are compared in figure 5.18, while velocity and workport pressures are compared in figure 5.19.

5.5.3 Boom Cylinder Simulations

Boom motion is more complicated. In the extender case, the boom has been positioned horizontally so that external forces that the extender pushes against are almost non existent, and only inertia effects are taken into consideration. In the case of boom motion, the mass and the external force that the cylinder has to push against change with the angle of the boom.

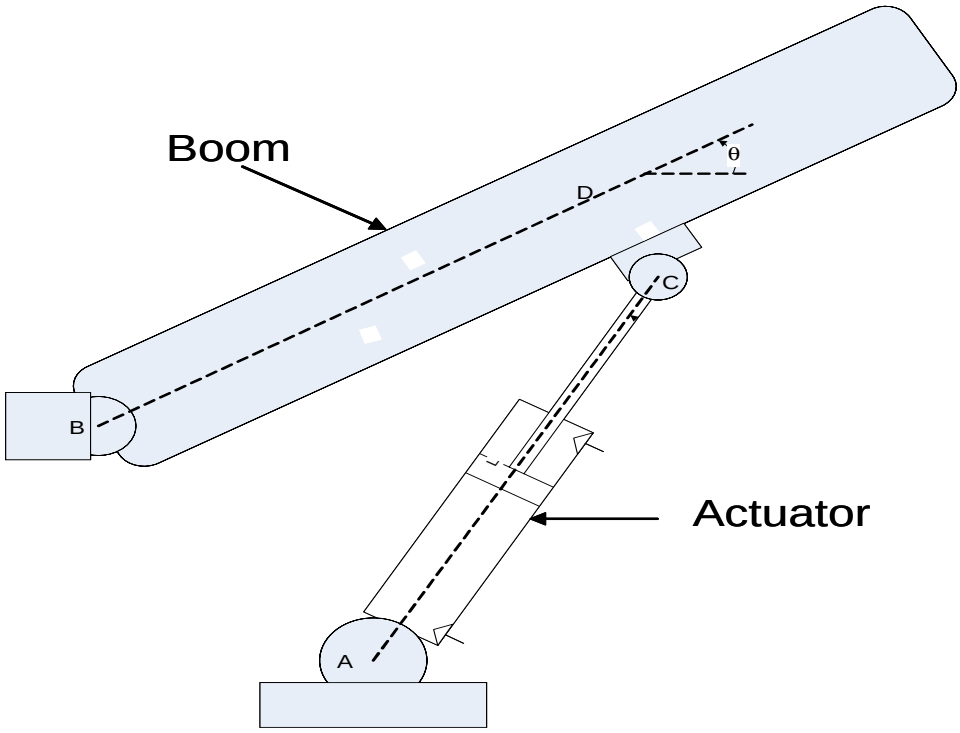

Figure 5.13: Boom motion

A separate test is done where the boom is positioned at different angles and the workport pressures are recorded along with angles. The angles correspond to boom actuator displacement. Consequently, a map between boom displacement and external force is constructed. The schematic is shown above in figure 5.13.

The joystick that controls the boom motion is moved to its extreme position, which translates into requiring highest speed possible by cylinder for this mode. The experimental results for the full stroke of the boom cylinder performed fully in Powered Extension mode along with the corresponding model predictions are shown in figures 5.20 and 5.21.

It is noted that the return pressure P_b is almost constant throughout the stroke, while P_a changes. P_a starts out with a large value because when the boom cylinder is fully retracted and the fork of the telehandler is touching the ground, a large force is needed to move the boom arm. As, boom moves up and the angle with the horizontal is positive the load decreases and that cause P_a to decrease.

It is noted that experimental workport pressures do not start from zero value like the

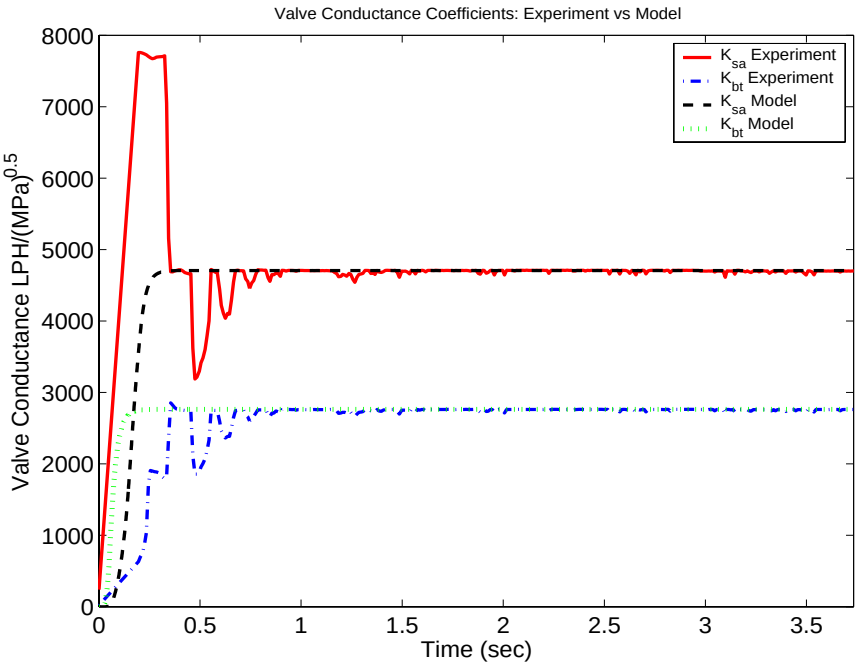

Figure 5.14: Valve conductance coefficients K_{sa} and K_{bt} experimental results versus model prediction for full extender stroke in Powered Extension Mode

model, where initial condition are chosen to be zero, and that explains the initial discrepancy. The model head chamber pressure P_a jumps almost instantaneously to provide the pressure difference needed for initial motion and acceleration

If the boom cylinder is in a fully retracted position, the load that the cylinder need to push to commence motion is very large and beyond the force capability of HSRE mode. HSRE mode capability is discussed in section 4.4.1 and is elaborated upon in chapter 6. As a consequence, the cylinder cannot perform the full stroke in HSRE. However, switching between PE and HSRE is important. Since high load is needed at the beginning of motion, the cylinder can start in PE mode to be able to provide high force capability. Then when not so much force is needed and a higher speed is more desirable, switching to HSRE is plausible. This scheme is studied in detail in chapter 7 along with the effect of this switching on the vibration of boom. Experimental results for boom clinder switching in mid motion is presented in chapter 7.

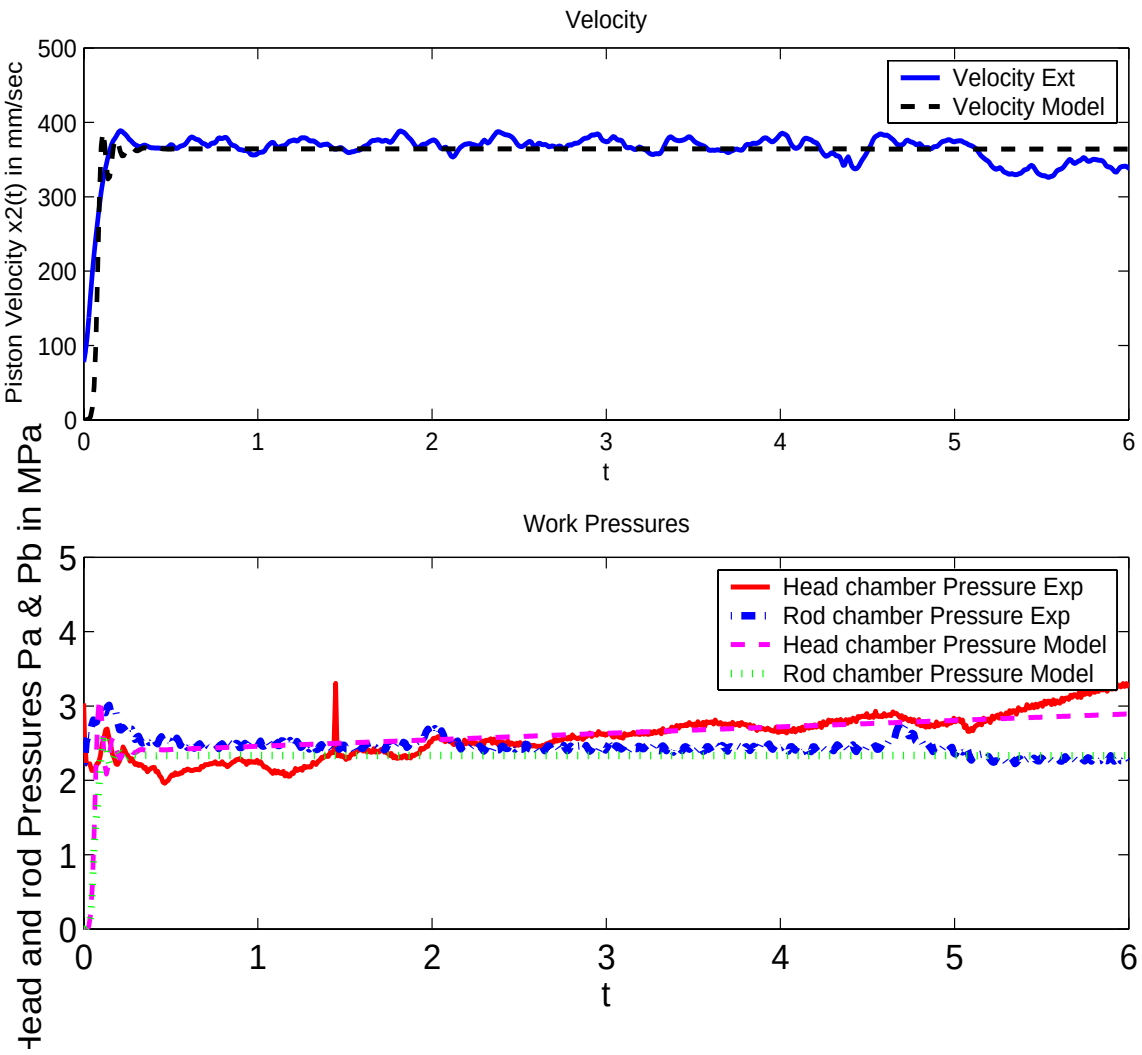

Figure 5.15: Velocity and workport pressures experimental results versus model prediction for full extender stroke in Powered Extension Mode

5.5.4 Remarks on Model Validity

From the plots in sections 5.5.2 and 5.5.3, it can be concluded that the model is credible. There are some factors that can explain the imperfect matching:

- Increase in structural friction of the vehicle as the cylinder extends.
- The joystick commands are essentially required velocities. These commands are translated into individual valve conductance values as explained in chapter 2. These control signals are under open loop control and thus there is no measure of how close the actual

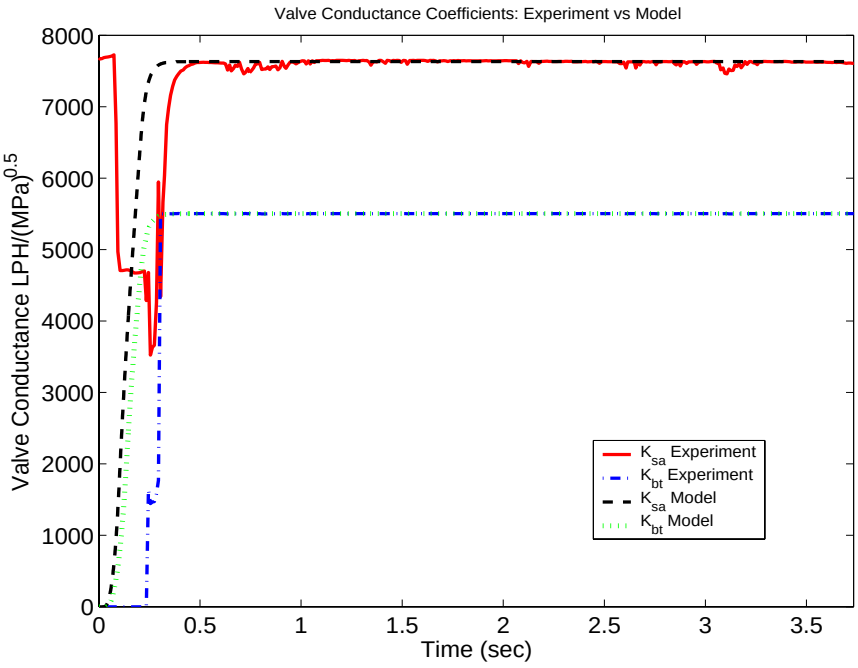

Figure 5.16: Valve conductance coefficients K_{sa} and K_{sb} experimental results versus model prediction for full extender stroke in High Side Regeneration Extension Mode

valve conductances are to the commanded signals.

- It has been stated in the assumptions sections that the model assumes that a change in orifice openings or pressure drop corresponds to instantaneous change in flow. A pure time delay inserted in the model might enhance the model prediction, but would add unnecessary complication for further dynamic analysis. Furthermore, if the system is assumed to be a linear time invariant systems, this time delay amounts to a response shift in time. Therefore, using a delay-fee model as a useful tool for further analysis is a very reasonable assumption.

- Supply pressure depends on workport pressures, i.e. load. If a load change happen and pressure set point is changed, the pump has to supply that new pressure with some dynamics inherent in its response characteristics. In the model, it has been assumed that this new supply pressure is achieved instantaneously and ignores the pump dynamics, since emphasis here is on the hydraulic actuator and the valves driving it. Pump dynamics are very fast yet this can still make a difference between

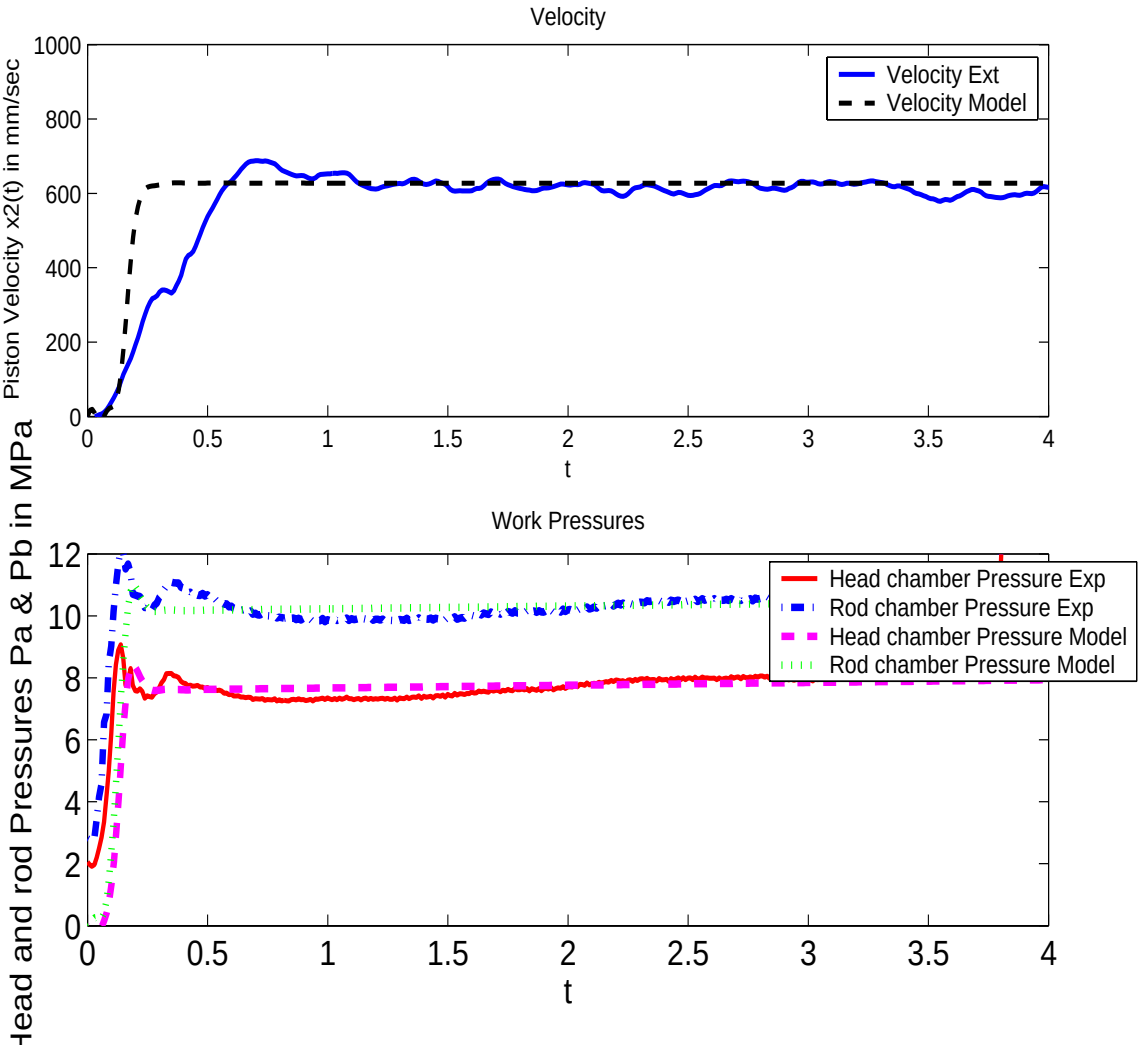

Figure 5.17: Velocity and workport pressures experimental results versus model prediction for full extender stroke in High Side Regeneration Extension Mode

the model and experimental results.

In conclusion, analytical results will not match experimental results perfectly. However, it is safe to say that the model matches the experimental results well enough and that it is practical to use it for further analysis.

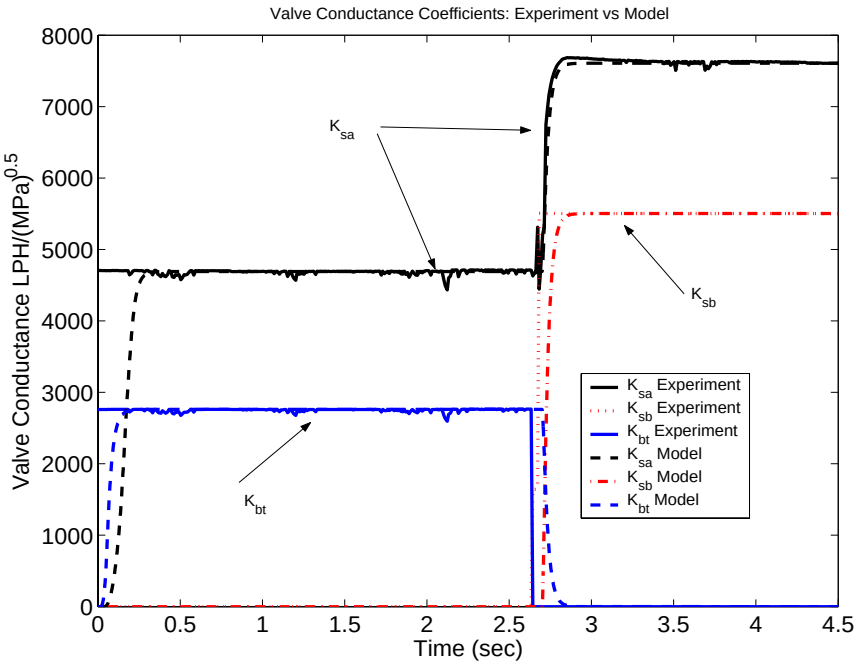

Figure 5.18: Valve conductance coefficients K_{sa}, K_{sb}, and K_{bt} experimental results versus model prediction for extender stroke starting in PE and switching to HSRE in mid-stroke

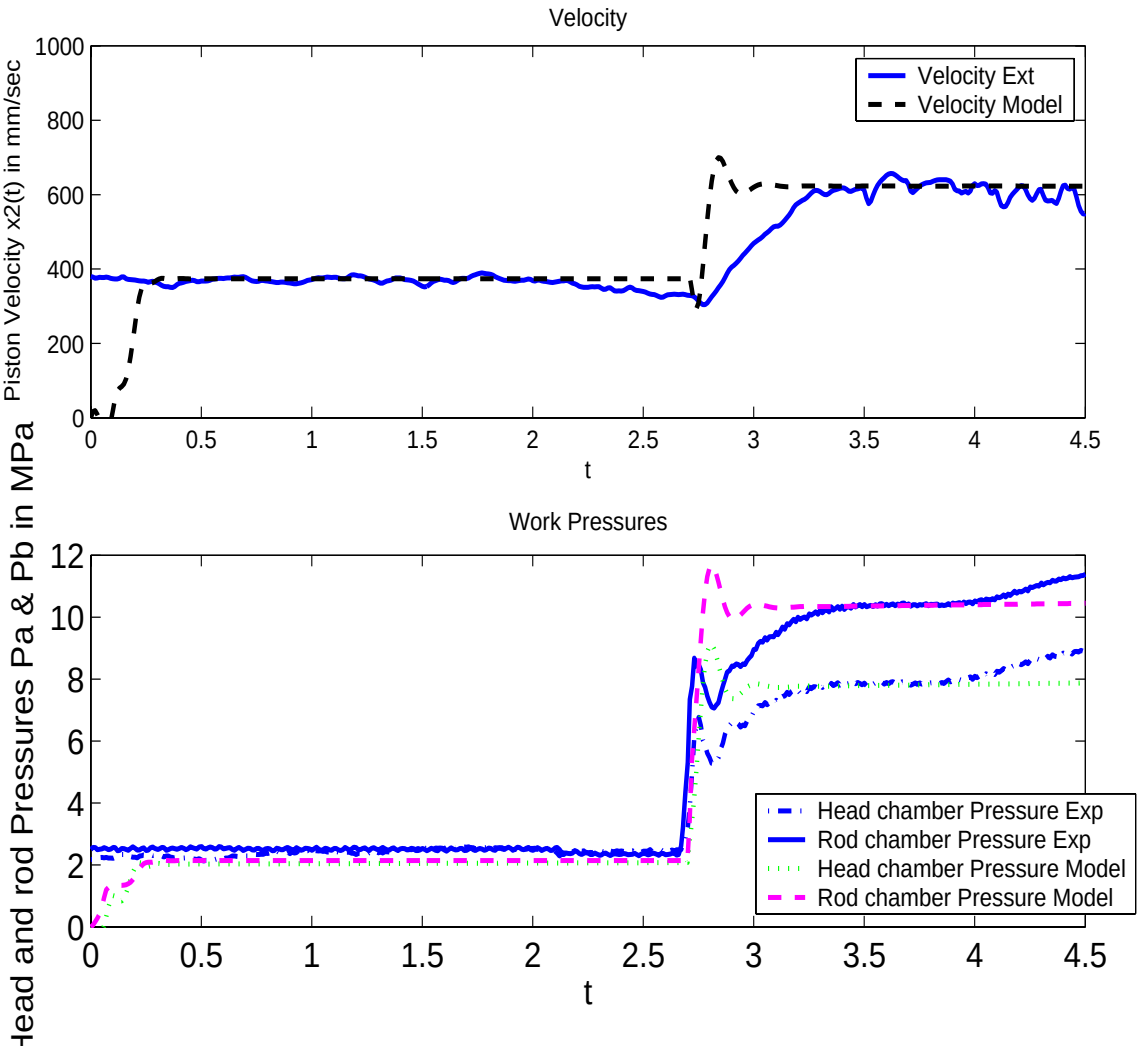

Figure 5.19: Velocity and workport pressures experimental results versus model prediction for extender stroke starting in PE and switching to HSRE in mid-stroke

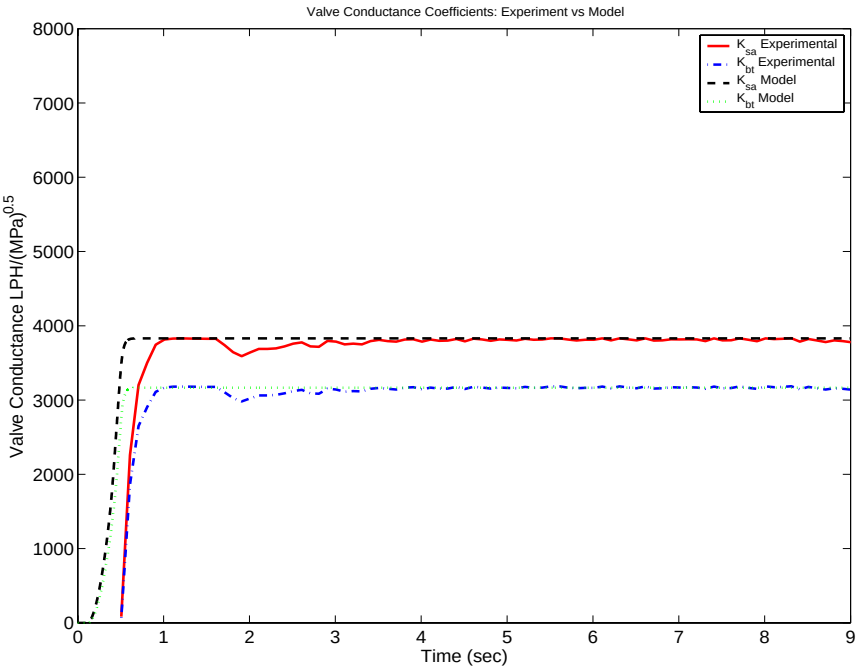

Figure 5.20: Valve conductance coefficients K_{sa} and K_{bt} experimental results versus model prediction for full boom cylinder stroke in Powered Extension Mode

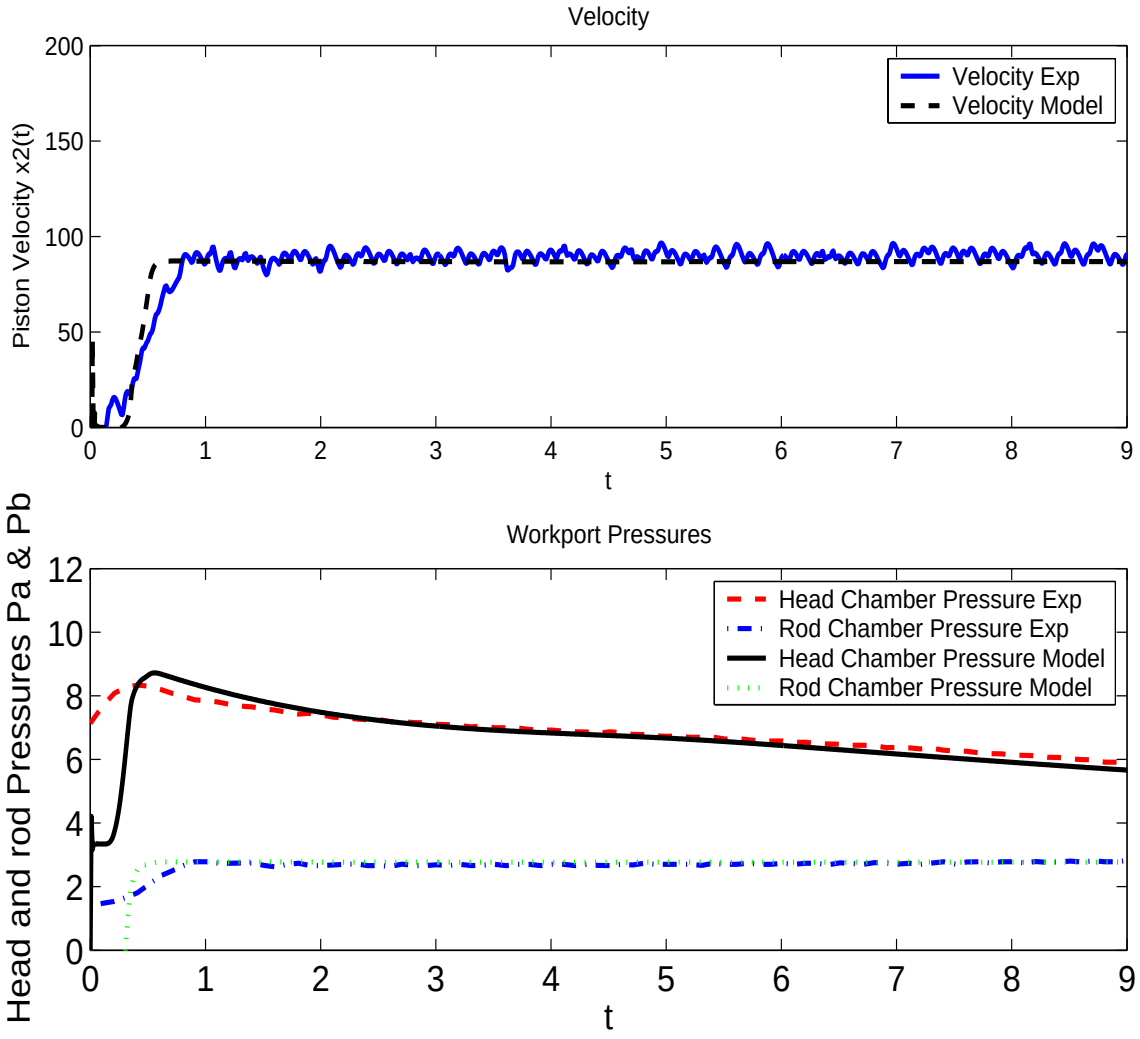

Figure 5.21: Velocity and workport pressures experimental results versus model prediction for full boom cylinder stroke in Powered Extension Mode

CHAPTER VI

OPTIMAL MODE SWITCHING

6.1 General

This chapter studies optimal mode switching. Specifically, it looks at the problem of switching between two modes as a problem of optimal switching of a switched dynamic system. This chapter develops the general theory for this problem first and then uses the dynamic model of chapter 5 to apply the theoretical results to the mode switching problem of the hydraulic system under investigation in this research. What complicates this mode switching problem is that not only the dynamics of the system changes upon mode switching, but the cost functional of the optimal control problem changes as well. Results are applied to switching of one actuator and then to switching of two actuators operating at the same time in a mobile hydraulics-like environment. The results of this chapter show that mode switching bears resemblance to automotive automatic transmission gear shifting. This analogy is built in this chapter and is used to inspire a real time algorithm for mode switching.

6.2 Switched Dynamic Systems

A switched dynamic system is such that its dynamic behavior can be described by a finite number of dynamic models, in the form of differential equations, and a set of rules that controls switching between these different dynamic models. These dynamic models describe discrete system behaviors with different characteristics.

The hydraulic system in this research can be portrayed as a switched dynamic system that has different dynamic behaviors based upon which metering mode it is operating in. For example, an actuator can start motion in PE mode then switches to HSRE mode, which has different dynamic behavior than PE with different force and speed capabilities.

The following mathematical expression is often used to describe switched dynamical

systems:

$$\dot{x}(t) \in \{f_\sigma(x(t), u(t))\}_{\sigma \in A} \tag{6.1}$$

where $x(t) \in \mathbb{R}^n$, $u(t) \in \mathbb{R}^k$, and $\left\{f_\sigma : \mathbb{R}^{n+k} \to \mathbb{R}^n\right\}_{\sigma \in A}$ is a group of continuously differentiable functions parameterized by σ which $\in$ a set A [24]. Time t is between 0 and T. Many applications in chemical, automotive, and manufacturing systems can be modeled by such switched systems representation [94].

Optimal control of these switched dynamical systems, which requires finding the optimal switching time between different continuous systems and at the same time the optimal continuous inputs has been under research recently [94, 13, 7, 36, 18, 43, 31, 46, 75, 67, 77, 86, 92] because of its importance in several applications. Control analysis and stability of such systems to achieve autonomous and intelligent control are under intense research activities. The reference mentioned here and the references therein are a good example of recent developments in the literature.

The work here, however, focuses on a class of autonomous systems where $u(t)$ is absent from the problem formulation because it is predetermined, and the variable to be controlled optimally is the switching time [33, 93].

In [93], an optimization problem is setup in terms of a cost functional of the state to be minimized with the control variable being the switching times. The results are then used for nonlinear programming algorithms. This reference provides a starting point for later work. However, a simpler cost functional gradient formula is derived here.

This optimal control problem where the cost function is the same throughout the time interval under consideration but the dynamics of the system change after a certain switching time has been considered and a simple solution has been found [24]. In the problem considered in this research, the cost function itself changes after switching happens not just the dynamics of the system. If the hydraulic system switches from PE to HSRE, the dynamics of the system change and also the pressure and flow characteristics change. If the cost functional is a function of pressure and flow, then the cost functional itself changes upon mode switching. This is going to be explained further in the problem formulation section.

6.2.1 Problem Formulation

Assume that a system behaves according to certain dynamics $\dot{x} = f_1(x,t)$ and then at time $\tau \in [0,T]$ the system dynamics change to $\dot{x} = f_2(x,t)$. This can be expressed by the following:

$$\dot{x} = \begin{cases} f_1(x,t) & t \in [0,\tau) \\ f_2(x,t) & t \in [\tau,T] \end{cases} \tag{6.2}$$

Now consider a continuously differentiable function $L : \mathbb{R}^n \to \mathbb{R}$ and the cost functional J where:

$$J = \int_0^T L(x(t))dt \tag{6.3}$$

In this problem we consider the control variable to be the switching time τ. If $L(x(t))$ is the same through out the time interval $[0,T]$, the solution to this optimal problem already exists in the literature [24, 75, 77, 93]. The gradient of J is found to be:

$$\frac{dJ}{d\tau} = \lambda(\tau)\left(f_1(x(\tau)) - f_1(x(\tau))\right) \tag{6.4}$$

Where the costate (Lagrange multiplier-like variable) equation is given by

$$\dot{\lambda} = -\frac{\partial L}{\partial x} - \lambda\frac{\partial f_2}{\partial x} \tag{6.5}$$

$$\lambda(T) = 0 \tag{6.6}$$

In this work, an extension is made to this result. The function $L(x(t))$ is **not** the same through out the time interval $[0,T]$. The cost functional can be expressed as:

$$J(\tau) = \int_0^\tau L_1(x(t))dt + \int_\tau^T L_2(x(t))dt \tag{6.7}$$

Thus, not the only the dynamics of the system change when switching happens, but the cost functional changes as well.

6.2.2 Gradient Calculation

In this section the gradient of the cost function J in equation 6.7 is calculated. Since τ is the control variable in this problem, consider a perturbation in τ: $\tau \to \tau + \epsilon\theta$, where $\epsilon \lll 1$.

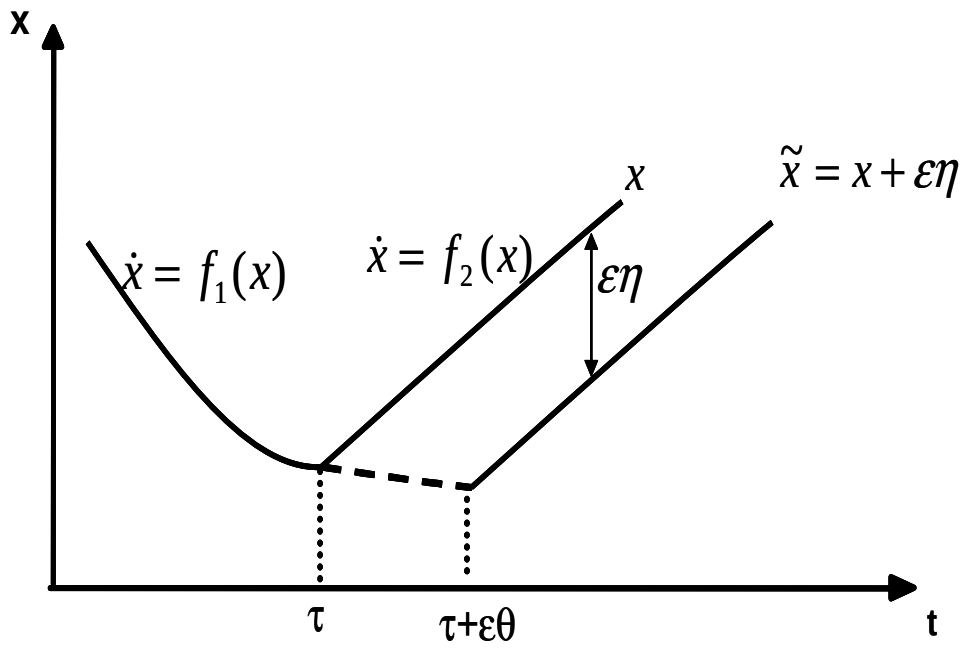

Figure 6.1: Switching and Perturbation

This perturbation in τ results in a change in the state $x \rightarrow x + \epsilon\eta$. This is shown in figure 6.1

The cost functional of the τ perturbed system is:

$$\begin{aligned} J(\tau + \epsilon\theta) = &\int_0^{\tau} [L_1(x(t)) + \lambda(f_1(x(t)) - \dot{x}(t))]dt + \\ &\int_{\tau}^{\tau+\epsilon\theta} [L_1(x + \epsilon\eta) + \lambda(f_1(x + \epsilon\eta) - \dot{x} - \epsilon\dot{\eta})]dt + \\ &\int_{\tau+\epsilon\theta}^{T} [L_2(x + \epsilon\eta) + \lambda(f_2(x + \epsilon\eta) - \dot{x} - \epsilon\dot{\eta})]dt \end{aligned} \tag{6.8}$$

$$\begin{aligned} \frac{J(\tau + \epsilon\theta) - J(\tau)}{\epsilon} = &\int_{\tau}^{\tau+\epsilon\theta} [L_1 + \frac{\partial L_1}{\partial x}\eta + \\ &\lambda(f_1 + \frac{\partial f_1}{\partial x}\eta - f_2 - \epsilon\dot{\eta}) - L_2]dt + \\ &\int_{\tau+\epsilon\theta}^{T} [\frac{\partial L_2}{\partial x}\eta + \lambda(\frac{\partial f_2}{\partial x}\eta) - \epsilon\dot{\eta})]dt \end{aligned} \tag{6.9}$$

Using mean value theorem:

$$\int_{\tau}^{\tau+\epsilon\theta} [L_1 - L_2 + \lambda(t)(f_1 - f_2)]dt = \epsilon\theta \Big[L_1(x(\tau)) - L_2(x(\tau)) + \lambda(\tau)[f_1(x(\tau)) - f_2(x(\tau))] \Big] \tag{6.10}$$

In the interval $\tau \rightarrow \tau + \epsilon\theta$ the terms multiplied by $\epsilon\eta$ are small higher order terms that can be ignored.

Using Integration by parts:

$$\int_{\tau}^{T} \lambda\dot{\eta}dt = \lambda(T)\eta(T) - \lambda(0)\eta(0) - \int_{\tau}^{T} \dot{\lambda}\eta dt \tag{6.11}$$

Note that $\eta(0) = 0$.

Obtaining the Gateaux derivative by taking the limit of the expression in equation 6.9 with respect to ϵ and combining with equations 6.10 and 6.11:

$$\begin{aligned} \delta J(\tau,\theta) = \lim_{\epsilon\rightarrow 0} \frac{J(\tau+\epsilon\theta) - J(\tau)}{\epsilon} = \\ \Big[L_1(x(\tau)) - L_2(x(\tau)) + \lambda(\tau)[f_1(x(\tau)) - f_2(x(\tau))]\Big] \\ + \int_{\tau}^{T} (\frac{\partial L_2}{\partial x} + \lambda\frac{\partial f_2}{\partial x} + \dot{\lambda})\eta dt + \lambda(T)\eta(T) \end{aligned} \tag{6.12}$$

Choosing λ (a Lagrange multiplier-like variable called costate) such that:

$$\begin{aligned} &\dot{\lambda} = -\tfrac{\partial L_2}{\partial x} - \lambda\tfrac{\partial f_2}{\partial x} \quad \textit{on } t \in [\tau, T] \\ &\lambda(T) = 0 \end{aligned} \tag{6.13}$$

the gradient is found out to be:

$$\frac{dJ}{d\tau} = L_1(x(\tau)) - L_2(x(\tau)) + \lambda(\tau)[f_1(x(\tau)) - f_2(x(\tau))] \tag{6.14}$$

Several numerical techniques can be used to obtain the optimal switching time τ_{opt}. A simple gradient descent algorithm can be used:

$$\tau_{k+1} = \tau_k - \gamma\frac{dJ}{d\tau} \tag{6.15}$$

In section 6.4 where these results are applied to the hydraulic system, a more complicated numerical technique built in `MATLAB` (Sequential Quadratic Programming) is used to calculate τ_{opt}.

6.2.2.1 Generalization to Multiple Switching Systems

The general expression for a multiple switching system can be found by following the same technique described above.

Let

$$\dot{x} = f_i(x(t)) \; on \; t \in [\tau_{i-1}, \tau_i], \; i = 1, 2, \cdots N \tag{6.16}$$

The gradient is found to be:

$$\frac{dJ}{d\tau_i} = L_i(x(\tau_i)) - L_{i+1}(x(\tau_i)) + \lambda(\tau_i)[f_i(x(\tau_i)) - f_{i+1}(x(\tau_i))] \tag{6.17}$$

Where the costate equation is obtained as follows:

$$\begin{aligned} \dot{\lambda} &= -\frac{\partial L_{i+1}}{\partial x} - \lambda \frac{\partial f_{i+1}}{\partial x} \quad on \; t \in [\tau_i, \tau_{i+1}] \\ \lambda(T) &= 0 \end{aligned} \tag{6.18}$$

6.3 Mode Capability: More on PE and HSRE Force-Speed Capabilities

In this section, the force and speed capabilities of modes are studied. Specifically, the force-speed characteristics of PE, HSRE, and LSRE are studied and compared. These characteristics are important to understand the optimal switching results as discussed in section 6.4. A quasi-static assumption is made here as well, and hydraulic line losses are neglected in the analysis

The speed that the actuator can achieve is limited by how much flow the pump can supply. The force capability that the actuator can provide depends on the load itself and the maximum supply pressure that the pump can supply.

6.3.1 PE Force-Speed Capability

The speed of the actuator can be expressed in terms of hydraulic force for PE mode by making use of equation 2.14 as follows:

$$F = P_a A_a - P_b A_b \tag{6.19}$$

$$\dot{x}_{PE} = \frac{K_{eq}\sqrt{(RP_s - P_r) + (-RP_a + P_b)}}{A_b} \tag{6.20}$$

$$\Rightarrow \dot{x}_{PE} = \frac{K_{eq}\sqrt{(RP_s - \frac{F}{A_b} - P_r)}}{A_b} \tag{6.21}$$

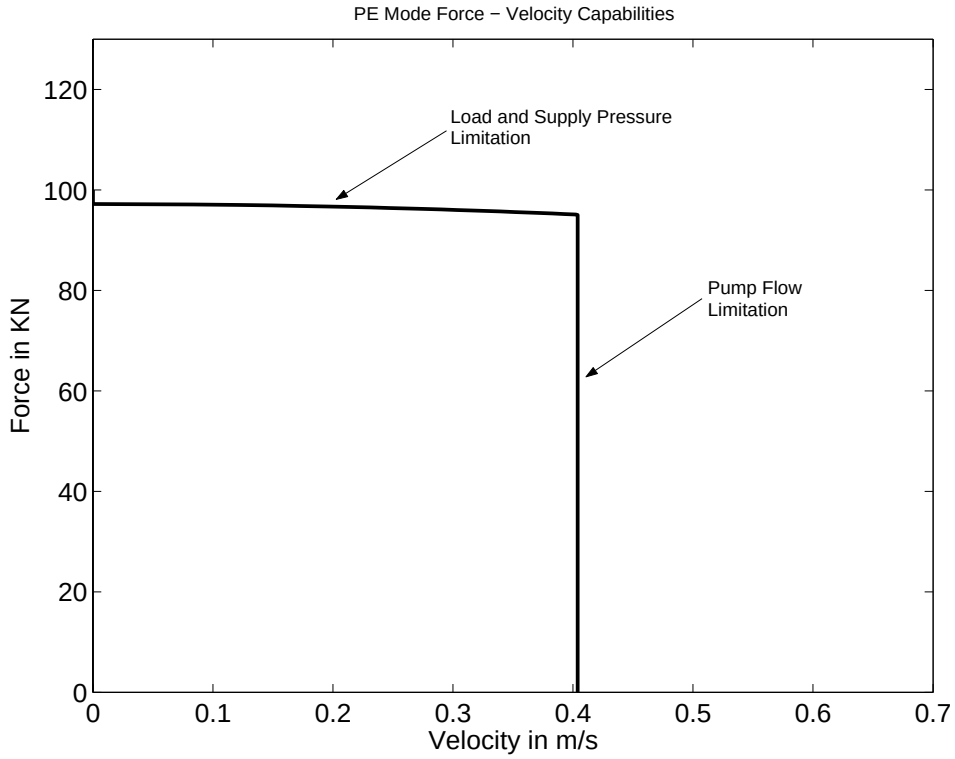

Figure 6.2: PE mode force-speed capability curve

The required power is used to quantify the force limitation due to supply pressure constraint and velocity limitation due to pump maximum flow restriction:

$$Power = P \cdot Q = F \cdot \dot{x} \tag{6.22}$$

$$P_s \cdot Q_{PE} = F_{max} \cdot \dot{x}_{PE} = (P_s A_a - P_r A_b)\dot{x}_{PE} \tag{6.23}$$

$$\Rightarrow Q_{PE} = \frac{(P_s A_a - P_r A_b)\dot{x}_{PE}}{P_s} \tag{6.24}$$

If Q_{PE} is calculated to be more than Q_{max}, then the speed $\dot{x}_{PE}$ is limited so that $Q_{PE} = Q_{max}$. Using equation 6.24:

$$\dot{x}_{PE} = \frac{Q_{max} P_s}{(P_s A_a - P_r A_b)} \tag{6.25}$$

The telehandler extender cylinder is used as an example. Assuming maximum valve opening, a force range from $0 \rightarrow 100\,KN$ is used to plot the force-speed curve for PE mode as shown in figure 6.2. The maximum pump flow is $5520\,L/h$.

6.3.2 HSRE Force-Speed Capability

A similar analysis is done for HSRE mode using equation 2.20 as follows:

$$F = P_a A_a - P_b A_b \tag{6.26}$$

$$\dot{x}_{HSRE} = \frac{K_{eq}\sqrt{(R-1)P_s + (-RP_a + P_b)}}{A_b} \tag{6.27}$$

$$\Rightarrow \dot{x}_{PE} = \frac{K_{eq}\sqrt{(R-1)P_s - \frac{F}{A_b}}}{A_b} \tag{6.28}$$

Again required power is used to quantify the force limitation due to supply pressure constraint and supply flow restriction due to pump maximum flow boundary:

$$P_s \cdot Q_{HSRE} = F_{max} \cdot \dot{x}_{HSRE} = P_s(A_a - A_b)\dot{x}_{HSRE} \tag{6.29}$$

$$\Rightarrow Q_{HSRE} = \frac{P_s(A_a - A_b)\dot{x}_{HSRE}}{P_s} = (A_a - A_b)\dot{x}_{HSRE} \tag{6.30}$$

If Q_{HSRE} is calculated to be more than Q_{max}, then the speed $\dot{x}_{HSRE}$ is limited so that $Q_{HSRE} = Q_{max}$. Using equation 6.30:

$$\dot{x}_{PE} = \frac{Q_{max}}{(A_a - A_b)} \tag{6.31}$$

The same telehandler extender cylinder is used as an example here as well. Assuming maximum valve opening, a force range from $0 \rightarrow 100\,KN$ is used to plot the force-speed curve for PE mode as shown in figure 6.3.

6.3.3 Remarks on Mode Capability

Figure 6.4 shows both mode capability curves superimposed on each other. The figure shows that PE mode has a higher force capability of about $97\,KN$ (in this example)than HSRE, which can push a maximum load of about $50\,KN$. However, HSRE has a maximum speed capability of about $0.8\,m/s$ while PE has a maximum speed capability of $0.4\,m/s$.

Coordination between using these two modes and optimally switching between them is essential to achieving high machine productivity and efficiency. This is the topic for the following section.

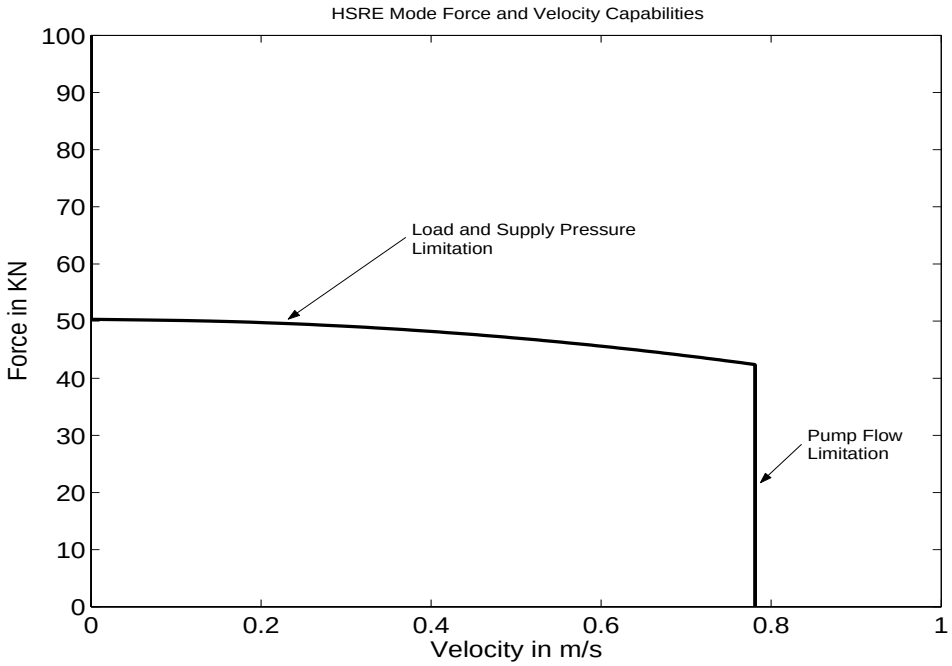

Figure 6.3: HSRE mode force-speed capability curve

It is also obvious from figure 6.4 that there are limitations to what the machine can do. For example, if the actuator needs to push a force of $50.3\,KN$, which is the maximum possible force using HSRE mode, at a commanded speed of $0.7\,m/s$ it cannot. To push such a load, the actuator would have to operate in PE mode at a lower speed than what is commanded. Then, as motion progresses and inertia effects decrease, i.e. load decreases, switching to HSRE mode may become possible and achieving the commanded speed becomes possible as well. Therefore, figure 6.4 also shows that these metering modes may not be the best control method for providing a flow path through the actuator and valve assembly. Other metering modes may exist that increase the capacity envelopes (force speed limitation) of these modes. This is the topic of chapter 8. In addition to mode capability limitations, switching between PE and HSRE during motion can have an effect on velocity performance, which is shown in chapter 7.

6.3.3.1 PE-only, HSRE-only, and Overlap Regions

Figure 6.5 shows that there are three different regions. First Region is the PE-only region which represents a region where only PE mode is possible to move the load, while the second

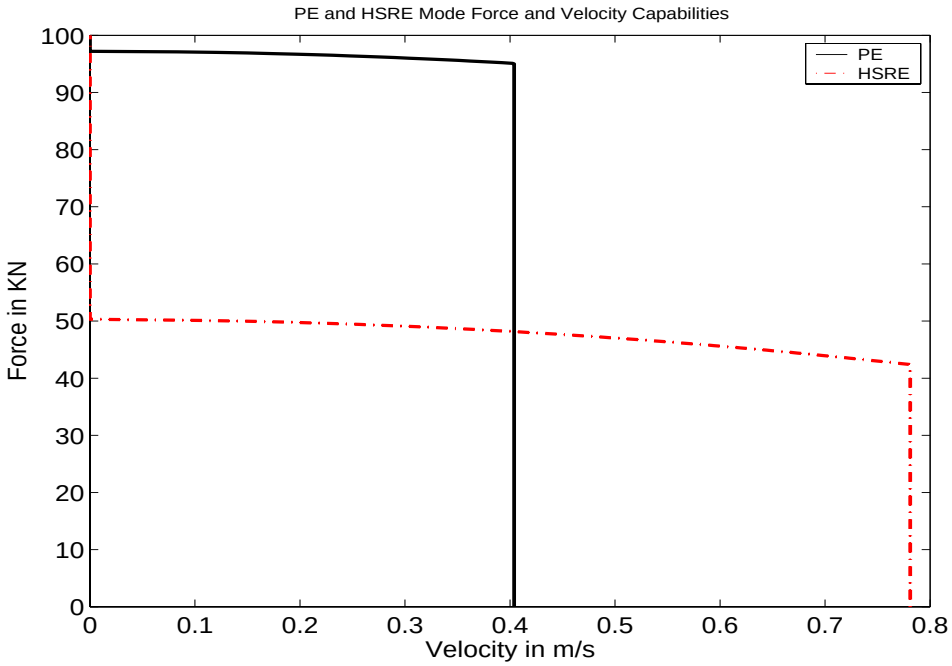

Figure 6.4: PE and HSRE mode force-speed capability curves

is the HSRE-only region, and finally the third is an overlap region where both modes can achieve the motion commanded.

In regions one and two, it is obvious which mode has to be used, while in region three it is not obvious which one is to be used. Applying the optimal switching theory developed in section 6.2 to the hydraulic system helps to decide which mode is to be used as discussed in section 6.4.

6.3.4 PE and LSRE Modes

Similar analysis can be done to compare PE and LSRE modes. LSRE mode is particularly useful when the actuator is assisted with gravity for example, which means that the actuator is subjected to negative loads. Figure 6.6 shows both mode capability curves superimposed on each other. LSRE can push a maximum load of about $1.4\,KN$ but is very useful for negative loads as it can achieve higher speeds than PE.

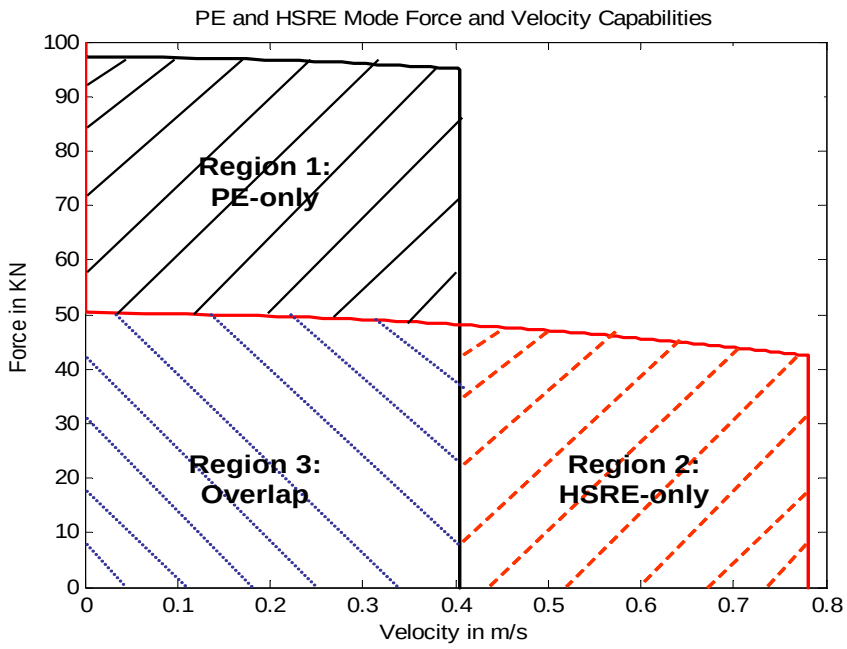

Figure 6.5: Three regions of capability

6.4 Application to Hydraulic Actuator and Four-Valve Assembly

The result derived in the 'Gradient Calculation' section is now applied to a hydraulic actuator controlled by the four-valve independent metering configuration. Focus is on a system that is assumed to start in Powered Extension mode for high force capability at the beginning of motion and then switches into High Side Regeneration mode to achieve the maximum speed possible.

The cost function is chosen to be the energy consumed by the machine in a fixed time T plus a penalty designed to force the system to achieve maximum speed which is only achievable in High Side Regeneration Mode. Time T is chosen to be sufficient to complete the task under all situations. In other words, the system is forced to switch to HSRE because otherwise the system will remain at low speed to save energy, if energy is the only concern.

$$J = \int_0^T P_s \cdot Q_s \, dt + \frac{1}{2}\rho \left(\dot{x}(T) - V_{max}\right)^2 \tag{6.32}$$

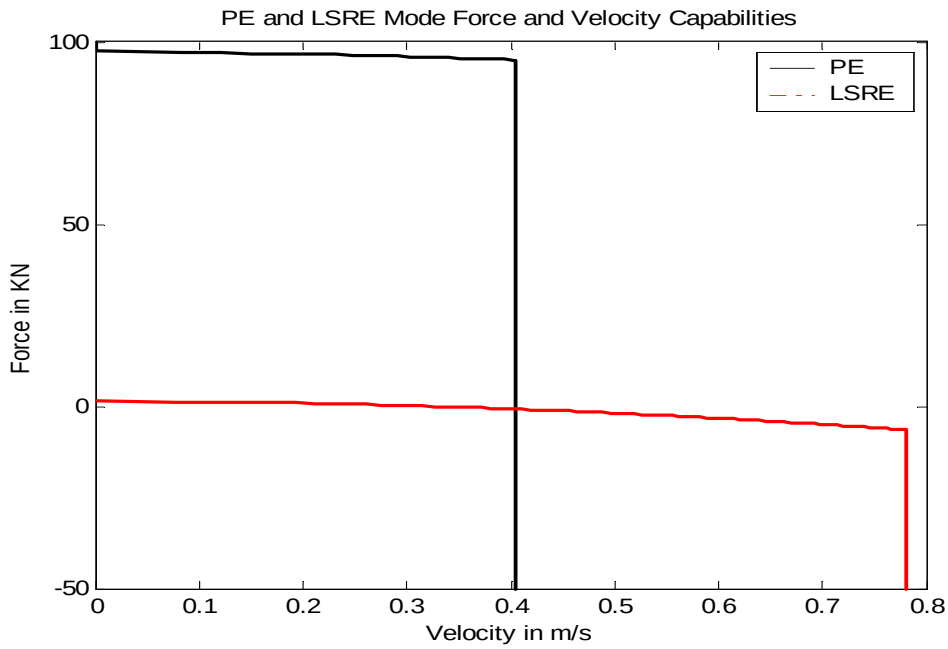

Figure 6.6: PE and LSRE mode force-speed capability curves

where P_s is the supply pressure and Q_s is the supply flow:

$$Q_s = Q_{sa} - Q_{sb} = K_{sa}\sqrt{P_s - P_a} - K_{sb}\sqrt{P_s - P_b} \tag{6.33}$$

For PE mode, $K_{sb} = 0$ and $Q_s = Q_{sa}$, while for HSRE K_{sb} is open and there is a flow Q_{sb}. In order to avoid make such distinctions, the valve switching function are used as explained in section 5.1 and a general expression can be used for supply flow as shown in equation 5.1.

Supply pressure required depends on the mode as well. Pressure set point equation for both PE and HSRE are written here again for convenience.

$$Peq_{min} = (R+1)\Delta P_{min} \tag{6.34}$$

$$Ps_{set-point,PE} = \frac{Peq_{min}}{R} + \frac{(RP_a - P_b)}{R} + \frac{P_r}{R} \tag{6.35}$$

$$Ps_{set-point,HSRE} = \frac{Peq_{min}}{R-1} + \frac{(RP_a - P_b)}{R-1} \tag{6.36}$$

Using the dynamic model developed in chapter 5, along with the supply pressure and

supply flow equations, the results developed in section 6.2.2 are applied to mode switching problem for the extender cylinder of the telehandler.

A computer simulation code consisting of two loops is built. An inner loop simulates the dynamics of the extender cylinder as it traverses from a fully retracted position to a fully extended position. Supply pressure and supply flow are calculated throughout the stroke. An outer loop optimizes switching time from PE to HSRE using the Sequential Quadratic Programming optimization functions in `MATLAB`.

Although Powered Extension mode consumes more flow because there is no regeneration flow and all the needed flow is consumed from the pump, the high pressure requirement for High Side Regeneration mode causes the system to consume more energy **as speed increases**. It is found that for a given fixed end time T switching happens at a point in time such that the maximum speed is achieved by the end time T as shown in figure 6.7.

For the simulation shown in figure 6.7 the end time used was $T = 0.8$ but the figure shows the extend simulation till $T = 1.0$ to show the settling down of the speed. It is noticed that the optimal switching time is such that at 0.8 seconds the speed is about the maximum speed. *This suggests that Powered Extension should be used whenever possible to save energy. If the speed needed is higher than the speed possible with Powered Extension then motion should still start in Powered Extension until the maximum speed possible with this mode is achieved then transition to High Side Regeneration Extension mode should occur.*

6.4.1 Interpretation on Mode Capability Curves

For efficient and proper motion path, this result implies motion starts in PE mode and should continue in PE mode until load is within the capability of HSRE mode then switching should occur. To illustrate this on the mode capability curve, refer to figure 6.8. The result entails that the optimal switching point is the intersection point shown in the figure.

This can be best explained by considering the quasi-static case. Ignoring the dynamics of the system, the gradient in equation 6.14 is reduced to the difference between the power consumed by both modes at the switching point. For the gradient to be zero, the power

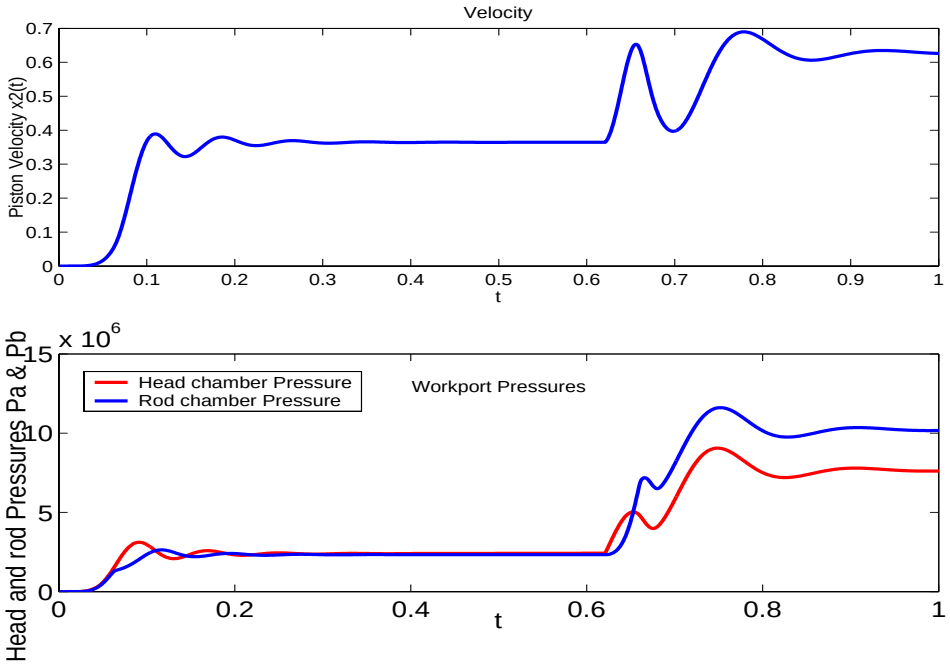

Figure 6.7: Optimal switching time τ between PE and HSRE

consumption has to be the same and that is achieved at the intersection point in figure 6.8 where the power consumption is equal in both modes.

A general closed form solution can be obtained for any case and any machine by equating the power consumption of PE and HSRE modes:

$$Power_{PE} = Power_{HSRE}$$

$$\Rightarrow F_{PE}\dot{x}_{PE} = F_{HSRE}\dot{x}_{HSRE} \tag{6.37}$$

Where:

$$F_{PE} = P_s A_a - P_r A_b \tag{6.38}$$

$$\dot{x}_{PE} = \frac{K_{eq}}{A_b}\sqrt{RP_s - P_r - \frac{F}{A_b}} \tag{6.39}$$

$$F_{HSRE} = P_s(A_a - A_b) \tag{6.40}$$

$$\dot{x}_{HSRE} = \frac{K_{eq}}{A_b}\sqrt{(R-1)P_s - \frac{F}{A_b}} \tag{6.41}$$

Substituting in equation 6.37:

$$\Rightarrow (P_s A_a - P_r A_b)\frac{K_{eq}}{A_b}\sqrt{RP_s - P_r - \frac{F}{A_b}} = P_s(A_a - A_b)\frac{K_{eq}}{A_b}\sqrt{(R-1)P_s - \frac{F}{A_b}} \tag{6.42}$$

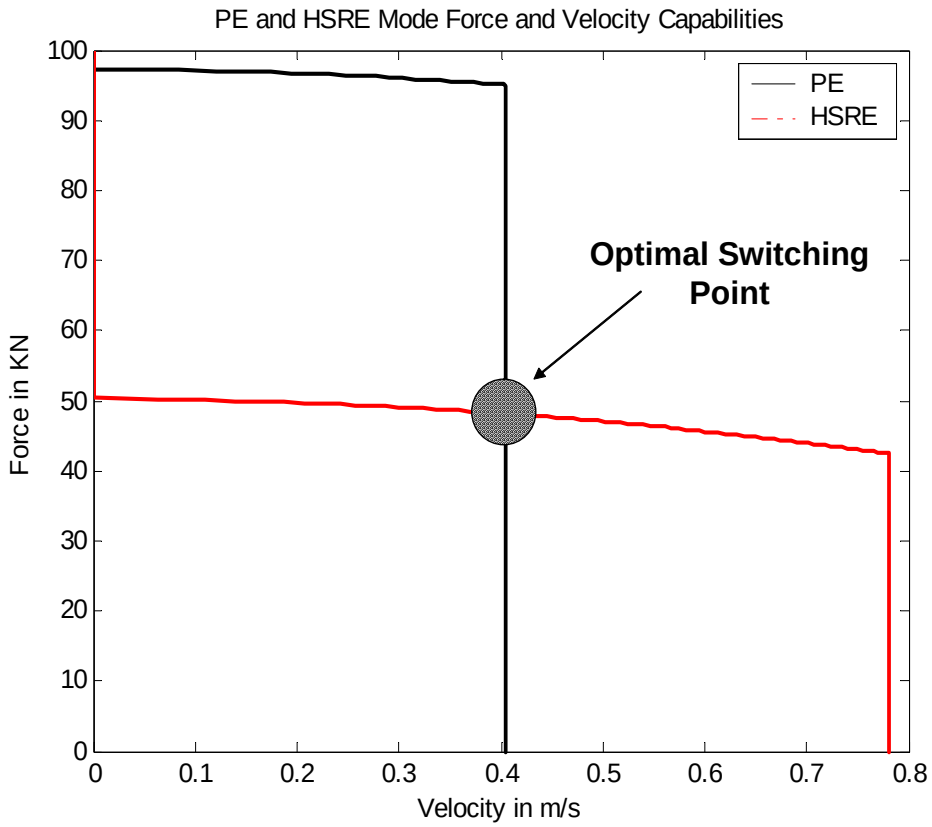

Figure 6.8: Optimal switching point

Assuming that $P_r \approx 0$, equation 6.42 can be solved for F, the load at which optimal switching should occur:

$$F = P_s A_b \frac{3R^2 - 3R + 1}{2R - 1} \tag{6.43}$$

Substituting F from equation 6.43 into equation 6.39 or 6.41, the corresponding optimal switching speed could be obtained.

An example motion path would be to start at zero speed with high force in the PE-only possible region, then traversing horizontally as speed increases with some down vertical motion as load decreases due to lowered inertia effects. This path continues until the maximum speed limit of PE mode is reached and the path become purely down and vertical along that boundary. This continues until the optimal switching point is reached and switching occurs to HSRE and motion path can start to go horizontal again allowing more speed. The effect of switching on the performance of the system is studied more closely in

Table 6.1: Extender Mode Switching Energy and Productivity Results

Where Mode Switching to HSRE Happen	Time Taken	Energy Consumed
No Switching (All in PE)	$6.6sec$	$46.212KJ$
Switching at $\frac{3}{4}$ Stroke	$5.9sec$	$49.8KJ$
Switching at $\frac{1}{2}$ Stroke	$5.6sec$	$57.77KJ$
Switching at $\frac{1}{4}$ Stroke	$4.7sec$	$65.1KJ$
Full stroke in HSRE	$4.1sec$	$66.7KJ$

the following chapters.

The behavior of this hydraulic system, the mode capability curve, and the optimal switching point bear close resemblance to automotive automatic transmission principles. This idea is explored in section 6.5 and inspires a real time algorithm that can be used for mode switching.

6.4.2 Experimental Results

An experiment is done to quantify the effect of changing switching time on telehandler productivity and efficiency. Productivity is measured by how long it takes to complete the full stroke of the extender and efficiency is measured by how much energy it consumes. The same telehandler in figure 5.11 is used. Boom is put in a horizontal position and the extender is retracted fully before giving it a maximum speed command and data is recorded throughout the full stroke.

Controlling mode switching is done by cylinder position. First the full stroke is done in PE. Then the stroke is repeated with transition into High Side Regeneration Extension mode happening after three quarters of the stroke is performed in PE, then with transition happening at half stroke, then at quarter the stroke, and finally the whole stroke is performed in High Side Regeneration Extension mode. Table 6.1

Thus, comparing full stroke in Powered Extension mode and full stroke in High Side Regeneration Extension mode, an energy saving of 30.7% is achieved but with a 37.6% loss in productivity (time to perform the stroke).

6.4.3 A Multi-Actuator System

The model for a two actuator system has been presented in section 5.4.4. The conclusion was that the different actuators can be treated independently provided that there are extra valves in the flow path that drop the supply pressure to the required pressure by the individual actuators. This allowed for treating each actuator independently.

The same independence applies to the optimal switching result in this chapter. If each actuator is treated separately, the optimal switching point is the intersection point between PE and HSRE mode capability curves pertinent to the specific actuator. However, if this is applied without further insight, a waste of energy could occur.

Assume that one actuator has to move a large load and thus demands a high pressure from the pump. The other actuator may be moving a smaller load but because the pump is already supplying a high pressure to the former actuator, it would save pump flow and thus pump power for the latter actuator to be operating in High Side Regeneration Mode (HSRE) than Powered Extension Mode (PE). As a consequence of this insight, the optimal switching point is no longer that intersection point but the second actuator should switch to HSRE.

To explain this further, suppose that the second actuator is operating in the overlap region in figure 6.8, i.e. the region where both PE and HSRE can move the load at the required speed. The results from previous section indicate that optimally the actuator should operate in PE until the intersection point or the maximum PE velocity boundary is reached then switch to HSRE mode. However, since pressure is up already and operation in HSRE is feasible, the second actuator should switch to HSRE and continue motion in HSRE to save flow (recall figure 4.15).

6.5 Automotive Automatic Transmission Analogy

Metering modes of the four-valve independent metering configuration and switching between them can be thought of as similar to automotive transmission different gears and shifting between them. Figure 6.9 shows first and second gears capability on a torque-speed graph. The capability figure for automotive transmission is very similar to mode capability figure

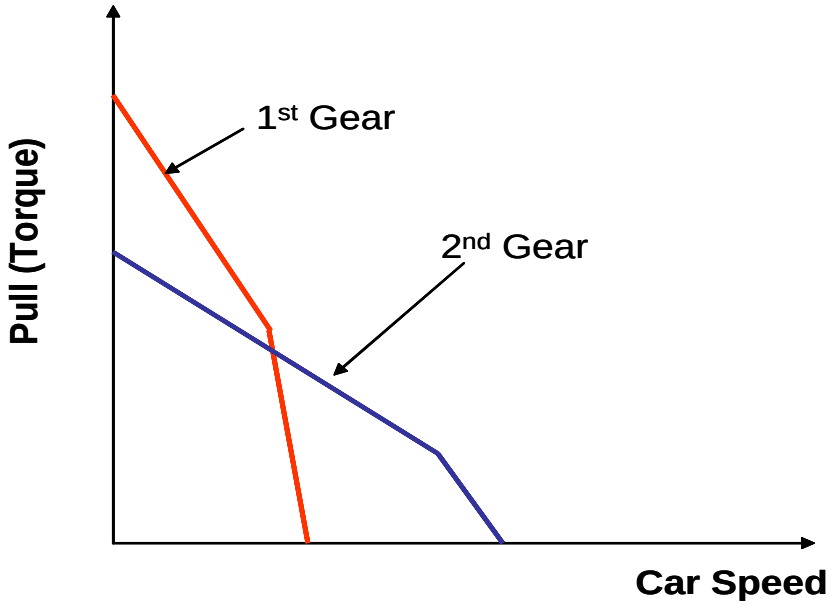

Figure 6.9: Torque versus speed curves for automotive automatic transmission 1^{st} and 2^{nd} gears

6.4. The first gear has a higher torque capability and a less speed capability than the second gear just as PE mode has a higher force capability and a less speed capability than HSRE mode.

Automatic transmission gear shifts depend on several input variables: throttle valve opening (pedal position), road condition (uphill or downhill), and speed of the vehicle. Optimal driving in terms of efficiency and exerting engine power is achieved when shifting occurs at the intersection between the two gears torque-speed curves as shown in figure 6.10 [98, 87]. This also similar to the optimal mode switching point depicted in figure 6.8.

Electronic gear shifting schedule or strategy is usually determined experimentally depending on priorities of the vehicle e.g. efficiency, performance...etc. A map is created between throttle valve opening and car speed as inputs and the gear the vehicle should be in as the output. A typical map is shown in figure 6.11 for shifts between 1^{st} and 2^{nd} gears. The throttle or pedal position is usually interpreted as a constant power demand

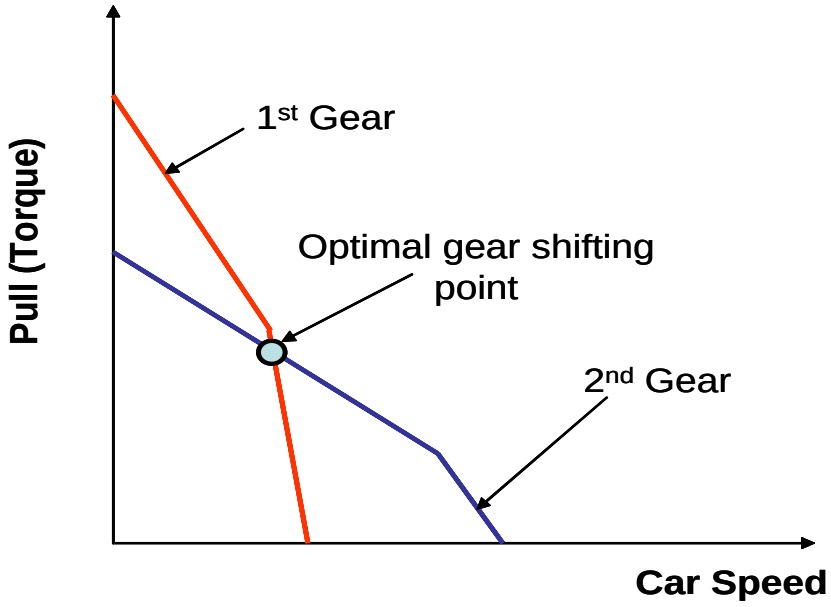

Figure 6.10: Optimal gear shifting point

or a constant torque output demand by the driver. This electronic automatic transmission schedule can inspire a real time algorithm for mode switching presented next.

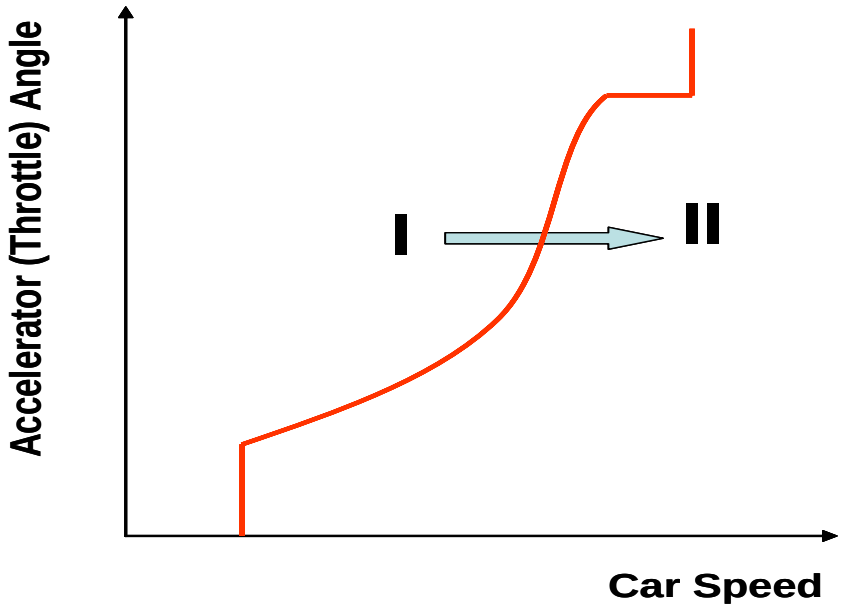

Figure 6.11: Gear shifting schedule

6.5.1 Real Time Algorithm for Mode Switching

The analogy of metering modes and mode switching to automatic transmission gears and gear shifting schedule can be used to design a real time algorithm for mode switching. Mode shifting logic between PE and HSRE is taken as an illustrative example. Similar developments can be made for other modes. The algorithm developed here can be thought of as a time optimal algorithm. The algorithm allows for shifting from PE to HSRE as soon as it is physically possible to achieve higher speeds, less flow requirement, and less time required to perform the motion.

As mentioned above, a specific throttle valve opening, which is the driver accelerator pedal position essentially, can be interpreted as a constant power demand from the engine. Similarly, a mobile hydraulic device such as an excavator or a telehandler usually has a joystick that the operator uses to command a certain speed from the hydraulic cylinder.

For this proposed real time algorithm, it is assumed that a joystick position corresponds to a power demand. This power demand is equal to the commanded velocity Vel_{Comm} multiplied by the load that needs to be moved F_{Load}. However, the current velocity $Vel_{Current}$ is not equal to the commanded velocity yet. Assuming that the current velocity is less than the commanded velocity, that means that the required force F_{Req} that the actuator needs to provide is larger than the load in order to instantaneously achieve the power demand. The ratio between the required force and the actual load, which is the same as the ratio between the current speed and the commanded speed is what is going to determine the operating mode at a particular instant. Define this ratio as r_{switch}. In equation format:

$$Power\,Demand = Vel_{Comm} \cdot F_{Load} = Vel_{Current} \cdot F_{Req} \tag{6.44}$$

$$r_{switch} = \frac{Vel_{Comm}}{Vel_{Current}} = \frac{F_{Req}}{F_{Load}} \tag{6.45}$$

It is noticed that $r_{switch} > 1$. As the actuator speeds up and current velocity approaches the commanded velocity, the ratio r_{switch} decreases and approaches 1 and the required force decreases as it approaches the actual load F_{Load}.

The maximum force capabilities of PE and HSRE modes can be derived from the supply

pressure set point equations 2.38, 2.43 as follows:

$$Ps_{,PE} = \frac{Peq_{min}}{R} + \frac{(RP_a - P_b)}{R} + \frac{P_r}{R} \tag{6.46}$$

$$Ps_{,HSRE} = \frac{Peq_{min}}{R-1} + \frac{(RP_a - P_b)}{R-1} \tag{6.47}$$

$$F_{PE,Max} = Ps_{,PE}A_a - PrA_b \tag{6.48}$$

$$F_{HSRE,Max} = Ps_{,HSRE}(A_a - A_b) \tag{6.49}$$

Define:

$$r_{mode} = \frac{F_{PE,Max}}{F_{HSRE,Max}} \tag{6.50}$$

It is clear that r_{mode} is a function of the load that the actuator has to move. This can be used to design a mode switching schedule.

r_{switch} is continuously evaluated during the motion of the actuator. At the beginning of motion, F_{Req} is larger than actual load F_{Load} because the current velocity is less than commanded velocity. This motion is only possible or achievable with PE mode. As current velocity increases and approaches the commanded velocity, the required load decreases and r_{switch} decreases until it becomes feasible to move the load with HSRE mode, which happens when $r_{switch} = r_{mode}$ and switching to HSRE occurs. Figure 6.12 illustrates this idea. Obviously, this schedule is also used for HSRE to PE switching which would happen if the current speed is higher than the commanded speed (operator trying to reduce the speed of the actuator). A hysteresis zone can be used to avoid having circular or frequent transition when operating near the transition line.

6.5.2 Algorithm Summary

The real time algorithm can be summarized as follows:

1. Assume motion starts from a still position and thus it starts in PE mode to provide the large force needed in the beginning.

2. Joystick command is a velocity command that can be considered as a constant power demand by multiplying that commanded velocity with the actual load to be moved.

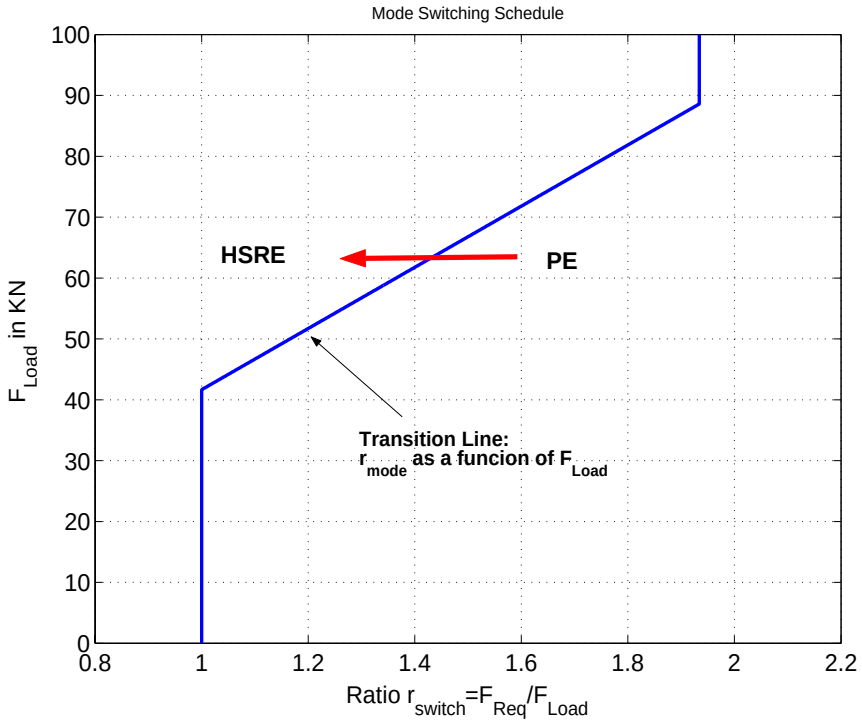

Figure 6.12: Load versus r_{mode} as a mode switching schedule

The required force is calculated by dividing the power demand just calculated by the current actuator velocity.

3. A switching ratio is calculated as the ratio of commanded velocity and current velocity, or required force and actual force.

4. This switching ratio is compared to r_{mode} at the given actuator load (the transition line in figure 6.12) If the ratio is to the right of the transition line, then the actuator should still be in PE mode. If it crosses to the left and $r_{switch} \leq r_{mode}$ then switching to HSRE mode should occur.

A schematic of the algorithm is shown in figure 6.13.

This chapter presented an optimal switching analysis and a possible real time algorithm mode switching with a focus on PE and HSRE modes as an example. The effect to mode switching on the dynamics and performance of the system is yet to be analyzed. First the effect of mode switching on vibration of the beam driven by the actuator is studied.

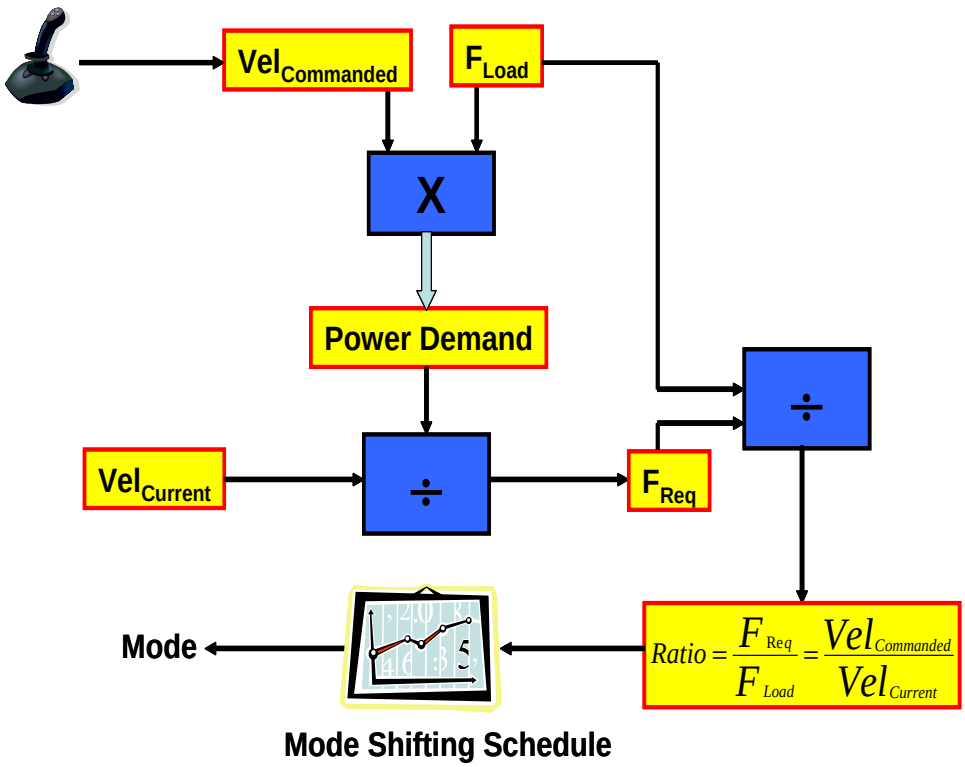

Figure 6.13: Schematic of real time algorithm for mode switching

CHAPTER VII

EFFECT OF MODE SWITCHING ON VIBRATION OF A ROTATING BEAM

7.1 General

The effect of mode switching on vibrational behavior of a rotating beam actuated by a hydraulic cylinder controlled by the four-valve configuration is studied in this chapter. This configuration is encountered quite often in mobile hydraulic equipment e.g. telehandlers, excavators and backhoes. The basic mechanical system in this case is a continuous rotating beam and a hydraulic actuator that drives this beam. The dynamic interaction between such a beam and its driving hydraulic cylinder actuator are presented here. The coupled dynamics of the beam and actuator can be simplified and generalized by using dimensionless analysis [63, 61, 62]. The goal of this development is to study the effect of mode switching on the vibration of this typical system. Since these beams are usually very rigid beams, only the rigid body mode and fundamental flexural mode is focused upon in this analysis. This allows for conducting the dynamic interaction investigation using a reduced order model analysis.

7.2 Brief Literature Review

Studying the dynamic response of rotating beams to actuation is not only important of the hydraulic system under research in this work, but it is essential to the control of flexible robots and space structures as well. That is why there has been a significant research activity in this area.

Book [10] applied the transfer matrix method introduced by Pestel and Leckie [64] to design, modeling, and control of flexible robots. To capture flexible link deformation, Book [11] suggested incorporating link flexibility into a recursive Lagrangian dynamic model using 4×4 transformation matrices. Chalhoub and Chen [16] extended this work by using

floating reference frame to include systems with prismatic joints, torsional and out-of-plane vibrations. The application of pole placement techniques to control of flexible systems is discussed in [12].

The dynamic response of rigid mechanisms driven by electric or hydraulic actuators at startup is analyzed in [55, 56]. The response of general, not necessarily rigid, systems has been studied in [72, 85]. It is shown that the actuator design parameters have a significant effect on the characteristics of the dynamic interaction between the actuator and the driven mechanism [85, 62, 61].

Vibration suppression and control of continuous beam models discretized by modal analysis have been examined in several references [39, 76, 45, 49, 52, 27, 74, 37, 17, 20].

In most of these studies, the actuator dynamics are assumed to be very fast and thus neglected in the overall analysis, or limited numerical results are presented with the main focus given to control. Groundwork has been done in [30, 63, 73] to study the effect of actuator dynamics on damping vibration of the driven mechanism.

In [61, 62] the dynamic interaction of a rotating flexible beam driven by a double acting hydraulic controlled by a spool valve has been investigated with a focus of how to tune the actuator parameters to reduce beam vibrations. The work herein follows the principles of that work but **extends** the analysis to the case of using a hydraulic actuator controlled by the four-valve independent metering configuration and the effect of mode switching on the vibrational behavior of the rotating beam.

7.3 Flexible Beam Dynamics

Figure 7.1 shows the system to be analyzed in this chapter. The beam is assumed to be an Euler-Bernoulli beam with a tip mass M_{tip} that represent, for example, the fork mass of the telehandler. The beam can be non-uniform with mass $m(x)$ and mass moment of inertia $I(x)$ being functions of position along the beam. The beam mass without tip mass is $m_b(x)$. The concentrated force F is the force applied by the actuator along the beam at position $x = L_a$ to move the beam. This force is related to and dependent upon the dynamics of the actuator.

The concentrated force F is usually represented using the Dirac Delta function [22, 52]. The general Euler-Bernoulli equation that govern the small dynamic beam perturbations $y(x,t)$ can therefore be written as:

$$x = \frac{\partial^2}{\partial x^2}\left[EI(x)\frac{\partial y^2}{\partial x^2}\right] + m(x)\frac{\partial y^2}{\partial t^2} = (F - F_s)\delta(x - L_a) \tag{7.1}$$

Where F_s is the static force the actuator needs to provide to balance the static friction and gravity forces.

Modal analysis can be used to discretize a continuous beam such as the one being modeled. Its dynamic motion $y(x,t)$ can be expressed through a modal or separable expansion utilizing a discrete set of mass normalized eigenfucntions $\phi_i(x)$ and modal coordinates $q_i(t)$:

$$y(x,t) = \sum_{i=0}^{n} \phi_i(x) q_i(t) \tag{7.2}$$

Orthogonality conditions for this beam with the boundary condition shown in figure 7.1 is found in [52, 82, 22]:

$$\int_0^L \phi_i(x)[m_b(x) + M_{tip}\delta(x - L)]\phi_j(x)dx = \delta_{ij} \tag{7.3}$$

$$\int_0^L \phi_i(x)\frac{d^2}{dx^2}\left[EI(x)\frac{d^2\phi_j(x)}{dx^2}\right]dx = \omega_{bi}^2\delta_{ij} \tag{7.4}$$

Using these orthogonality conditions, second order differential equations in the modal coordinates $q_i(t)$ can be obtained. Assuming Rayleigh modal damping [52, 82, 22] with modal damping factors ζ_i:

$$\frac{d^2 q_i(t)}{dt^2} + 2\zeta_i\omega_{bi}\frac{dq_i(t)}{dt} + \omega_{bi}^2 q_i(t) = (F - F_s)\phi_i(L_a)$$
$$i = 0, 1, ...n \tag{7.5}$$

Several methods can be used to determine $\phi_i(x)$ and ω_{bi}, which are the only quantities needed for equation 7.5. Rayleigh-Ritz functions are one way to determine them [52].

In mobile hydraulic equipment, like telehandlers, the rotating beams are rigid semi-definite hinged free beams with a tip mass. The $i = 0$ mode can be interpreted as the rigid body motion of such a beam. From modal expansion (separability), the rigid body mode motion can be separated as:

$$\phi_0(x)q_0(t) = x\theta(t) \tag{7.6}$$

An equation associated with this rigid body mode is:

$$J\frac{d^2\theta}{dt^2} = (F - F_s)L_a \cos\gamma \tag{7.7}$$

J is the beam and tip mass moment of inertia around the hinge point. The modes from $i = 1, ...N$ in equation 7.5 correspond to beam bending modes.

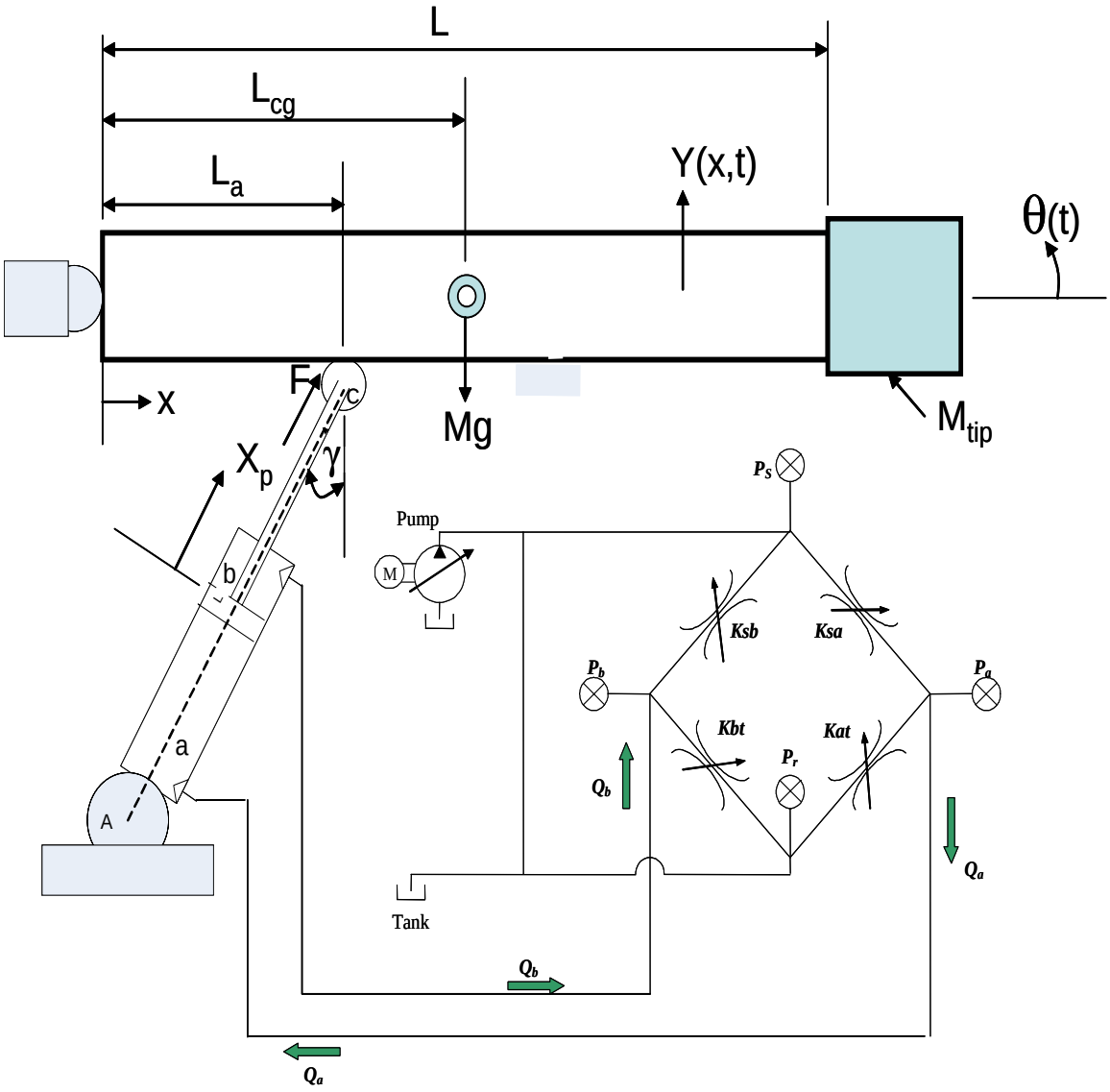

Figure 7.1: A rotating beam driven by a hydraulic cylinder actuator controlled by four-valve assembly

7.4 Actuator Dynamics

Details of the actuator dynamics have been presented in in chapter 5. Brief presentation of actuator dynamics is given here to couple these dynamics to the discretized beam motion through the concentrated force F:

$$F = P_a A_a - P_b A_b \tag{7.8}$$

The static force is related to the initial value of head and rod chamber pressures P_{a0} and P_{b0}

$$F_s = P_{a0} A_a - P_{b0} A_b \tag{7.9}$$

Cylinder piston mass and flexibility have secondary effects regarding actuator-beam dynamic interaction and are thus neglected here [61].

Orifice Flows: Assuming a turbulent flow, the following square root relationship between flow and pressure can be used [53]

$$Q_{sa} = K_{sa}\sqrt{|P_s - P_a|}sgn(P_s - P_a) \tag{7.10}$$

$$Q_{sb} = K_{sb}\sqrt{|P_s - P_b|}sgn(P_s - P_b) \tag{7.11}$$

$$Q_{at} = K_{at}\sqrt{|P_a - P_r|}sgn(P_a - P_r) \tag{7.12}$$

$$Q_{bt} = K_{bt}\sqrt{|P_b - P_r|}sgn(P_b - P_r) \tag{7.13}$$

Compressibility:

$$\begin{aligned} Q_{ca} &= \frac{CV_a}{B_e}\dot{P}_a \\ Q_{cb} &= \frac{CV_b}{B_e}\dot{P}_b \end{aligned} \tag{7.14}$$

where,

$$CV_a = V0_a + A_a x \tag{7.15}$$

$$CV_b = V0_b - A_b x \tag{7.16}$$

$V0_a$ is the initial volume of head chamber (a), and $V0_b$ is the initial volume of rod chamber (b)

Conservation of Mass:

$$Q_{sa} - Q_{at} = Q_{ca} + A_a\dot{x}$$
$$Q_{sb} - Q_{bt} = Q_{cb} - A_b\dot{x} \tag{7.17}$$

Assuming rigid connection between piston rod and beam, piston velocity can be expressed in terms of beam velocity at the connection point:

$$\dot{x}_p = \frac{dy(L_a,t)}{dt}\cos\gamma = L_a\frac{d\theta}{dt}\cos\gamma + \sum_{i=1}^{n}\phi_i(L_a)\frac{dq_i(t)}{dt}\cos\gamma \tag{7.18}$$

Where the first term on the right hand side represents the rigid body motion and the second term represents the flexural modes of the beam motion. Substituting equation 7.18 into equations 7.17 and using equations 7.14

$$\frac{CV_a}{B_e}\dot{P}_a + A_aL_a\frac{d\theta}{dt}\cos\gamma + A_a\cos\gamma\sum_{i=1}^{n}\phi_i(L_a)\frac{dq_i(t)}{dt} = Q_{sa} - Q_{at} \tag{7.19}$$
$$\frac{CV_b}{B_e}\dot{P}_b - A_bL_a\frac{d\theta}{dt}\cos\gamma - A_b\cos\gamma\sum_{i=1}^{n}\phi_i(L_a)\frac{dq_i(t)}{dt} = Q_{sb} - Q_{bt} \tag{7.20}$$

7.5 Non-Dimensional Analysis

Equations from 7.5 till 7.20 represent the actuator and flexible beam dynamics in actual system parameters. In order to generalize this analysis to different designs and to reduce the number of parameters that need to be defined, a non-dimensional analysis proves to be useful. This makes general system behavior assessment and analysis possible and also proves to be an insightful approach into the dynamic interaction of actuator and beam [61].

Natural dimensionless quantities are first defined and then the non-dimension groups are obtained from these basic quantities. Mostly, non-dimensional parameters are characterized by a ratio of some dynamic variable and another variable that serves as a reference. A fundamental dimensionless quantity is dimensionless time. After defining this quantity, actuator dynamics are first non-dimensionlized followed by the dynamic coupling equations and finally the beam dynamic equation.

7.5.1 Dimensionless Time

Dimensionless time is an essential parameter for the non-dimensional analysis undertaken here. A quantity found in [85] appropriate for this type of systems defines the reference time to be the time required for a rigid load to reach steady state motion assuming constant acceleration throughout the motion. This reference time is found to be [61]:

$$t_r = \frac{J}{A^{*2} L_a^2 R^*} \tag{7.21}$$

Where $A^* = A_b \cos\gamma$ and R^* is a quantity that represents the total fluid resistance including line losses and other losses in the flow path such that $R^* Q = P$. Reference time t_r can also be looked at as the time constant of a stiff hydraulic system (low capacitance) driving a rigid beam.

The reciprocal of reference time t_r can be defined as reference natural frequency ω_r:

$$\omega_r = \frac{A^{*2} L_a^2 R^*}{J} \tag{7.22}$$

The dimensionless time can thus be defined as:

$$T = \frac{t}{t_r} = \frac{A^{*2} L_a^2 R^*}{J} t \tag{7.23}$$

It is important to define the derivatives with respect to dimensionless time [61]:

$$\frac{d}{dt} = \frac{dT}{dt}\frac{d}{dT} = \frac{A^{*2} L_a^2 R^*}{J}\frac{d}{dT} = \omega_r \frac{d}{dT} \tag{7.24}$$

$$\frac{d^2}{dt^2} = \frac{d}{dt}\left[\frac{dT}{dt}\frac{d}{dT}\right] = \left[\frac{dT}{dt}\right]^2 \frac{d^2}{dT^2} = \frac{A^{*4} L_a^4 R^{*2}}{J^2}\frac{d^2}{dT^2} = \omega_r^2 \frac{d^2}{dT^2} \tag{7.25}$$

7.5.2 Actuator Dynamics in Non-Dimensional Format

In order to non-dimensionalize the hydraulic actuator equations, the following dimensionless parameters are defined.

Non-dimensional flows:

$$\begin{aligned} Q_1 &= \frac{Q_{sa}}{P_s/R^*} \\ Q_2 &= \frac{Q_{at}}{P_s/R^*} \\ Q_3 &= \frac{Q_{sb}}{P_s/R^*} \\ Q_4 &= \frac{Q_{bt}}{P_s/R^*} \end{aligned} \tag{7.26}$$

For the analysis done in this chapter assume that supply pressure P_s is not a function of workport pressures of the actuator being analyzed here. For example, assume that there is another actuator working at the same time as this actuator and that this other function dictates pump pressure.

Consider equation 7.20, dividing the equation by supply pressure P_s and noticing that $\frac{dP}{dt} = \omega_r \frac{dP}{dT}$:

$$\frac{CV_a}{B_e}\frac{\omega_r}{P_s}\frac{dP_a}{dT} + \frac{A_a L_a}{P_s}\frac{d\theta}{dT}\cos\gamma + \frac{A_a}{P_s}\cos\gamma \sum_{i=1}^{n} \phi_i(L_a)\frac{dq_i(t)}{dt} = \frac{Q_{sa}}{P_s} - \frac{Q_{at}}{P_s} = \frac{Q_1}{R^*} - \frac{Q_2}{R^*} \quad (7.27)$$

Multiplying by R^*:

$$\Rightarrow R^*\frac{CV_a}{B_e}\frac{\omega_r}{P_s}\frac{dP}{dT} + R^*\frac{A_a L_a}{P_s}\frac{d\theta}{dT}\cos\gamma + R^*\frac{A_a}{P_s}\cos\gamma \sum_{i=1}^{n} \phi_i(L_a)\frac{dq_i(t)}{dt} = Q_1 - Q_2 \quad (7.28)$$

Notice that $A_a = RA_b$. Define non-dimensional angular rotation Φ and non-dimensional beam flexural modal coordinate Z_i as:

$$\Phi = \frac{A^{*3}L_a^3 R^{*2}}{P_s J}\,\theta \quad (7.29)$$

$$Z_i = \frac{A^{*3}L_a^2 R^{*2}\phi_i(L_a)}{P_s J}\,q_i \quad (7.30)$$

A dimensionless hydraulic capacitance can be defined as:

$$K_C = \frac{CVA^{*2}L_a^2 R^{*2}}{B_e J} \quad (7.31)$$

As a consequence of the definitions in 7.30, reference frequency, and dimensionless hydraulic capacitance 7.31, equation 7.28 can be written as follows:

$$K_C\frac{1}{P_s}\frac{dP_a}{dT} + R\frac{d\Phi}{dT} + R\sum_{i=1}^{n}\frac{dZ_i}{dT} = Q_1 - Q_2 \quad (7.32)$$

And similarly:

$$K_C\frac{1}{P_s}\frac{dP_b}{dT} - \frac{d\Phi}{dT} - \sum_{i=1}^{n}\frac{dZ_i}{dT} = Q_3 - Q_4 \quad (7.33)$$

7.5.3 Beam Dynamics in Non-Dimensional Format

Assuming initial pressures $P_{a0} = P_{b0} = 0$, equation 7.7 can be written as:

$$J\omega_r^2\frac{d^2\theta}{dT^2} = (P_a A_a - P_b A_b)L_a\cos\gamma = (RP_a A^* - P_b A^*)L_a \quad (7.34)$$

Dividing by $P_s A^* L_a$ and making use of 7.30:

$$\frac{d^2\Phi}{dT^2} = R\frac{P_a}{P_s} - \frac{P_b}{P_s} \tag{7.35}$$

Equation 7.5 can be written in dimensionless format as follows:

$$\omega_r^2 \frac{d^2 q_i(t)}{dT^2} + 2\zeta_i \omega_{bi} \omega_r \frac{dq_i(t)}{dT} + \omega_{bi}^2 q_i(t) = (RP_a A^* - P_b A^*)\phi_i(L_a) \tag{7.36}$$

Define a dimensionless parameter K_{Bi} as the ratio of the i^{th} mode beam flexural frequency to the reference frequency ω_r. It contains both beam and actuator parameters and it is an important for describing their dynamic interaction [61]:

$$K_{Bi} = \frac{\omega_{bi}}{\omega_r} = \frac{\omega_{bi} J}{A^{*2} L_a^2 R^*} \tag{7.37}$$

Dividing 7.36 by ω_r^2:

$$\frac{d^2 q_i(t)}{dT^2} + 2\zeta_i K_{Bi} \frac{dq_i(t)}{dT} + K_{Bi}^2 q_i(t) = \frac{(RP_a - P_b)A^* \phi_i(L_a) J^2}{A^{*4} L_a^4 R^{*2}} \tag{7.38}$$

Defining a modal mass coefficient $K_{Mi} = \frac{L_a^2}{J\phi_i^2(L_a)}$ and making use of definition in 7.30 and equation 7.35:

$$\frac{d^2 Z_i(t)}{dT^2} + 2\zeta_i K_{Bi} \frac{dZ_i(t)}{dT} + K_{Bi}^2 Z_i(t) = \frac{RP_a}{P_s K_{Mi}} - \frac{P_b}{P_s K_{Mi}} = \frac{1}{K_{Mi}} \frac{d^2\Phi}{dT^2} \tag{7.39}$$

Taking the derivative of both sides of equation 7.35 and defining a non-dimensional rigid body angular speed $\Omega = \frac{d\Phi}{dT}$:

$$\frac{d^2\Omega}{dT^2} = \frac{d^3\Phi}{dT^3} = \frac{R}{P_s}\frac{dP_a}{dT} - \frac{1}{P_s}\frac{dP_b}{dT} \tag{7.40}$$

Substituting the dimensionless time derivatives of pressures from equations 7.32 and 7.33 into equation 7.40

$$\begin{aligned} \frac{d^2\Omega}{dT^2} &= \frac{R}{K_C}\left[Q_1 - Q_2 - R\frac{d\Phi}{dT} - R\sum_{i=1}^{n}\frac{dZ_i}{dT}\right] - \frac{1}{K_C}\left[Q_3 - Q_4 + \frac{d\Phi}{dT} + R\sum_{i=1}^{n}\frac{dZ_i}{dT}\right] \\ &\Rightarrow \frac{d^2\Omega}{dT^2} + \frac{1+R^2}{K_C}\Omega + \frac{1+R^2}{K_C}\sum_{i=1}^{n}\frac{dZ_i}{dT} = \frac{R}{K_C}(Q_1 - Q_2) - \frac{1}{K_C}(Q_3 - Q_4) \end{aligned} \tag{7.41}$$

7.6 Dynamic Interaction of Actuator and Flexible Beam

In mobile hydraulic systems, the rotating beams actuated by hydraulic cylinders are usually very rigid. The rest of the analysis in this chapter focuses on the rigid body mode of the beam and the first fundamental flexural frequency and ignores higher modes, which is a very reasonable assumption given the rigidity of the beams. Moreover, this allows for a simplified analysis that gives insight into the system dynamic coupling and behavior and leads to a simulation of mode switching effect on the beam vibration.

The equations above can be reduced to a fourth order system of two coupled second order ordinary differential equations. Equations 7.39 and 7.41 can be written in a matrix form including the fundamental flexural frequency:

$$\begin{bmatrix} 1 & 0 \\ 0 & K_C \end{bmatrix} \begin{bmatrix} \frac{d^2 Z_1}{dT^2} \\ \frac{d^2 \Omega}{dT^2} \end{bmatrix} + \begin{bmatrix} 2\zeta_1 K_{B1} & \frac{-1}{K_{M1}} \\ 1+R^2 & 0 \end{bmatrix} \begin{bmatrix} \frac{dZ_1}{dT} \\ \frac{d\Omega}{dT} \end{bmatrix} + \begin{bmatrix} K_{B1} & 0 \\ 0 & 1+R^2 \end{bmatrix} \begin{bmatrix} Z_1 \\ \Omega \end{bmatrix} = \begin{bmatrix} 0 \\ R(Q_1 - Q_2) + (Q_4 - Q_3) \end{bmatrix} \tag{7.42}$$

Z_1 represents the beam vibration at the fundamental frequency and Ω represents the rigid body angular speed of the beam. Coupling between these two parameters appears in the off diagonal terms of the damping matrix, which have opposite signs, i.e. a gyroscopic type of coupling. This implies that there is dynamic interaction between the actuator and the beam and that the specific parameters of the actuator affect the beam vibration.

In equation 7.42 calling the mass matrix M, the damping matrix D, and the stiffness matrix K, the characteristic equation is obtained by taking the determinant $|s^2M + sD + K|$ and equating it to zero, where s is the Lapalce variable:

$$K_C \mathbf{s^4} + 2\zeta_1 K_{B1} K_C \ \mathbf{s^3} + [K_{B1} K_C + (1+R^2)(1 + \frac{1}{K_{M1}})]\mathbf{s^2} + 2\zeta_1 K_{B1}(1+R^2)\mathbf{s} + K_{B1}(1+R^2) = 0 \tag{7.43}$$

The parameter K_{M1}, which appears off diagonally in damping matrix in equation 7.42 and thus causes the actuator-beam coupling, shows in the collection of terms multiplying $\mathbf{s^2}$.

Consequently, the non-dimensional parameters K_C and K_{B1} affect the degree of beam-actuator coupling. The following remarks can be made about the characteristics of this coupling and the effect of the K_C and K_{B1} [61]:

- The parameter K_{M1} is fixed by a given actuator connection point to the beam, i.e. by the value of L_a.
- When K_{B1} is very large, it renders K_{M1} negligible and thus the coupling is insignificant. It also implies that the actuator dynamic response is slow relative to beam vibration
- On the other hand, a small value K_{B1} implies a fast actuator response and allows for beam-actuator dynamic coupling. Very small values of K_{B1} entails full coupling as if the actuator and beam are one physical entity and the actuator does not affect the beam vibration.
- The range $2 \leq K_{B1} \leq 4$ is a transition between a full coupling and no coupling system behavior.
- Intermediate values of K_{B1} may be best for overall dynamic response as it permits the actuator's response to suppress the beam vibration.
- Considering the definition K_C in equation 7.31, it is noticed that there are no beam flexural parameters. This indicates that it does not have an effect on dynamic coupling between beam and actuator.
- It has been shown in [85] that the typical range for the dimensionless capacitance is $0.1 \leq K_C \leq 0.4$.

It is shown in [62] that the ranges indicated above for K_C and K_{B1} allow for actuation process to suppress beam vibration. In the analysis conducted here, K_C and K_{B1} values are chosen in these ranges and focus will be upon the effect of mode switching on beam vibration, which is presented next.

7.7 Effect of Mode Switching

Assume that the actuator shown in figure 7.1 drives the beam and that it starts in PE mode to allow for a high force capability at the commencement of motion then in mid motion the actuator switches to HSRE mode to allow for high speed capability. Although this is appropriate use of modes, mode switching entails closing a poppet valve and opening another. These poppet valves are ***not*** infinitely fast and, as a consequence of that, mode switching has dynamic effects on the performance of the system. This is the subject of this section. The dynamic non-dimensional equations derived above are first put in a state space format, simulated, and then experimental validation follows.

7.7.1 State Space Representation of Non-Dimensional System Equations

This system can be considered as a multi-input system where the inputs are the flows Q_1, Q_2, Q_3, and Q_4, which in turn depend on valve conductances K_{sa}, K_{sb}, K_{at}, and K_{bt}:

$$\begin{aligned} Q_1 &= \frac{Q_{sa}}{P_s/R^*} = \frac{K_{sa}\sqrt{P_s - P_a}}{P_s/R^*} \\ Q_2 &= \frac{Q_{at}}{P_s/R^*} = \frac{K_{at}\sqrt{P_a - P_r}}{P_s/R^*} \\ Q_3 &= \frac{Q_{sb}}{P_s/R^*} = \frac{K_{sb}\sqrt{P_s - P_b}}{P_s/R^*} \\ Q_4 &= \frac{Q_{bt}}{P_s/R^*} = \frac{K_{bt}\sqrt{P_b - P_r}}{P_s/R^*} \end{aligned} \tag{7.44}$$

The following set of first order differential equations can be written and will be used for simulation and analysis. The state variables are non-dimensional fundamental modal coordinate Z_1, its dimensionless derivative, non-dimensional rigid body angular speed, and its derivative, or non-dimensional rigid body angular acceleration:

$$\begin{aligned} x_1 &= Z_1 \\ x_2 &= \frac{dZ}{dT} \\ x_3 &= \Omega \\ x_4 &= \frac{d\Omega}{dT} \\ \frac{dx_1}{dT} &= x_2 \end{aligned}$$

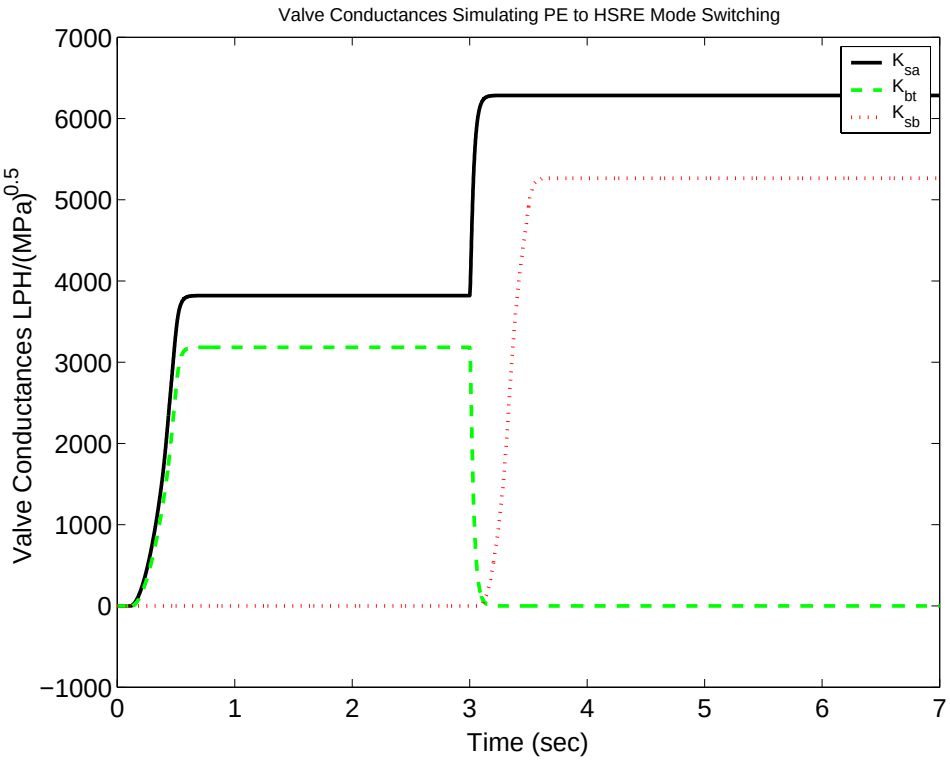

Figure 7.2: Valve conductance coefficients that simulate mid-motion PE to HSRE mode switching

$$\frac{dx_2}{dT} = -2\zeta_1 K_{B1} x_2 - K_{B1} x_1 + \frac{1}{K_{M1}} x_4$$

$$\frac{dx_3}{dT} = x_4$$

$$\frac{dx_4}{dT} = -\frac{1+R^2}{K_C} x_3 - \frac{1+R^2}{K_C} x_2 + \frac{R}{K_C}(Q_1 - Q_2) - \frac{1}{K_C}(Q_4 - Q_3) \tag{7.45}$$

The system is simulated with valve openings K_{sa}, K_{sb}, and K_{bt} affecting a motion that starts in PE mode and then at some point during the motion, the hydraulic actuator switches to HSRE as shown in figure 7.2.

The system is simulated using the values $K_{B1} = 2$, $K_{M1} = 0.5$, $K_C = 0.1$, and $\zeta_1 = 0.6$, which are typical values with the actuator located at mid length on the beam. The simulation results are shown in figure 7.3. Ignoring the transients in the beginning of the motion, it is noticed that mode switching in mid motion induces heavy vibration that is indicated in the fluctuation in Z_1 and Ω at about 20 units of dimensionless time (the fluctuation in Ω is circled).

The rigid body angular speed Ω increases as desired by switching to HSRE, but during mode switching, the beam almost halts and then picks up speed. This fluctuation in rotational speed and the fundamental modal coordinate (and their derivatives obviously) is very noticeable and could potentially causes the whole vehicle to vibrate. ***This is unacceptable velocity performance***.

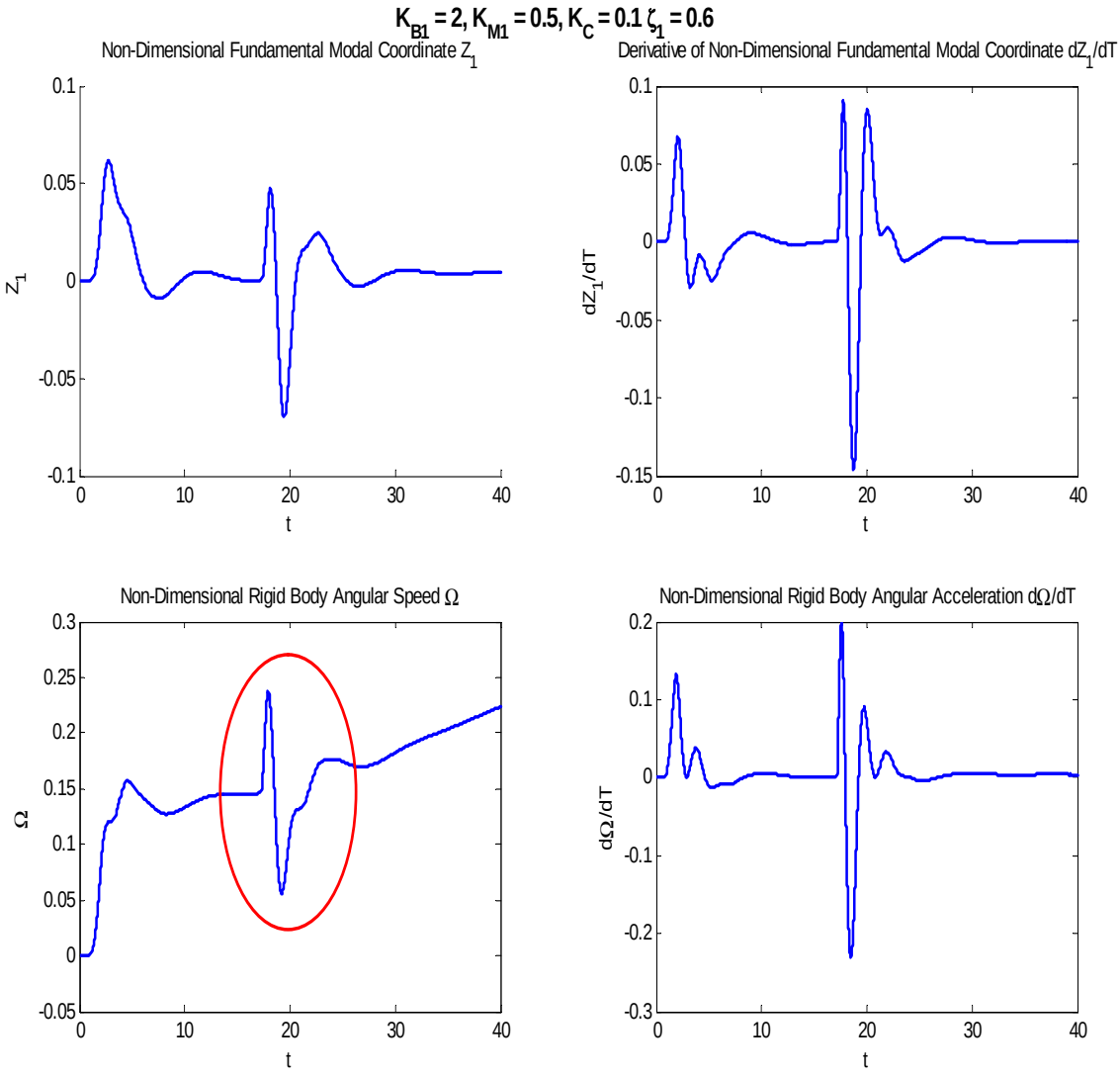

Figure 7.3: Beam Vibrations

7.7.2 Experiment: Boom Vibration

In order to see the effect of mode switching on velocity performance on a real vehicle, a simple experiment has been done on the boom of the telehandler in figure 5.11. The hydraulic cylinder actuating the boom of the telehandler is a typical practical embodiment of what is depicted in figure 7.1.

The stroke of this boom cylinder is $845\,mm$. When the cylinder is fully retracted the load is very large and therefore motion has to start in PE. Then when the actuator is extended to $400\,mm$, a little less than half the stroke, mode switching is commanded and the rest of the stroke is completed in HSRE. Valve commands are given in figure 7.4 and the actuator position and speed in addition to workport pressures throughout the motion are shown in figure 7.5.

These results confirm the simulations in figure 7.3. Although workport pressures do not show irregular fluctuation in head or rod chamber pressures, position and velocity curves show the effect of mode switching clearly. In the circled portion of position curve in figure 7.5, it is noticed that the beam halts for $\approx 0.2sec$. The vibration is even clearer in the velocity curve and is also circled in figure 7.5. The velocity goes down to zero, which explains the halt in the position curve and also shows that the beam shakes with speed going back and forth.

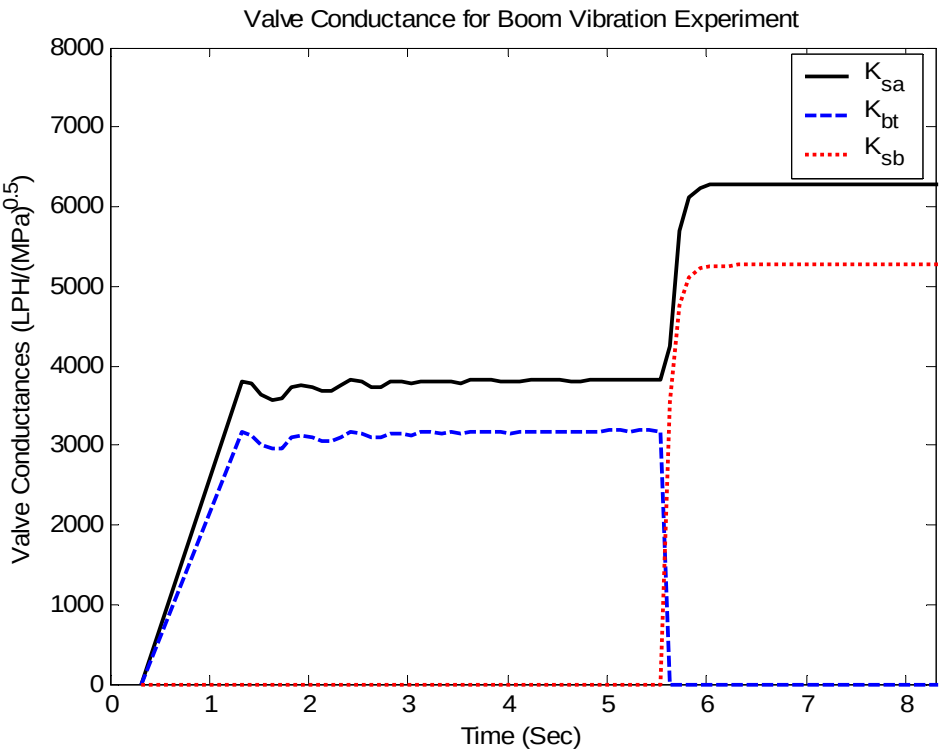

Figure 7.4: Valve conductance commands for motion starting in PE and switching to HSRE in mid motion

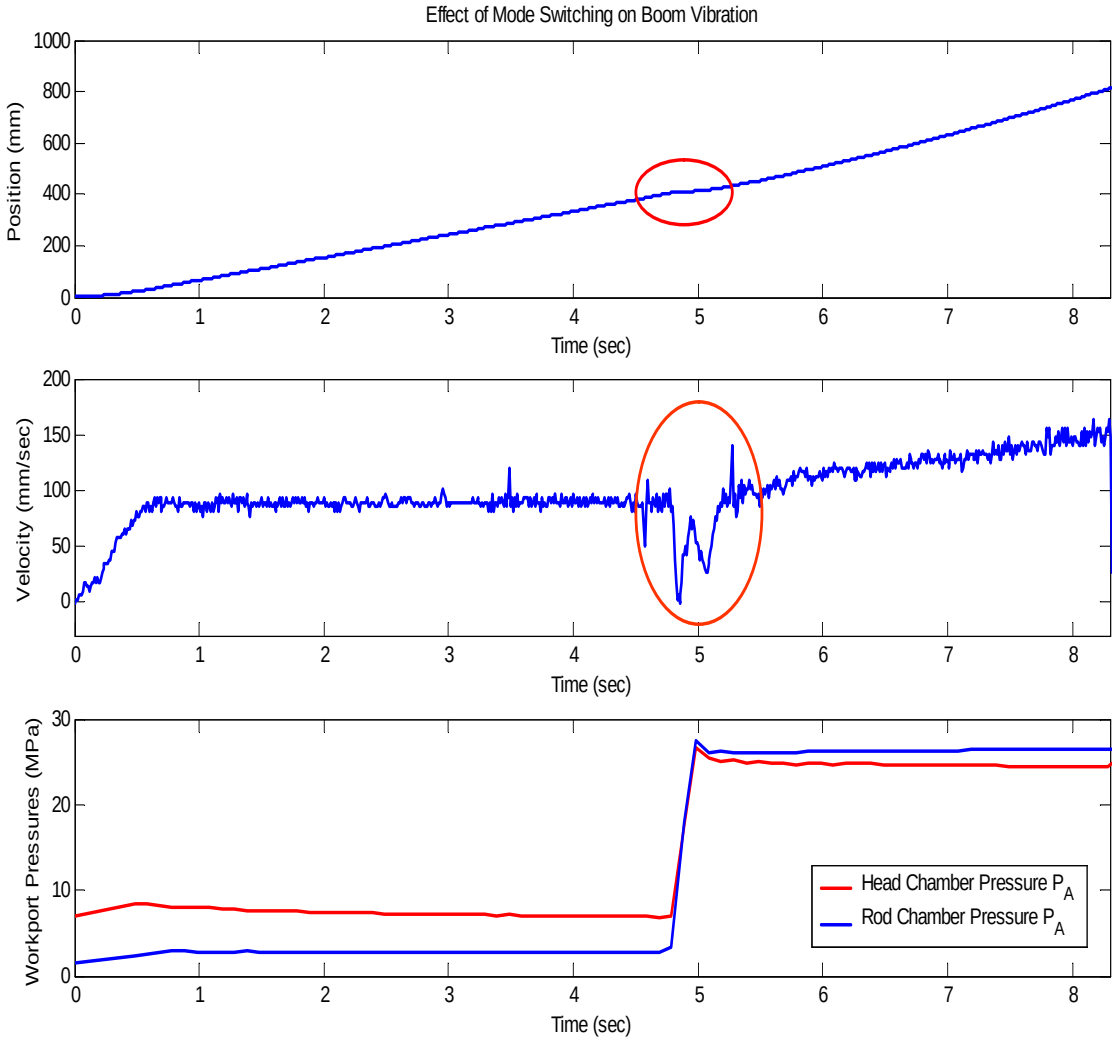

Figure 7.5: Effect of mode switching on boom vibration of telehandler

7.8 Remarks: Motivation of Continuously Variable Modes

In this chapter the equations describing the dynamic interaction of a rotating beam and a hydraulic actuator controlled by a four-valve independent metering configuration was derived and then converted to non-dimensional format. A reduced order model including the rigid body mode of the beam and the first flexural mode was the focus. Although the actuator-beam dynamic interaction can be a focal point that motivates tuning the design parameters of both the beam and the actuator to achieve favorable performance, the analysis in this chapter has concentrated on mode switching effect on beam vibration.

A telehandler boom has been used as an example of the system analyzed. The effect of mode switching between PE and HSRE in mid motion illustrated the effect on beam vibration. Both simulation and experiment has showed that despite the highly desirable gain in speed capability and reduction of pump flow that result from switching to HSRE, the beam vibration and the resulting disruption of beam velocity behavior are unacceptable and make mode switching practically infeasible.

The vibration and velocity performance problems in addition to the limited capability of discrete modes such as PE and HSRE, show that these modes may not be a good way to control the four-valve independent metering configuration. In the next chapter a different idea that has the potential of solving these problems is explored. Instead of using two-valve discrete modes as has been described until now, the idea of three-valve continuously variable modes is introduced. It is shown that these new modes can enhance the mode force-speed capabilities of the actuator in addition to alleviating beam vibration and velocity performance problems.

CHAPTER VIII

CONTINUOUSLY VARIABLE MODES

8.1 General

Thus far the focus of this work has been on the distinct metering modes, e.g PE, HSRE. Their potential to save energy and optimal switching between modes has been studied in previous chapters. It has also been shown that these distinct metering modes may not be a good way of controlling the four-valve independent metering modes configuration. Switching between modes, for example, involves closing one poppet valve and opening another. These valves are not infinitely fast and thus an interruption in the fluid flow path resulting from mode switching causes a disruption in the velocity of the actuator and some vibration in the mechanical system being driven by that actuator.

This chapter introduces the idea of Continuously Variable Modes (CVMs). Instead of having five distinct modes that determines the flow path by opening two of the four valves in the assembly, three Continuously Variable Modes are presented as an alternative way of controlling the four-valve configuration. These three CVMs combine the distinct modes and use three of the four valves to provide the fluid flow path. Therefore, these modes could alternatively be called *Three-Valve Modulation Modes*. The five distinct modes become a special case of these three CVMs.

It will be shown that CVMs have more force-speed capabilities than the distinct modes and provide for better velocity and vibrational performance by virtue of always offering a continuous flow path even when closing one poppet valve and opening another. The first mode is Powered-High Side Regeneration Extension mode (PHSRE), the second is Powered-Low Side Regeneration Retraction mode (PLSRR), and the third is Powered-Low Side Regeneration Extension mode (PLSRE). CVMs involve modulating three valves and imply continuous variation between two distinct modes, hence the name Continuously Variable Modes.

Modeling of these modes is presented next. The issue of mode capability, which has been discussed in section 6.3 for PE versus HSRE and LSRE modes, is revisited again to show that CVMs offers more force-velocity capability than the distinct modes. Following this, PLSRE is used as an example of how to control these modes since this mode is used as an example for experimental verification in chapter 9. These modes require different supply pressure set point calculations than presented for the distinct modes in chapter 2 and these calculations are presented later. A simulation of the effect of using CVMs on beam vibration is finally given as an example for CVMs enhanced performance.

In the rest of this chapter and the following chapters, continuously variable modes are referred by their names followed by "*CVM*" or just by the word "*mode*". For example, PHSRE is referred to as either PHSRE CVM or PHSRE mode.

8.2 Powered-High Side Regeneration Extension Mode (PHSRE)

This mode uses the valves K_{sa}, K_{sb}, and K_{bt} as shown in figure 8.1. This system can be thought of as equivalent to an electric circuit with a pressure source, a resistance, a transformer, two other resistances leading to two voltage sources as shown in figure 8.2. The difference is that the hydraulic system is nonlinear due to the square root relationship between flow and pressure across the valves $Q = K\sqrt{\Delta P}$, while electric resistances are generally considered to be linear and follow ohms law $V = IR$.

Modeling this mode is a two step process. The first step focuses on the reducing the rod side branch including rod chamber pressure P_b, two valves K_{sb} and K_{bt}, in addition to supply and return pressures P_s, P_r to an intermediate effective pressure $P_{CVM,\,Inter}$ and intermediate effective valve conductance $K_{CVM,\,Inter}$. The resulting system is the same as a standard PE mode and subsequently can be reduced to a single pressure source P_{CVM} and a single valve conductance K_{CVM}. This modeling sequence is shown in figure 8.3. **In the following modeling process a quasi-static system behavior and turbulent flow characteristics are assumed**.

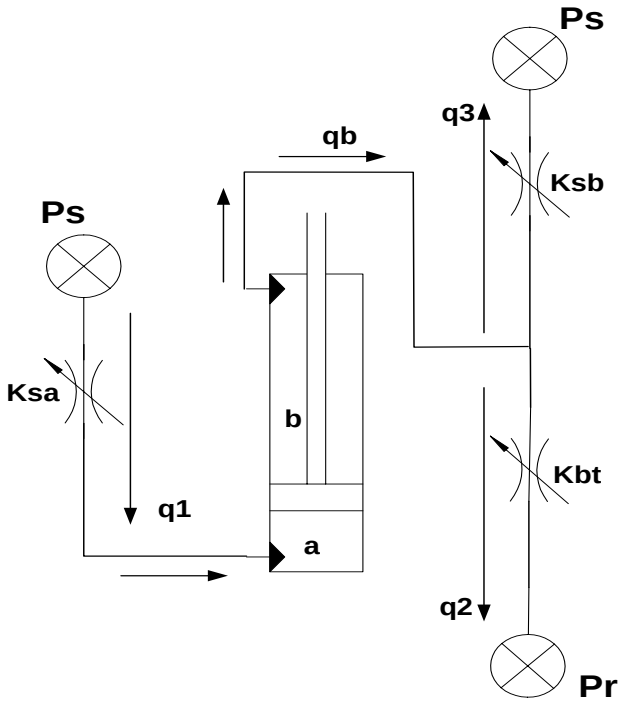

Figure 8.1: Powered-High Side Regeneration Extension CVM

8.2.1 $P_{CVM,Inter}$ and $K_{CVM,Inter}$ for PHSRE

Figure 8.4 shows the first step of the PHSRE mode modeling process. The following equations can be deduced from the figure:

$$\begin{aligned} q_b &= q_2 + q_3 \\ \Rightarrow K_{CVM,Inter}\sqrt{P_b - P_{CVM,Inter}} &= K_{bt}\sqrt{P_b - P_r} + K_{sb}\sqrt{P_b - P_s} \\ \Rightarrow K_{CVM,Inter}^2(P_b - P_{CVM,Inter}) &= K_{bt}^2(P_b - P_r) + K_{sb}^2(P_b - P_s) + \\ & \quad 2K_{bt}K_{sb}\sqrt{(P_b - P_r)(P_b - P_s)} \\ \Rightarrow K_{CVM,Inter}^2 P_b - K_{CVM,Inter}^2 P_{CVM,Inter} &= (K_{bt}^2 + K_{sb}^2)P_b - K_{bt}^2 P_r - \\ & \quad K_{sb}^2 P_s + 2K_{bt}K_{sb}\sqrt{(P_b - P_r)(P_b - P_s)} \end{aligned} \tag{8.1}$$

As a consequence, $P_{CVM,Inter}$ and $K_{CVM,Inter}$ can be defined as:

$$\Rightarrow P_{CVM,Inter} = \frac{K_{bt}^2 P_r + K_{sb}^2 P_s - 2K_{bt}K_{sb}\sqrt{(P_b - P_r)(P_b - P_s)}}{K_{bt}^2 + K_{sb}^2} \tag{8.2}$$

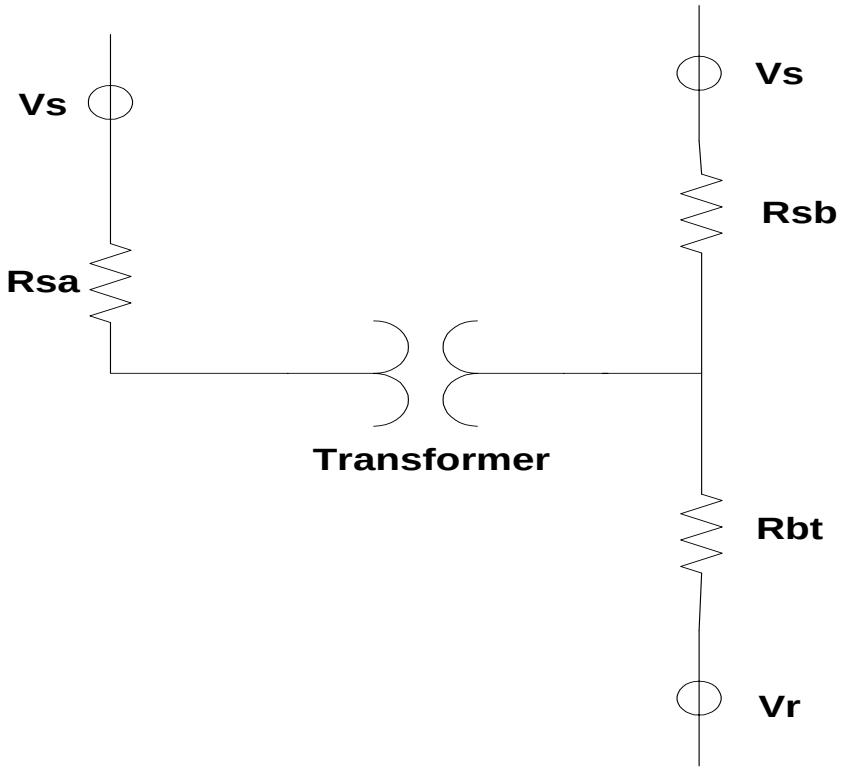

Figure 8.2: Electric circuit equivalent to PHSRE mode

$$\Rightarrow K_{CVM,\,Inter} = \sqrt{K_{bt}^2 + K_{sb}^2} \tag{8.3}$$

8.2.2 P_{CVM} and K_{CVM} for PHSRE

The second step involves the same system topology used for reducing the PE mode with valves K_{sa} and K_{bt} into an effective pressure source and an effective valve conductance in section 2.3.2 and figure 2.7. Therefore, P_{CVM} and K_{CVM} can be written here without re-deriving the methodology:

$$P_{CVM} = R(P_s - P_a) + (P_b - P_{CVM,\,Inter})$$

$$K_{CVM} = \frac{K_{sa}K_{CVM,\,Inter}}{\sqrt{K_{sa}^2 + R^3 K_{CVM,\,Inter}^2}} = \frac{K_{sa}\sqrt{K_{bt}^2 + K_{sb}^2}}{\sqrt{K_{sa}^2 + R^3(K_{bt}^2 + K_{sb}^2)}} = \frac{\dot{x}A_b}{\sqrt{P_{CVM}}} \tag{8.4}$$

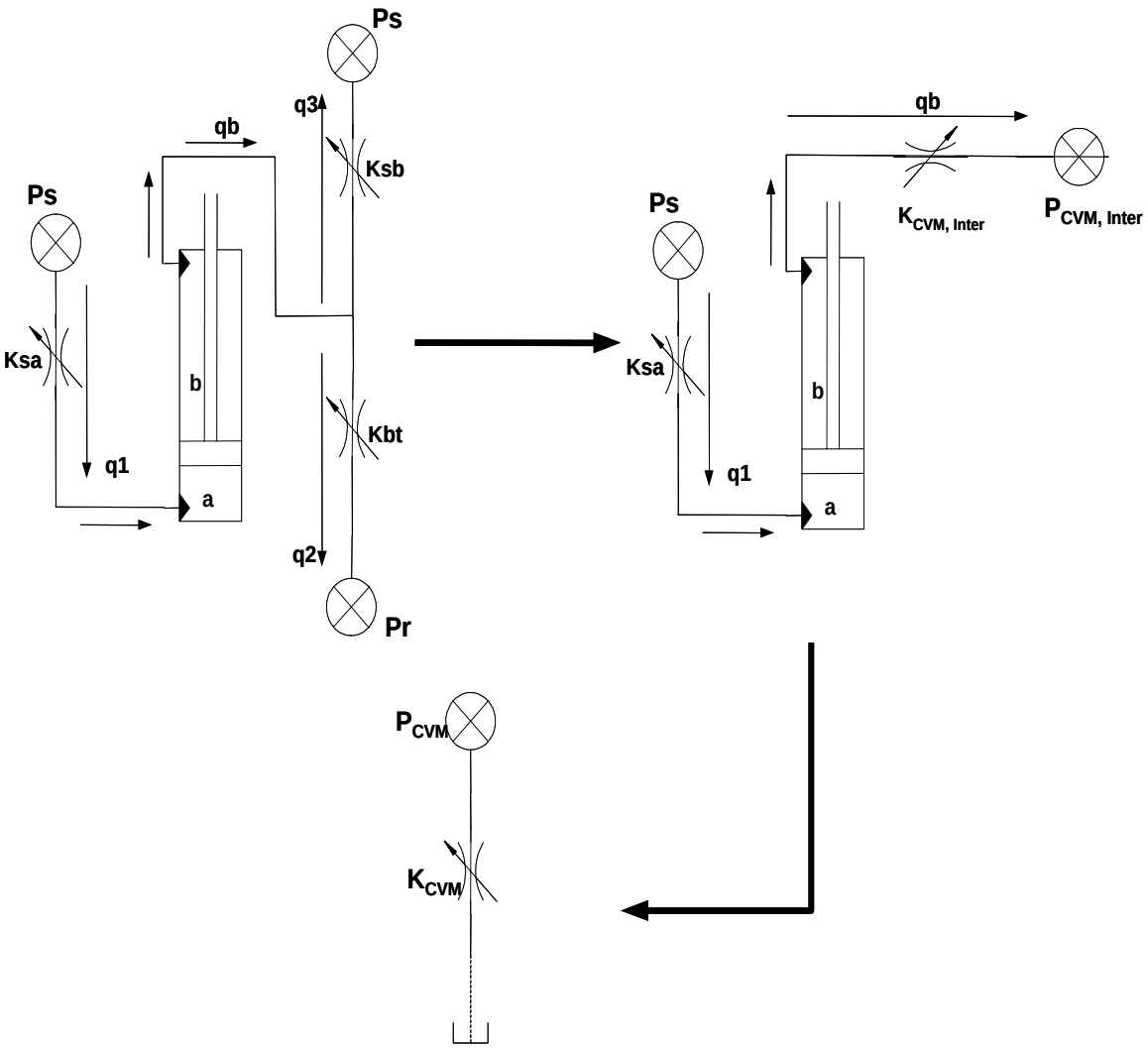

Figure 8.3: Modeling steps of PHSRE mode: a two step process

8.3 Powered-Low Side Regeneration Retraction Mode (PLSRR)

This mode uses the valves K_{at}, K_{sb}, and K_{bt} as shown along with a portrayal of the modeling process in figure 8.5. The same two step modeling process is followed for this mode as well. First step reduces the rod side branch including rod chamber pressure P_b, two valves K_{sb} and K_{bt}, in addition to supply and return pressures P_s, P_r to an intermediate effective pressure $P_{CVM,\,Inter}$ and intermediate effective valve conductance $K_{CVM,\,Inter}$. The resulting system is the same as a standard Powered Retraction (PR) mode and subsequently can be reduced to a single pressure source P_{CVM} and a single valve conductance K_{CVM}.

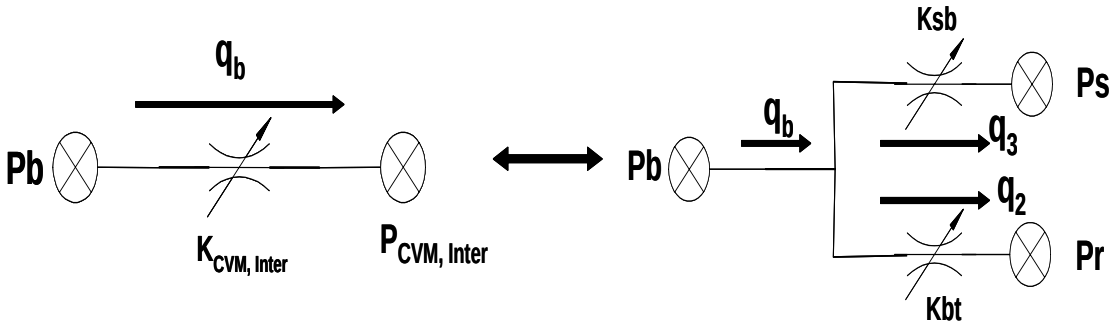

Figure 8.4: First step in modeling PHSRE

8.3.1 $P_{CVM,Inter}$ and $K_{CVM,Inter}$ for PLSRR

Figure 8.6 shows the first step of the PHSRE mode modeling process. The following equation sequence can be deduced from the figure:

$$\begin{aligned} q_b &= q_1 + q_3 \\ \Rightarrow K_{CVM,Inter}\sqrt{P_{CVM,Inter} - P_b} &= K_{bt}\sqrt{P_r - P_b} + K_{sb}\sqrt{P_s - P_b} \\ \Rightarrow K^2_{CVM,Inter}(P_{CVM,Inter} - P_b) &= K^2_{bt}(P_r - P_b) + K^2_{sb}(P_s - P_b) \\ &\quad +2K_{bt}K_{sb}\sqrt{(P_r - P_b)(P_s - P_b)} \\ \Rightarrow K^2_{CVM,Inter}P_{CVM,Inter} - K^2_{CVM,Inter}P_b &= -(K^2_{bt} + K^2_{sb})P_b + K^2_{bt}P_r \\ &\quad +K^2_{sb}P_s + 2K_{bt}K_{sb}\sqrt{(P_r - P_b)(P_s - P_b)} \end{aligned} \tag{8.5}$$

As a consequence, $P_{CVM,Inter}$ and $K_{CVM,Inter}$ can be defined as:

$$\Rightarrow P_{CVM,Inter} = \frac{K^2_{bt}P_r + K^2_{sb}P_s + 2K_{bt}K_{sb}\sqrt{(P_r - P_b)(P_s - P_b)}}{K^2_{bt} + K^2_{sb}} \tag{8.6}$$

$$\Rightarrow K_{CVM,Inter} = \sqrt{K^2_{bt} + K^2_{sb}} \tag{8.7}$$

8.3.2 P_{CVM} and K_{CVM} for PLSRR

The second step involves the same system topology used for reducing the PR mode with valves K_{sb} and K_{at} into an effective pressure source and an effective valve conductance. Consequently, P_{CVM} and K_{CVM} can be written as:

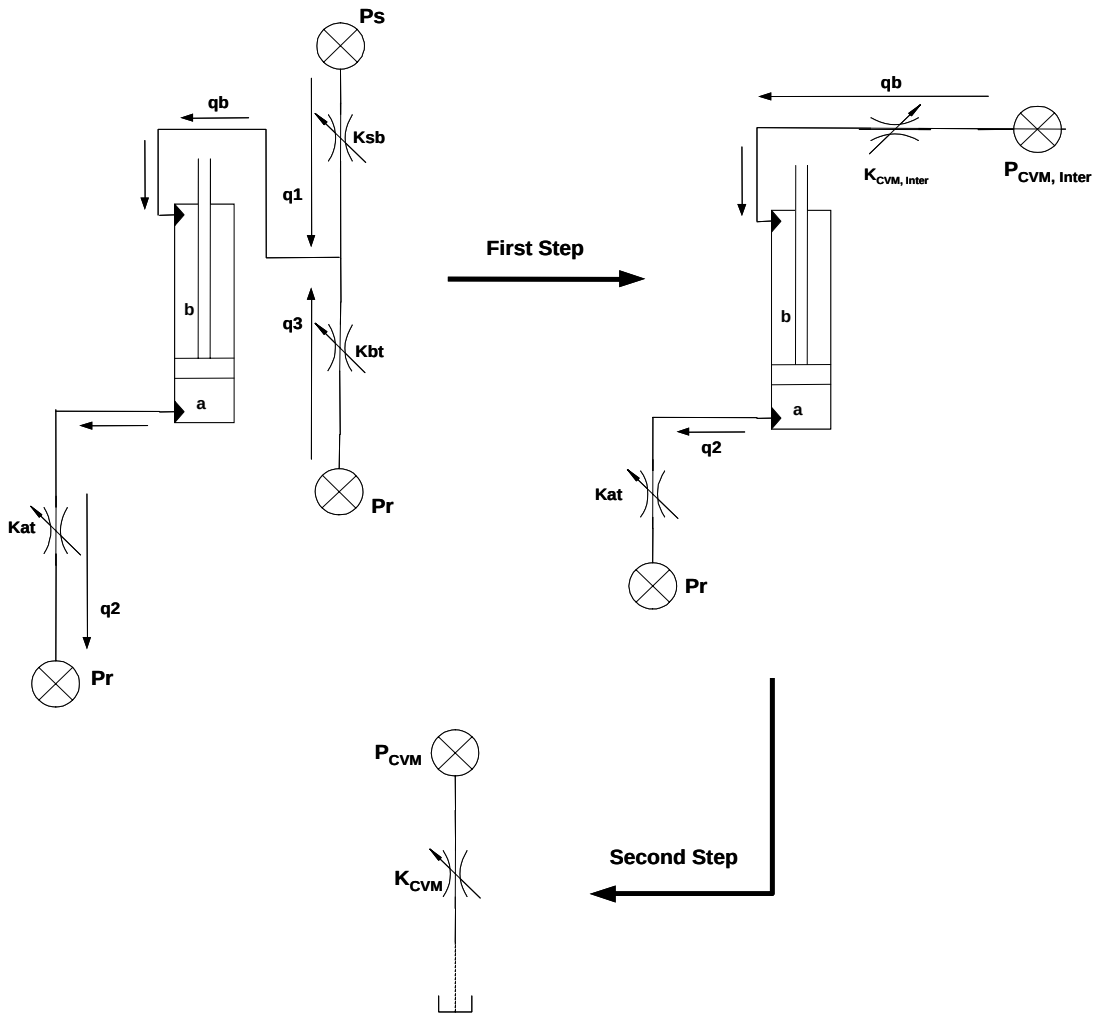

Figure 8.5: Modeling steps of PLSRR CVM

$$P_{CVM} = R(P_a - P_r) + (P_{CVM,Inter} - P_b)$$

$$K_{CVM} = \frac{K_{at}K_{CVM,Inter}}{\sqrt{K_{at}^2 + R^3 K_{CVM,Inter}^2}} = \frac{K_{at}\sqrt{K_{bt}^2 + K_{sb}^2}}{\sqrt{K_{at}^2 + R^3(K_{bt}^2 + K_{sb}^2)}} = \frac{\dot{x}A_b}{\sqrt{P_{CVM}}} \tag{8.8}$$

8.4 Powered-Low Side Regeneration Extension Mode (PLSRE)

This mode uses the valves K_{sa}, K_{at}, and K_{bt} as shown along with a depiction of the modeling process in figure 8.7. Again, the same two step modeling process is followed for this mode

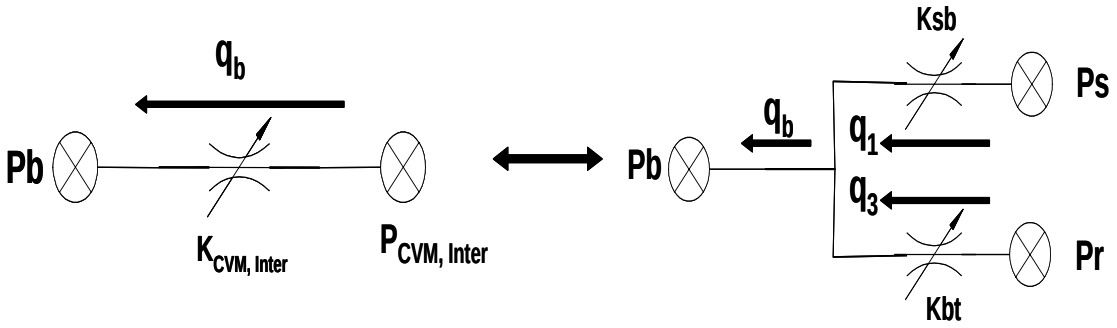

Figure 8.6: First step in modeling PLSRR

also. First step reduces the head side branch including supply and return pressures P_s, P_r, two valves K_{sa} and K_{at}, in addition to head chamber pressure P_a, to an intermediate effective pressure $P_{CVM,Inter}$ and intermediate effective valve conductance $K_{CVM,Inter}$. The resulting system is the same as a standard Powered Extension (PE) mode and subsequently can be reduced to a single pressure source P_{CVM} and a single valve conductance K_{CVM}.

8.4.1 $P_{CVM,Inter}$ and $K_{CVM,Inter}$ for PLSRE

Figure 8.8 shows the first step of the PLSRE mode modeling process. The following equation sequence can be deduced from the figure:

$$\begin{aligned} q_a &= q_1 + q_3 \\ \Rightarrow K_{CVM,Inter}\sqrt{P_{CVM,Inter} - P_a} &= K_{sa}\sqrt{P_s - P_a} + K_{at}\sqrt{P_r - P_a} \\ \Rightarrow K^2_{CVM,Inter}(P_{CVM,Inter} - P_a) &= K^2_{sa}(P_s - P_a) + K^2_{at}(P_r - P_a) \\ &\quad + 2K_{sa}K_{at}\sqrt{(P_s - P_a)(P_r - P_a)} \\ \Rightarrow K^2_{CVM,Inter}P_{CVM,Inter} - K^2_{CVM,Inter}P_a &= -(K^2_{sa} + K^2_{at})P_a + K^2_{at}P_r \\ &\quad + K^2_{sa}P_s + 2K_{bt}K_{sb}\sqrt{(P_r - P_a)(P_s - P_a)} \end{aligned} \tag{8.9}$$

As a consequence, $P_{CVM,Inter}$ and $K_{CVM,Inter}$ can be defined as:

$$\Rightarrow P_{CVM,Inter} = \frac{K^2_{at}P_r + K^2_{sa}P_s + 2K_{at}K_{sa}\sqrt{(P_s - P_a)(P_r - P_a)}}{K^2_{sa} + K^2_{at}} \tag{8.10}$$

$$\Rightarrow K_{CVM,Inter} = \sqrt{K^2_{sa} + K^2_{at}} \tag{8.11}$$

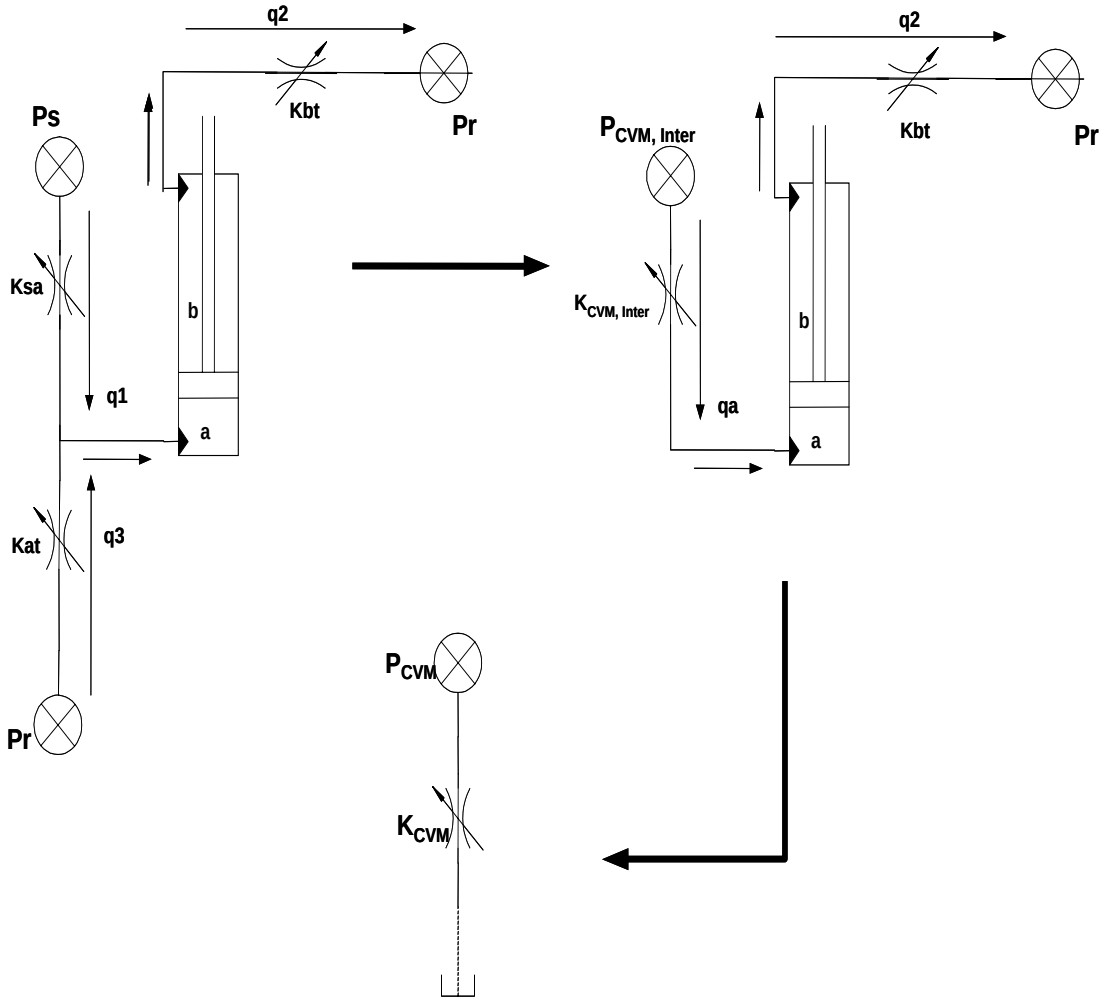

Figure 8.7: Modeling steps of PLSRE CVM

8.4.2 P_{CVM} and K_{CVM} for PLSRE

The second step involves the same system topology used for reducing the PE mode with valves K_{sa} and K_{bt} into an effective pressure source and an effective valve conductance. Consequently, P_{CVM} and K_{CVM} can be written as:

$$P_{CVM} = R(P_{CVM,\,Inter} - P_a) + (P_b - P_r)$$

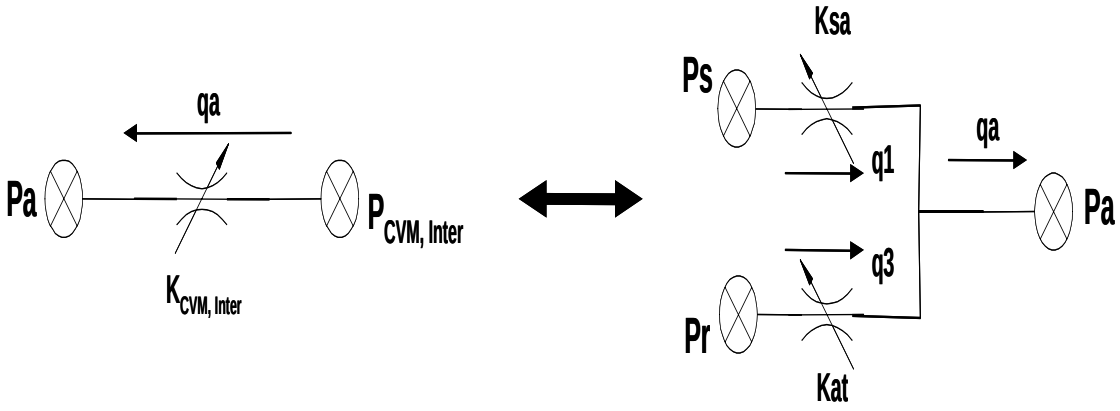

Figure 8.8: First step in modeling PLSRE

$$K_{CVM} = \frac{K_{bt}K_{CVM,Inter}}{\sqrt{K_{CVM,Inter}^2 + R^3K_{bt}^2}} = \frac{K_{bt}\sqrt{K_{sa}^2 + K_{at}^2}}{\sqrt{K_{sa}^2 + K_{at}^2 + R^3K_{bt}^2}} = \frac{\dot{x}A_b}{\sqrt{P_{CVM}}} \tag{8.12}$$

8.5 Mode Capability of Continuously Variable Modes and Comparison with Distinct Modes

In this section, the force and speed capabilities of CVMs are studied. The force-speed characteristics of PHSRE are compared to those of PE and HSRE, which has been shown in section 6.3 and the force-speed characteristics of PLSRE are compared to those of PE and LSRE. It is shown that CVMs have more force-speed capability than the distinct modes.

8.5.1 PHSRE CVM versus PE and HSRE Distinct Modes

PE and HSRE can be considered as special cases of PHSRE modes, and as a consequence of that, PHSRE mode can definitely achieve the same force-speed capability of PE and HSRE. Moreover, by changing the ratio of K_{sb} and K_{bt} it is shown that PHSRE can increase the performance envelope.

Following the analysis shown in section 6.3, the speed that the actuator can achieve is limited by how much flow the pump can supply. The force capability that the actuator can provide depends on the load itself the maximum supply pressure that the pump can supply.

The speed of the actuator can be expressed in terms of hydraulic force for PHSRE mode

as follows:

$$F = P_a A_a - P_b A_b \tag{8.13}$$

$$\dot{x}_{PHSRE} = \frac{K_{CVM}\sqrt{(RP_s - P_{CVM,Inter}) + (-RP_a + P_b)}}{A_b} \tag{8.14}$$

$$\Rightarrow \dot{x}_{PHSRE} = \frac{K_{CVM}\sqrt{(RP_s - \frac{F}{A_b} - P_{CVM,Inter})}}{A_b} \tag{8.15}$$

K_{CVM} has been derived in equation 8.4 and $P_{CVM,Inter}$ in equation 8.2. To quantify the force limitation due to supply pressure constraint and supply flow restriction due to pump maximum flow boundary, required power is used:

$$Power = P \cdot Q = F \cdot \dot{x} \tag{8.16}$$

$$P_s \cdot Q_{PHSRE} = F_{max} \cdot \dot{x}_{PHSRE} = (P_s A_a - P_{CVM,Inter} A_b)\dot{x}_{PHSRE} \tag{8.17}$$

$$\Rightarrow Q_{PHSRE} = \frac{(P_s A_a - P_{CVM,Inter} A_b)\dot{x}_{PHSRE}}{P_s} \tag{8.18}$$

If Q_{PHSRE} is calculated to be more than Q_{max}, then the speed $\dot{x}_{PHSRE}$ is limited so that $Q_{PHSRE} = Q_{max}$:

$$\dot{x}_{PHSRE} = \frac{Q_{max} P_s}{(P_s A_a - P_{CVM,Inter} A_b)} \tag{8.19}$$

The telehandler extender cylinder is again used as an example. K_{sa} valve opening is assumed to be maximum, while K_{sb} and K_{bt} are varied by a parameter $0 \leq \alpha \leq 1$ such that:

$$K_{bt} = \alpha K_{max}$$

$$K_{sb} = (1 - \alpha) K_{max} \tag{8.20}$$

When $\alpha = 0$, K_{bt} is closed while K_{sb} is opened and this simulates HSRE mode as a special case of PHSRE mode. On the other hand, if $\alpha = 1$, K_{bt} is opened while K_{sb} is closed and this simulates PE mode as a special case of PHSRE mode. As α varies between 0 and 1 the capabilities of PHSRE mode are explored. A force range from $0 \rightarrow 100\,KN$ is used to plot

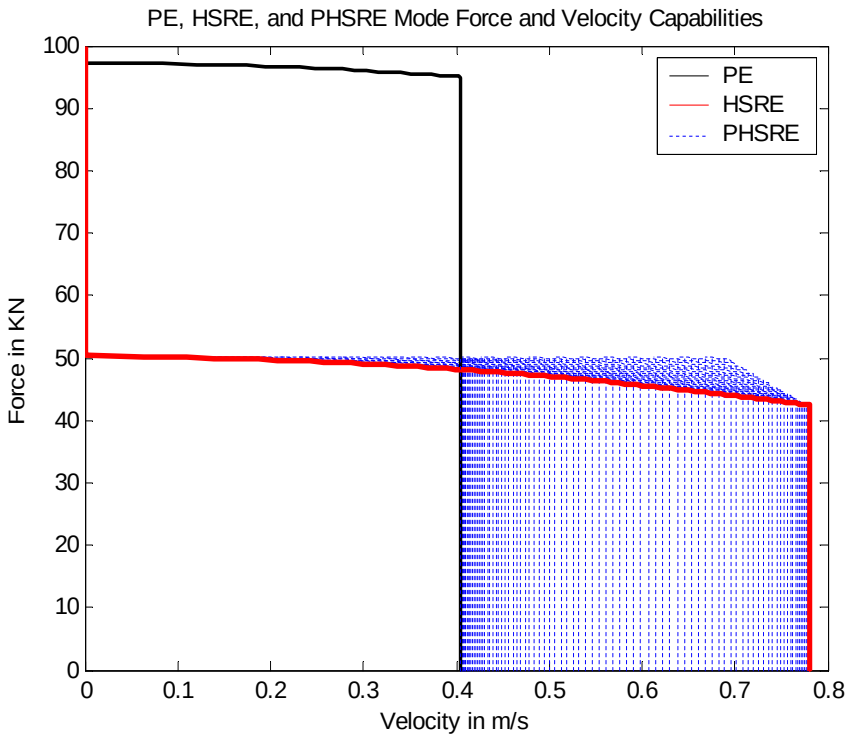

Figure 8.9: PHSRE mode force-speed capability curves

the force-speed curve for PHSRE mode as shown in figure 8.9. The maximum pump flow is $5520\,L/h$.

Figure 8.9 shows that as α varies and force-speed curve of PHSRE is varied as well between PE and HSRE curves. PHSRE, consequently, adds another region of capability that cannot be reached by PE or HSER. It pushed the capability envelope to include operating points, i.e. moving loads at certain speeds, that are not possible with distinct PE and HSRE modes.

The limitations mentioned in section 6.3 are no longer limitations. It has been mentioned that if the actuator needs to push a force of $50.3\,KN$ at a commanded speed of $0.7\,m/s$ it cannot. However, with PHSRE CVM concept, this operating point is achievable and the actuator can push a load of $50.3\,KN$ at a commanded speed of $0.7\,m/s$.

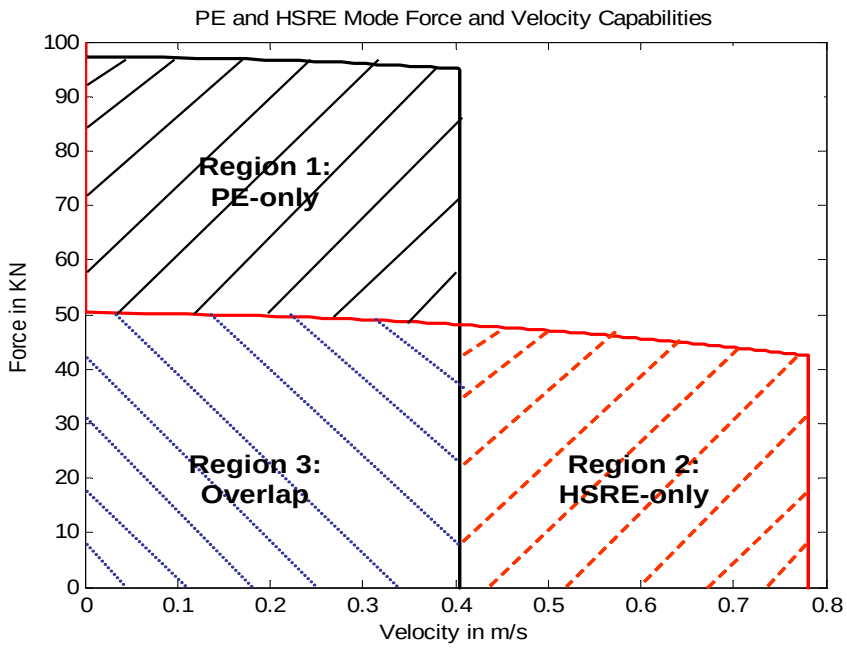

Figure 8.10: Three regions of capability

In addition to expanding the capability or performance envelope, no switching is required. Using PHSRE entails keeping three valves opening most of the time and consequently closing a poppet valve and opening another to switch modes and access a different capability region is not required anymore. This promises to alleviate velocity and vibration performance problems as will be discussed in this chapter and the next chapter as well.

8.6 PLSRE CVM Quasi-Static Valve Control

PLSRE is chosen to be an example of how to control individual valves in CVMs. Valve control implies choosing individual valve openings that achieve a specific K_{CVM} which translates into a specific actuator speed that is commanded by the operator through a joystick for example. Valve control in CVM case is more complicated than for distinct modes that has been explained in chapter 2 because three valves are involved in addition to the dependence of $P_{CVM,Inter}$, and thus P_{CVM}, on valve openings.

Assuming that that commanded speed is $\dot{x}_{com}$, K_{CVM} can be calculated from:

$$K_{CVM} = \frac{A_b \dot{x}_{com}}{\sqrt{P_{CVM}}} = \frac{A_b \dot{x}_{com}}{R(P_{CVM,Inter} - Pa) + (P_b - P_r)} \tag{8.21}$$

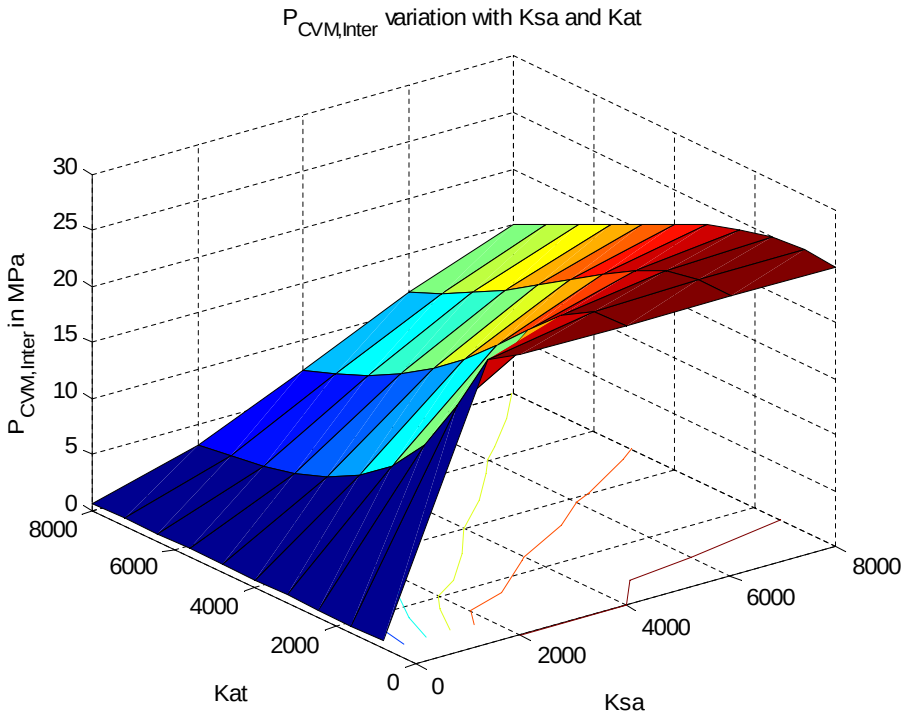

Figure 8.11: 3D surface showing variation of $P_{CVM,\,Inter}$ with K_{at} and K_{sa}

Where:

$$P_{CVM,\,Inter} = \frac{K_{at}^2 P_r + K_{sa}^2 P_s + 2K_{at}K_{sa}\sqrt{(P_s - P_a)(P_r - P_a)}}{K_{sa}^2 + K_{at}^2} \tag{8.22}$$

and:

$$K_{CVM} = \frac{K_{bt}\sqrt{K_{sa}^2 + K_{at}^2}}{\sqrt{K_{sa}^2 + K_{at}^2 + R^3 K_{bt}^2}} \tag{8.23}$$

It is clear that $P_{CVM,\,Inter}$ and P_{CVM} depend not only on load and supply and return pressures, but on K_{at} and K_{sa} as well. Figure 8.11 shows the $P_{CVM,\,Inter}$ as a surface and its contour plot as a function of K_{at} and K_{sa} and figure 8.12 shows the variation of P_{CVM}. The contour plots imply that an infinite number of linear combinations corresponding to a specific ratio of K_{at} and K_{sa} realize the same pressure $P_{CVM,\,Inter}$. Same is true for P_{CVM}.

Considering equation 8.23 for K_{CVM}, if $K_{sa} = 0$, the system is reduced to LSRE mode configuration discussed in chapter 2 and the 3D surface describing the variation of K_{CVM} with K_{at} and K_{bt} would be the same as figure 2.8. However, for PLSRE mode generally $K_{sa} \neq 0$ and the 3D surface describing the variation of K_{CVM} with K_{at}

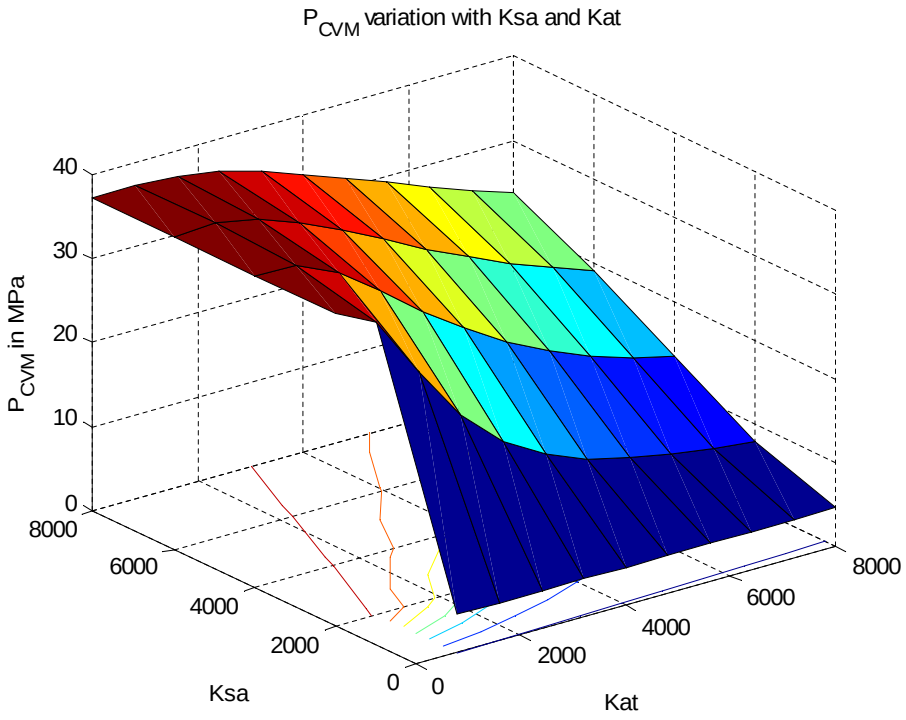

Figure 8.12: 3D surface showing variation of P_{CVM} with K_{at} and K_{sa} (PLSRE)

and K_{bt} is different. Several of these 3D surfaces are shown in figure 8.13 for K_{sa} = 0, 2000, 4000, 6000, 8000 $\frac{LpH}{\sqrt{MPa}}$. It is obvious that the K_{CVM} surface for $K_{sa} \neq 0$ is different than the surface in figure 2.8, which is for a value of $K_{sa} = 0$ or the LSRE mode. To further visualize the effect of K_{sa}, the contour plot of K_{CVM} versus K_{at} and K_{bt} for values of $K_{sa} = 3000$, 5000 $\frac{LpH}{\sqrt{MPa}}$ is shown in figures 8.14 and 8.15, respectively.

In figure 8.14, it is shown that for low values of K_{CVM} e.g. 500, 1000 $\frac{LpH}{\sqrt{MPa}}$ the contour plot is almost a line indicating that the effect of K_{at} is minimal and that almost any value of K_{at} gives the same K_{CVM} with very little variation. K_{CVM} is dominated by K_{sa} and K_{bt}. For example, choosing a value for $K_{sa} = 3000$ $\frac{LpH}{\sqrt{MPa}}$ and $K_{bt} = 1000$ $\frac{LpH}{\sqrt{MPa}}$ varying K_{at} from 0 to 1000 $\frac{LpH}{\sqrt{MPa}}$ and finally to 8000 $\frac{LpH}{\sqrt{MPa}}$, which is the maximum physical value varies K_{CVM} from 888.2 $\frac{LpH}{\sqrt{MPa}}$ to 897.7 $\frac{LpH}{\sqrt{MPa}}$ and to 983.9 $\frac{LpH}{\sqrt{MPa}}$ only, which show slight variation given the wide variation in K_{at}.

This behavior can be explained by observing that small K_{CVM} values imply small commanded speeds and, therefore, a small amount of flow is needed and the maximum amount

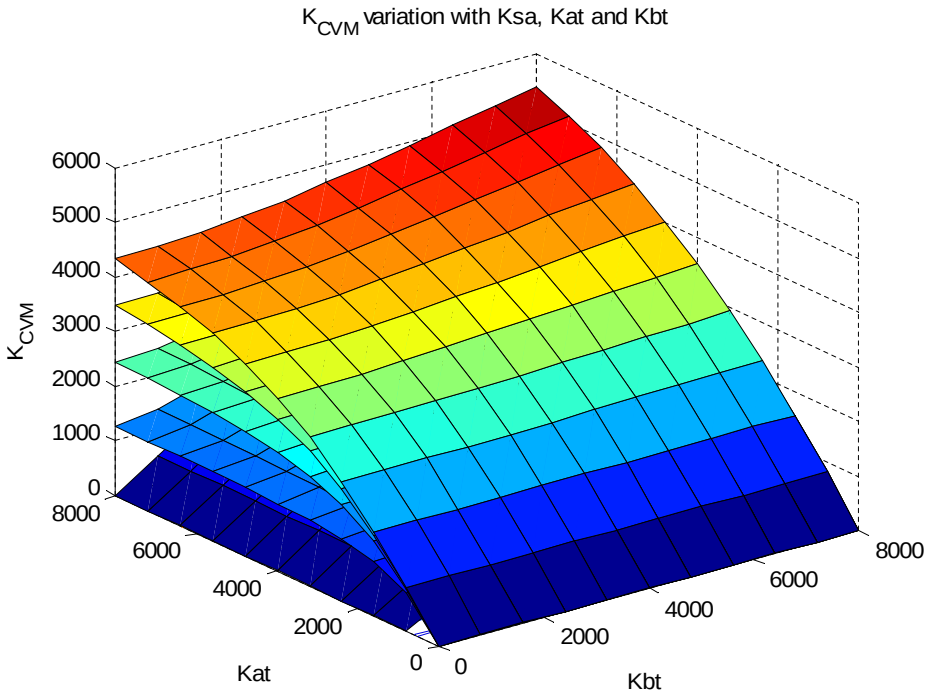

Figure 8.13: 3D surfaces showing variation of K_{CVM} with K_{at} and K_{bt} for several values of K_{sa} (PLSRE)

of flow allowed to regenerate can be recirculated with a small value of K_{at} and further opening the valve does not affect the overall system behavior.

However, for larger values of K_{CVM} e.g. $2000\,\frac{LpH}{\sqrt{MPa}}$ and larger values, the variation behavior of K_{CVM} with K_{at} and K_{bt} is similar to that illustrated in figure 2.9, except that the whole contour plot is shifted upwards. This affects the sensitivity concerns explained in section 2.4.1. As a result of this upward shift in the contour plot, reducing valve sensitivity effects entails choosing the smallest K_{at}. However, choosing a small K_{at} results in minimized flow regeneration and consequently reduces potential energy savings. A compromise between such requirements is resolved by setting system priorities like those explained in section 2.4.4.

Figure 8.15 shows a similar behavior for $K_{sa} = 5000\,\frac{LpH}{\sqrt{MPa}}$ except that even larger values of K_{CVM} illustrate independence of specific K_{at} values and domination of K_{sa} and K_{bt}, which is expected when increasing K_{sa} or inlet flow.

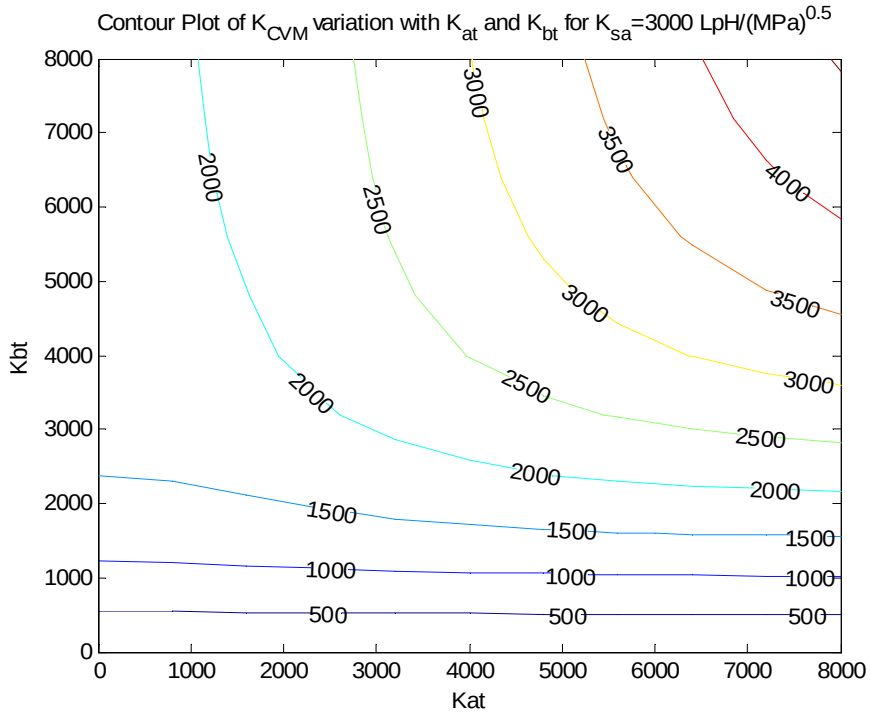

Figure 8.14: Contour plot of K_{CVM} variation with K_{at} and K_{bt} for $K_{sa} = 3000 \frac{LpH}{\sqrt{MPa}}$

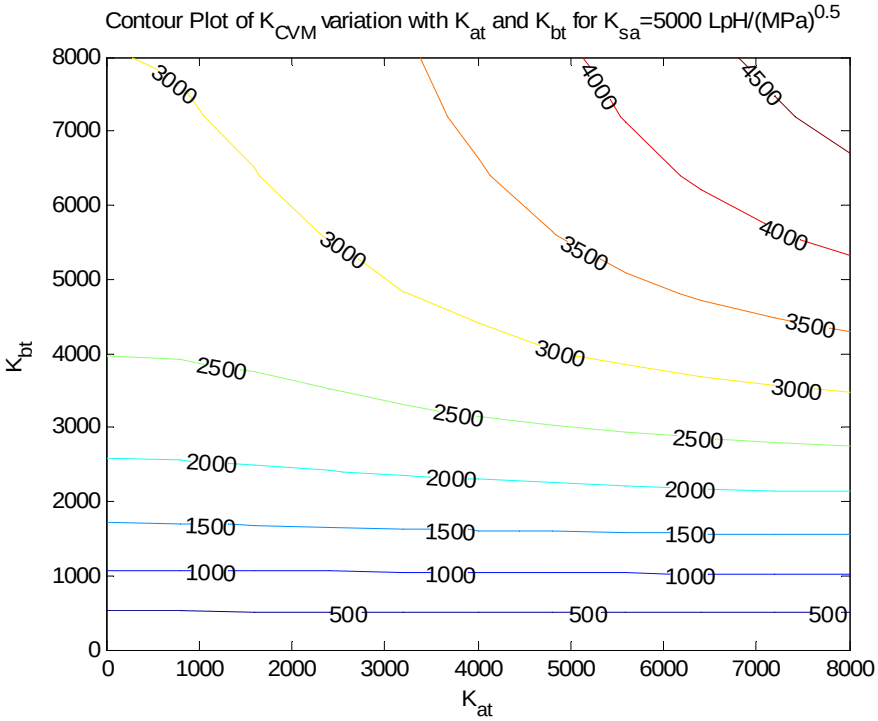

Figure 8.15: Contour plot of K_{CVM} variation with K_{at} and K_{bt} for $K_{sa} = 5000 \frac{LpH}{\sqrt{MPa}}$

8.6.1 Valve Control Methodology

In this section a valve control methodology is suggested. In other words, given a supply pressure P_s, return pressure P_r, a load F, and a commanded speed $\dot{x}_{Com}$, how the three valve openings K_{sa}, K_{at}, and K_{bt} are determined to move the load at the commanded speed. Assume that the ratio between K_{sa} and K_{at} is γ:

$$K_{sa} = \gamma K_{at} \tag{8.24}$$

Then:

$$K_{CVM,\,Inter} = \sqrt{K_{sa}^2 + K_{at}^2} = \sqrt{\gamma^2 K_{at}^2 + K_{at}^2} = \sqrt{\gamma^2 + 1} K_{at} \tag{8.25}$$

Assuming that K_{bt} is specified to achieve minimum possible throttling losses across the outlet valve, then desired workport pressures $P_{b,\,Des}$ and $P_{a,\,Des}$ are determined for a given load and a commanded speed according to the following equations.

$$P_{b,\,Des} = \frac{(\dot{x}_{Com} A_b)^2}{K_{bt}^2} + P_r \tag{8.26}$$

$$P_{a,\,Des} = \frac{F}{A_a} + \frac{P_{b,\,Des}}{R} \tag{8.27}$$

Thus, $P_{CVM,\,Inter}$ can be calculated:

$$P_{CVM,\,Inter} = \frac{K_{at}^2 P_r + \gamma^2 K_{at}^2 P_s + 2\gamma K_{at}^2 \sqrt{(P_s - P_{a,\,Des})(P_r - P_{a,\,Des})}}{\gamma^2 K_{at}^2 + K_{at}^2} \tag{8.28}$$

Dividing numerator and denominator of 8.28 by K_{at}^2, $P_{CVM,\,Inter}$ can be written with just the ratio γ appearing in the equation and without any specific valve opening:

$$P_{CVM,\,Inter} = \frac{P_r + \gamma^2 P_s + 2\gamma \sqrt{(P_s - P_{a,\,Des})(P_r - P_{a,\,Des})}}{\gamma^2 + 1} \tag{8.29}$$

Consequently, for a given γ, $P_{CVM,\,Inter}$ can be determined from equation 8.29 for a given load and return and supply pressures and subsequently, P_{CVM} can be easily calculated:

$$P_{CVM} = R(P_{CVM,\,Inter} - P_{a,\,Des}) + (P_{b,\,Des} - P_r) = P_{CVM} = R P_{CVM,\,Inter} - \frac{F}{A_b} - P_r \tag{8.30}$$

As a result of having calculated P_{CVM} a commanded speed can be translated into a specific K_{CVM} for the value of $P_{a,\,Des}$ determined by the choice of K_{bt}:

$$K_{CVM} = \frac{\dot{x}_{Com} A_b}{\sqrt{P_{CVM}}} \tag{8.31}$$

The purpose of being able to control PLSRE mode is to convert the K_{CVM} that corresponds to a certain commanded speed into individual valve opening K_{sa}, K_{at}, and K_{bt}.

$$K_{CVM} = \frac{K_{CVM,\,Inter} K_{bt}}{\sqrt{K_{CVM,\,Inter}^2 + R^3 K_{bt}^2}} = \frac{\sqrt{\gamma^2+1} K_{at} K_{bt}}{\sqrt{(\gamma^2+1)K_{at}^2 + R^3 K_{bt}^2}} \tag{8.32}$$

$$\Rightarrow K_{CVM}^2[(\gamma^2+1)K_{at}^2 + R^3 K_{bt}^2] = (\gamma^2+1)K_{at}^2 K_{bt}^2 \tag{8.33}$$

From equation 8.33 valve opening for K_{at} can be evaluated given K_{bt} as follows:

$$K_{at}^2 = \frac{R^3 K_{CVM}^2 K_{bt}^2}{(\gamma^2+1)[K_{bt}^2 - K_{CVM}^2]}$$

$$\Rightarrow K_{at} = \frac{R^{3/2} K_{CVM} K_{bt}}{\sqrt{(\gamma^2+1)[K_{bt}^2 - K_{CVM}^2]}} \tag{8.34}$$

In summary, as a result of this analysis, given a specific load F and certain supply and return pressures P_s and P_r in addition to the ratio γ, and choosing a specific K_{bt} that leads to desired workport pressures, then K_{CVM} can be determined from equation 8.31 and accordingly K_{at} is determined from equation 8.34.

Multiplying K_{at} by γ results in K_{sa} and thus the three valve openings are determined for the commanded speed.

It is worth noting that selecting γ is crucial for PLSRE mode capability. A higher γ means a larger ratio $\frac{K_{sa}}{K_{at}}$ and it indicates a higher force capability and less speed capability when compared with a smaller γ.

Although, this control methodology is parallel to the discrete modes velocity control method presented in chapter 2, it is not perfectly analogous. K_{eq} in chapter 2 represents a surface of solution points that could achieve the commanded speed for a given load, supply pressure, and return pressure. This is due to the fact that P_{eq} is constant for a given load, and does not depend on an individual workport pressure.

In the PLSRE CVM control methodology represented in this section, P_{CVM} depends on an individual workport pressure through its dependence on $P_{CVM,\,Inter}$. Therefore, K_{CVM} does not represent a surface of solutions but a contour or a curve in the $3D$ space of valve openings K_{sa}, K_{bt}, and K_{at} depending on the individual workport pressure P_a.

8.7 Supply Pressure Set Point

As in the case of distinct modes, based on the load that the actuator has to move and the minimum pressure that needs to be maintained across poppet valves, a particular pump supply pressure is needed. In this section, the supply pressure set point required for an actuator to operate in CVMs is derived. A different supply pressure is needed for each of the three CVMs. Derivation of supply pressure set point in the case of PHSRE mode is presented. Instead of repeating similar derivations for PLSRE and PLSRR modes, the final results for supply pressure set point are given.

8.7.1 Supply Pressure Set Point for PHSRE CVM

Figure 8.16 shows valves involved in PHSRE mode. The following equation can be written:

$$P_s A_a - P_r A_b - P_s A_b = \Delta P_1 A_a + (P_a A_a - 2P_b A_b) + A_b \Delta P_2 + A_b \Delta P_3 \tag{8.35}$$

Where:

$$\Delta P_1 = P_s - P_a$$

$$\Delta P_2 = P_b - P_r$$

$$\Delta P_3 = P_b - P_s$$

Dividing by A_b:

$$\Rightarrow (R-1)P_s - P_r - RP_a + 2P_b = R\Delta P_1 + \Delta P_2 + \Delta P_3 \tag{8.36}$$

EHPV valves need a minimum pressure ΔP_{min} across them for satisfactory performance. Supply pressure set point $Ps_{set-point}$ needs to supply this minimum pressure across the valves even if the velocity requirements do not demand such a supply pressure. Thus, if each of these $\Delta P's$ in equation 8.36 is replaced by this minimum pressure ΔP_{min}, then solving for P_s in equation 8.36:

$$\Rightarrow Ps_{set-point} = \frac{(R+2)\Delta P_{min}}{R-1} + \frac{RP_a - 2P_b + P_r}{R-1} \tag{8.37}$$

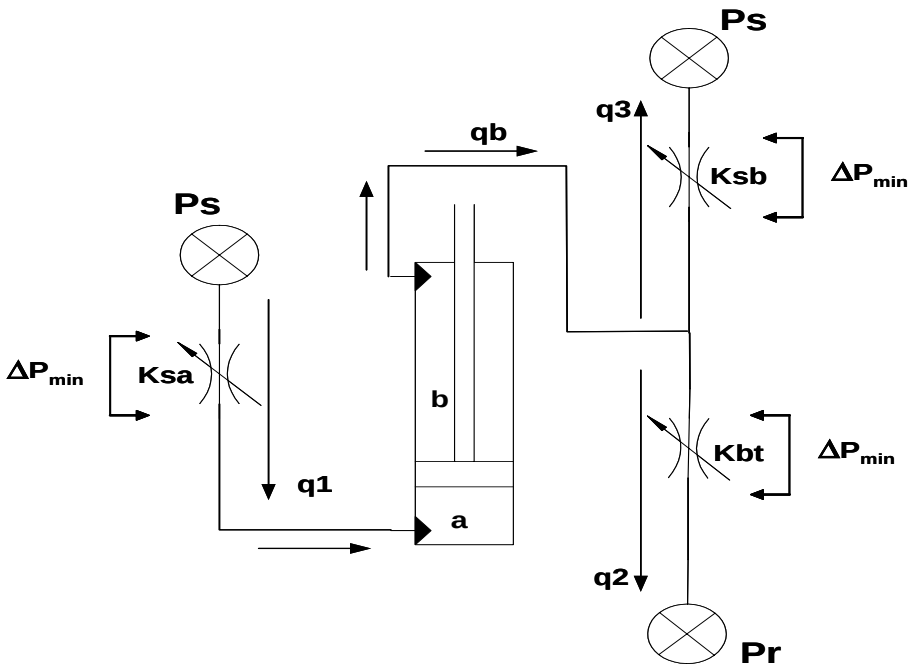

Figure 8.16: Calculating $Ps_{set-point}$ for PHSRE mode

8.7.2 Supply Pressure Set Point for PLSRR and PLSRE CVM

Following a similar analysis to the one performed for PHSRE, $Ps_{set-point}$ can be calculated for PLSRR and PLSRE modes. For PLSRR mode it is found to be:

$$Ps_{set-point} = (R+2)\Delta P_{min} - RP_a + 2P_b + (R+1)P_r \tag{8.38}$$

while for PLSRE mode it is found to be:

$$Ps_{set-point} = \frac{(2R+1)\Delta P_{min}}{R} + \frac{2RP_a - P_b - (R-1)P_r}{R} \tag{8.39}$$

8.8 Effect of Using CVMs on Beam Vibration

In section 7.7 the effect of mode switching from PE to HSRE on beam vibration has been discussed. In this section, PHSRE mode is used to to perform the beam motion, i.e. cylinder extension, instead of using the distinct modes PE and HSRE. In other words, a CVM where three valves are modulated instead of closing a valve and opening another to switch modes.

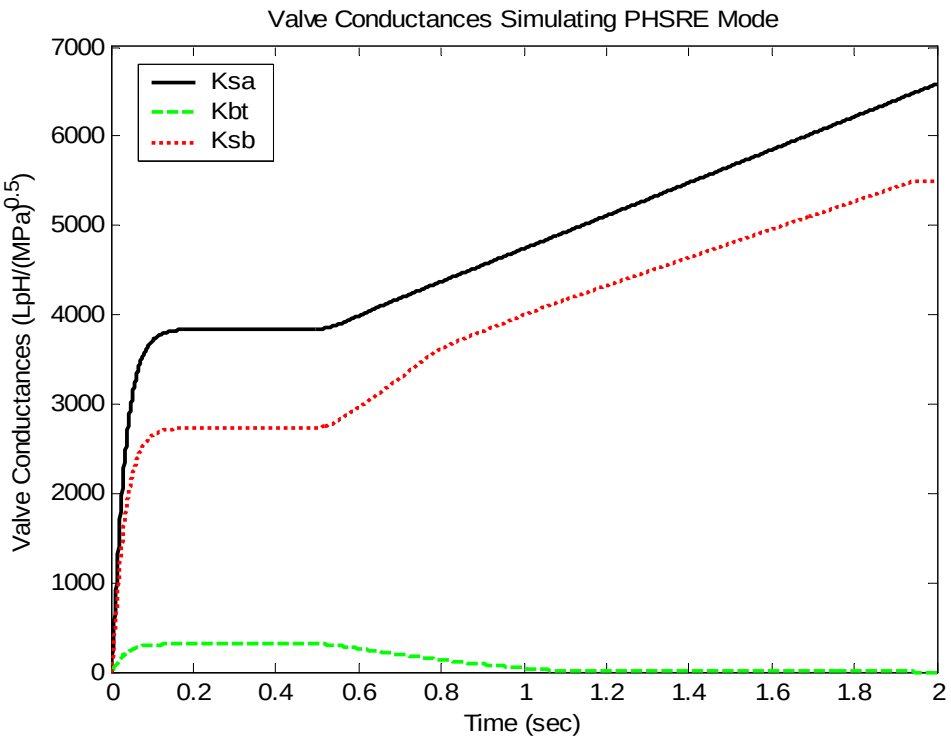

Figure 8.17: Valve conductance coefficients that simulate PHSRE mode

Using the same state space model derived in section 7.7, the system is simulated with valve openings K_{sa}, K_{sb}, and K_{bt} being controlled as shown in figure 8.17.

The system is again simulated using the values $K_{B1} = 2$, $K_{M1} = 0.5$, $K_C = 0.1$, and $\zeta_1 = 0.6$, which are the same typical values used in section 7.7. The simulation results are shown in figure 8.18. Ignoring the transients in the beginning of the motion, it is noticed that motion is very smooth as opposed to the vibration that has been shown in figure 7.3 as a result of mode switching in mid motion. Figure 8.17 shows three valves opened at the beginning of motion. Then, valve K_{bt} closes gradually when high force capability is no longer needed and the actuator thus operates in a special case of PHSRE CVM, which is HSRE mode. In this case, however, no abrupt poppet closure happens while another is opened from a fully closed position, which is the case in discrete mode switching. A continuous flow path has existed all the time, and that is why no flow or velocity disruption has occurred.

Increase in the rigid body angular speed Ω is achieved smoothly without having to close and open valves and thus the hydraulic oil flow path is not disturbed enough to cause beam stopping and vibration. Comparing the performance using PHSRE to that of starting motion in PE and switching to HSRE in figure 7.3 shows a *significant improvement in velocity performance.*

8.9 Remarks on CVMs

This chapter has introduced the idea of CVMs. Modeling and controls techniques have been suggested as well. These modes promise to achieve a smoother velocity performance in addition to higher force and speed capabilities. Simulations show that velocity performance is enhanced and vibration effects of mode switching are alleviated by using CVMs as opposed to discrete modes and switching between them. It is suggested that this due to providing a continuous flow path by modulating three valves and avoiding closing and opening poppet valves to achieve mode switching. The following chapter presents a set of experiments that shows the practical capability of CVMs.

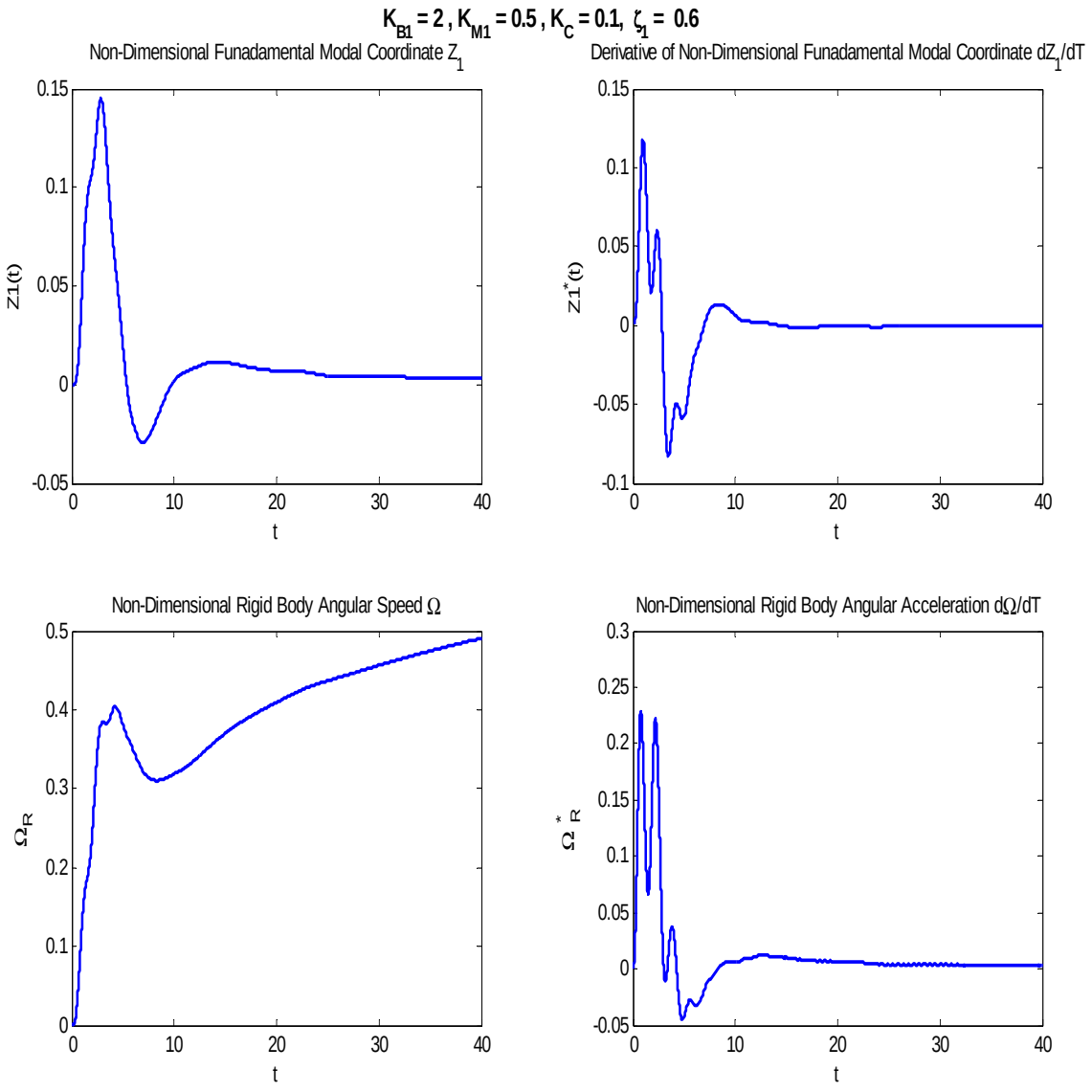

Figure 8.18: No mid motion beam vibrations when using PHSRE mode

CHAPTER IX

EXPERIMENTAL VALIDATION OF CONTINUOUSLY VARIABLE MODES CONCEPT

9.1 General

The previous chapter introduced CVMs and presented a modeling technique and a control method. It showed that CVMs have better force-velocity capabilities than the distinct modes and claims to provide better velocity performance. This chapter experimentally verifies this better velocity performance assertion.

The HUSCO International machine used to perform these experiments is a mid size Tractor Loader Backhoe (TLB) shown in figure 9.1. The Crowd function is chosen for the experiment. If the crowd cylinder is fully retracted and then an extend command is given to the cylinder with the whole stroke done in the air without digging in the ground, gravity assists this extension at first until a point is reached where gravity is not assisting this extend motion anymore and the cylinder needs to provide power to continue extending the crowd. This means that the Low Side Regeneration Extension Mode (LSRE) could be used during the gravity assisted part of the cylinder stroke to save energy and then Powered Extension (PE) could be used to power the rest of the extension stroke.

This motion does not always occur fully in the air, but most of the time some digging in the ground is required. So, for example, motion should start in LSRE then when the bucket touches the ground and starts to meet heavy resistance and requires large force capability, switching to PE should occur. Of course the entire stroke could be performed with PE but it is considered a waste of energy since this does not make use of gravity assistance and regenerative flow.

An experiment is done for both cases: full motion conducted in air, and then the experiment is redone to include a digging scenario. Four controllers are used. The first one

Figure 9.1: Mid size Tractor Loader Backhoe

performs all motion in PE. The second uses LSRE for part of the motion until the load reaches a certain value and then switching to PE occurs. The third controller uses the same scenario as in second controller except that switching does not happen suddenly at a particular load, but transition happens gradually over a range of loads with an interpolation being done between calculations for both LSRE and PE modes throughout this transition range. Finally, the continuous variable mode PLSRE, explained in chapter 8 is used. More about these controllers is said later in the chapter. This constitutes eight experiments; two path conditions: air, and digging, with four different controllers in each condition. Performance comparison follows and superior performance of PLSRE, in terms of velocity performance and energy savings, is established.

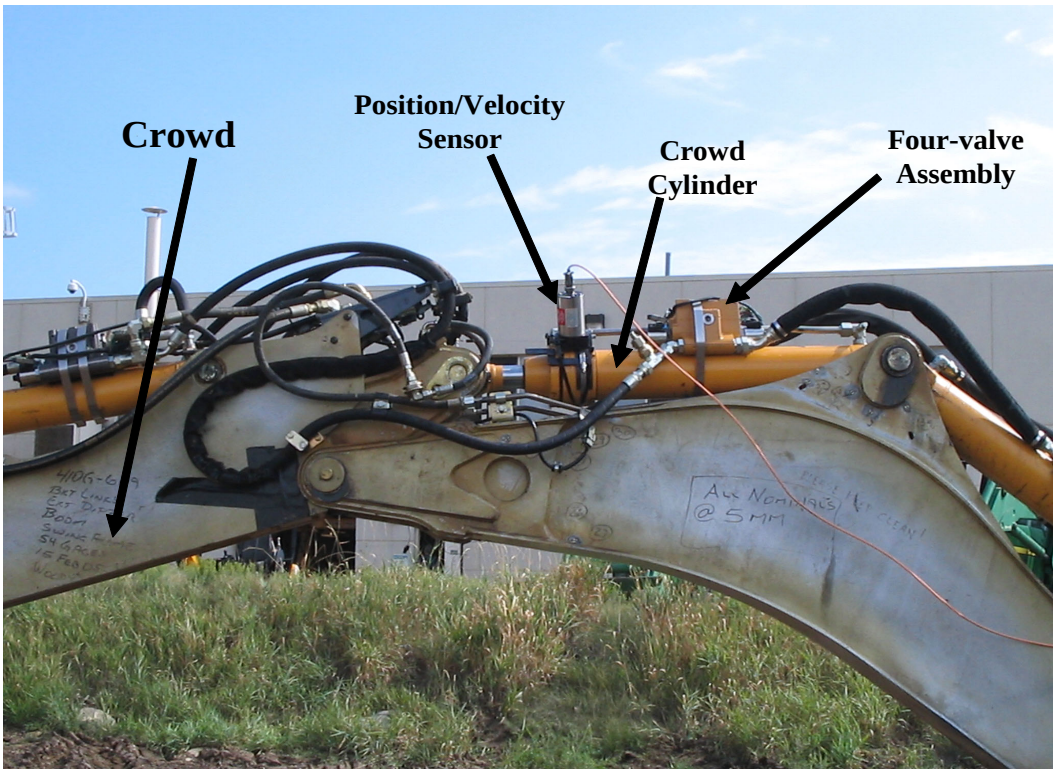

Figure 9.2: Test Setup

9.2 Experiment

9.2.1 Test Setup

Figures 9.2 and 9.3 show a close up on the crowd of the mid size TLB shown in this experiment, which is shown in figure 9.1. The four-valve assembly mounted on the cylinder is shown and the position / velocity sensor is shown is as well.

The valves used in this experiment are a $40\,GPM$ capacity EHPVs. The pump can supply a pressure between $\approx 3\,MPa$ and $25\,MPa$. The maximum pump flow is $8316\,lph$. The stroke of the crowd cylinder is $810\,mm$, the head chamber piston area is $A_a = 7854\,mm^2$, and the rod chamber piston area is $A_b = 4737\,mm^2$.

The crowd cylinder has been fully retracted and then given a speed command of 0.5 Kph (A software change is necessary to ensure that no matter what the joystick position is, the same speed of 0.5 Kph is commanded). The Crowd cylinder is then allowed to fully extend ("Crowd In" motion). In the first set of experiments, all the extend stroke has been

Figure 9.3: Test Setup

done in the air, with no touching or digging the ground. The same set of experiments has been then repeated for a digging condition.

The bucket cylinder is fully extended and kept fully extended throughout the experiment (dead headed) to drive the pump pressure to a high value. As a result of dead heading the bucket, the pump pressure is held almost constant at 25 MPa.

9.2.2 Four Controllers

As mentioned above, four controllers are used and compared. The four controllers are:

1. All the extension stroke is preformed in PE with no switching to any other mode.

2. Motion is started in LSRE to exploit gravity assistance, then at a specific loading condition of $-13.5\,KN$ mode switching to PE occurs in a step, or abrupt, fashion. This is plausible since the remaining part of the motion needs higher force capability when gravity stops being an assisting force and starts to be an opposing force. This

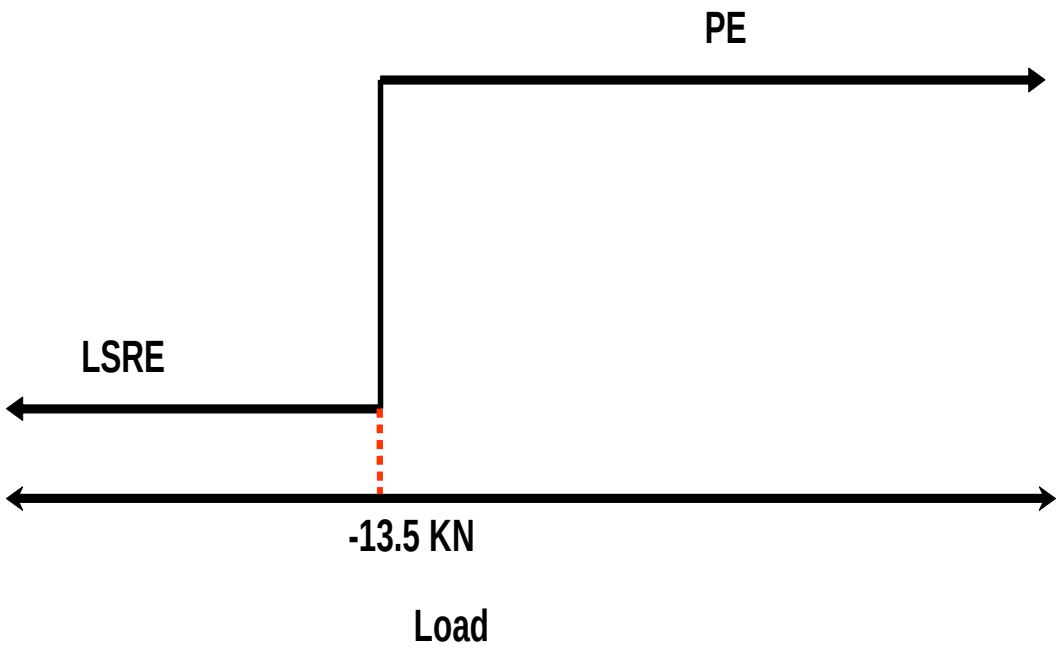

Figure 9.4: Control scheme 2: abrupt mode switching from LSRE to PE

scheme is depicted in figure 9.4.

3. As in the previous controller, motion commences in LSRE to take advantage of gravity assistance. However, instead of abruptly switching to PE, a linear transition between both modes is used as shown in figure 9.5. The range of load over which this transition occurs is between $-13.5\,KN$ and $+5.2\,KN$. In this transition period, calculations are done separately for PE mode and for LSRE modes in terms of required pressure, and valve openings. Linear interpolation then occurs to interpolate between the values calculated for the two modes.

4. The fourth controller uses three valve modulation and specifically PLSRE CVM explained in chapter 8 through out the whole motion.

9.2.3 Flow and Energy Calculation

Pump Flow Calculation:

The flow consumed from the pump is Q_s and it is equal to the flow through valve K_{sa} since there is *no* recirculation through valve K_{sb} in this experiment. Pump flow is then

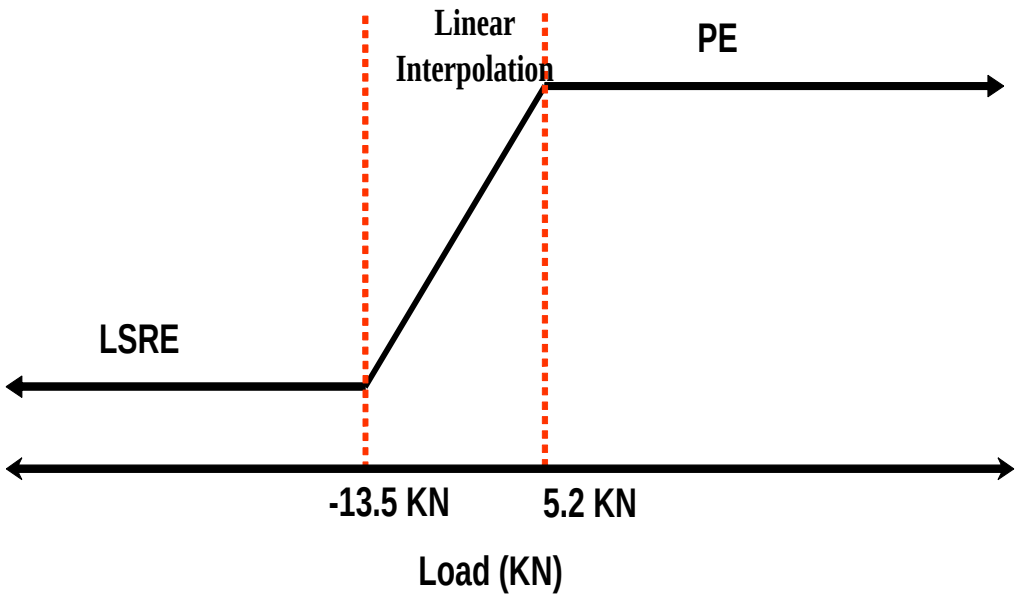

Figure 9.5: Control scheme 3: Linear interpolation transition from LSRE to PE

calculated as follows:

$$Q_s = Q_{sa} = K_{sa}\sqrt{P_s - P_a} \tag{9.1}$$

All the valve coefficients as well as supply pressure and workport pressures P_a and P_b are recorded throughout the experiment and thus the supply flow Q_s can be calculated.

Energy Calculation:

The instantaneous power consumed from the pump is calculated by:

$$Power = P_s \cdot Q_s \tag{9.2}$$

Energy consumed during the full extend stroke of the crowd is the time integral of the instantaneous power:

$$Energy = \int_0^T P_s \cdot Q_s \, dt = \int_0^T P_s \cdot K_{sa}\sqrt{P_s - P_a} \, dt \tag{9.3}$$

All the data in the integrand above are available (measured) as a function of time over the extend stroke and the integration is done numerically in `MATLAB`.

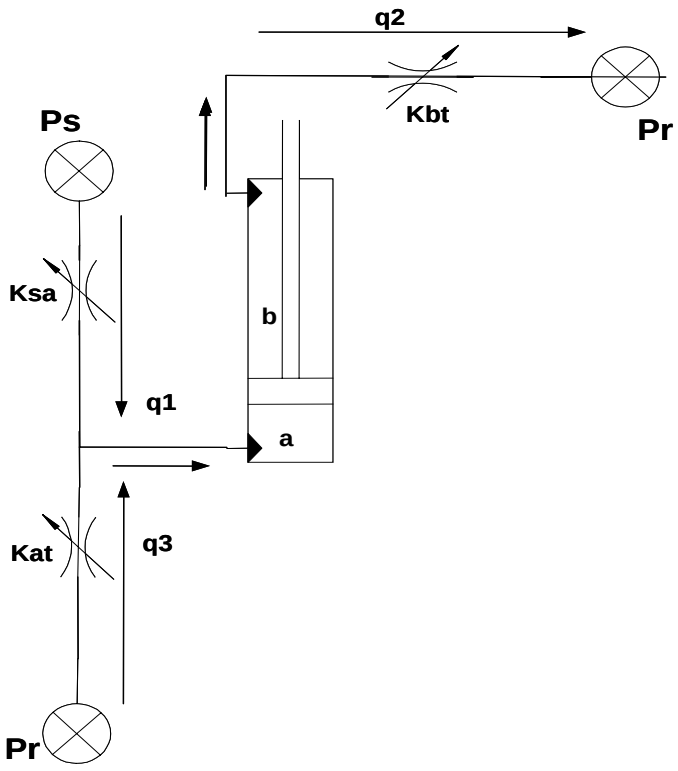

Figure 9.6: Valves being modulated in the different modes

9.3 Results

In this section, the result for the eight experiments conducted are presented. First, the results for the full motion conducted in free air with no digging are presented for the four different controllers. Then, results for the repeated experiments with digging in the ground are presented.

9.3.1 Full Extend Stroke Conducted in The Air with No Digging

As explained above four control schemes are used. First the free motion is fully conducted with PE mode, then same extend stroke is repeated with motion starting in LSRE then abrupt transition to PE occurs when the load reaches $-13.5KN$, then the same motion is repeated with the transition from LSRE to PE happening gradually with a linear interpolation transition across a range of loads from $-13.5\,KN$ to $+5.2\,KN$, and finally PLSRE CVM is used.

9.3.1.1 Controller I: Full Stroke in PE

Figures 9.7, 9.8, and 9.9 show the velocity of the crowd cylinder, valve openings K_{sa} and K_{bt}, and workport pressures P_a and P_b, respectively, when the full stroke is done in PE mode.

Ignoring the transients at the beginning and ending of motion, these plots show that the velocity performance of the crowd cylinder in PE mode is not consistent throughout the stroke. When a positive load is encountered close to the four second mark, the cylinder slows down and this indicates any of these possible causes:

- Since control is based on quasi-static behavior and does not include dynamic behavior, this velocity inconsistency occurs.
- The valves did not re-adjust their openings fast enough to keep the same cylinder speed.

It is clear from workport pressures that rod chamber pressure P_b is higher than head chamber pressure P_a, which is expected since the load is negative. It is also noticed that P_a increases because load is increasing as the cylinder is extending.

The energy consumed in this case according to equation 9.3 is $653.8\,KJ$.

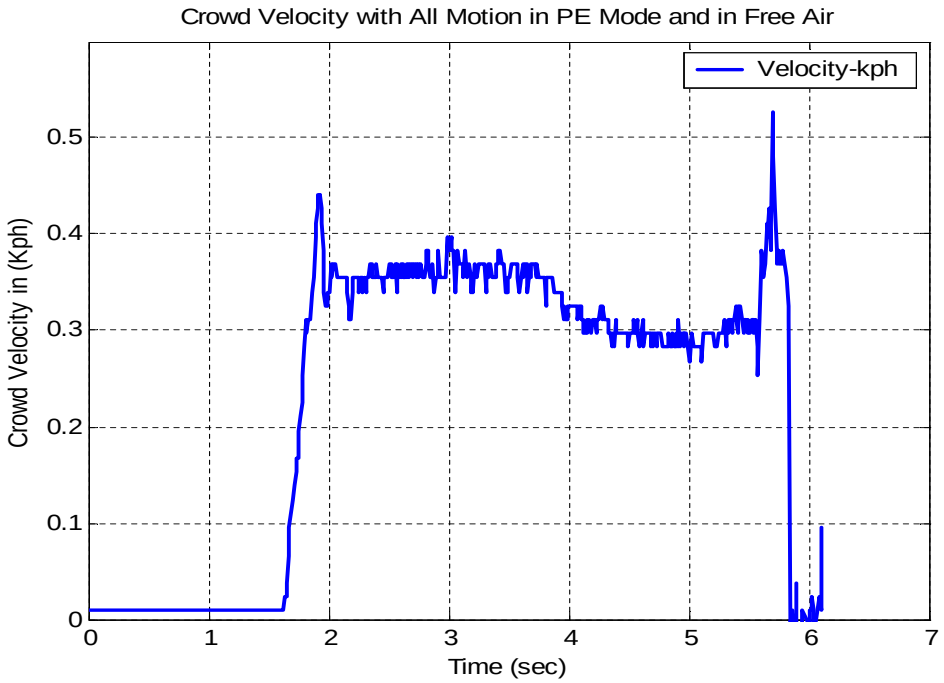

Figure 9.7: Crowd cylinder velocity with all motion in PE and in free air

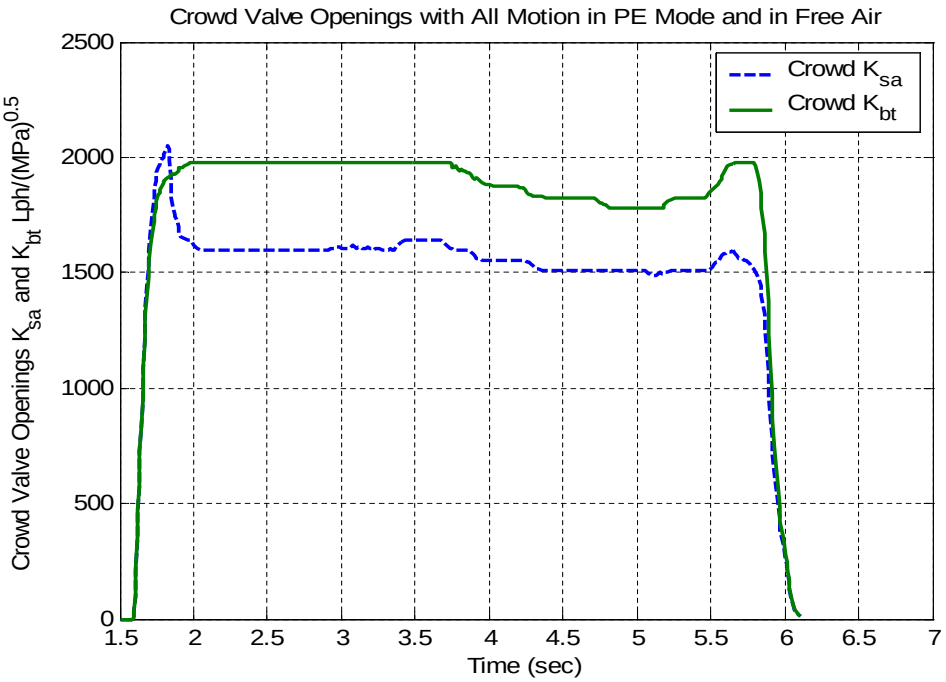

Figure 9.8: Valve openings K_{sa} and K_{bt} for the crowd cylinder with all motion in PE and in free air

Figure 9.9: Workport pressures P_a and P_b for the crowd cylinder with all motion in PE and in free air

9.3.1.2 Controller II: Abrupt Mode Switching from LSRE to PE

Figures 9.10, 9.11, and 9.12 show the velocity of the crowd cylinder, valve openings K_{sa}, K_{at}, and K_{bt}, and workport pressures P_a and P_b, respectively, when the stroke commences in LSRE mode until the load reaches a value of $-13.5\,KN$ then full or abrupt mode switching to PE occurs.

Velocity performance in this case in unacceptable. Looking at figure 9.10, it is observed that speed decreases close to the transition load, then a sudden increase in speed takes place at the transition load. Obviously, any backhoe operator can feel this irregular and rough velocity behavior.

Figure 9.11 shows mode switching by noticing which valves are open. In the LSRE part of the motion, valves K_bt and K_at are opened and provide for velocity control, while K_{sa} is opened a little bit to provide for the difference in flow needed to compensate for area difference between head side of the piston and rod side of the piston. This extra flow can come from another valve not necessarily one of the four-valve assembly controlling the cylinder. When mode switching to PE happens, K_{at} is closed while K_{sa} increases, while K_{bt} remains at the same value. Workport pressures figure 9.12 also shows the mode switching where a sudden increase in pressures is readily noticed.

The energy consumed in this case according to equation 9.3 is $135.1\,KJ$.

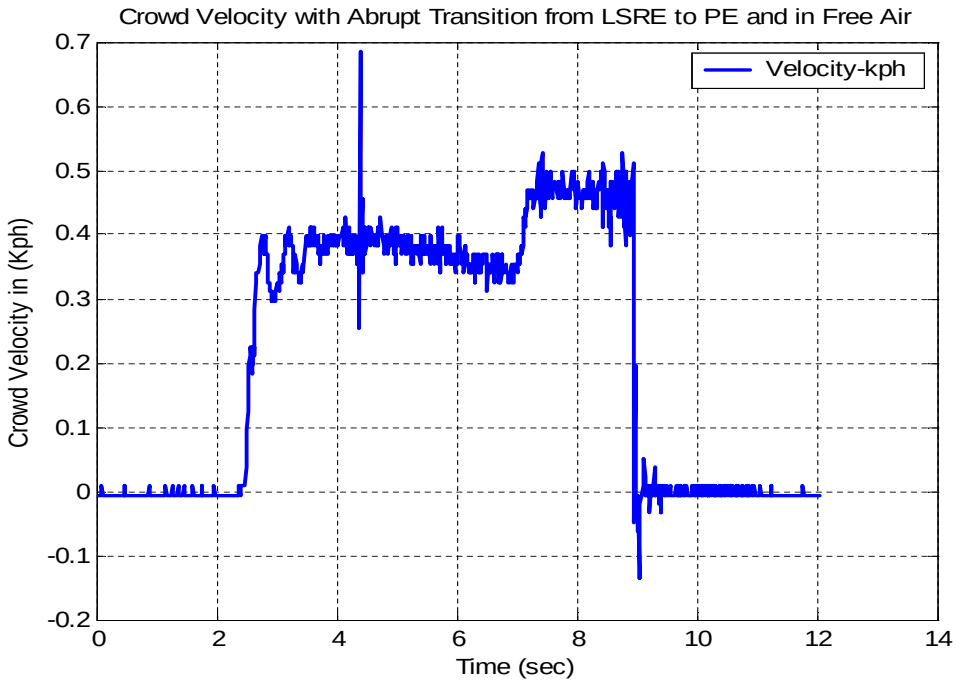

Figure 9.10: Crowd cylinder velocity with abrupt transition from LSRE to PE and in free air

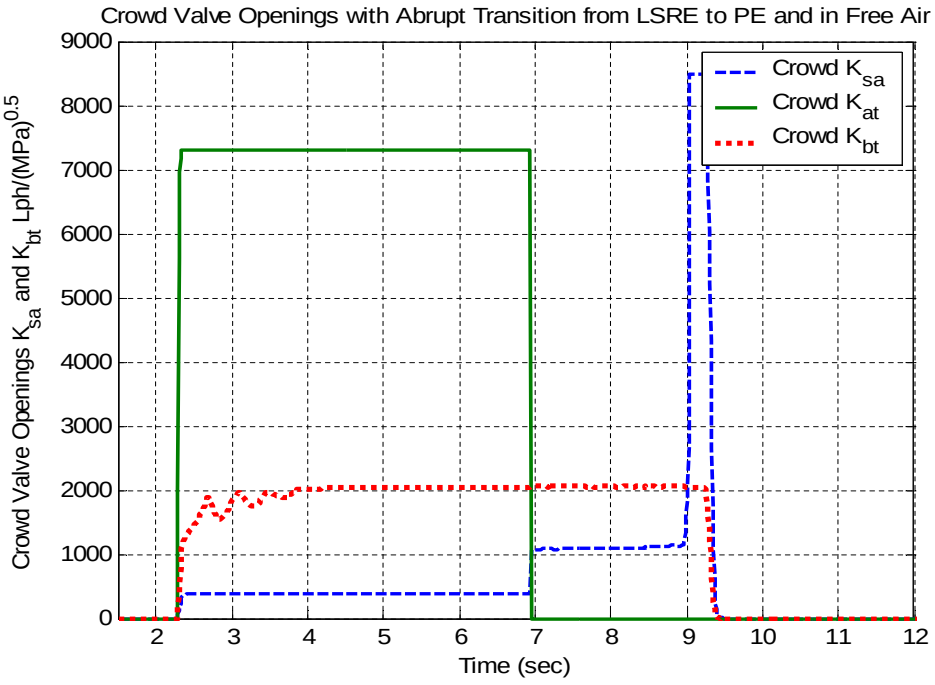

Figure 9.11: Valve openings K_{sa}, K_{at}, and K_{bt} for the crowd cylinder with abrupt transition from LSRE to PE and in free air

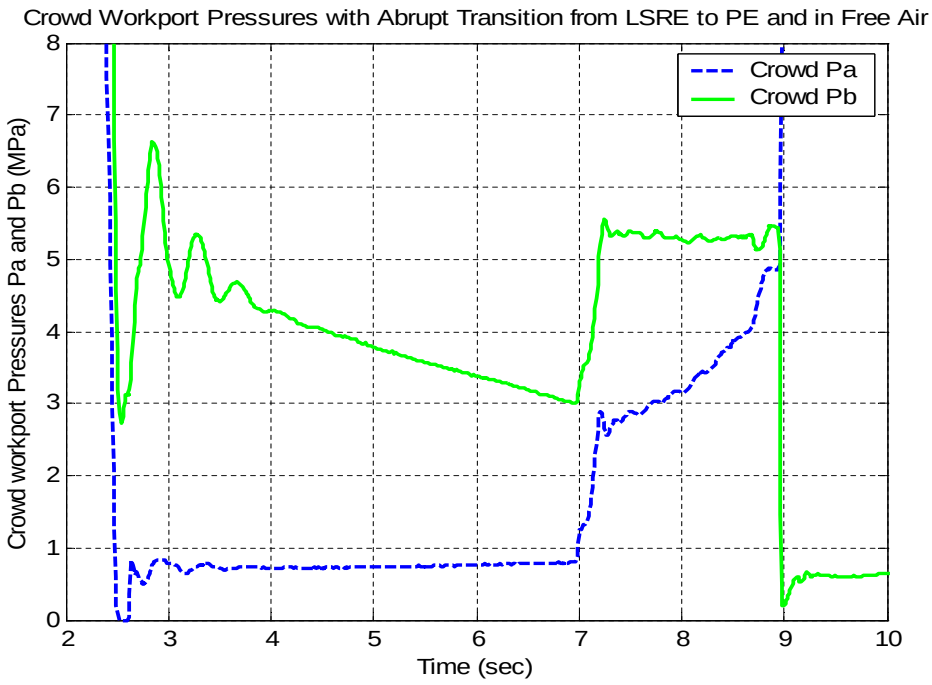

Figure 9.12: Workport pressures P_a and P_b for the crowd cylinder with abrupt transition from LSRE to PE and in free air

9.3.1.3 Controller III: Linear Transition in Mode Switching from LSRE to PE

Figures 9.13, 9.14, and 9.15 show the velocity of the crowd cylinder, valve openings K_{sa}, K_{at} and K_{bt}, and workport pressures P_a and P_b, respectively, when the stroke commences in LSRE mode until the load reaches a value of $-13.5\,KN$ then a linear interpolation between LSRE and PE takes place constituting a transition region until a load of $+5.2\,KN$ where the transition is completed and the cylinder operates fully in PE.

Velocity performance in this case in unacceptable as well. Figure 9.13 again reveals that speed decreases close to and throughout the transition period, then a sudden increase in speed takes place at the end of the transition region. Backhoe operator can feel this irregular and rough velocity behavior in this case as well.

Figure 9.14 shows the gradual mode switching where instead of valve K_{at} closing suddenly, it gradually closes in a linear fashion, while K_{sa} increases linearly also instead of a sudden increase in its value. This is less noticeable in the workport pressure figure 9.15 where workport pressures change gradually as opposed to the sudden change depicted in figure 9.12.

The energy consumed in this case according to equation 9.3 is $129.1\,KJ$.

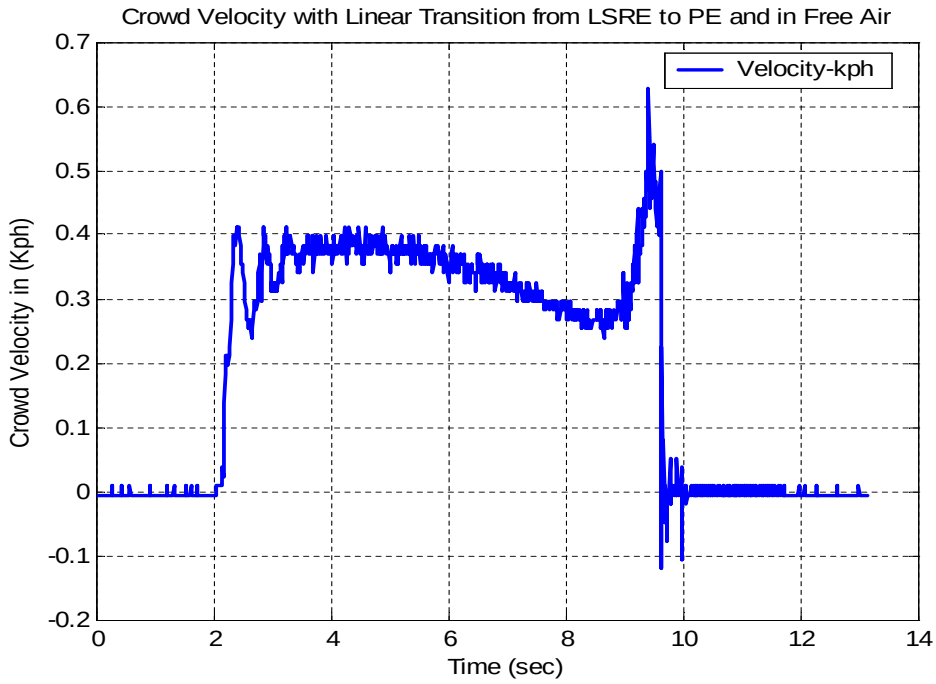

Figure 9.13: Crowd cylinder velocity with linear transition from LSRE to PE and in free air

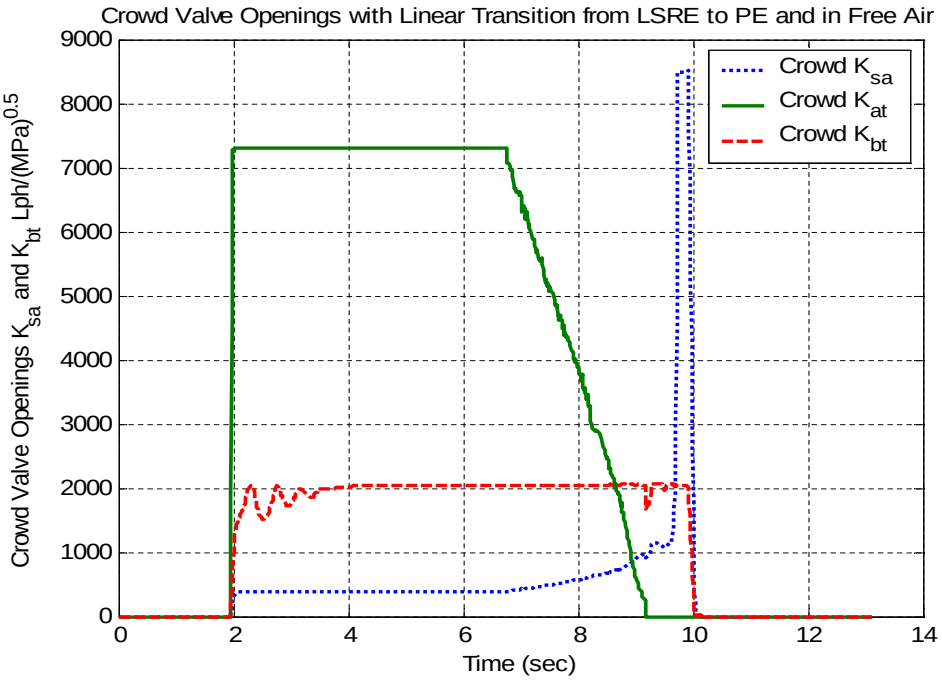

Figure 9.14: Valve openings K_{sa}, K_{at}, and K_{bt} for the crowd cylinder with linear transition from LSRE to PE and in free air

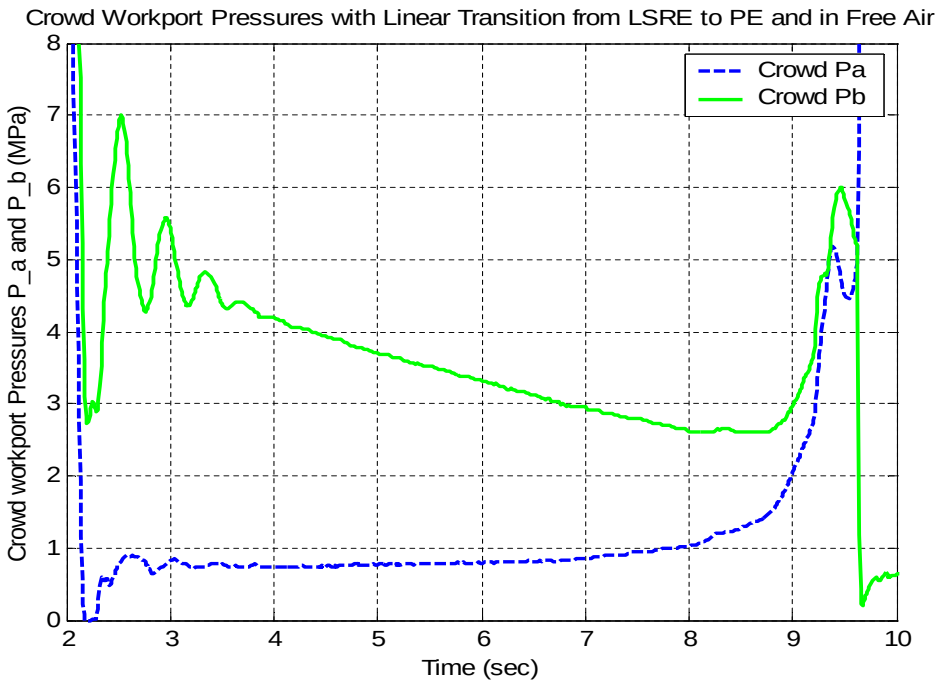

Figure 9.15: Workport pressures P_a and P_b for the crowd cylinder with linear transition from LSRE to PE and in free air

9.3.1.4 Controller IV: PLSRE CVM Control

Finally, the concept of CVM is tested as controller IV. PLSRE CVM control explained in the previous chapter is used to control the extend stroke of the crowd cylinder. Three 2-D tables have been generated: one for each of the three valves K_{sa}, K_{at}, and K_{bt}. Each of these tables is a mapping between the supply pressure, load, and a valve opening. These tables have been designed for the same velocity requirement of $0.5\,Kph$. The tables have been downloaded into the controller and a flag has been used to bypass the regular controller and use the tables instead.

Figures 9.16, 9.17, and 9.18 show the velocity of the crowd cylinder, valve openings K_{sa}, K_{at} and K_{bt}, and workport pressures P_a and P_b, respectively, when the entire stroke is performed in PLSRE CVM. It is worth noting that as soon as the 2D tables referred to above are downloaded into the controller, the crowd function starts moving without a joystick command because the tables are designed for a certain speed. This explains that truncation in the initial transients since it takes fraction of a second between finishing the download process and starting to record data.

Velocity in this case is smoother than the three previous control methods in terms of performance. Figure 9.16 shows that there are *no* noticeable disruptions to the velocity as a result of increasing loads like the behavior manifested in figures 9.7, 9.10, and 9.13. Backhoe operators will not feel any transitions and will not any irregular or rough velocity behavior in this case. This proves superiority of this control method based on the CVM concept.

Figure 9.17 shows the gradual increase in K_{bt} and decrease in K_{at}. It is clear that the value of K_{sa} jumps up very fast when the load turn into positive range. Although K_{at} closes off completely, no perceptible disruption happens to the flow path since at any given time, at least two valves are open and there is a continuous flow path with enough flow to provide for the velocity commanded at the given load.

Similar to controller III, workport pressures in figure 9.18 demonstrates gradual change in P_a and P_b in contrast to the sudden change illustrated in figure 9.12.

The energy consumed in this case according to equation 9.3 is $190.23\,KJ$. Table 9.1

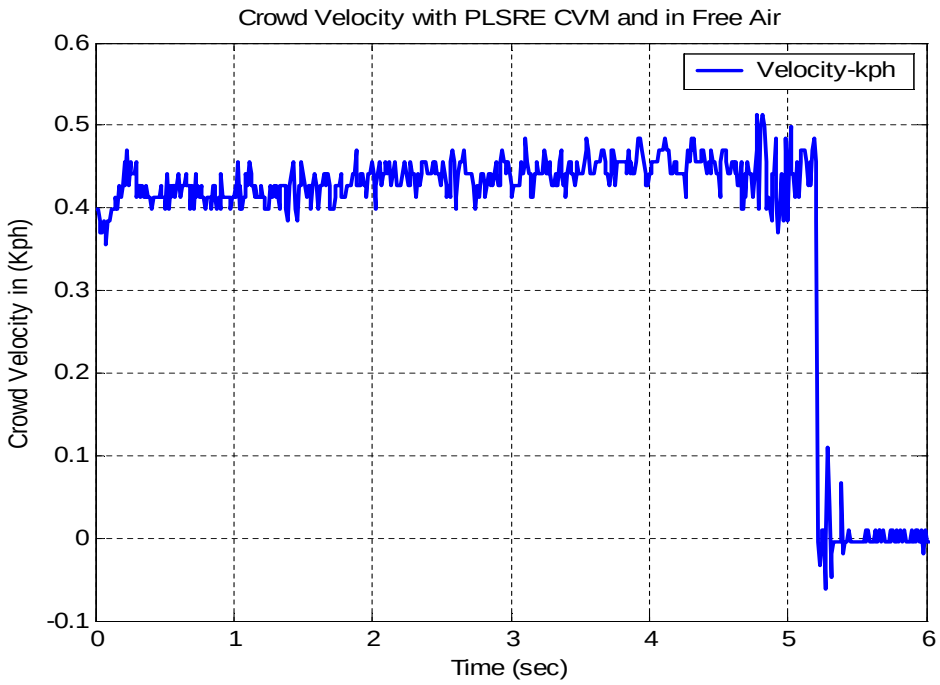

Figure 9.16: Crowd cylinder velocity with PLSRE CVM and in free air

Table 9.1: Energy Consumed by the Four Controllers

Controller	**Energy Consumed in KJ**
I	653.8
II	135.1
III	129.1
IV	190.23

combines the results for the energy consumed by all four controllers for comparison.

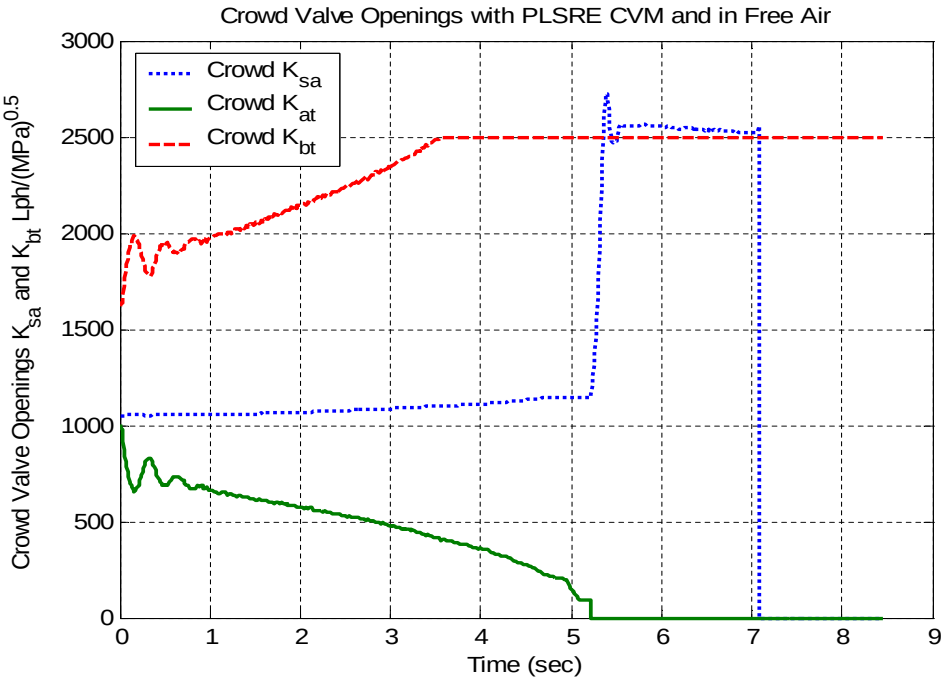

Figure 9.17: Valve openings K_{sa}, K_{at}, and K_{bt} for crowd cylinder with PLSRE CVM and in free air

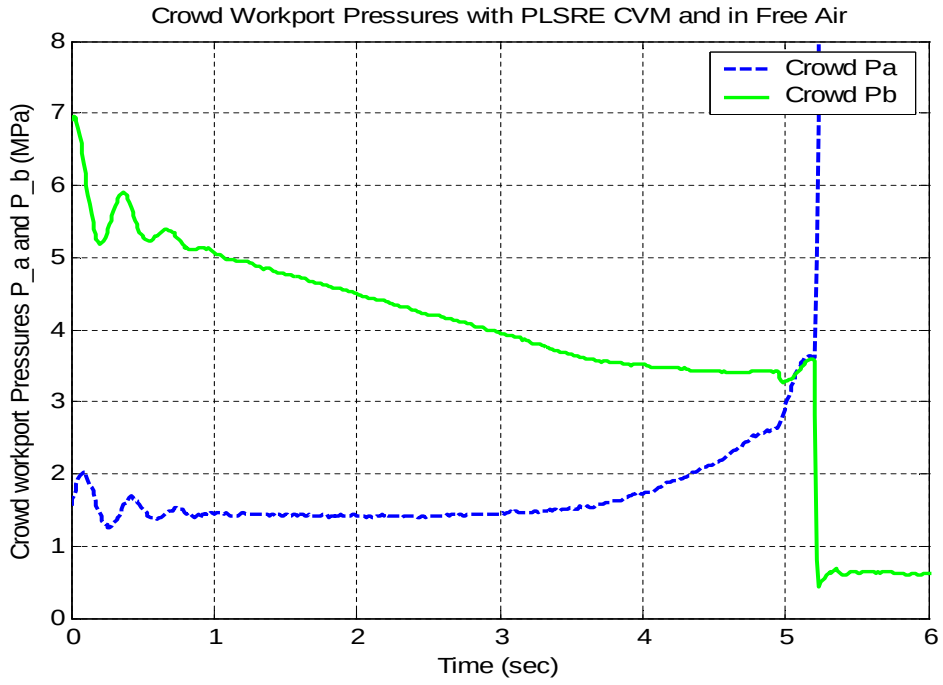

Figure 9.18: Workport pressures P_a and P_b for crowd cylinder with PLSRE CVM and in free air

9.3.2 Extend Stroke Conducted in a Digging Condition

The set of experiments presented in section 9.3.1 are for the full stroke conducted in free air with no digging. This is a rare scenario for mobile hydraulic equipment. Most of the time digging is involved and in this section the same four controllers are compared but with a scenario that involves digging in the ground.

Creating the same exact soil condition for every one of the four trials is extremely difficult. Soil and ground condition are different from a spot to another. Also, due to limitation in hardware availability, the experiments were not repeated enough time to establish statistical significance. However, the velocity performance results in this section gives a reasonably good comparison of the four controllers.

It is worth noting that when using controller II or III, fluctuations between LSRE and PE modes can take place as a result of continuous fluctuations in the load experience by the crowd cylinder. However, it is expected that most of the stroke will be performed in PE mode since digging represent a high load on the cylinder.

9.3.2.1 Controller I: Full Stroke in PE with a Digging Scenario

Figures 9.19 shows the velocity of the crowd cylinder when the full stroke is done in PE mode. Velocity fluctuations are conspicuous. It even shows that the cylinder comes to a complete stop while digging between roughly $t = 2\,sec$ and $t = 4\,sec$.

Obviously, there are a lot of speed fluctuations as the crowd and bucket are going though earth due to the fact that the load is itself, irregular, fluctuating, and unpredictable. The figure also indicates that PE mode, which like any of the other four distinct modes depends on a two-valve flow path, does not adapt fast enough to load fluctuations and this results in the velocity variations.

9.3.2.2 Controller II: Abrupt Mode Switching from LSRE to PE with a Digging Scenario

Figures 9.20 shows the results when the experiment is repeated with controller II. Controller II puts the cylinder in LSRE mode if load is smaller than $-13.5\,KN$, and puts it in PE if the load is larger than $-13.5\,KN$. As a result of large force fluctuations as digging in the ground

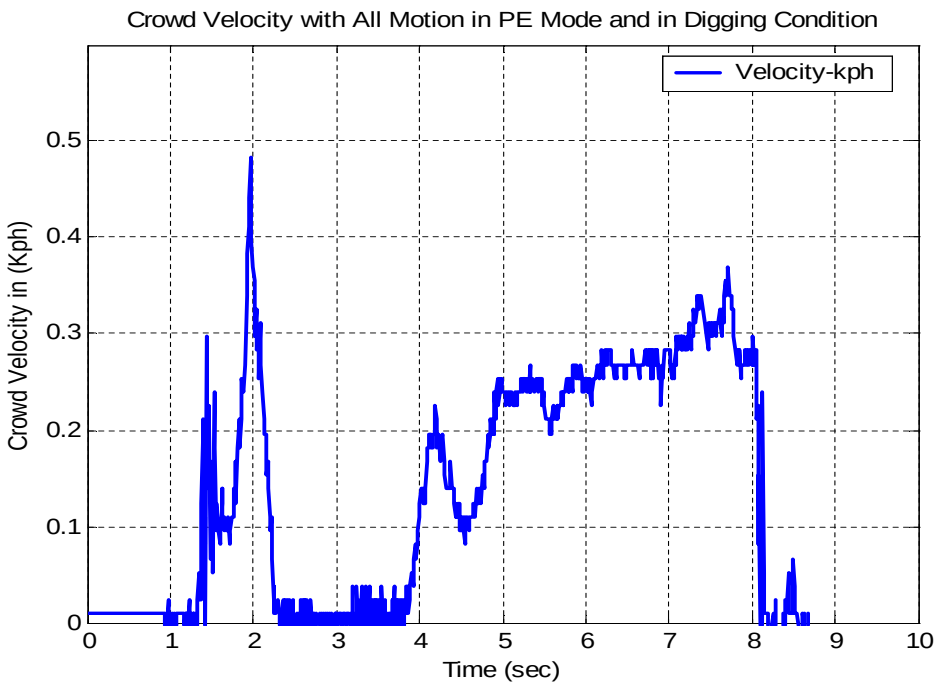

Figure 9.19: Crowd cylinder velocity with all motion in PE and in digging condition

is taking place, the $-13.5\,KN$ mark is crossed several times back and forth. Mode switching entails closing a valve and closing another every time that load is crossed. This explains the large variations and disruptions in the velocity shown in figure 9.20. Multiple mode switching can be avoided by adding some kind of hysteresis to the mode switching causing load or using a linear transition like Controller III, but no dramatic velocity improvement can be expected.

9.3.2.3 Controller III: Linear Transition in Mode Switching from LSRE to PE with a Digging Scenario

Controller III is then used tried and figures 9.21 shows the cylinder velocity results. Because of the linear transition region, velocity irregularities and fluctuations are less and are an improvement over the velocity performance portrayed in figure 9.20. Still, velocities are almost reduced to zero and then jump back up depending on the load, which is highly variable when digging in the earth.

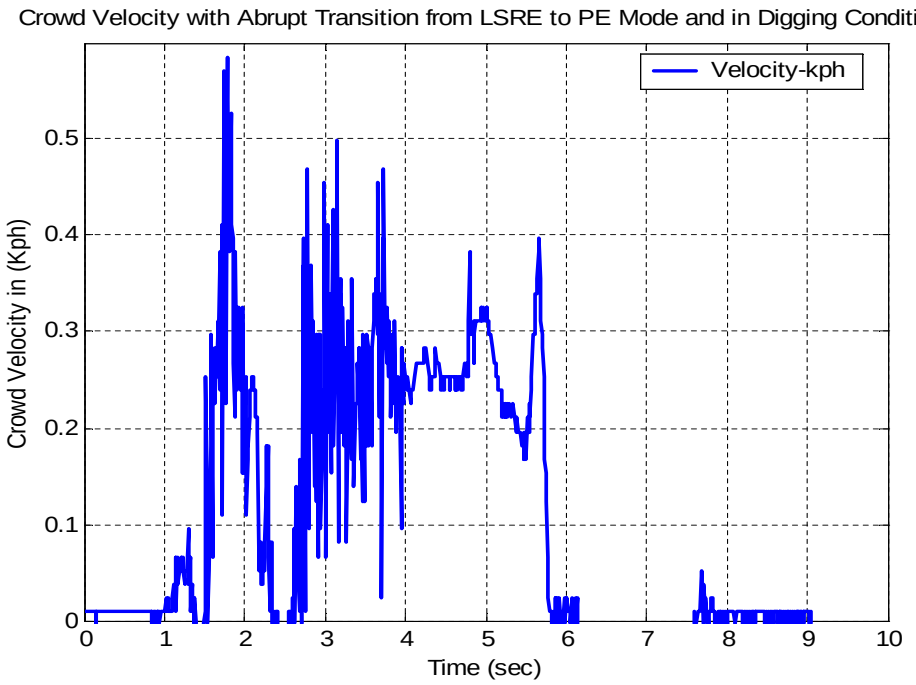

Figure 9.20: Crowd cylinder velocity with abrupt transition from LSRE to PE and in digging condition

9.3.2.4 Controller IV: PLSRE CVM Control with a Digging Scenario

The PLSRE CVM is finally applied the same digging scenario. The same 2-D tables are used to determine valve openings for K_{sa}, K_{at}, and K_{bt} based on load and supply pressure.

Figure 9.22 illustrates a significant improvement in velocity performance over any of the previous three controllers. Other than some fluctuation at about $t = 3\,sec$, velocity is relatively smooth and obviously having three valves opened and being modulated provides a continuous flow path most of the time resulting in this much enhanced velocity compared to the previous three controllers. Again, this proves the better velocity performance of this control method based on the CVM idea.

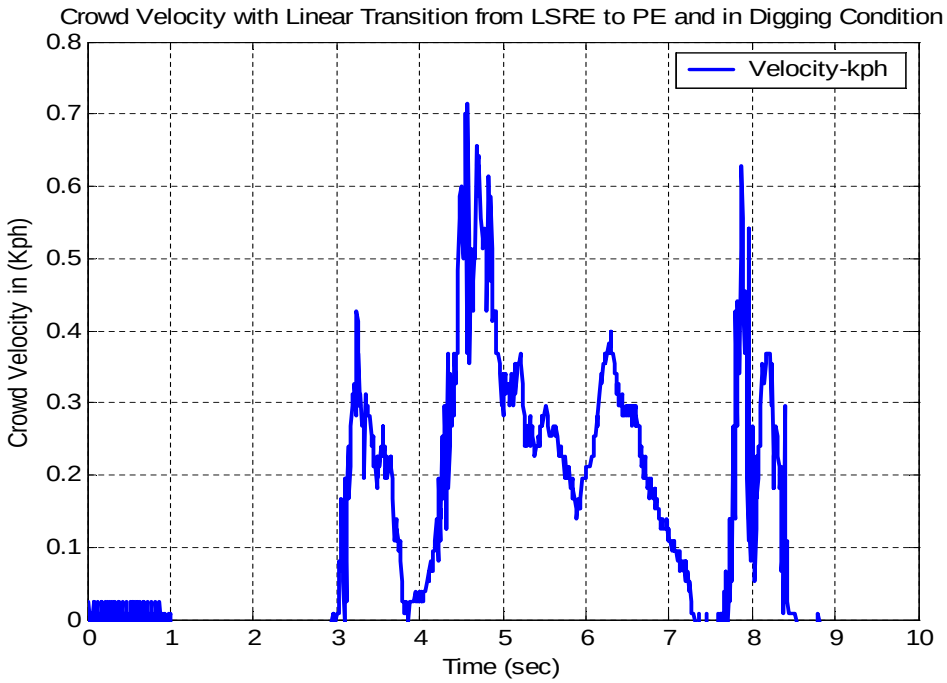

Figure 9.21: Crowd cylinder velocity with linear transition from LSRE to PE and in digging condition

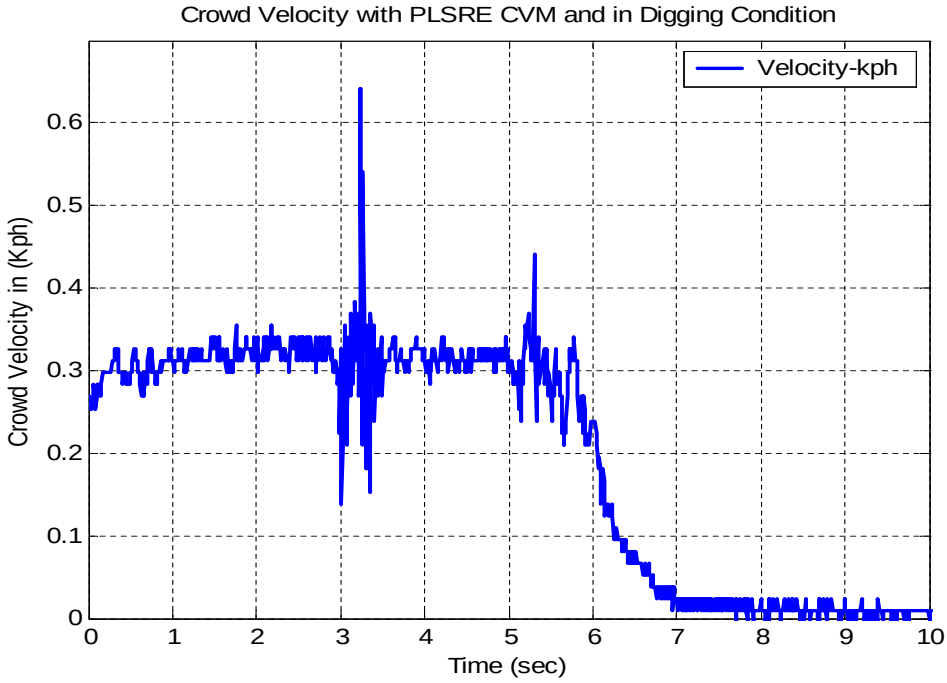

Figure 9.22: Crowd cylinder velocity with PLSRE CVM and in digging condition

9.4 Remarks

The following remarks can be made as a conclusion to this chapter:

- When the entire stroke is performed in the air and is done in PE mode, controller I, the velocity performance is relatively smooth except that towards the end of the stroke as the load increases, the cylinder slows down. But the overall velocity performance is acceptable. The energy consumed in this case, however, is large. It is about 5 times the energy used in controller II and III.

- When controllers II and III are used, where LSRE mode is used along with some scheme of mode switching to PE, velocity performance is *not* acceptable. Velocity decreases towards the end of the Low Side Extend part of the cycle then it goes up again when complete transition to PE takes place. However, the energy consumed is much less than that required to perform the entire stroke in PE because these two controllers allow for flow recirculation throughout the LSRE part of the stroke.

- When three-valve modulation PLSRE CVM controller IV is used, velocity performance is the smoothest among all controllers.

- In the free air experiment, the energy required for PLSRE CVM is higher than the energy required by controllers II and III, but it is still about $\frac{1}{4}$ of the energy required by controller I.

- Controllers I, II, and III are based on two-valve modulation for velocity control that provides a flow path for the hydraulic oil. Since mode switching between these two-valve modulation modes necessitates closing a valve and opening another, flow path and, consequently velocity, disruptions are expected. Three-valve modulation based CVMs provide a continuous flow path to the oil, since at least two valves are always open, and thus much less velocity disruption occurs.

- In conclusion, the experiments shown in this chapter have proved that three-valve modulation or the CVMs concept achieves the best velocity performance while the

increase in energy requirements is not significant compared to the energy used when using discrete mode switching from LSRE to PE but is significantly less than the energy consumed if the whole stroke is performed in PE. Velocity performance and energy requirements make this control method attractive.

CHAPTER X

CONCLUSIONS & FUTURE WORK

10.1 Conclusions

The four-valve independent metering configuration has been investigated including its potential for saving energy and switching between different metering modes.

Independent metering promises intuitively to be more energy efficient than coupled metering. This hypothesis has been mathematically validated. This analysis included three studies. First it has been shown that even if the independent metering four-valve assembly is used in a Pressure Compensated Load Sense (PCLS) type control strategy, power can be saved by virtue of having a two degree of freedom system and being able to control the pressure in the return chamber in addition to the speed of the actuator. Then, power savings have been quantified when using an actuator force feedback control method which takes full advantage of electronic control and independent metering configuration. Lastly, the power savings that could result from using regenerative modes as opposed to powered modes were also computed.

A nonlinear mathematical model of a hydraulic cylinder controlled by a four-valve independent metering configuration has been developed. The model has been experimentally validated using a telehandler machine. Both the extender and boom functions of the telehandler have been simulated with the state space model and then the compared with experimental results from the telehandler. This nonlinear model was useful in conducting the optimal switching analysis that followed.

Optimal control of mode switching has been one of the major objectives of this research. First, switching between two discrete modes has been studied as a problem of optimal switching of a switched dynamic system. Alternatively, other metering modes were developed in this research that provide better performance.

For the former direction of switching between two discrete modes, the general theory

has been developed and then the dynamic model of the hydraulic system has been used to apply the theoretical results to the mode switching problem.

The best way to explain the results of this optimal control problem has been to interpret the result on the mode capability curve. An example of switching between PE and HSRE mode has been used for illustration. It was shown that for efficient and proper motion path, motion should start in PE mode and should continue in PE mode until load is within the capability of HSRE mode then switching should occur. The result showed that the optimal switching point is the intersection point shown on the mode capability curve (refer to figure 6.8).

The results showed that mode switching bears resemblance to automotive automatic transmission gear shifting. This analogy has inspired a real time mode switching algorithm. Mode shifting logic between PE and HSRE has been used as an illustrative example. Similar developments can be made for other modes.

There are points on the capability curves that are beyond the capability of discrete modes. This means that some loads cannot be moved at some commanded velocities using discrete modes. Research showed that this is a control system limitation not a physical limitation in the system. Moreover, switching between discrete modes entails closing one poppet valve and opening another. Since these poppet valves are not infinitely fast, the closing and opening of poppet valves causes a disruption in the flow path and consequently in the velocity of the hydraulic cylinder controlled by the valves. Mode switching was shown to cause beam vibration and undesirable disruption in flow path and thus velocity of the actuator driving the beam.

Solving these discrete modes problems led to the idea of Continuously Variable Modes (CVMs). Instead of having five distinct modes that determines the flow path by opening two of the four valves in the assembly, three Continuously Variable Modes are presented as an alternative way of controlling velocity. In these new modes, three valves are continuously modulated to achieve velocity control as opposed to two valves in the discrete modes. CVMs always provide a continuous flow path. Even if one of the three poppet valves being modulated is closed, the other two poppet valves remain opened during this transition and

thus the continuity of the fluid path is insured. This alleviates the mode switching problem between discrete modes that caused disruption of flow path and cylinder velocity.

The first these CVMs is Powered-High Side Regeneration Extension mode (PHSRE), the second is Powered-Low Side Regeneration Retraction mode (PLSRR), and the third is Powered-Low Side Regeneration Extension mode (PLSRE). The five distinct modes become a special case of these three CVMs. It has been shown that CVMs have more force-speed capabilities than the distinct modes and provide for better velocity and vibrational performance by virtue of always offering a continuous flow path.

Although these modes promise to provide a smoother velocity performance and better energy efficiency than using discrete modes and having to switch between them, they are more complex from a controls point of view than the discrete modes.

The concept of continuously variable modes was experimentally validated in chapter 9. An experiment was conducted on the crowd function of a mid size tractor loader backhoe. Four control techniques were tried. First technique involves using a conventional (or standard) mode that corresponds to using a spool valve with no regenerative modes possible. Then, two controllers allow for switching between regenerative modes and standard modes. One of them allows for abrupt switching, while the other allows for gradual transition between modes. Finally the continuously variable mode control is used. The crowd is given the same speed command in all four trials and the experiment conditions are the same. In the first set of experiments, the Crowd moves in free air without doing any earth digging as the cylinder is extended. The same set of experiments have been then repeated but with the bucket digging in the ground. The experiments showed that the continuously variable modes achieve superior velocity and energy consumption performance (refer to sections 9.3 and 9.3.2 for more details about the results of these experiments).

This research proposes the use of CVMs to achieve superior velocity performance while maintaining an energy savings advantage over conventional technologies.

10.2 Future Work

This work can be extended in several directions:

- The four valve independent metering configuration has been retrofitted to existing mobile hydraulics equipment. In chapter 7, a non-dimensional analysis has been conducted, where beam and actuator parameters have been grouped into non-dimensional parameters that can describe the overall beam-actuator interaction and can help in designing both concurrently to achieve good performance. Some other group parameters can be derived that would include the valve openings of the four valve independent metering configurations to study the influence of these valve openings on the overall system behavior. This analysis can lead to an overall design approach for the valves, their control strategy, and mobile hydraulic equipment design.

- The crowd of a mid size tractor loader backhoe operating in the PLSRE mode was used to demonstrate the capability of CVMs. This concept is yet to be extended to the rest of the functions: boom and bucket and that would allow for testing the other CVMs PHSRE and PLSRR. In the experiment conducted in this work, 2D tables were generated for each of the valve openings for a specific speed. Alternatively, a parametric representation of the controls of CVMs will help the universal implementation of the control algorithm for different speeds, different machines, and various operating conditions.

- The experiments done in this research were conducted on specific types of machines and under a limited range of loading conditions. Using a Hardware-in-the-Loop setup to test the control methodology with various loading conditions, and different simulated machines can be extremely helpful in conducting thorough testing and in universally validating the ideas presented in this dissertation.

- Current research is being done to implement a learning algorithm for the EHPVs and to better understand their dynamics.

- The ideas presented in this dissertation were developed with mobile hydraulic machines in mind. Industrial applications can also be a good target for these ideas. Extensions into other industrial applications can lead to implementation improvements and generalization of the ideas.

REFERENCES

[1] Aardema, J. A., "Hydraulic circuit having dual electrohydraulic control valves." United States Patent, (5,568,759), 1996.

[2] Aardema, J. A. and Koehler, D. W., "System and method for controlling an independent metering valve." United States Patent, (5,947,140), 1999.

[3] Adrian Bonchis, P. I. C. and Rye, D. C., "A pressure-based, velocity independent, friction model for asymmetric hydraulic cylinders," in *In Proc of IEEE International Conference on Robotics and Automation*, (Detroit, Michigan), May 1999.

[4] Andersen, B. R. and Ayres, J. L., "Load sensing directional valves, current technology and future development," in *In The Fifth Scandinavian International Conference on Fluid Power*, 1997.

[5] Andersson, B. R. and Ayres, J. L., "Load sensing directional valves, current technology and future development," in *The Third Scandinavian International Conference on Fluid Power*, (Linkoping, Sweden), May 1993.

[6] Backe, W., "Hydraulic drives with high efficiency," in *In ASME Fluid Power Systems and Technology , FPST-Vol. 2*, pp. 45–73, 1995.

[7] Bemporad, A., Borrelli, F., and Morari, M., "Optimal controllers for hybrid systems: stability and piecewised linear explicit form," *In 39th Proceedings of IEEE Conference on Decision and Control*, 2000.

[8] Book, R. and Goering, C. E., "Programmable electrohydraulic valve," *In SAE paper*, vol. 1, no. 2, pp. 28–34, 1999.

[9] Book, R., *Programmable electrohydraulic valve*. PhD dissertation, University of Illinois at Urbana-Champaign, 1998.

[10] Book, W. J., *Modeling, Design and Control of Flexible Manipulator Arms*. PhD dissertation, Massachusetts Institute of Technology, Boston, MA, April 1974.

[11] Book, W. J., "Recursive lagrangian dynamics of flexible manipulator arms," *The International Journal of Robotics Research*, vol. 3, pp. 87–101, 1984.

[12] Book, W. J., Maizza-Neto, O., and Whitney, D. E., "Feedback control of two beam, two joint systems with distributed flexibility," *Journal of Dynamic Systems, Measurement and Control, Transactions of ASME*, vol. 97 Ser G, pp. 424–431, December 1975.

[13] Branicky, M. S., Borkar, V. S., and Mitter, S. K., "A unified framework for hybrid control: Model and optimal control theory," *IEEE Transactions on Automatic Control*, vol. 43, pp. 31–45, January 1998.

[14] Bu, F. and Yao, B., "Adaptive robust precision motion control of single-rod hydraulic actuators with time varying unknown inertia: a case study," in *In ASME International Mechanical Engineering Congress and Exposition (IMECE), FPST-Vol. 6*, pp. 131–138, 1999.

[15] Carlson, R., "The correct method of calculating energy savings to justify adjustable-frequency drives on pumps," *IEEE Trans. on Industry Applications*, vol. 36, November/December 2000.

[16] Chalhoub, N. G. and Chen, L., "A structural flexibility transformation matrix for modeling open-kinematic chains with revolute and prismatic joints," *Journal of Sound and Vibration*, vol. 218, pp. 45–63, November 1998.

[17] Chalhoub, N. and Ulsoy, A. G., "Control of a flexible robot arm: Experimental and theoretical results," *ASME Journal of Dynamic Systems, Measurement, and Control*, vol. 109, pp. 299–309, 1987.

[18] Chudoung, J. and Beck, C., "The minimum principle for deterministic impulsive control systems," *IEEE Conference on Decision and Control*, vol. 4, pp. 3569–3574, December 2001.

[19] Curtis, C. H., "Energy storage systems for public service vehicles," *Integrated Engine Transmission Systems, IMechE*, vol. C186/86, pp. 117–126, 1986.

[20] Dancose, S., Angeles, J., and Hori, N., "Optimal vibration control of a rotating flexible beam," *Proceedings of* 12^{th} *ASME Conference on Mechanical Vibration and Noise*, September 1989.

[21] DeBoer, C. C. and Yao, B., "Velocity control of hydraulic cylinders with only pressure feedback," in *In ASME International Mechanical Engineering Congress and Exposition (IMECE), DSC-2B-3*, 2001.

[22] deSilva, C. W., *Vibration Fundamentals and Practice*. Boca Raton, FL: CRC Press, 1999.

[23] Edge, K. A., "The control of fluid power systems - responding to challenges," *Journal of Systems & Control Engineering*, vol. 211, no. 2, pp. 91–110, 1997.

[24] Egerstedt, M., Wardi, Y., and Delmott, F., "Optimal control of switching times in switched dynamical systems," in *IEEE Conference on Decision and Control*, (Maui, Hawii), December 2003.

[25] Elfving, M. and Palmberg, J. O., "Distributed control of fluid power actuators - experimental verification of a decoupled chamber pressure controlled cylinder," in *4th International Conference on Fluid Power*, 1997.

[26] Frankenfield, T. and Stavrou, P., "Developing trends in hydraulics tied to electronic controls," *Control Engineering*, vol. 40, no. 5, pp. 62–66, 1993.

[27] Fukuda, T., "Flexible control of elastic robotic arms," *Journal of Robotic Systems*, vol. 2, no. 1, pp. 73–88, 1985.

[28] Garnjost, K. D., "Energy-conserving regenerative-flow valves for hydraulic servomotors." United States Patent, (4,840,111), 1989.

[29] Grabbel, J. and Ivantysynova, M., "Integrated servo joint actuators for robotic application," in *6th Scandinavian International Conference of Fluid Power*, (Tampere, Finland), pp. 1253–1265, May 1999.

[30] Harakopos, E. G. and Mayne, R. W., "Motor characteristics in the control of a compliant load," *Journal of Guidance, Control, and Dynamics*, vol. 9, pp. 113–118, Jan-Feb 1986.

[31] Hedlund, S. and Rantzer, A., "Optimal control of hybrid systems," *Proceedings of 38th IEEE Conference on Decision and Control*, vol. 4, pp. 3972–3977, December 1999.

[32] Holzbock, P. E., "Energy saving electrohydraulic systems," in *Proceeding of The National Conferences on Fluid Power*, pp. 324–331, 1977.

[33] Hristu-Varsakelis, D., "Feedback control systems as users of shared network: Communication sequences that guarantee stability," *IEEE Conference on Decision and Control*, pp. 2063–2068, 2001.

[34] Hu, H., Zhang, Q., and Alleyne, A., "Multi-function realization of a generic programmable e/h valve using flexible control logic," in *Proceedings of the Fifth International Conference on Fluid Power Transmission and Control*, (International Academic Publishers, Beijing, China), pp. 107–110, 2001.

[35] Jansson, A. and Palmberg, J.-O., "Separate control of meter-in and meter-out orifices in mobile hydraulic systems," *SAE technical Paper Series*, no. 901583, 1990.

[36] Johansson, M., *Piecewise Linear Control Systems*. PhD dissertation, Lund Institute of Technology, Lund, Sweden, 1999.

[37] Juang, J.-N. and Horta, L. G., "A slewing control experiment for flexible structures," *Journal of Guidance*, vol. 9, pp. 599–607, Sept-Oct 1986.

[38] Kramer, K. D. and Fletcher, E. H., "Electrohydraulic valve system." United States Patent, (Re. 33,846), 1990.

[39] Lew, J. Y. and Book, W. J., "Hybrid control of flexible manipulators with multiple contact," *Proceedings - IEEE International Conference on Robotics and Automation*, vol. 2, pp. 242–247, 1993.

[40] Liang, X. G., Virvalo, T., and Linjama, M., "The influence of control valves on the efficiency of a hydraulic crane," in *6th Scandinavian International Conference of Fluid Power*, (Tampere, Finland), pp. 381–394, May 1999.

[41] Liang, X. and Virvalo, T., "Energy reutilization and balance analysis in a hydraulic cranes," in *Fifth International Conference on Fluid Power Transmission and Control (ICFP)*, (Hangzhou, China), 2001.

[42] Liang, X. and Virvalo, T., "What's wrong with energy reutilization in hydraulic cranes," in *Fifth International Conference on Fluid Power Transmission and Control (ICFP)*, (Hangzhou, China), 2001.

[43] Lincoln, B. and Benhardsson, B. M., "Efficient pruning of search trees in lqr control of switched linear systems," *In Proceedings of 39th IEEE Conference on Decision and Control*, vol. 4, pp. 1828–1833, December 2000.

[44] Liu, S. and Yao, B., "Energy saving control of single-rod hydraulic cylinders with programmable valves and improved working model selection," *National Fluid Power Association*, vol. 102, no. 2.4, pp. 81–91, 2002.

[45] Loper, J. C., *Vibration cancellation and disturbance rejection in serially linked micro/macro manipulators*. MS thesis, Georgia Institute of Technology, Atlanta, GA, March 1998.

[46] Lu, J., Liao, L., Nerode, A., and Taylor, J. H., "Optimal control of systems with continuous and discrete states," *In Proceedings of 32nd IEEE Conference on Decision and Control*, pp. 2292–2297, 1993.

[47] Luomaranta, M. K., Vilnius, M. J., and Ahonoja, I., "Microcontroller makes a flexible electrohydraulic valve, mechatronics spells profitability," in *International Conference of Machine Automation*, (Tampere, Finland), Feb 1994.

[48] Luomaranta, M. K., Vilnius, M. J., and Ahonoja, I., "Can bus for advanced electrohydraulic remote valves," in *Industrial Vehicle Technology '97 Off-Highway*, (UK & International Press, Dorking, Surrey, UK.), pp. 134–137, 1997.

[49] Magee, D. P., *Optimal Arbitrary Time-Delay Filtering to Minimize Vibration in Elastic Manipulator Systems*. PhD dissertation, Georgia Institute of Technology, Atlanta, GA, August 1996.

[50] Mattila, J. and Virvalo, T., "Computed force control of hydraulic manipulators," in *5th Scandinavian International Conference on Fluid Power*, 1997.

[51] McCloy, D. and Martin, H. R., *The Control of Fluid Power*. New York, NY: John Wiley & Sons, 1973.

[52] Meirovitch, L., *Analytical Method in Vibrations*. New York, NY: The Macmillan Company, 1967.

[53] Merritt, H. E., *Hydraulic Control Systems*. New York, NY: John Wiley & Sons, Inc, 1967.

[54] Munzer, M. E., "Control of mobile hydraulic cranes," in *In Proc of 1st FPNI-PhD Symp*, (Hamburg, Germany), pp. 475–483, 2000.

[55] Mykleburst, A., "Dynamic response of an electric motor linkage system during startup," *ASME Journal of Mechanical Design*, vol. 104, no. 1, pp. 137–142, 1982.

[56] Mykleburst, A., Fernandez, E. F., and Choy, T. S., "Dynamics response of slider-crank machines during startup," *ASME Journal of Mechanism, Transmissions, and Automation in Design*, vol. 106, pp. 452–457, December 1984.

[57] Noack, S. and Riede, H., "Calculation of the energy balance of complex hydraulic drives," in *6th Scandinavian International Conference of Fluid Power*, (Tampere, Finland), pp. 903–920, May 1999.

[58] O'Hara, D. E., "The smart valve," *Industrial Applications of Fluid Mechanics*, vol. 100, pp. 95–99, 1990.

[59] Opdenbosch, P. and Sadegh, N., "Control electro-hydraulic poppet valves via online learning and estimation," in *Proceedings of IMECE 2005*, (Orlando, FL), pp. 57–62, November 2005.

[60] Opdenbosch, P., Sadegh, N., and Book, W., "Modeling and control of an electro-hydraulic poppet valve," in *Proceedings of IMECE 2004*, (Anaheim, CA), pp. 103–110, November 2004.

[61] Panza, M. J., *Actuator, Load, and Control Considerations in the Dynamics of a Flexible Beam-Like Member*. PhD dissertation, State University of New York at Buffalo, Buffalo, NY, 1989.

[62] Panza, M. J. and Mayne, R. W., "Theoretical and experimental investigation of hydraulic actuator interaction in the dynamics of a rotating flexible beam," *Journal of Vibration and Acoustics*, vol. 116, pp. 113–119, January 1994.

[63] Panza, M. J., Sah, J. F., Mayne, R. W., and Inman, D. J., "Prospects of damping structures via actuator interaction," *Proceedings of International Conference on Computational Engineering Science*, pp. 44.6.1–4, 1988.

[64] Pestel, E. C. and Leckie, F. A., *Matrix Methods in Elastomechanicsl*. New York, NY: McGraw Hill, 1963.

[65] Pfaff, J. and Tabor, K., "Method of sharing flow of fluid among multiple hydraulic functions in a velocity based control system." United States Patent, (6,779,340), August 2004.

[66] Pfaff, J. and Tabor, K., "Velocity based electronic control system for operating hydraulic equipment." United States Patent, (6,732,512, May 2004.

[67] Piccoli, B., "Hybrid systems and optimal control," *In Proceedings of 37th IEEE Conference on Decision and Control*, pp. 13–18, 1998.

[68] Plummer, A. R. and Vaughan, N. D., "Robust adaptive control for hydraulic servosystems," *Transactions of the ASME, Journal of Dynamic Systems, Measurement and Control*, vol. 118, no. 2, pp. 237–143, 1996.

[69] Punyapas, N., *The Design of Hydraulic Valve Circuit under Microprocessor Control for Increasing Efficiency of Hydraulic Servo system*. PhD dissertation, Georgia Institute of Technology, March 1982.

[70] Rahmfeld, R. and Ivantysynova, M., "Energy saving controlled linear drive with differential cylinder." 2.IFK, 2000.

[71] Rahmfeld, R. and Ivantysynova, M., "Displacement controlled linear actuator with differential cylinder- a way to save primary energy in mobile machines," in *Fifth International Conference on Fluid Power Transmission and Control (ICFP)*, (Hangzhou, China), 2001.

[72] Sadler, J. P., Mayne, R. W., and Fan, K. C., "Generalized study of crank-rocker mechancism driven by a dc motor, part i: Mathematical model, and part ii: Appications," *Mechanisms and Machine Theory*, vol. 15, pp. 435–461, 1980.

[73] Sah, J. F. and Mayne, R. W., "Modeling of a slewing motor-beam system," *Proceedings of ASME International Computers in Engineering Conference*, August 1990.

[74] Sakawa, Y., Matsunno, F., and Futsushima, S., "Modeling and feedback control of a flexible arm," *Journal of Robotic Systems*, vol. 2, no. 5, pp. 453–472, 1985.

[75] Shaikh, M. S. and Caines, P., "On trajectory optimization for hybrid systems: Theory and algorithms for fixed schedules," *IEEE Conference on Decision and Control*, December 2002.

[76] Siciliano, B. and Book, W. J., "A singular perturbation approach to control of lightweight flexible manipulators," *The International Journal of Robotics Research*, vol. 7, pp. 79–90, August 1988.

[77] Sussmann, H. J., "Set-valued differentials and the hybrid maximum principle," *IEEE Conference on Decision and Control*, vol. 1, pp. 558–563, December 2000.

[78] Tabor, K., "Velocity based method for controlling a hydraulic system." United States Patent, (6,718,759), April 2004.

[79] Tabor, K., "Velocity based method for controlling an electro-hydraulic proportional control valve." United States Patent, (6,775,974), August 2004.

[80] Tabor, K., "A novel method of controlling a hydraulic actuator with four valve independent metering using load feedback," in *SAE Commercial Vehicle Engineering Conference*, (Chicago, Illinois), November 2005.

[81] Tabor, K., "Optimal velocity control and cavitation prevention of a hydraulic actuator using four valve independent metering," in *SAE Commercial Vehicle Engineering Conference*, (Chicago, Illinois), November 2005.

[82] Tse, F. S., Morse, I. E., and Hinkle, R. T., *Mechanical Vibrations, Theory and Applications*. Boston, MA: Allyn and Bacon, Inc, 1978.

[83] Vaughan, N. D. and Dorey, R. E., "Hydraulic accumulator energy storage in a city bus, integrated engine transmission systems," *Integrated Engine Transmission Systems, IMechE*, vol. C186/86, pp. 105–116, 1986.

[84] Vaughan, N. D. and Gamble, J. B., "The modeling and simulation of a proportional solenoid valve," *Transactions of the ASME, Journal of Dynamic Systems, Measurement and Control*, vol. 118, no. 1, pp. 120–125, 1996.

[85] Venkatraman, V. and Mayne, R. W., "Dynamics behavior of a hydraulically actuated mechanism, part i: Small perturbations, and part ii: Nonlinear character," *ASME Journal of Mechanisms, Transmissions, and Automation in Design*, vol. 108, pp. 245–254, June 1986.

[86] Wang, L. Y., Beydoun, A., Cook, J., Sun, J., and Kolmanovsky, I., "Optimal hybrid control with applications to automotive powertrain systems," *In Control Using Logic-Based Switching*, vol. 222, pp. 190–200, December 1997.

[87] Wang, X., Xu, C., Zhao, K., Zhao, D., and Nie, F., "Simulation of automatic shift-control on construction vehicle," *China Journal of Highway and Transport*, vol. 14, no. 3, pp. 113–116, 2001.

[88] Weber, R. T., "Controlling pumps for performance efficiency," *Hydraulics and Pneumatics*, May 1994.

[89] Wieber, R. H., "Time optimal electrohydraulic servopositioning system for replaceable disk," in *Proceeding of The National Conferences on Fluid Power*, pp. 306–320, 1970.

[90] Wilke, R. A. and Yang, X., "Pilot solenoid control valve and hydraulic control system using same." United States Patent, (5,878,647), March 1999.

[91] Wu, B., "Optimization of power management strategies or a hydraulic hybrid medium truck," in *Proceeding of the 2002 Advanced Vehicle Control Conference*, (Hiroshima, Japan), September 2002.

[92] Xu, X. and Antsaklis, P. J., "An approach for solving general switched linear quadratic optimal control problems," *In Proceedings of 40th IEEE Conference on Decision and Control*, pp. 2478–2483, 2001.

[93] Xu, X. and Antsaklis, P., "Optimal control of switched autonomous systems," *IEEE Conference on Decision and Control*, pp. 2063–2068, December 2002.

[94] Xu, X. and Antsaklis, P., "Optimal control of switched dynamical systems based on parameterization of switching instants," *IEEE Transactions on Automatic Control*, vol. 49, pp. 2–16, January 2004.

[95] Yang, X., "Pilot solenoid control valve with pressure responsive diaphragm." United States Patent, (6,149,124), November 2000.

[96] Yang, X., Pfaff, J. L., and Paik, M. J., "Pilot operated control valve having a poppet with integral pressure compensating mechanism." United States Patent, (6,745,992), June 2004.

[97] Yang, X., Stephenson, D. B., and Paik, M. J., "Bidirectional pilot operated control valve." United States Patent, (6,328,275), 2001.

[98] Zhu, Z. and Xu, C., "Experimental study on intelligent gear-shifting control system of construction vehicle based on chaotic neural network," *Nature and Science*, vol. 1, no. 1, pp. 86–90, 2003.